Characterisation and application of olfactory ensheathing cells for glaucoma induced optic nerve damage

Sauparnika Rayapureddi

This thesis is submitted to

University College London

for the degree of

Doctor of Philosophy

UCL Institute of Ophthalmology

October 2012

Declaration

I, Sauparnika Rayapureddi, confirm that the work presented in this thesis is my own. Where information has been derived from other sources, I confirm that this has been indicated in the thesis.

Acknowledgements

First, I would like to thank my supervisors Prof Peng Khaw and Prof Geoff Raisman for allowing me to do this work and continuous guidance throughout. A big thanks to Prof Khaw and Mrs Peggy Khaw for their invaluable encouragement, suggestions and support for the last four years.

I am forever grateful to Dr Annegret Dahlmann-Noor, who had been the rock of support that I always turned to, who taught me all the necessary skills in the lab, patiently corrected my grammar mistakes and always found time to talk to me, irrespective of the time I called her. I am indebted to Dr Astrid Limb for her invaluable suggestions in numerous experiments and writing for publications. I am very thankful to Dr Maryse Bailly who found the time and energy to teach me a numerous microscopy skills, despite me blowing off her light bulbs a hundred times. I would also thank Prof Julie Daniels and Prof. Clare Futter for their clever suggestions for better assays.

Thank you to my great friends Dr Ashkan Khalili, Dr Alistair Lockwood, Dr Daniel Paull, Dr Sumit Dhingra and Dr Amir Samsuddin for always lending your ears to my chit-chat. I greatly appreciate all the constructive criticisms from Ashkan; I hugely appreciate Alistair and Sumit for the training for talks and presentations; I am grateful to Dan for always helping me out with the Mac. Above all, I am most thankful to Peggy for all her support, but more importantly for the brownies, chips etc on so many hungry and dull afternoons.

A special thanks to Dr Richard Foxton who kindly provided the ganglion cells; Dr Silke Becker and Dr Hari Jayaram for teaching me electrophysiology and refining my writing skills. I cannot forget all the help I received from Dr Shweta Singhal, Dr Bhairavi Bhatia, Ms Megan Jones, Dr Philippa Cotrill, Mr Joe Wiseman, Dr Hannah Levis, Dr Anna Harris, Ms Amanda Vernon, Dr Antony Vugler, Dr Ioannis Kokinopoulas, Dr Maayan

Semo, Dr Jean Lawrence, Prof James Morgan, Prof Tom Salt, Dr Peter Munro and Mr Peter Marshall.

I gratefully acknowledge the funding from Dorothy Hodgkins Postgraduate Award, Medical Research Council, UK, Fight for Sight, Helen Hamlyn Trust, NIHR BRC for Ophthalmology, Moorfields Eye Hospital and UCL Institute of Ophthalmology.

Finally, I would not have written this thesis without the love and support from my parents and brother, although they are far away and my husband, who put up with my numerous PhD prangs and mood swings very patiently.

I dedicate my thesis to my teacher, Udith Chaitanyaji, who has been my inspiration for the last ten years of my life.

Abbreviation List

Ab Alamar blue

AC anterior chamber

AMP adenosine monophosphate

ANOVA analysis of variance

ANP atrial natriuretic peptide

BDNF brain derived neurotrophic factor

BSS balanced salt solution

cAMP cyclic adenosine monophosphate

CNS central nervous system

CNTF ciliary neurotrophic factor

CMFDA 5-chloromethylfluorescein diacetate

CS corticosteroids

DAPI 4',6-diamidino-2-phenylindole

DI dynamic index

DMEM Dulbecco's modified Eagle medium

DNA deoxyribonucleic acid

ECM extracellular matrix

EGF epidermal growth factor

eGFP enhanced green fluorescent protein

EM electron microscopy

ERG electroretinography

FBS fetal bovine serum

FGF fibroblast growth factor

GCL ganglion cell layer

GDNF glial derived neurotrophic factor

GFAP glial fibrillary acidic protein

GFP green fluorescent protein

HSP heat shock protein

ICA irido-corneal angle

ICC immunocytochemistry

IgG immunoglobulin G

IHC immunohistochemistry

IOP intraocular pressure

LAMP1 Lysosomal-associated membrane protein 1

LC lamina cribrosa

LCC lamina cribrosa cells

OCT optimal cutting media

OEC olfactory ensheathing cells

OB olfactory bulb

OM olfactory mucosa

ONF olfactory nerve fibroblasts

ONH optic nerve head

OPC oligodendrocyte precursor cells

MMP matrixmetallo proteinase

Mn manganese

mRNA messenger ribonucleic acid

MSC mesenchymal stem cells

NGF nerve growth factor

NMDA N-Methyl-D-Aspartic acid

NOS nitric oxide synthase

nSTR negative scotopic threshold response

NT neurotrophins

NTR neurotrophin receptor

PBS phosphate buffered saline

PCR polymerase chain reaction

PFA paraformaldehyde

PI propidium iodide

POAG primary open angle glaucoma

pSTR positive scotopic threshold response

PNS peripheral nervous system

RNA ribonucleic acid

RGC retinal ganglion cells

RT room temperature

SC scleral canal

SEM standard error of mean

STR scotopic threshold response

TACE TNF alpha converting enzyme

TBS tris buffered saline

TEM transmission electron microscopy

TM trabecular meshwork

TNF tumour necrosis factor

Trk tyrosine kinase

TUNEL terminal deoxynucleotidyl transferase dUTP nick labelling

Abstract

Glaucoma is the term used to describe a group diseases characterised by a specific type of damage to the optic nerve head (ONH) known as cupping and a characteristic type of visual field loss. This loss is associated with progressive atrophy and loss of the retinal ganglion cells. Glaucoma is a leading cause of irreversible blindness in the world.

This project was aimed at investigating olfactory ensheathing cells (OEC), a population of radial glia proven to be neuroprotective in central and peripheral nerve injury models, and their potential to protect the retinal ganglion cells in glaucoma.

We studied the interactions of RGC and OEC in culture. We show that OEC can straighten, ensheath and bundle RGC neurites as well as support the survival of RGC and their synapses in culture. We also show that OEC endocytose dead RGC in culture.

We modified a rat model of glaucoma (where paramagnetic microbeads are injected into the anterior chamber of the rat eyes) and characterised the early and late functional changes in the glaucomatous retina. We showed that RGC function was compromised in the early stages of glaucoma, before histological changes set in.

We injected OEC into glaucomatous rat eyes to study the effects of OEC on optic nerve damage. The presence of OEC in the vitreous cavity of the glaucomatous rat eye significantly reduced the optic nerve damage in glaucomatous eyes.

In summary, the work presented in this thesis provides an insight into

- The functional changes of RGC in the early stages of experimental glaucoma and
- Protection of RGC in experimental glaucoma by introduction of OEC into the vitreous.

Table of Contents

Table of figures

List of tables

Introduction

Glaucoma

Glaucoma is the term used to describe a group diseases characterised by a specific type of damage to the optic nerve head (ONH) known as cupping and a characteristic type of visual field loss. This loss is associated with progressive atrophy and loss of the retinal ganglion cells (Quigley and Green, 1979, Quigley and Broman, 2006, Liao et al., 2003).

Glaucoma is the leading cause of irreversible blindness in the world (Quigley and Broman, 2006). About 60.5 million people worldwide had glaucoma in 2010 and the figures are expected rise to 79.6 million by 2020 (Quigley and Broman, 2006). About 50% of patients are unaware of their disease before irreversible loss of sight has occurred (Tielsch et al., 1991). About 70% of glaucoma is found in the developing countries, and the disease is detected at the very late stages (Quigley and Broman, 2006). With the increase in ageing population, glaucoma will affect a rising number of individuals and its socio-economic burden will increase.

In the eye, the structures significant for glaucoma are located in the anterior chamber, the retina and the optic nerve. Figure 1 is a diagrammatic representation of the section of human eye.

The anterior chamber of the eye

The space between the iris and the cornea is referred to as the anterior chamber (AC). This chamber is filled with a fluid, the aqueous humour.

Aqueous humour

Aqueous humour is composed of water and dissolved salts, gases (oxygen and carbondioxide), proteins and carbohydrates (Kinsey, 1951).

Figure 1 A diagrammatic representation of the section of human eye.

Adapted from www.removingblindness.com/e_anatomy.htm

Figure 2 Direction of aqueous humour circulation in the anterior chamber.

The aqueous humour secreted by the ciliary epithelium travels to the anterior chamber through the pupil and drains through the trabecular meshwork in the iridocorneal angle, into Schlemm's canal. The dotted arrows indicate the course of aqueous. (Adapted from anesthesia.org.cn).

It is important that the aqueous remains transparent because it is in the path of light rays to the retina. The cornea and lens being avascular, the aqueous humour provides oxygen and metabolites for these structures. It also regulates the pH balance and provides antioxidants. Secreted by the ciliary epithelium of the ciliary body, the aqueous humour enters the anterior chamber through the pupil and drains out mainly through the trabecular meshwork (TM) into Schlemm's canal and finally into the episcleral veins (Cole, 1977). A fraction of aqueous (about 40% in humans) drains directly through the connective tissue out into the sclera; this is referred to as the "uveo-scleral outflow" (Alm and Nilsson, 2009). The secretion, circulation and drainage of aqueous humour are well balanced and create a pressure referred to as the intraocular pressure (IOP). When the volume of aqueous humour in the AC increases, this can give rise to ocular hypertension, which is one of the major risk factors for glaucoma. The volume of aqueous can increase due to increased secretion, blockage of outflow or both.

In the ciliary epithelium, solutes are secreted actively (Civan and Macknight, 2004), followed by passive diffusion of water aided by aquaporins, specialised water channels on cell membranes (Yamaguchi et al., 2006). In humans, the secretion of aqueous humour follows a circadian rhythm (Maus et al., 1994). In humans, the normal IOP is about 16 Hgmm (Sommer et al., 1991). The normal aqueous turnover in adults is about 1.5% of the total volume per minute (Goel et al., 2010), but flow is reduced during the night (Liu et al., 2011).

Aqueous humour secretion is in part controlled by the enzyme carbonic anhydrase, which regulates bicarbonate concentration and subsequent regulation of osmosis of water into the anterior chamber (Becker, 1959). Carbonic anhydrase and its mRNA are over-expressed in cultured ciliary epithelial cells from human glaucomatous eyes which suggests that over production of aqueous humour may be present in some eyes with high

IOP and may contribute to glaucoma (Liao et al., 2003). However, this is an unusual cause for intraocular pressure.

Aqueous humour outflow can be blocked at any part of the drainage pathways: trabecular meshwork/Schlemm's canal or uveoscleral pathway. Deposition of proteins, blood cells, etc, can block these aqueous humour outflow pathways. Pseudo-exfoliation syndrome is one risk factor for glaucoma. Deposition of microfibrillar exfoliative material on lens capsule, zonules, iris and ciliary processes and subsequent elevation of IOP lead to glaucoma in affected patients (Jeng et al., 2007).The susceptibility to harm from elevated IOP increases with age, female sex, Afro-Asian race and family history (Yang et al., 2004). Hypermetropia is considered a risk factor for developing the closed angle type glaucoma (Lowe, 1977).

The most common clinical types of glaucoma are primary open angle glaucoma (POAG) and primary angle closure glaucoma (PACG). Angle closure glaucoma is caused by the apposition of iris and TM, blocking the aqueous humour outflow. In POAG, the iris does not block the aqueous flow through the TM, and on clinical examination, the iridocorneal angle appears patent.

Trabecular meshwork

The trabecular meshwork is a porous structure composed of connective tissue lamellae which contain collagen and elastin, and lined with cells called trabecular meshwork cells (Tamm, 2009). These endothelial cells of the TM can phagocytose debris that would otherwise block the pores (Rohen and van der Zypen, 1968). TM cells have been cultured and studied *in vitro* to enhance the understanding of their cell biology.

Mechanical stretching of the porcine TM cells up regulates extracellular matrix (ECM) proteins like collagen and fibronectin, and cytoskeletal proteins like vimentin and tubulins (Keller et al., 2007) (Tumminia et al., 1998, Vittal et al., 2005). In eyes with POAG, there is irregular thickening of the TM due to the deposition of ECM proteins (plaques); the amount of

depositions correlates with optic nerve damage (Lutjen-Drecoll et al., 1981, Gottanka et al., 1997). The amount of ECM content in the TM is strongly linked to matricellular proteins like SPARC, thrombopsodins and tenascins (Rhee et al., 2003, Rhee et al., 2009, Flugel-Koch et al., 2004). Matricellular proteins are bioactively secreted glycoproteins, which modulate the interactions between cells and their ECM environment (Bornstein and Sage, 2002). The over-expression of these proteins may raise IOP by TM remodelling, deposition of ECM and tissue adhesion to the ECM preventing the outflow of the aqueous (Rhee et al., 2009).

In POAG, the TM cell count is significantly reduced (Alvarado et al., 1984). Mitochondrial damage triggers apoptosis in TM cells (He et al., 2008). The TM of glaucomatous human eyes displays high levels of calcification markers (Xue et.al., 2007). A recent study has shown that POAG and pseudo-exfoliation glaucoma are the only two glaucomas where TM cells are subjected to oxidative stress due to defective mitochondria (Izzotti et al., 2011). In other types of glaucoma, oxidative stress does not appear to correlate with mitochondrial damage.

Use of corticosteroids to combat inflammation in the eye or elsewhere in the body can result in a secondary glaucoma termed steroid induced glaucoma. Eventhough only a small percentage of the general population is at risk of developing steroid-induced glaucoma; people with predisposition for POAG are at increased risk when using steroids (Armaly, 1965, Tektas 2009). The TM of eyes with steroid induced glaucoma is obstructed by fibrillar basement membrane material (Tawara et al., 2008). Hypercholesterolemia, obesity and smoking are associated with increased IOP (Stewart et al., 1996, Mori et al., 2000, Lee et al., 2003). In the elderly, reduced uveoscleral outflow may be another trigger for the onset of glaucoma (Toris et al., 1999).

The first line treatment is conservative: eye drops or systemic drugs to reduce aqueous production (beta blockers, alpha agonists, CA inhibitors) or facilitators of uveoscleral outflow (prostaglandin analogues). Laser can

be applied to the TM (laser trabeculoplasty) to stimulate cellular activity including the phagocytic cells and increase outflow in the short to medium term. Blockage at the level of the TM can also be surgically treated by Glaucoma Filtration Surgery (most commonly a procedure called trabeculectomy) where an opening is made in the eye which allows an alternate path for the outflow of aqueous from the AC to reduce the IOP. However, the healing and scarring of the wound cause the closure of the surgical aperture and the aqueous humour can build up again (Georgoulas et al., 2008).

Raised intraocular pressure (IOP) causes RGC loss in many cases although lower levels of IOP produces effects similar to that of high IOP in some individuals (Trick, 1993) (Guo et al., 2005). In some cases, vision loss progresses despite lowering of IOP.

Vitreous humour

The gel-like vitreous fills the posterior part of the eye between the lens and retina. The vitreous in the adult is devoid of blood vessels and this is important as it maintains transparency to facilitate the passage of light. 98% of the vitreous is water. The vitreous also contains collagen fibrils, some of which insert into the inner limiting membrane of the retina (Bos et al., 2001) (Bishop, 2000) as well as hyaluronic acid, proteins, salts and sugars. The vitreous is a reservoir of extracellular matrix proteins and acts as a “sink” for retinal potassium ions pumped out by the Müller glia.

Hyalocytes, the cells in the vitreous humour, are capable of ECM protein secretion and phagocytosis (Sakamoto and Ishibashi, 2011, Bos et al., 2001, Bishop, 2000). The adult vitreous has a canal stretching from the optic nerve head to the back of the lens - the hyaloid canal/ Cloquet’s canal which is the remnant of embryonic blood vessels that nourish the anterior chamber (Mann, 1928).

Figure 3 Histology of the trabecular meshwork.

The section at the top shows the relative positions of anterior chamber (AC), ciliary muscle, Trabecular meshwork (TM) and Schlemm's canal (SC) in a meridional section of the human eyeball. The figure at the bottom is the magnification of the area in the rectangular box in the figure above. It shows the arrangement of the pores of varying sizes in the TM. The figure is adapted from Tamm, 2009.

Anatomy of the optic nerve head

The point where the RGC meet and form the beginning of the optic nerve is called optic nerve head (ONH). The ONH is composed of connective tissue, glial cells, RGC axons and blood vessels.
The connective tissue may mechanically support the ONH. Three zones have been distinguished: lamina cribrosa (LC), peripapillary sclera and scleral wall (Burgoyne et al., 2005).

Lamina cribrosa

In humans, RGC axons leave the eye and pass through the LC, a fenestrated, reticulated tissue that supports the optic nerve head, and travel to the superior colliculus or lateral geniculate nucleus in the thalamus of the brain from where the impulses are transferred to the visual cortex in the occipital lobe (Quigley et al., 1983) (Isenmann et al., 2003). The LC is composed of laminin, fibronectin, elastin, proteoglycans, tenascin and several types of interstitial collagen. The LC is lined by astrocytes that may be responsible for the generation and maintenance of the unique ECM in this region (Morrison et al., 1995a). Elevated hydrostatic pressure changes the shape of human lamina cribrosa cells (LCC) in culture, and cells increase the synthesis of collagen type I, III and IV (Luo et al., 1998).

The LCC from glaucomatous eyes show oxidative stress, impaired mitochondrial function and calcium homeostasis but it is not clear whether the oxidative stress is causative or a result of glaucoma (McElnea et al., 2011).

In healthy eyes, the pores of the lamina are rounded (Miller and Quigley, 1988). The human lamina has a lower density of connective tissue at the superior and inferior poles which makes the fibres passing through these areas more susceptible to damage from increased pressure (Radius and Gonzales, 1981) (Quigley et al., 1983).

Figure 4 Frontal view of human lamina cribrosa (Scanning electron micrograph).

Source: Quigley et al., 1983.

Unlike primates, the rat, commonly used in experimental models of glaucoma, has a less-developed collagenous LC. However, cross sections through the ONH show multilayered vertical laminar beams within the sclera. The lamina in rat is composed of collagen types I, III and IV, chondroitin-4 sulfate, chondroitin-6 sulfate and dermatan sulfate proteoglycans. The rat ONH is of bottleneck configuration, horizontally oval and tapering towards the retina (Morrison et al., 1995a).

In mice, a meshwork of astrocytes starts from the region where the nerve enters the scleral canal and extends to the point where myelination begins (Howell et al., 2007). The cells of ONH and astrocytes secrete neurotrophins (Lambert et al., 2001). Astrocytes are connected by closely apposed connexins forming tight junctions facilitating their functioning as a syncytium for calcium signalling (Newman, 2001) (Zahs et al., 2003). In the CNS, glia are known to transport ribosomes and possibly RNA to the axoplasm (Court et al., 2008).

The individual pores of the lamina in glaucomatous human eyes are elongated and decrease in size although the total area of pores increases (Tezel et al., 2004). The vertical layers of laminar sheets are rearranged

as a result of compression even during the initial stages of glaucoma. In humans and in some animal models of glaucoma, loss of RGC axons and the bowing of the connective tissue matrix of LC cause cupping of the ONH (Morrison et al., 2005).

In a genetic mouse model of raised IOP, the point of initial damage is the glial lamina corresponding to the LC in humans. In eyes with early glaucoma, axonal swellings occur in the laminar region, but not in the pre-laminar or nerve fibre layers (Howell et al., 2007).

In the mouse model, RGC damage occurs in a well-defined sequence of events. The axons in the optic nerve are the first to be affected followed by the accumulation of phosphorylated neurofilament and loss of axonal transport in the intraocular part of optic nerve before the actual death of RGC soma. In rat models of glaucoma with elevated IOP, the sequence of damage is similar (Soto et al., 2010). The pattern of RGC death in the DBA/2J mouse model and the various rat glaucoma models is sectorial, indicating focal damage of axons within the lamina (Soto et al., 2010) (Morrison et al., 1997) (Levkovitch-Verbin et al., 2002b).

In glaucoma models, where reactive gliosis occurs in response to raised IOP, the connexin arrangement is largely disrupted (Malone et al., 2007).

Mechanisms of RGC death

The precise mechanism of RGC damage in glaucoma is not known although there is evidence that the RGC undergo the apoptotic cascade (Quigley et al., 1995) (Kerrigan et al., 1997).

Raised IOP as the main cause of RGC death

When exposed to high IOP, RGC undergo specific cellular and extracellular changes, which are summarised below.

Blockade of axonal transport

In the retina, neurotrophins (NT) are retrogradely transported from optic nerve targets in the brain through optic nerve axons, in the form of

neurotrophin-receptor complexes (Ginty and Segal, 2002). Axonal transport slows down in the ONH region in healthy eyes, probably due to the peculiar anatomy of the ONH. In glaucomatous eyes, where the structures are remodelled, axonal transport is completely obstructed (Hollander et al., 1995). In experimental models, axonal transport slows down from as soon as one hour of elevated IOP. Transport blockade only affects a proportion of axons. IOP normalisation rapidly reverses the blockade (Quigley and Anderson, 1976). Due to lack of axonal transport, neurotrophic factors and receptors crucial for the survival of RGC may fail to reach their target (Quigley and Anderson, 1976). However, Müller glial cells are known to secrete NTs and might provide trophic support within the retina (Seki et al., 2005).

BDNF is also anterogradely transported from the RGC soma; lack of BDNF leads to the apoptosis of the target neurons in the brain (Caleo et al., 2000).

Immuno-labelling for BDNF and its receptor TrkB is increased in the ONH in a rat glaucoma model (Pease et al., 2000), probably due to blockade of retrograde transport. TrkB gene expression is also down-regulated in rats with raised IOP (Jia et al., 2004). However, another study on an experimental glaucoma model did not demonstrate a correlation of raised IOP and the levels of NT and their receptors in the retina (Guo et al., 2009).

Intravitreal injections of manganese chloride in a rat model of glaucoma results in the accumulation of manganese ions in the vitreous and ONH at six weeks after the induction of glaucoma. This accumulation could be due to blockade of axonal transport and reduction in the number of RGC. However, the presence of superoxide dismutase 2 in glaucomatous ONH to reduce the oxidative damage could also contribute to the elevated levels of Mn^{2+} (Chan et al., 2008).

Dendrite loss of RGC

In primates, the presence of raised IOP causes shrinkage of the dendritic tree of RGC, followed by a reduction in size of cell body and axons (Weber et al., 1998). In glaucomatous monkey eyes, the postsynaptic dendrites in the lateral geniculate nucleus are swollen, disrupted and fragmented and the dendritic field area is reduced (Gupta et al., 2007). In a rat glaucoma model, synaptic function is affected in the early stages of glaucoma (Fu et al., 2009).

Role of MMPs

Increased immunostaining for matrix metalloproteinases (MMP-1, 2, 3 and 9) and MT1-MMP (an integral membrane MMP) was observed in the ONH of human and rat eyes with raised IOP (Agapova et al., 2001, Yan et al., 2000, Guo et al., 2005). MMPs degrade ECM proteins like collagens, elastin, gelatin, proteoglycans and glycoproteins (Ohuchi et al., 1997, Matrisian, 1992) (Imper and Van Wart, 1998). Moreover, MMP-9 inhibition is protective against RGC death and retinal thinning in NMDA and optic nerve ligation models of RGC destruction in mice (Manabe et al., 2005, Chintala et al., 2002).

Reactivation of glia and ECM remodelling

The ganglion cell soma are ensheathed by thin processes of Müller glia, as far as the axon segment. The initial parts of these long axons are partially ensheathed by plump processes of astroglia and Müller glia. This area, called the axon hillock, has the highest density of sodium channels and is therefore important in the generation of action potential (Sekirnjak et al., 2008, Black et al., 1984). Electron dense node-like specialization is found beneath the axolemma in the areas where glial processes are in contact with axon segments. These glial arrangements may enhance conduction in the non-myelinated part of the optic nerve (Black et al., 1984, Waxman and Black, 1984). Mechanical stimulation of retinal astrocytes activates calcium waves that travel through both astrocytes and Müller glia (Newman, 2001). In glaucoma models, where reactive gliosis

occurs in response to raised IOP, the connexin arrangement is largely disrupted, resulting in the collapse of intercellular communication (Malone et al., 2007).

In glaucoma, the Müller glia in the retina become activated and over express GFAP and TNF alpha, the receptors for which are situated on RGC (Tezel et al., 2001). In a recent study of optic nerve transection, glial TNF alpha was shown to induce apoptosis of RGC (Lebrun-Julien et al., 2010). TNF alpha secreted by activated Müller glia might therefore contribute to RGC apoptosis in glaucomatous retina.

Elevated IOP may induce abnormal deposition of ECM materials such as interstitial collagens and basement membrane components (Morrison et al., 1990), especially within laminar pores of the optic nerve head that are usually occupied by axon bundles (Johnson et al., 1996). These changes in ECM macromolecules may reflect activation of astrocytes. Reactive astrocytes over-express endothelins (Prasanna et al., 2002), which may mediate the extensive tissue remodelling observed in glaucomatous ONH and LC (Hernandez, 2000) (Rao et al., 2007) through the over expression of MMPs (Chauhan, 2008) (He et al., 2007). Astrocyte cell bodies also form a “glial scar” in CNS diseases and injuries (Yang et al., 2004), a process which may be similar to the changes observed in glaucoma.

When reactive, mature astrocytes re-express molecules characteristic of immature astrocytes but not usually expressed in the adult stage. Reactive astrocytes at the ONH synthesize Nitric oxide synthase-2 (NOS-2) (Neufeld et al., 1999, Neufeld et al., 1997). An increase in nitric oxide production in the retina is seen in rats with elevated IOP (Siu et al., 2002). Although NOS-2 inhibitors reduce RGC death in a rat model of glaucoma (Neufeld et al., 2002), this effect is not observed in a NOS knockout mouse glaucoma model and other authors have not replicated these findings.

Glutamate toxicity

Excessive secretion of excitatory neurotransmitters including glutamate damages neurons and glia. All major neuron types in the retina are glutamatergic. In the vitreous of glaucomatous human and monkey eyes glutamate levels had been reported to be elevated while other amino acid levels were unchanged (Dreyer et al., 1996).

However, the above-mentioned paper has been discredited and further research on primates (Carter-Dawson et al., 2002) as well as rats (Levkovitch-Verbin et al., 2002a) have subsequently reported unchanged levels of glutamate in glaucoma.

Vascular hypothesis of glaucoma

High IOP causes reduction in blood flow in choroid, optic nerve and retina (Geijer and Bill, 1979) (Gasser, 1989) and impairs anaerobic glycolysis in the retina (Sperber and Bill, 1985). However, high IOP does not always cause glaucomatous optic neuropathy, for example in normal tension glaucoma (NTG). A reduction in choroidal blood flow is more significant in NTG than in glaucomas with ocular hypertension (Duijm et al., 1997). Glaucomatous eyes may also have slower blood flow in the retinal artery than eyes with ocular hypertension only (Nicolela et al., 1996).

A reduction in blood flow can cause gliosis and RGC death in the retina (Osborne et al., 1991) (Katai and Yoshimura, 1999, Cioffi and Sullivan, 1999). An animal model has been reported showing that restricted blood flow to the optic nerve can cause loss of axons and optic nerve head changes with some features of characteristic of glaucoma (Cioffi and Sullivan, 1999).

Ocular vasospasm impairs visual function in patients with vasospastic syndrome (Gasser and Flammer, 1987), and treatment with calcium antagonists may bring about a reversal of visual field defects in selected vasospastic patients (Gasser et al., 1988) although this has not been confirmed by any prospective randomised clinical trials.

These data suggest that a reduction in ocular blood flow could play a role in glaucoma along with other risk factors, although this has been difficult to confirm clinically.

RGC death via a mitochondria-mediated apoptotic pathway

There is some evidence about the role of mitochondria in RGC death *in-vitro* (Osborne, 2008). The non-myelinated part of the RGC is particularly rich in mitochondria (Bristow et al., 2002) and is exposed to light entering the globe. Deprivation of serum, concentration of anti-oxidants etc may make the RGC more susceptible to damage from light (Osborne et al., 2006) (Mandel et al., 2005). The mitochondrial respiratory chain is associated with light-induced damage of RGC and subsequent down-regulation of characteristic proteins like tubulins and neurofilaments (Osborne et al., 2008).Therefore, in diseases like glaucoma, the progressive apoptosis of RGC might be partially due to light induced damage to already compromised RGC.

Autoimmunity in glaucoma

Elevated levels of autoantibodies in the serum and aqueous humour of glaucoma patients raises the possibility of autoimmunity as a possible contributive factor in glaucoma. Antibodies against glycosaminoglycans, HSPs, gamma-enolase and glutathione-S-transferase in retina or ONH have been detected in the serum of glaucoma patients (Tezel et al., 1998, Tezel et al., 1999, Tezel et al., 2000) (Maruyama et al., 2000, Yang et al., 2001). Glaucoma patients also may have a greater incidence of autoimmune diseases (Wax, 2000). Antibodies against HSPs (HSP 70 and αB-crystallin) and vimentin were found in the aqueous humour of NTG patients (Joachim et al., 2007).

Molecular Genetics of glaucoma

Mutations of the myocilin gene (MYOC) have been investigated as possible causative agents in primary open angle glaucoma (Stone et al., 1997). More than 70 mutations of the gene have been detected (Gong et al., 2004) in which the mutants misfold to form aggregates (Yam, 2006)

and suppress the secretion of endogenous myocilin (Jacobson et al., 2001), leading to elevated IOP. Atrial natriuretic peptide (ANP) receptor-A gene maps to chromosome 1q21-q22 (Lowe et al., 1990). ANP levels are elevated in rabbit models of glaucoma; this elevation may be secondary to a decrease in their binding sites (Fernandez-Durango et al., 1990, Fernandez-Durango et al., 1991). Further, intravenous administration of ANP considerably reduces IOP (Diestelhorst and Krieglstein, 1989).

Mutation of the gene CYP1B, a member of the P450 cytochrome super family, was described as a possible causative of primary congenital glaucoma (Stoilov et al., 1997). Normal aqueous humour formation and maintenance of lenticular transparency may be affected by the modulation of metabolic pumps due to cytochrome P-450 dependent metabolism of arachidonic acid (Schwartzman et al., 1987).

DNA sequence variants in lysyl oxidase−like 1 protein (LOXL1) gene are associated with pseudo exfoliative glaucoma (Fan et al., 2008). LOXL1 is specifically involved in elastogenesis and elastin homoeostasis (Liu et al., 2004).

Animal models of glaucoma

The main risk factor associated with glaucoma is elevated IOP. Animal models therefore mainly aim at raising IOP, usually by blocking the aqueous humour outflow through various mechanisms.

Argon laser scarring model

The first model was described by Gaasterland and Kupfer in 1974 on monkey eyes by scarring the TM with argon laser, thereby increasing the IOP and decreasing aqueous humour outflow (Gaasterland and Kupfer, 1974). Quigley refined this method by developing consistent IOP elevation with minimal damage to the ciliary body with optimal delivery of laser energy so as to reduce side effects (Quigley et al., 1983).

Latex microspheres

Latex micro spheres can be used to block aqueous humour flow through the TM in primates as a cost effective model of inducing glaucoma (Weber and Zelenak, 2001).

Ghost red blood cells

A major disadvantage of blocking aqueous humour with foreign materials or scarring is that the inflammatory responses may cause changes that could be wrongly attributed to elevated IOP. Quigley and Addicks introduced autologous ghost red blood cells into the AC to raise IOP; this method did not create inflammation, but the retina and ONH could not be visualized (Quigley and Addicks, 1980).

In order to reduce costs and ethical concerns, monkeys are often replaced by rodents, especially rats, in glaucoma studies.

Translimbal laser photocoagulation

Translimbal laser photocoagulation successfully raises IOP in rats (Levkovitch-Verbin et al., 2002b). Ueda et al., injected India ink into the anterior chamber of rats to block aqeous outflow. The deposited carbon visualises the TM, facilitating laser photocoagulation without the aid of a gonio-lens (Ueda et al., 1998). Unfortunately this model is often associated with significant corneal oedema.

Episcleral vein cauterisation

Episcleral vein cauterisation (Shareef et al., 1995) provides another way of blocking aqueous humour outflow. With this model there have been concerns about the ischaemic effects on the rest of the eye.

Hypertonic saline injection model

Injection of hypertonic saline into the episcleral veins of rats induces scarring of the TM and blocks aqueous humour outflow (Morrison et al., 1997). This model produces damage to RGC and nerve fibre layer without many side effects, though repeated injections are needed in some

animals. The degree of damage can be evaluated by quantifying degenerating axons in the optic nerve 2mm away from the eye or by grading optic nerve damage.

Ligation of episcleral veins

Ligation of the episcleral veins using nylon sutures raises the IOP, but not consistently (Yu et al., 2006b).

Polystyrene bead injection model

Recently the injection of polystyrene microbeads into the AC of rats and mice has been described as a method of raising IOP. Axon damage in this model is only 30% despite repeated injections (Sappington et al., 2009a). One problem might be the lack of targeting of beads to the TM.

Magnetic microbeads injection model

The main disadvantage of polystyrene bead injection is the lack of control over the position of the beads in the AC. Soto et al targeted microbeads to the iridocorneal angle by using magnetic microbeads. Magnetic beads are injected into the AC and then pulled into the iridocorneal angle using a strong hand held neodymium magnet.

The elevation in IOP in this model correlates with the reduction in the number of RGC. The major advantage of this model is the relative ease of the surgical procedure and high success rate in raising the IOP. However, repeated injections may be required to maintain high IOP.

Intravitreal injection of NMDA

N-methyl-D-aspartate (NMDA), when injected into the vitreous in front of the retina, causes RGC death and visual dysfunction by triggering calcium ion influx and apoptosis (Lam et al., 1999). Therefore NMDA injections are used as laboratory models of RGC damage.

NMDA is known to affect the activity of Müller glia, the principal glia in the retina (Puro et al., 1996). Therefore, the effects of intravitreal injection of

NMDA might not be restricted to ganglion cells. The use of NMDA as a glaucoma model has to be used with these limitations in mind.

Genetic model of glaucoma

A genetic mouse model of glaucoma (DBA/2J) with a recessive mutation in the genes Gpnmb and Tyrp1 may be similar to the human version of disease in many aspects (Chang et al., 1999). Affected mice exhibit raised IOP after reaching adulthood and gradually lose a majority of RGC. Although a majority of the mice with the mutation develop glaucoma, few of the animals remain normal. In addition, age of onset of the disease is unpredictable.

The model has been used to study various aspects of glaucoma, however, caution must be applied before extrapolating the findings to human forms of glaucoma, the causes of which are not yet clear.

Treatments for glaucoma

Treatment for glaucoma aims at reducing IOP to slow down the progression of RGC and axonal damage, even in the case of normal tension glaucoma. Medications are available to reduce the production of aqueous humour in the eye, for example beta-blockers, alpha-agonists and carbonic anhydrase inhibitors.

However, in many cases, RGC death continues at a lower rate leading to blindness in some patients, particularly if severe loss has occurred. Therefore neuroprotection strategies along with IOP control might provide better results.

Neuroprotection

The expression of heat shock proteins may be protective to RGC in glaucoma. HSP induced by Zinc, gerarylgeralylacetone and hyperthermia reduce loss of RGC in rat models of glaucoma (Ishii et al., 2003).

RGC express NT- NGF, BDNF, NT3, NT4 and CNTF and receptors- TrkA, TrkB, p75 receptor (von Bartheld and Butowt, 2000, Endres et al., 2000,

Harada et al., 2005) (Agarwal et al., 2007). In addition, RGC also receive BDNF from the brain through retrograde transport through the optic nerve. Elevation of IOP induces blockade of retrograde transport of BDNF from the brain to the retina (Quigley et al., 2000). As NT may have a number of different effects on axons and cell bodies, the NT transported from the brain are the topic of ongoing research (Johnson et al., 2009a). In xenopus, the dendritic arborization of RGC depends on the availability of BDNF (Lom and Cohen-Cory, 1999).

P75 mRNA levels in the retina increase with increasing IOP in a rat glaucoma model; however the protein expression does not alter (Guo et al., 2009). There is contradictory evidence about the expression of p75 and its role in RGC apoptosis in different disease forms (Hu et al., 1999) (Coassin et al., 2008). Lebrun-Julien et al., have described the expression of p75 receptor in Müller glia which mediates the secretion of TNF alpha and subsequent apoptosis of RGC in an optic nerve transection model. Whether a similar mechanism is present in glaucoma needs to be investigated (Lebrun-Julien et al., 2010).

Administration of NT significantly delays RGC death. Brain derived neurotrophic factor (BDNF) and ciliary neurotrophic factors (CNTF) provide neuroprotection to RGC in experimental glaucoma (Martin et al., 2003) (Ko et al., 2001, Ji et al., 2004).

Further upregulation of the receptor TrkB enhances BDNF-induced RGC survival by many fold (Cheng et al., 2002). CNTF injection encourages regeneration of RGC axons *in vivo* (Muller et al., 2009).

Pharmaceutical approaches to assist optic nerve regeneration or prevent degeneration are mainly based on prevention of apoptosis of RGC and promotion of axonal growth by disintegration of astroglial scars. A study which used astrotoxin along with lithium supplements demonstrated that removal of scar along with apoptosis inhibitors may enhance regeneration of RGC axons (Cho and Chen, 2008).

Table 1 Animal models of glaucoma.

Glaucoma model	First described	Animals tested	Caveats
Argon laser scarring of TM	Gaasterland and Kupfer, 1974	Primates	Inconsistent IOP rise and inflammation
Ghost red blood cells	Quigley and Addicks; 1980	Primates	Retina or ONH could not be viewed.
Episcleral vein cauterisation	Shareef et al., 1995	Rats	Inflammation and inconsistent IOP rise.
Hypertonic saline injection into episcleral veins	Morrison et al., 1997	Rats	Technically very difficult and unpredictable IOP rise
India ink injection into the anterior chamber followed by laser photocoagulation	Ueda et al., 1998	Rats	Large-scale macrophage migration to the site, which makes it uncomparable to human form of the disease.
Genetic model of glaucoma	Chang et al., 1999	Mice	Unpredictable development of glaucoma.
NMDAinjection into the vitreous	Lam et al., 1999		Complete death of RGC and causative factors never

			comparable to human disease forms
Latex microspheres injection into the anterior chamber	Weber and Zelenak, 2001	Primates	
Episcleral vein ligation	Yu et al., 2006	Rats	Very slow and inconsistent IOP rise
Polystyrene microbeads injection into anterior chamber	Sappington et al., 2009	Rats and mice	Very low IOP rise
Magnetic microbeads injection into the anterior chamber and use of a hand held magnet to direct the beads into the limbus	Soto et al., 2011	Rats	Fast rise in IOP following bead injection.
Topical administration of steroids	Sawaguchi et al., 2008	Rats	IOP rise after two weeks of dexamethasone treatment

In transgenic mice, RGC apoptosis is considerably reduced by over expression of BCL-2, an anti-apoptotic protein (Martinou et al., 1994). Sigma-1 receptor agonists may protect RGC from glutamate-induced apoptosis. The receptor ligands down-regulate Bax and caspase-3 activity and interfere with the calcium influx to prevent apoptotic cell death (Tchedre and Yorio, 2008).

Phenytoin, a sodium channel blocker was discovered as protective against RGC as well as axonal loss in rat models of glaucoma (Hains and Waxman, 2005).

Calcium channel blockers like flunarizine and verapamil were found to lower IOP in glaucomatous eyes of rabbits (Campana et al., 2002), monkeys (Siegner et al., 2000, Wang et al., 2008) and humans (Abelson et al., 1988, Goyal et al., 1989). Flunarizine reduces IOP by increasing aqueous humour outflow (Wang et al., 2008) and prevent calcium overload by blocking entry of excess calcium into the cells thereby offering neuroprotection (Todd and Benfield, 1989).

Low doses of N-β-Alanyl-5-S-glutathionyl-3,4-dihydroxyphenylalanine(5-S-GAD), derived from flesh fly, offers neuro-protection to RGC against apoptosis induced by NMDA or crush injury. 5-S-GAD increases the expression of cell survivor molecules like phospho-Akt and Bcl-2 but does not affect microglial activation (Koriyama et al., 2008).

Neurons, particularly those of the central nervous system are considered to have little regenerative abilities. However, recent studies have shown that axotomised RGC regenerate into a peripheral nerve graft and form functional synapses in the brain (Carter et al., 1989, Keirstead et al., 1989). This demonstrates that RGC axons are capable of long distance regeneration and formation of functional reconnections under suitable conditions.

Over expression of BCl-2 in immature astrocytes facilitates regeneration and re-innervation of the optic nerve in very young mice (Cho et al., 2005),

which suggests that postnatal down-regulation of this protein might be one of the factors preventing regeneration.

Cellular rescue strategies

A variety of cells of glial, neuronal and mesenchymal lineages secrete neurotrophic molecules *in vitro*. Many of these have been found to be neuroprotective *in vivo* as well. Specifically studied in glaucoma models were Müller glial cell lines, oligodendrocyte precursor cells (OPC) and mesenchymal stem cells (MSC).

Müller cells

The ability to regenerate damaged retinal neurons is limited to lower vertebrates like fish and amphibians. In zebra fish, after injury to the retina, Müller cells undergo dedifferentiation to progenitor cells and then give rise to retinal neurons (Bernardos et al., 2007) (Thummel et al., 2008).

In the mammalian retina, Müller glia and the different neurons are derived from a single progenitor cell (Turner and Cepko, 1987). However, the Müller glia in adult mammals seem to have a limited potential to dedifferentiate to stem cells and re-differentiate to neurons following injury (Ooto et al., 2004) (Kohno et al., 2006). However mammalian Müller glia forms neurospheres in culture, which indicates that these cells have stem cell properties. When transplanted into the eye, they can also be induced to differentiate towards a neuronal lineage (Das et al., 2006).

Spontaneously immortalized Müller-glial cells of the retina were first described by Limb et al., 2002 and further characterized as stem cells capable of migration and differentiation under appropriate conditions (Lawrence et al., 2007, Limb et al., 2002). Human Müller glial cell lines injected into the sub-retinal space of glaucomatous rat eyes integrate into the different retinal layers and express the corresponding markers, indicating their differentiation into various neurons like photoreceptors, amacrine and RGC *in vivo* (Bull et al., 2008). Müller cells also secrete a variety of NT that may encourage RGC survival. Since these cells lines

were used as xeno-transplants, their survival rate was limited. The functional state of the cells was not determined (Bull et al., 2008).

Human trials on retinal progenitor cells are difficult to set up, due to the lack of sufficient numbers of autologous cells. Human allografts require local or systemic immunosuppression.

Oligodendrocyte precursor cells (OPC)

Oligodendrocyte precursors are multipotent stem cells in the CNS that can give rise to neurons, astrocytes and oligodendrocytes (Kondo and Raff, 2000). OPC injected into glaucomatous retina with inflammatory responses are protective to the RGC. OPC differentiate into glial and neuronal lineages and partially myelinate the RGC. The protective role of OPCs might be due to NT secretion (Bull et al., 2008) (Johnson et al., 2008a).

Mesenchymal stem cells

MSCs are pluripotent stem cells able to differentiate into neurons and secrete NT. MSC can be cultured from the patient's own bone marrow and therefore avoid the risk of allograft immune-rejection (Chen et al., 2005) (Inoue et al., 2007) (Dezawa et al., 2004) (Crigler et al., 2006).

MSCs support RGC survival in a glaucoma model, mainly by the secretion of a combination of NT (Johnson et al., 2010) (Yu et al., 2006a).

Even though many studies have demonstrated the integration and partial differentiation of progenitor cells into the RGC layer, none could demonstrate the complete differentiation of these cells into neurons or elongated axons that would finally establish functional synapses in the brain.

A variety of stem cells including neural progenitor cells from the brain and embryonic stem cells are able to integrate into the different layers of retina when injected into the eye (Mizumoto et al., 2003) (Guo et al., 2003) (Carr et al., 2009). However, their functional impact remains to be elucidated.

Olfactory ensheathing glia

The olfactory ensheathing glia are a special population of glia in the olfactory mucosa and bulb. These cells support neuron regeneration in the adult olfactory system (Doucette et al., 1983) (Field et al., 2003).

Cultured olfactory glia injected into the vitreous settle near the RGC layer. Since these cells secrete NT and promote neuronal regeneration *in vitro* (Woodhall et al., 2001), the finding could be of relevance to the treatment of glaucoma (Li et al., 2008). In this first publication of OEC transplantation into the eye, OEC were injected trans-sclerally and transretinally, from behind the eyeball. Due to the high risk of complications from this route, this approach cannot easily be used in human patients.

The role of OEC in the olfactory mucosa

Axotomy of the olfactory neurons results in the death of the neurons which are replaced by new neurons formed from stem cells in the epithelium. Injured olfactory neurons do not regenerate their axons, unlike axotomised neurons in the peripheral nervous system (Ide, 1996). The axons of the new neurons extend from the nasal epithelium to the olfactory bulb, where they form synapses with their glomerular target neurons (Graziadei and Monti Graziadei, 1980). The axons are brought together as fascicles by the cytoplasmic processes of the ensheathing glia that is situated in the lamina underneath the epithelium. The glia in the olfactory mucosa and bulb provide a favourable environment for the growth of new axons (Doucette et al., 1983).

Doucette called the olfactory glia “olfactory Schwann cells” as they ensheath the axons of the olfactory neurons. No other myelinating cells are present in the olfactory system, and the olfactory glia resemble Schwann cells in their properties. However, he observed astrocytes in the same tissue, which differ from ensheathing glia by the presence of bundles of intermediate filaments as well as a less electron dense cytoplasm. Olfactory glia differ from oligodendrocytes and microglia in that they contain intermediate filaments in the cytoplasm (Doucette, 1984).

It is hypothesised that one function of OEC in the adult mucosa is to maintain open channels through which the regenerating axons can reach their targets in the bulb (Li et al., 2005). OEC also phagocytose axonal debris in the nasal mucosa and in the olfactory bulb (Chuah et al., 1995) (Wewetzer et al., 2005).

Anatomy of Olfactory Mucosa

In higher vertebrates such as mammals the olfactory nerve running from the olfactory mucosa to the bulb is the only cranial nerve capable of regeneration and functional restoration.

The olfactory epithelium (OE) is a pseudostratified epithelium consisting of supporting / sustentacular cells, olfactory receptor neurons (ORNs) and basal progenitor cells. Immediately below the OE lies the lamina propria, which contains axons of ORNs, OEC, connective tissue, blood vessels and glands.

ORNs are bipolar cells, the cell bodies of which lie below the supporting cells and express olfactory marker protein when mature. The supporting cells maintain the ORNs by regulating the ionic environment and phagocytosing degenerating epithelial cells (Farbman and Margolis, 1980, Suzuki et al., 1996). Beneath the ORNs lies the basal progenitor cell layer constituted of a heterogeneous population of globose and horizontal basal cells (Murdoch and Roskams, 2007). Globose cells divide continuously and can differentiate into neurons or supporting cells (Chen et al., 2004, Caggiano et al., 1994). Horizontal cells are more quiescent and multi-potent and divide only when extensive repopulation is required (Carter et al., 2004, Leung et al., 2007).

The non-myelinated axons of the ORNs are ensheathed by the cytoplasmic processes of OEC which lead the axons from the mucosa through the cribriform plate of the skull to form the *glia limitans* and the olfactory nerve layer around the bulb (Doucette et al., 1983, Doucette, 1984) (Doucette, 1991, Raisman, 1985). From this point the axons are

independent of the OEC and enter the glomeruli to form synapses. OEC secrete a range of molecules that promote nerve regeneration. Among these are NT such as NGF, BDNF, GDNF, CNTF, OP-1, artemin, neurotrophic receptors like p75 and TrkC and cell adhesion molecules like laminin, L1, etc (Woodhall et al., 2001) (Lipson et al., 2003) (Kafitz and Greer, 1997). Direct membrane contact of OEC with regenerating axons may be equally required for effective regeneration (Chung et al., 2004).

OEC express Lyz proteins, which are major immune regulators of the OM (Getchell and Getchell, 1991). OEC highly express interleukin 6(IL-6) responsive transcription factor and respond to macrophage infiltration by up-regulating IL-6 receptors which could eventually lead to the cascade of OEC preparing an environment suitable for axonal regeneration (Vincent et al., 2005, Nan et al., 2001). OEC express vascular endothelial growth factor and CTGF, the proteins that assist in ECM remodelling and angiogenesis (Au and Roskams, 2003). OEC promote angiogenesis (Lopez-Vales et al., 2004) and deposits laminin after transplantation into spinal cord (Ramer et al., 2004).

Cell types in the olfactory mucosa/bulb cultures

Along with OEC, cultures contain cells called Olfactory nerve fibroblasts (ONF), which express fibronectin (Franceschini and Barnett, 1996). Li et al., 1997 reported co-expression of p75NTR and fibronectin in the cultures from OM. However, after 10- 14 days in culture, cells expressed only one of the markers. ONF are considered a contamination by many of the researchers who separate the two groups by various immunology techniques (Ramer et al., 2004, Au and Roskams, 2003). Among the different populations, P75-positive OEC were shown to be more effective in promoting neurite outgrowth than any other cell type from the culture or a mixture of cell types (mainly p75NTR negative OEC and ONFs), irrespective of whether their source was the mucosa or the bulb (Kumar et al., 2005). This is in contradiction to the findings of Li et al., 1997, that ONFs are essential for the reparative functions of OEC.

Markers for Olfactory ensheathing cells

In culture, the marker protein for OEC is mainly the P75 receptor and that for ONFs is fibronectin (Moreno-Flores et al., 2003). Thy-1 is also regarded as a marker of ONF (Kueh et al., 2011). Depending on the culture conditions and the number of days in culture, some OEC express S100 (Schwann cell marker protein), GFAP (Glial fibrillary acidic protein), or O4 (Oligodendrocyte marker protein) (Pixley, 1992) (Pastrana et al., 2006), (Moreno-Flores et al., 2003). Positivity to O4 is due to axonal fragments sticking to OEC rather than expression of O4 on the membrane of OEC.

Keuh et al., described a population of highly proliferative cells isolated from adult rat mucosa that maintained co-expression of OEC and ONF markers for over two weeks in culture (Kueh et al., 2011).

Sources of OEC for transplants

Initially, OEC isolated from the olfactory bulb were used in animal models of transplantation. However, to avoid the complications of craniotomy for future cell transplants in humans, harvest of OEC from more accessible OM is more relevant.

OEC cultures from the adult rat bulb possess a higher proportion of p75NTR positive cells (about 50%) than the mucosal cultures (about 10-15%) (Li et al., 2008) (Roux and Barker, 2002) (Kueh et al., 2011). The p75 positive OEC start expressing fibronectin and lose p75 reactivity after about two weeks in culture (Kueh et al., 2011).

OEC have been widely studied for their potential therapeutic properties to assist in the regeneration of peripheral and central nervous systems.

Figure 5 A diagrammatic representation of the distribution of OEC, ORN and progenitor cells in the adult olfactory mucosa.

Basal lamina seperates the olfactory epithelium from the underlying lamina propria. Mature olfactory receptor neurons (ORN) and immature olfactory neurons lie in the epithelium along with globose and horizontal basal cells situated near the basal lamina which are the progenitors of the epithelium. Olfactory ensheathing cells (OEC) lie at the lamina propria ensheathing the axons of ORN. The diagram is adapted from Murdoch and Roskams, 2007.

OEC transplantation was reported to have contributed to the regeneration of axons with minimal branching and restoration of functional connections after spinal cord lesions (Li et al., 1997, Verdu et al., 2001) (Lu et al., 2002, Guntinas-Lichius et al., 2002). In successful axonal regeneration after transplantation, OEC exhibit spindle shape, which may provide scaffold facilitating the regeneration of axons (Li et al., 1998).

Ensheathing cells and fibroblasts reportedly form “conduits”, which allow the passage of regenerating axons through the otherwise hostile environment of a glial scar laden with molecules inhibitory to axon growth. The OEC cytoplasm ensheathes the regenerating axons, and the olfactory fibroblasts form a perineurium-like covering around the OEC Figure 7 (Li et al., 1998). In another study on OEC from the mucosa, nerve function was restored after OEC transplant without noticeable axon regeneration; the mechanism behind the functional restoration was unclear (Yamamoto et al., 2009).

OEC-filled conduits transplanted between transsected facial motor neurons encourage axonal sprouting, but no functional improvement (Guntinas-Lichius et al., 2001). However, OEC transplantation along with microsurgical repair results in regeneration of sciatic nerve axons, myelin formation and functional recovery. New nodes of Ranvier form and conduction velocity is enhanced due to OEC ensheathment of the regenerated axons (Sasaki et al., 2006) (Radtke et al., 2009).
In the above studies, OEC migrated towards the axonal target when transplanted into the CNS. However, OEC transplanted into CNS sites that migrated in the direction opposite to that of axon targets were not able to support regeneration (Gudino-Cabrera et al., 2000).
Adult RGC cultured on OEC mono-layers have shown that OEC can promote RGC neurite extension up to 360μm while the controls form neurites up to 150μm long (Moreno-Flores et al., 2003).

Bulbar OEC versus Mucosal OEC

There is significant evidence to suggest that OEC derived from olfactory bulb (OB OEC) and mucosa (OM OEC) have different effects when transplanted to sites of neuronal injury. OM OEC are more migratory and reduce formation of cavities at lesion sites and increase angiogenesis (Richter et al., 2005) (Gorrie et al., 2010). OB OEC are associated with actual axonal regeneration and functional improvement (Li et al., 1998, Guerout et al., 2011b) (Guerout et al., 2011a) with some exceptions of no regeneration (Riddell et al., 2004) or little functional recovery (Takami et al., 2002). OM OEC failed to induce axonal (Lu et al., 2002) regeneration in several *in-vivo* studies (Yamamoto et al., 2009) (Guerout et al., 2011b). However, some studies were able to demonstrate successful axonal regeneration and functional recovery (Lu et al., 2002). OM OEC induce side effects like autotomy (Richter et al., 2005) and aberrant muscle movements (Paviot et al., 2011). A combination of bulbar and mucosal OEC in transplant may induce maximum axonal regeneration and functional recovery compared to any one the groups alone (Guerout et al., 2011b).

OEC, Schwann cells and astrocytes

OEC have been compared to glial cells like Schwann cells and astrocytes. OEC are similar to Schwann cells in terms of function, antigen expression, cell-cell communication, ability to remyelinate spinal cord axons, etc (Doucette, 1990) (Barnett et al., 1993, Barnett et al., 2001) (Franklin et al., 1996), but differ in their interaction with astrocytes.

OEC mingle well with astrocytes while Schwann cells do not integrate into the astrocytic environment, making OEC better candidates for neuroregeneration in the CNS (Lakatos et al., 2000, Taniuchi et al., 1988). OEC reduce the reactive gliosis by astrocytes whereas Schwann cells do not have such an effect (Lakatos et al., 2003, Barnett et al., 1993, Barnett et al., 2001), but both OEC and Schwann cells induce proliferation of astrocytes in culture (O'Toole et al., 2007).

P75 receptor expression is upregulated after axotomy in both Schwann cells of peripheral nerves (Taniuchi et al., 1988) and OEC (Gong et al., 1994).

P75 receptor expression is indispensable for migration (Bentley and Lee, 2000) and remyelination by Schwann cells (Tomita et al., 2007), but the role of the P75 receptor in OEC is not yet established.

Mechanisms of OEC mediated neuro-regeneration

Role of calcium ions

External calcium ions play a major role in regulating axonal growth and path finding by controlling calcium in growth cones (Gomez and Spitzer, 1999). OEC have non-voltage gated calcium channels (Davies et al., 2004). Calcium ions released by OEC affect the regeneration of RGC *in vitro.* Pharmacological blockage of calcium channels on the OEC has detrimental effects on RGC neurite elongation (Hayat et al., 2003a, Hayat et al., 2003b).

P75 neurotrophin receptor expression of OEC

P75NTR is a low affinity neurotrophin receptor that was the first described receptor for NT and binds to all the known NT with an affinity lesser than that of Tyrosine kinase receptors (Trk) (Roux and Barker, 2002). The P75NTR is part of numerous pathways and acts in partnership with various co-receptors effecting survival, regeneration, migration, growth inhibition, degeneration and apoptosis, depending on the molecular clues from the surrounding cells/tissues (Anton et al., 1994, Lebrun-Julien et al., 2009) (Lebrun-Julien et al., 2009) (Singh et al., 2008) (Naska et al., 2010) (Cragnolini and Friedman, 2008). Generally, the function of the p75NTR is attributed to the specific ligand(s) binding to the receptor and subsequent cleavage, internalisation and transportation of intracellular/ extracellular domains (Kanning et al., 2003) (Frade, 2005). Because of the complexity of the pathways involved, relatively little knowledge is available on the details of the mechanisms involved (Cragnolini and Friedman, 2008).

P75NTR expression of OEC is down regulated when OEC are in contact with axons. The p75NTR is strongly expressed by embryonic cells, but down regulated post-natally. However, when OEC are isolated from the mucosa and placed in culture, the cells that initially express negligible amount of p75NTR but up-regulate the receptor after several days in culture (Wewetzer et al., 2005) (Kueh et al., 2011). This up regulation may occur due to the phagocytic removal of axonal fragments attached to the surface of OEC (Wewetzer et al., 2005).

Although the exact function of the p75NTR on OEC is not understood, the expression of p75NTR correlates with their neuro-regenerative properties. A pure population of p75NTR positive OEC enhances RGC growth *in vitro* significantly more than p75NTR negative OEC (Kumar et al., 2005). This effect is disputed by Li et al, who report that p75NTR positive OEC along with the p75NTR negative fibroblasts in equal proportions facilitate maximum axonal regeneration (Li et al., 2003) (Li et al., 1998).

P75NTR expression by OEC is reduced after several passages in culture; at the same time cells attain a flattened, fibroblast-like morphology.

Phagocytic properties of OEC

Olfactory neurons exposed to the external environment may transmit infections to the brain via the olfactory nerve (Mori et al., 2005) (Harberts et al., 2011). OEC can endocytose bacteria *in vitro* (Leung et al., 2008). OECs express Lyz protein and mRNA, major immune regulators of the OM (Getchell and Getchell, 1991). *In vitro*, OEC phagocytose axonal debris resulting from dissociation of the tissue for cell culture (Wewetzer et al., 2005). Immunoreactivity of OEC for the marker O4 is in fact due to axonal fragments adhering to OEC. O4 reactivity disappears as the fragments are phagocytosed by OEC (Wewetzer et al., 2005). After injury of olfactory neurons, OEC in the olfactory mucosa form a barrier to microbes and phagocytose the debris. Damaged axon fragments are found inside OEC in injured olfactory bulb (Li et al., 2005).

Morphology

The morphology of OEC depends on culture conditions. *In vitro*, OEC are highly dynamic and switch between different shapes ranging from flat, spindle shaped to stellate or triangular multipolar or filamentous cells (Doucette, 1995, Vincent et al., 2003) (Au and Roskams, 2003) (van den Pol and Santarelli, 2003). Morphology is affected by the presence or absence of serum. Serum free culture conditions switch OEC towards a more fusiform morphology. This correlates with the fact that in serum free media OEC are more migratory, fusiform morphology might reflect migration of OEC. Spindle shaped OEC may migrate faster than the other forms *in vitro,* indicating that these cells can change their forms according to the requirements of their micro-environment (Huang et al., 2008).

Figure 6 A diagrammatic representation of olfactory system.

The diagram on the right is a representation of a sagittal section through ahuman head showing the relative positions of olfactory mucosa and bulb. The picture on the left is a magnification of the highlighted area. This drawing illustrates the arrangement of different cell types of the olfactory system. Olfactory receptor neurons lie in the olfactory epithelium. The axons pass through the pores in the cribriform plate of the skull. The axons are lined by the olfactory ensheathing glia, which occupy the region below the epithelium, until they enter the bulb, where they make synapses with their target neurons (Thuret et al., 2006).

Figure 7 The relative positions of olfactory ensheathing glia and olfactory fibroblasts that facilitate the regeneration of axons across a lesion.

The figure is a diagrammatic representation of the role of olfactory ensheathing glia (red) and fibroblasts (green) in axonal (black) regeneration. In figure A, after the injection of ensheathing cells and fibroblasts into an area of lesion (grey), the ensheathing glia aligns around the sprouting axonal tip and leads it through the lesion area. In successful regeneration of axons across the lesion, as represented by figure b, the cytoplasm of ensheathing glia forms a tube around the regenerated axon around which, the fibroblasts form a perineurial layer. The blue cells represent the oligodendrocytes that normally myelinate the axons on either side of the lesion. The diagram is taken from Li et al., 1998.

Electroretinography

Electrical potentials generated by the various cell types of the retina in response to light stimuli of different intensities can be measured using electrodes placed on the cornea, in the vitreous or in the retina. The major components of the electroretinogram were first described by the Nobel laureate Ragnar Granit (Granit, 1933).

Electroretinography is a useful tool to study the functional status of retinal cells. ERG recordings from the cornea are non-invasive and facilitate repeated measurements from the same animal at different stages of an experiment without having to sacrifice the animal.

The origin of the different components of the ERG are attributed to different regions/cell types of the retina, based on their anatomy as well as by blocking the activities of the cells. Pharmacological agents are used to selectively deplete the activity of certain cell types to study their contributions to the ERG. At low intensities of stimulation, potentials from RGC can be measured, while stronger intensities measure the photoreceptor, bipolar cell, Müller glia and interneuron activities. The radial orientation of cells in the retina creates current flow in one direction resulting in a massive field potential, which is easier to record. The origin of the potentials varies between different species.

In our experiments, the following components of the ERG were particularly relevant

A wave

The fast, negative potential that appears in response to a high intensity light stimulus until about 25ms is termed “A wave”. In dark-adapted conditions, the A wave mainly represents the activity of rod photoreceptors.

B wave

Granit attributed the b wave to the radial cells internal to the outer nuclear layer and photoreceptors. The exact cellular origins of the b wave are disputed. The two radial cell types in the inner layers of the retina are the bipolar neurons and Müller cells. Two theories for the origin of b wave are termed the “Müller cell theory” and the “bipolar theory”.

A light stimulus causes an increase in the extracellular potassium in the retina. These potassium ions depolarize the membrane of Müller glia and the ions flow to the vitreous via Müller cells, generating a positive b wave (Karwoski et al., 1989) (Newman et al., 1984) (Wen and Oakley, 1990). Current source density analyses revealed that the current that gives rise the b wave extends from outer plexiform layer to the vitreal surface. The only cell in the retina that spans this entire depth is the Müller glia.

The main criticism of the Müller theory of the b wave stems from experiments on mammalian retina, which show that intravitreal barium ions that block potassium channels can amplify the b wave instead of abolishing it (Frishman and Steinberg, 1989) (Stockton and Slaughter, 1989). However, at low concentrations, barium attenuates the b wave.

The radial arrangement of photoreceptors, Müller glia and bipolar cells contributes to the large field potentials responsible for the a wave and b waves. The ganglion cells are oriented perpendicular to the radial components and therefore, the current they generate is much weaker and difficult to detect.

Scotopic threshold Response (STR)

The negative potential in response to a very dim intensity of light stimulation in dark-adapted eyes is termed “scotopic threshold response (STR)” (Sieving et al., 1986). It is generally accepted that the STR is generated by the innermost part of the retina. Since the optic nerve is composed of axons of the RGC, optic nerve transection is used to selectively destroy RGC to study potentials arising from RGC. A positive

component of the STR termed the pSTR precedes the negative component, the nSTR. In monkeys and rats, the STR is attributed mainly to the RGC and a small percentage to amacrine cells (Bui and Fortune, 2004), whereas in cats and humans the major part of the STR is generated by amacrine cells (Sieving, 1991).

In a primate model of glaucoma, the negative STR is highly diminished, while a and b waves are unaffected. This correlates well with IOP elevation and reduction in RGC density (Frishman et al., 1996).

Functional deficits in rat models of glaucoma are less well characterised than histological changes. In the hypertonic saline glaucoma model, IOP less than 30 mm of Hg selectively diminishes the pSTR, but higher IOP affects a and b waves as well. In mild IOP elevation, pSTR reduction precedes the onset of structural changes in the optic nerve on histology.

Aims

The aim of this project were to

Study the basic cell biology of the OEC

1. The antigenic expression of OEC.
2. The factors controlling OEC migration and proliferation
3. Develop a technique of serum-free culture of OEC.
4. Phagocytic properties of OEC.

Study the interactions of RGC and OEC *in vitro* using

1. Co-culture of RGC5 cell line and OEC
2. Co-culture of primary RGC and OEC
3. Co-culture of retinal explants and OEC

Develop a glaucoma model and characterise the pathology

1. Elevation of IOP
2. Changes of the retinal glia

3. Changes at the optic nerve
4. Changes at the optic nerve head.

Characterise the functional changes of retinal neurons in our glaucoma model

1. Electroretinography to assess the functional outcome of experimental glaucoma.
2. Study the early and late functional changes in glaucoma.
3. Correlate the elevation of IOP to functional changes.
4. Correlate the structural changes in the retina/optic nerve to functional changes.

Effects of OEC in glaucomatous retina and optic nerve

1. Identify the safest injection technique to introduce OEC near the RGC.
2. Study the pattern of migration and interaction of OEC in the retina/vitreous.
3. Inject the OEC into glaucomatous retina/vitreous.
4. Study the changes in optic nerve axonal loss in glaucoma due to OEC.

General Methods

Main materials and methods are discussed in this section. Additional methods are discussed in the relevant chapters.

Cell culture techniques

OEC culture

OEC culture techniques were based on Bianco et al., (Bianco et al., 2004). Rats were injected intra-peritoneally with 0.1ml of pentobarbital per 100 gm of body weight. Young rats between postnatal day one and day five were used for cell cultures. The rats were decapitated and a midline skin incision was made on the skull followed by a para-sagital skull incision next to the nasal septum. The OM was identified by its amber coloration and the branching blood vessels.

The posterior part of the mucosa was collected from both the sides of the septum and placed in cold carbondioxide independent medium (Invitrogen) and stored in ice until use. The medium was aspirated and treated with dispase (2.3mg/ml) for 30 minutes. The epithelium was removed as much as possible using a fine forceps; the tissue was then digested with 0.05% collagenase for 15 minutes, both at 37°C. After centrifugation, collagenase was aspirated and the tissue was resuspended in 0.05% trypsin (GIBCO). After 5 minutes trypsin was denatured with serum containing media and the tissue was centrifuged and the supernatant was aspirated. The cells were resuspended in DMEM/F12+Glutamax (Gibco)/10% FBS (Invitrogen)/ Penicillin/Streptomycin (100mg/ml) (Invitrogen) and sent through a 40µm cell strainer (BD Falcon). The resulting cell suspension was plated on cell culture flasks (Nunc Life Technologies) or labtek multichambered glass slides (VWR international) coated with matrigel (BD biosciences). The cell density was adjusted to about 20,000 cells per cm^2 of surface area. When

confluent, cells in a T25 flask were trypsinised with 0.5% trypsin for 4 minutes. The trypsin was deactivated with serum containing culture medium and centrifuged at 1400rpm for four minutes at 4^0C. The cells were resuspended in the medium and passaged to four T25 flasks or used for experiments.

Primary RGC culture

Sprague Dawley (SD) rat pups of postnatal day one/two were used for RGC culture. Retinas were isolated in a similar fashion to that of retinal culture (see below). Tissue was dissociated by centrifugation at 70g, triturated by pipetting, and incubated for 15 minutes at 37°C in 1 mg/ml papain (Worthington, Lakewood, NJ) and 0.005% DNase I in Earles balanced salt solution. Viability was assessed by trypan blue exclusion and was found to be greater than 98%. The cell suspension was centrifuged at 250g and resuspended in DMEM with antibodies against cell type– specific markers. To isolate RGC, we followed published studies and used a monoclonal anti–Thy1.1 (CD90) antibody (5 g/mL; BD PharMingen, San Diego, CA), again applying microbeads conjugated with antimouse IgG.

Cells positively selected by the anti-Thy1.1 antibody were plated at a density of approximately 2 x 10^4 cells in each well of two-chamber glass slides or 3 x 10^3 cells in each well of eight-chamber glass slides (Labtek; Nalge-Nunc) coated with laminin (0.01mg/mL; Sigma, St.Louis, MO) and poly-D-lysine (0.01mg/mL; Sigma) and grown in serum free, B27-supplemented neurobasal medium (Gibco), as previously described. The growth medium also contained 2mM glutamine, 0.1% gentamycin, 1% N2 supplement (insulin 500g/mL; transferrin 10mg/mL; progesterone 630ng/mL; putrescine 1.6mg/mL and selenite 520 ng/mL; Gibco), 50ng/mL BDNF (Invitrogen, Carlsbad, CA), 20ng/mL CNTF (Invitrogen), 10ng/mL FGF (Invitrogen), and 100M inosine (Sigma). Before our timed experiments, RGCs were maintained with the medium described above in

a standard incubator with 5% CO_2 until homeostasis was reached, as determined by neurite outgrowth and a stable level of viability (4-6 days).

3D culture of cells

Thick gels were used to create a 3dimensional scaffold to mimic the in-vivo environment for the cells.

Collagen gel

Gels were made of 14.5% FBS, 14% concentrated medium and 71.5% volume percentage of first link type I collagen solution (2.2 mg/ml in 0.6% acetic acid). The final concentration of collagen was 1.5mg/ml. Cells were suspended in a mixture of FBS and concentrated medium. Collagen solution was mixed with the cells and the solution was neutralized with NaOH solution. About 150µl of the collagen was quickly cast into the wells of Mattek dishes and allowed to set for 30 minutes. (If the cells were not added to the collagen solution before setting, they were added on top the gel after the gel was set and left to adhere for about 15 minutes). After the gel had set, about 2ml of normal culture media was added.

Matrigel thick gel

Matrigel was used to cast gel to study the three-dimensional behaviour of OECs as well as retinal neurites. Matrigel is composed of laminin, collagen and growth factors. Matrigel was cast on Mattek dishes (Mattek) at 4.5mg/ml concentration and allowed to solidify at 37^0C for 30 minutes. OECs were added on top of the gel with 2µl of media and left in the incubator for 20 minutes before adding the media.

Retinal culture

Rat pups of postnatal day one to three were used for different sets of experiments. The eye was dissected out and placed on ice-cold carbon dioxide independent media (Invitrogen). The cornea was dissected using fine scissors. Lens and vitreous were removed using a fine forceps. Four cuts were made along the equators of the eyecup so that the cup lay flat. The retina was gently peeled off the sides using a fine forceps. The retina

was then cut into square pieces, roughly 1mmx1mm and stored in CO_2 independent media on ice until used. The pieces were then placed on top of just set Matrigel gels

a) With OECs- to study the interaction of OECs with neurites
b) Without OECs as controls.

The samples were incubated at normal culture conditions. The tissues were fixed after 4 days (or 14 days for long term cultures) with 4%PFA and processed for immunostaining.

The samples were examined under a fluorescent confocal microscope and images were captured. Three-dimensional reconstruction of the series of images was performed using the software Volocity (version 4.0).

Protein detection

Immunostaining

Immunocytochemistry (ICC)

The cells from culture flasks were trypsinised and plated onto labtek slides for ICC. The cells were fixed with 4% PFA for 10 minutes and washed thoroughly with phosphate buffered saline (PBS) before blocking with 5% donkey serum (Stratech) and 0.3% Triton (Sigma) in PBS for an hour. Cells were incubated at 4°C overnight with primary antibodies diluted in blocking solution. The controls were incubated in blocking solution only. The cells were washed thrice with PBS and incubated with secondary antibodies raised in donkey and conjugated to Alexafluor488 or Alexafluor555 (Invitrogen), applied at 1:500 for 2 hours at room temperature. Non-adherent antibodies were washed off thrice with PBS. The cells were cover slipped with vectashield with Diaminopyridine imidazole (DAPI) (Vector Laboratories) for nuclear visualization.

Immunohistochemistry (IHC)

The tissue was sectioned using a cryotome and collected on positively charged glass slides (Superfrost plus, VWR international). The slides were

dried thoroughly and then blocked for immunostaining purposes. The protocol for ICC was followed for IHC as well. The sections were viewed using confocal microscope and digital images were captured.

Terminal deoxynucleotidyl transferase mediated dUTP Nick End Labelling (TUNEL) assay

Dead End fluorimetric Tunel system from Promega (G3250) was used for detection of cell apoptosis. DNA of apoptotic cells get fragmented producing free 3' hydroxyl ends. In TUNEL assay, these hydroxyl ends are labeled by fluorescin-12 dUTP and the process is catalyzed by the enzyme, terminal deoxynucleotidyl transferase (TdT).

Retina were fixed using 4% PFA for three hours, washed in PBS and permeabilised using 2% triton for 30 minutes and rinsed again in PBS before incubating with TdT and dUTP overnight at 4°C.

RNA detection

Reverse Transcription-PCR

RNA isolation

The reagents for RT-PCR were from Roche unless stated otherwise. OECs were trypsinised from confluent T75 flasks. The trypsin was inactivated with medium and the cells were pelleted by centrifugation. The pellet was washed with PBS and centrifuged in an Eppendorf tube at 3000rpm for 5 minutes. The pellet was broken by flicking and resuspended in RLT-buffer to lyse the cell membranes and b-mercaptoethanol (Sigma-aldrich) to eliminate the RNA released during the lysis. The solution could be used PCR or stored at -80^0 C for future use. The amount of RNA was determined using a spectrometer (Eppendorf biophotometer).

Genomic DNA was removed by treating the mixture with DNAse along with reaction buffer for 15 minutes at room temperature. The DNAse was inactivated with EDTA solution and heated for 10 minutes at 60^0 C.

Table 2 List of primary antibodies used for immunostaining.

Primary antibody	Supplier	Dilution
Alexafluor 488 Phalloidin	Invitrogen A12379	1:500
Anti-glial fibrillary acidic protein (GFAP)	Dako	1:200
Anti-human fibronectin	Dako A0245	1:200
Anti-$Na_v1.6$ (voltage gated sodium channel)	Alomone labs	1:100
Anti-nerve growth factor antibody (NGFR p75)	Sigma N3908	1:200
Anti-neuronal nuclei	Millipore	1:100
Anti-postsynaptic density	Millipore	1:500
Anti-RT97 (phosphorylated neurofilament heavy chain)	Developmental Studies Hybridoma Bank (DSHB)	1:100
Anti-s100	Sigma	1:200
Anti-synaptotagmin	Abcam	1:500
Anti-Thy-1	Santa Cruz sc-9163	1:200
Anti-β3tubulin	Abcam	1:100

Reverse Transcription (RT)

20µl of reaction mixture was made with 10mM reaction buffer, 5mM $MgCl_2$, 1mM dNTP, 1U/µl RNAse inhibitor, 80ng/µl oligo dT-15 primers, 0.8 U/µl AMV reverse transcriptase and RNase free water to reverse transcribe 1µg of RNA. The mixture was vortexed and briefly centrifuged and incubated for 10minutes at 25^0 C, 60 minutes at 42^0 C, 5 minutes at at 99^0 C and 5 minutes at 4^0 C in a thermal cycler (Eppendorf). The primers were specific for nestin, Pax6, Sox2, Chx10, Hes5 and Notch1.

PCR

The PCR reaction mixture consisted of 2.5µl cDNA, 0.25µl DNA polymerase, 10µM each of dNTP mix, 2µl of forward and reverse primers, 5µl of reaction buffer with 10 mmol/L of Tris/HCl buffer with $MgCl_2$. The mixture was incubated for 2 minutes at 94^0 C followed by 34 cycles at the following temperatures- 94^0 C for 30 seconds, 58^0 C for 30 seconds, 72^0 C for 1 minute. After holding at 72^0 C for 7 minutes, the mixture was analyzed by gel electrophoresis with 1% agarose gel.

Agarose was mixed with TAE buffer and heated in a microwave till it dissolved and boiled. Once the solution was cooled, gel red was mixed with 2% agarose gel and was poured to mould.
The PCR products were inserted into the wells of the gel and electric current was passed through the gel.

Proliferation assay

Alamar blue (Ab) is a nontoxic dye that readily enters the cells and is an indicator of cell viability and proliferation. Upon entering the cell, the active ingredient, resazurin, which is nearly non-fluorescent, is reduced to red fluorescent resorufin. The measurement of the resulting fluorescence facilitates the quantification of cell proliferation.

To study the effects of forskolin and EGF on OEC proliferation, four groups were set up- media with serum, serum free media with forskolin,

serum free media with EGF (40ng/ml), serum free media with forskolin and EGF. For proliferation assay, OEC were isolated and plated on Matrigel coated 48 well plates. DMEM/F12 media was supplemented with serum/forskolin/EGF according to the group. 24 hours after plating, Ab (AbD serotech) was diluted 1:10 with the media in wells, and incubated at 37^0 C for an hour. The absorbance of media containing Ab was read using a plate reader (Safire, Tecan) at an excitation of 570nm and emission of 600nm. Half of the media containing supplements were renewed every alternate day. The Ab assay was repeated for all the groups after five days and seven days. The absorbance of media with Ab from different groups was compared with two-way ANOVA using the Prism software.

Quantification of cell dynamics

OEC in culture displayed dynamic extension and retraction of cell processes. We quantified these extensions and retractions from time-lapse microscopic images.

P1 OEC were plated on matrigel coated glass bottom Mattek dishes (13mm in diameter) at a density of 10,000 cells per well with normal culture media with serum. The cells were allowed to settle for four hours after plating. For microscopy, the cells were kept in a specially designed chamber where temperature was set at 37°C and carbondioxide levels were maintained at 5%. Phase images were captured with the 20x objective at every two minutes using the automated camera fitted to the Leica microscope. The field of imaging was chosen such that the cells were not adherent to each other and there were at least six cells per field. After 18 minutes, p75 antibody was added to the medium and imaging was continued for another 45 minutes. We imaged five Mattek dishes with OEC.

The series of images were opened with Image J software. After setting the scale for measurements, the outline of the cell of interest was drawn manually using the ‘wand’ tool of the software on every image of the time-

lapse series and the traces were stored in the software for future reference. We used a plug-in which automatically calculated the retractions and protrusions as well as the area of cell in each frame in the order of the manual traces.

The values for retraction, protrusion and area of the cells were imported to microsoft excel where we calculated the dynamic index of the cell at each time point.

Dynamic index= (extension + retraction)/ area at each time point.

To study the pattern of cell movement, the dynamic index of the cells was plotted versus the time point.

Scratch wound assay

We used a scratch wound assay to study the role of the p75NTR in OEC proliferation and migration *in vitro*. The area of wound healing/migration was quantified using Image J software (Yue et al., 2010). P1 OEC were plated on 96 well flat bottom plates (Nunc) at a density of 3 x 10^4 cells per well. The cells were incubated in DMEM/F12 media with 10% serum for 24 hours. The wound was made by scratching a straight line on the well using a sterile 10µl pipette tip (Starlabs) held perpendicularly to the surface of the well. Fresh media with inhibitors replaced the old media. The inhibitors used in the assay are listed in Table 3. Controls received standard medium without inhibitors.

Table 3 Inhibitors of p75 NTR used in the scratch wound assay.

Type of inhibitor	Action
TACE	Sheds ectodomains from p75 and nogo receptors
NGF inhibitor	Inhibits binding of NGF to p75 receptor and/or TrkA receptor
P75 antibody	Binds to p75 receptor

TACE

TNF alpha converting enzyme (TACE/ADAM17) cleaves ectodomains from a number of proteins including p75 and Nogo receptors(Ahmed et al., 2006). Recombinant human TACE (R&D Systems, Cat. No: 930-ADB) was used in the culture systems at 100ng/ml.

NGF inhibitor

2,3,4,10-tetrahydro-7,10-dimethyl-2,4-dioxobenzo[g]pteridine-8-carboxaldehyde (TOCRIS bioscience, Cat. No: 2272) is a non-peptide inhibitor of NGF dimer causing a conformational change inhibiting its binding to P75 NTR and TrkA. This effect is concentration dependent (Niederhauser et al., 2000).

P75 antibody

The antibody to P75 receptor was a kind donation from Prof Chao. The antibody competitively binds to the neurotrophin-binding site of the receptor rendering it inactive.

Calculation of the rate of wound closure

Phase contrast images of the wound were captured at time points of 0 and 16 hours using a Leica inverted microscope. The images were uploaded in Image J software. The area of wound was measured using the 'polygon selection tool' of Image J software.

The data was analysed using one-way ANOVA.

Labeling of cells

Cell tracker dye

The green cell tracker dye, CMFDA (5-chloromethylfluorescein diacetate) from Invitrogen (C7025) was used to label the OEC. According to the manufacturer's information, the choloromethyl group of CMFDA reacts with thiol in the cells, which emits green fluorescence upon action of

intracellular esterases. CMFDA enters the cells passively, but is retained in the cells after reaction with thiols and esterases.

Cells in flasks were incubated with pre-warmed probe (final concentration of 10μM /ml in serum free media) for thirty minutes. The probe was removed and the cells were treated with culture medium with serum for another thirty minutes before the flask was trypisinised. The trypsin was deactivated with serum containing media and then the suspension was centrifuged at 1400rpm for four minutes and the cells were re-suspended in serum free medium and stored on ice till use.

Quantom dots

Q-tracker 525 cell labelling kit from Invitrogen (A10198) was used to label OEC green. Fluorescent nanocrystals of 10-20nm in diameter are made of fluorescent semiconductor material coated with water-soluble polymer. The crystals are bound to a targeting peptide that helps in the internalisation of the crystals into the cell cytoplasm. The crystals remain in the cytoplasm in vesicles and emit fluorescence upon excitation.

eGFP labelled OEC

Transgenic Sprague–Dawley rats [SD-Tg(CAG-EGFP)Cz-004Osb] carrying the enhanced green fluorescent protein (eGFP) transgene were obtained from Japan SLC., Inc. (Hamamatsu, Japan). This transgenic rat line expresses the *eGFP* gene under the control of the cytomegalovirus enhancer and the chicken β-actin promoter. The e-GFP gene was inserted randomly into the genome and therefore the exact location of the gene is not known *(Marano et al., 2008)*.

eGFP labelled OEC were used for *in vivo* transplantation experiments because the cell trackers or quantum dots was not efficiently retained by the OEC for several weeks.

Quantification of synapses in-vitro

Synaptotagmin, a membrane trafficking protein, present in the synaptic vesicles was detected by immunostaining. Synaptotagmin was labelled with green fluorescent secondary antibody.

The images were uploaded in ImageJ software and converted into 8 bit images and thresholded to avoid background. The staining was then quantified using the “analyse” particles menu of Image J. The data was exported to Prism software for analysis.

Animal use for in-vivo experiments

Before surgical procedures, Brown Norway rats were housed with adequate light, temperature and humidity in a controlled environment and had access to standard rat chow and water ad-libitum.

Rats were anaesthetised with a mixture of ketamine hydrochloride (Ketaset) 65mg/kg and medetomidine (Domitor) 50 mg/kg intra-peritoneally. Atipamezole (Antisedan) 1mg/kg was injected intra-peritoneally for recovery from anaesthetics. The animals were constantly monitored, kept warm and offered hydrogel to prevent dehydration until they regained their balance. The rats were checked regularly for any signs of distress or deviations from normal grooming patterns. In the event of excess pain or suffering, the animal was terminated immediately by intraperitoneal injection of pentobarbital solution (0.1 mg per kg of body weight of the animal).

Injection of hypertonic saline into episcleral veins

The injection of 1.75M hypertonic saline solution into the episcleral vein causes sclerosis of Schlemm’s canal, blocking the outflow of aqueous humour and leading to an increase in IOP (Morrison et al., 1997).

Borosilicate glass micropipettes of inner diameter of 75µm were pulled through a pipette puller (Sutter instruments Co., P-97) to achieve a long tapering tip. The tip was broken at ~1.5cm from the tip in order to get a lumen with an outer diameter of ~15µm. The tip was held against the abrasive surface of a moist rotating beveller (Dremel) coated with aluminium oxide for about five seconds in order to get a long bevel. The shape of the bevel was confirmed under a microscope before attaching it to tubing. A 5ml syringe was attached to the tubing of a butterfly needle (metallic tip of the needle and the plastic wings were removed) and the pipette tip was inserted into the lumen of the tubing and glued with superglue. The apparatus was left overnight to dry.

A hypertonic saline solution (1.75M) was prepared for injection and filtered using a 0.22µm filter to prevent clogging of the tiny lumen of the needle.

Morrison et al studied the limbal vasculature of the rat eye using microvascular castings, demonstrating the connections between Schlemm's canal, venous plexus in the limbus and episcleral veins through which the aqueous humour drains (Morrison et al., 1995b). A polypropylene ring (donated by Prof. Morrison) with 5.5 mm internal diameter and a groove of 1mm was used to hold the globe in place, obstruct the blood flow through the episcleral veins except for the one to be cannulated for the injection of hypertonic saline. Under the dissection microscope, the conjunctiva was incised using Vanass scissors.

The needle, held with a curved forceps, was inserted into the vein, and ~50 µl of saline solution was injected manually. The saline was injected slowly to avoid the displacement of the needle inside the vein. Blanching of the vessels, limbal flush, clouding of the anterior chamber and appearance of lens vacuoles indicate successful injection. The hypertonic saline solution scleroses the blood vessels that drain the aqueous humour and Schlemm's canal and block the aqueous outflow.

The ring was removed and a drop of antibiotic (chloramphenicol) was applied. Only one eye of an animal was injected with saline. The un-operated eye served as control. IOP was measured using a rebound tonometer calibrated for use in rats (TonoLab, Tiolat), three times a week at the same time every day to avoid variations due to circadian fluctuations.

Calculation of Integral IOP

Integral IOP is a measure of IOP rise, which is the difference in IOP between the treated and the untreated eye, expressed as a function of number of days after the injection (Guo et al., 2005).

Inttegral IOP= (Average IOP of treated eyes- average IOP of untreated eyes) x number of days after the injection.

Tissue processing for Flourescent microscopy

The animals were transcardially perfused with 4% PFA and the tissue of interest was dissected out. The tissue was then post fixed for four hours at room temperature or overnight at 4^0 C and then cryoprotected in 30% sucrose solution. The tissue was then embedded in Optimal cutting media which was frozen rapidly with the help of liquid nitrogen. Sections of 20µm thickness were collected on glass slides.

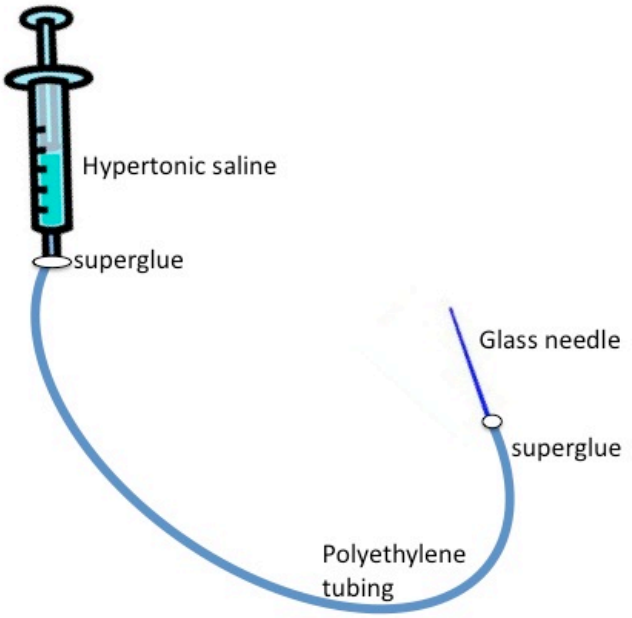

Figure 8 Hypertonic saline injection apparatus.

The figure is a diagrammatic representation of the hypertonic saline injection apparatus demonstrating the beveled glass needle glued to polyethylene tubing which is glued to the injection syringe.

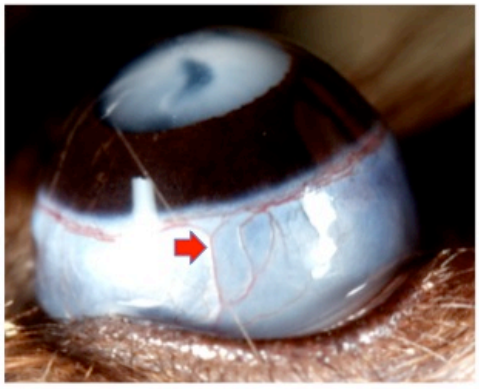

Figure 9 Episcleral vein on the rat eye.

The arrow indicates the episcleral vein on the rat eye. Veins are distinguished from arteries by their limbal morphology. Arteries bifurcate in the shape of a "T" into two branches at right angle to the supplying artery. Several small veins merge into a larger vein as they take blood from the limbus to the peri-ocular vessels. In addition, the direction of blood flow was confirmed by occluding the blood vessels with a forceps.

Tissue processing for light/electron microscopy

The reagents were from Agar Scientific. The animals were transcardially perfused with 3% glutaraldehyde and 1% PFA; eyes were enucleated and rinsed in sodium cacodylate buffer and treated with 1% aqueous osmium tetroxide in the dark for 2 hours at 4^0C with agitation followed by passage through a series of ascending alcohols-50%, 70%, 90% and 100%. Following ethanol dehydration, tissue blocks were passed through two changes of propylene oxide, prior to 12 hours immersion in a 1:1 mixture of propylene oxide and araldite and 3 to 6 hours in full resin. Tissue samples were embedded in fresh resin, labelled and placed in a 60^0C oven overnight to cure.

For light microscopy, semi-thin sections of 0.75 micrometer thickness were cut using a Reichert Jung microtome and dried on a hot plate with a drop of water and stained with 1% methylene blue.

For electron microscopy, ultra-thin sections of about 70nm were cut using diamond knife and collected on copper grids. The sections were dried for two hours at least before staining with Reynold's lead citrate solution. The grids were then washed thoroughly and dried before imaging using the electron microscope.

Imaging

The confocal microscopes used for imaging are Zeiss microscopes (series 700 and 710) and Biorad Leica epifluorescent microscope (DMIRB). Electron microscopy was carried out using JEOL Transmission electron microscope.
Images were analysed using ImageJ software.

Quantification of retinal ganglion cell from retinal whole mounts

Eye were post fixed in 4%PFA for four hours. To prepare retinal whole mounts, the cornea and lens were removed and four partial cuts were made in order to flatten the eyecup. A moist, fine paintbrush was used to separate the retina from the underlying pigment epithelium. Finally, the connection at the optic nerve head was incised using curved Vanass scissors to obtain four equal sized lobes of retina connected at the centre. The retina was washed four times in PBS to remove PFA which could cause background fluorescence. After washing, the retina was spread out on a glass slide with a drop of PBS. Excess liquid was removed using blotting paper. The retina was immediately cover-slipped using Vectashield with DAPI to stain for the nuclei and viewed under Leica confocal microscope.

Twelve images were captured from every retina, three from each of the four lobes using the x20 objective. Care was taken to consistently image similar areas from each lobe Figure 10. The top most layers of nuclei (which consists of RGC nuclei mainly and some displaced amacrine cells) were imaged. The images were opened with ImageJ software and the cell counter plug-in was installed. The nuclei stained blue were selected manually by mouse click, which was counted by the cell-counter plug-in. The nuclei counts from the twelve images were added up and the sum was assigned to each retina.

Even though this method may count misplaced amacrine cells as well, the technique is well established as giving an overall reflection of the loss of RGC (Samsel et al., 2010).

Quantification of optic nerve axons

Optic nerve axon damage is characteristic of glaucomatous pathology and therefore quantification of these axons indicates the severity of glaucomatous damage.

The optic nerve was collected from 2mm behind the globe of the rat eye, where myelination begins, because here individual axons are easily recognisable due to their myelin sheaths, which stain darker than axoplasm and axolemma.

The nerves were fixed in Karnovsky's fixative, processed with the same protocol for EM specimen preparation and embedded in plastic. Semithin cross sections were cut and stained with toluidine blue and cover-slipped. The sections were imaged using a light microscope.

Four non-overlapping images of the optic nerve sections were captured at a magnification of 60x. About 40% of the total area of the cross-section was covered by the four images. The number of axons in each of this image was counted using imageJ software. The images were manually thresholded and counted automatically.

The various steps in counting axons are as follows:

Colour images were converted into 8bit images and the contrast was enhanced by 0.5%. The image was converted into binary and thresholded so that healthy axons with clear cytoplasm appear as solid particles. These particles were counted using the 'analyze particles' plug-in of ImageJ software.

Statistics

Prism, version 5.0, GraphPad Software, Inc., was used to perform t-tests and analysis of variance (ANOVA). Where possible, the observer was masked to the study groups (except in the case of obvious differences

between the groups, for example, during the IOP measurements, it was impossible to be masked between the beads injected eyes and PBS injected eyes).

t-test

When the number of groups for comparison was less than three, then t-test was used. Standard error of means was used to represent the error in each group. Statistical significance was accepted at $p<0.05$.

Analysis of variance (ANOVA)

To compare three or more groups, ANOVA was employed. When the parameter of comparison was restricted to one, we selected one-way ANOVA. The different groups were compared by applying Bonferroni's correction to reduce the chances of a false positive. Standard error of mean was used to determine the error in each group. Statistical significance was accepted at $p<0.05$

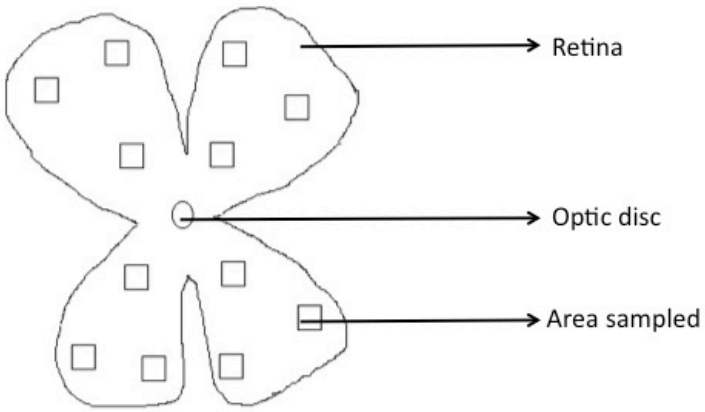

Figure 10 Schematic diagram representing the areas of retinal whole mounts photographed for quantification of RGC.

The eye was fixed in 4% PFA for four hours. The cornea and lens were removed and four partial cuts were made in order to flatten the eyecup. The retina was removed using a paintbrush and was cut at the optic disc. The retina was washed in PBS and flattened on a glass side with the RGC layer facing up. The tissue was cover-slipped using vectashield with DAPI and imaged using the x20 objective of a Zeiss 700 confocal fluorescent microscope. Three images were captured from each lobe of the retina so that a total of 12 images were obtained per eye. The images were uploaded in ImageJ software and RGC were selected manually and counted using the cell-counter plugin. Care was taken to exclude vascular endothelial cell nuclei.

Chapter one: Cell biology of olfactory glia

OEC are one of the most promising cell types in neuro-regeneration experiments in animal models of spinal cord injury (Ramer et al., 2004) (Li et al., 1998, Yamamoto et al., 2009) as well as other parts of the CNS (Guntinas-Lichius et al., 2002, Guntinas-Lichius et al., 2001, Gudino-Cabrera et al., 2000, Nivet et al., 2011). Autologous OEC transplantation in humans is safe; to date no side effects such as tumours, cavity formation or neuropathic pain have been observed. The beneficial effects of OEC are yet to be evaluated (Mackay-Sim et al., 2008). Although the therapeutic effects of OEC are well established *in vitro*, the mechanisms involved in regeneration and neuroprotection are poorly understood.

As cell cultures techniques in different laboratories vary, we began our investigations by characterising the expression of our OEC cultures for their marker proteins, neurotrophic factors and migratory properties.

In order to use OEC in humans, it will be ideal to develop a culture technique that does not require animal derived substances like serum, trypsin etc and this will be important to try to prevent infectious diseases.

We also wanted to explore the OEC derived factor(s) facilitating regeneration of neurons as well as migration. The expression of p75 receptor following injury is similar to OEC and Schwann cells and could be very important to facilitate regeneration.

The rate of migration of cells differs according to the surface, nutrients in the serum, etc. The role of binding of neurotrophins to the low affinity nerve growth factor receptor p75 receptor in Schwann cell migration following peripheral nerve injury is well documented (Anton et al., 1994). Blocking either the neurotrophin or the p75 receptor stops the migration of Schwann cells (Anton et al., 1994).

Therefore, the up-regulation of p75 receptor immediately after injury could be a mechanism to induce migration in an otherwise static population of OEC. We hypothesised that P75 might have a role in OEC migration.

House keeping roles of OEC such as phagocytosis of neuronal debris is well established in drosophila, but less clear in mammals (Doherty et al., 2009) (Suzuki et al., 1996). We studied the phagocytic potential of OEC using cultured RGC, which could give an insight to the phagocytic property of OEC in transplanted areas.

Aims

We have discussed the main aims of this thesis in the last section. In order to explore the possibilities of OEC in RGC protection, we require thorough knowledge about the basic cellular properties of OEC. The aims of this chapter are to:

1. Establish a cell culture technique to selectively grow sufficient number of OEC for transplantation.
2. Characterise the purity of OEC in culture by studying the expression of cell-specific markers.
3. Study the ultrastructure of the cytoplasmic components of OEC.
4. Study the expression of progenitor markers and neurotrophins by OEC.
5. Identify the role of p75 neurotrophin receptor in the migratory properties of OEC.
6. Analyse the role of OEC in phagocytosis/efferocytosis of apoptotic neurons.

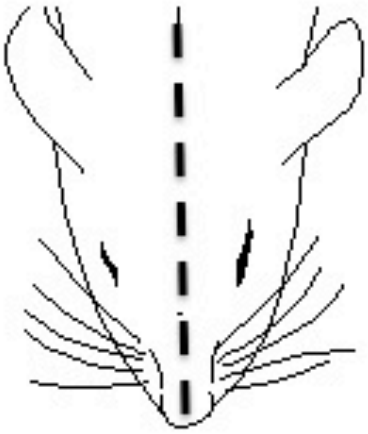

Figure 11 To obtain mucosa from the nasal mucosa, a midline structure, we split the rat skull in a paramedian section.

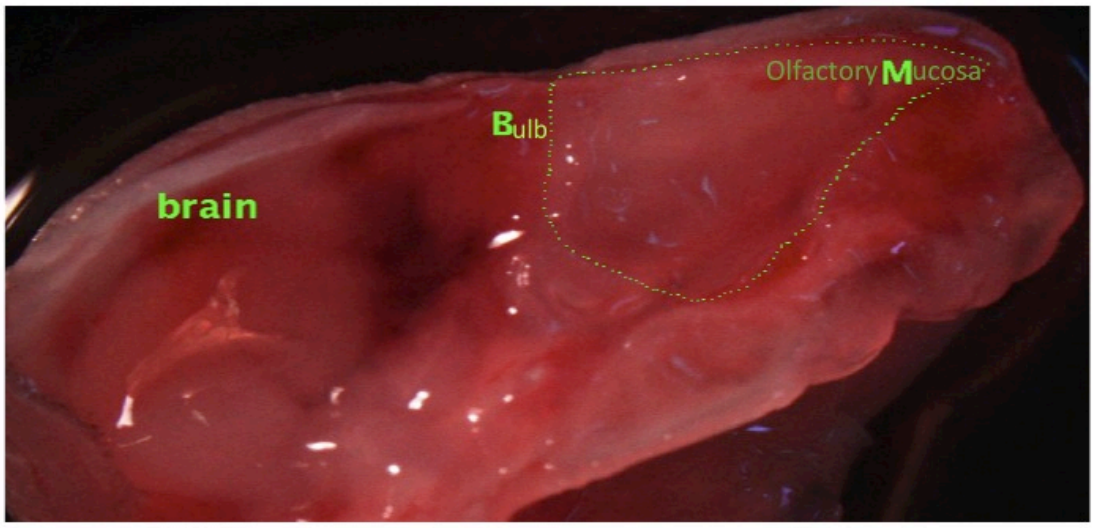

Figure 12 The paramedian section exposes the nasal mucosa and the olfactory bulb.

The anterior part of the nasal mucosa has more glands and the posterior part has a higher concentration of olfactory neurons and ensheathing cells (Graziadei and Graziadei, 1979).

Immunohistochemistry on rat mucosa

We performed immunostaining on cryosections of adult rat mucosa. We used Beta III tubulin to stain neurons and GFAP for OEC. We found tightly

packed neuronal cell bodies in the epithelium of the olfactory mucosa. The GFAP positive cells were located exclusively in the lamina propria region, immediately below the epithelium. These cells (OEC) were found at the junction of the lamina propria and the epithelium and were arranged perpendicular to the epithelium. The GFAP positive OEC also appeared interspersed within axonal bundles in the lamina propria which was identified by beta III tubulin staining. OEC in the mucosa did not stain for p75 neurotrophin receptor, which is the marker for OEC in culture. Fibronectin staining was similar to that of GFAP staining. Cells positive for fibronectin lay at the junction of lamina propria and epithelium as well as in the bundles in lamina propria.

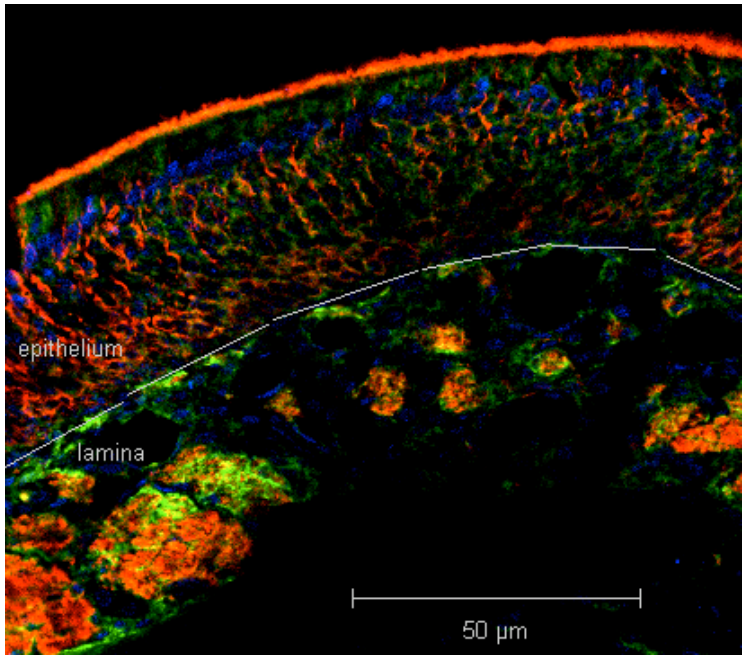

Figure 13 Olfactory glia are present in the lamina propria of olfactory mucosa in adult rat, as shown by the distribution of GFAP.

Olfactory mucosa of adult rat was fixed and immunostained for GFAP (green) for OEC, beta-3 tubulin (red) for neurons and (blue) for neurons. In the lamina, OEC lie interspersed with axon bundles (see ***Figure 14*** *for higher magnification) arising from the neurons in the epithelium; OEC are also found at the junction between the epithelium and lamina.*

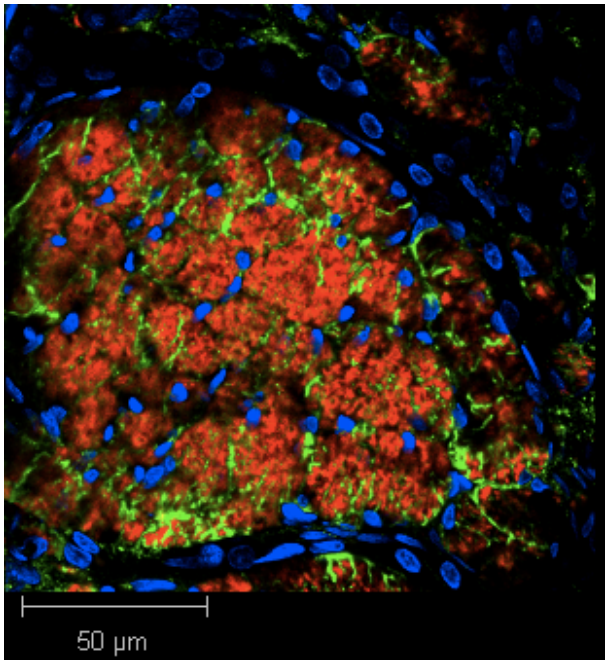

Figure 14 Olfactory glia ensheath axons in the lamina of olfactory mucosa of adult rat.

Olfactory mucosa of adult rat was fixed and immunostained for GFAP (green) for OEC, beta-3 tubulin (red) for neurons and DAPI (blue) for nuclei. The figure shows an axon bundle in the lamina of olfactory mucosa interspersed with OEC processes. Since axons do not contain nuclei, all the nuclei in the picture belong to OEC.

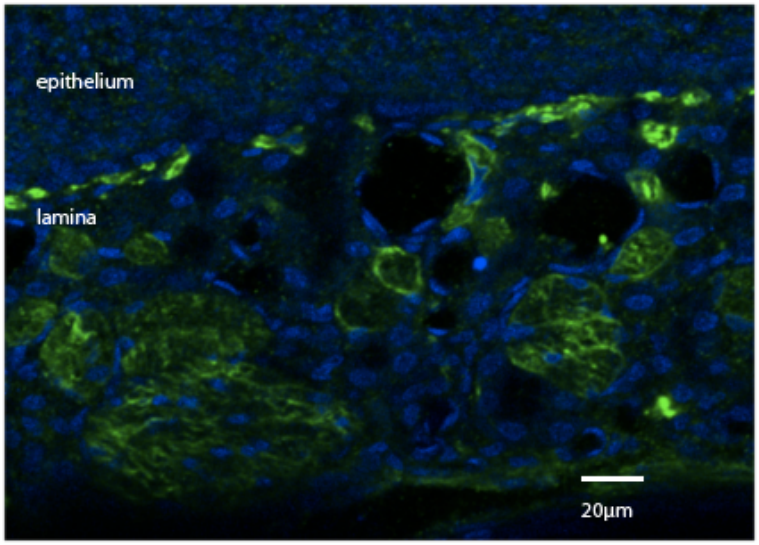

Figure 15 Fibronectin expression in the olfactory mucosa is similar to that of GFAP, confirming the presence and location of olfactory glia.

Olfactory mucosa of adult rat was fixed and immunostained for fibronectin (green). The expression pattern of fibronectin was similar to that of GFAP; it was expressed in the lamina as well as at the junction of lamina and epithelium. OEC in culture express both GFAP and fibronectin.

OEC culture

Expression of olfactory glial marker proteins

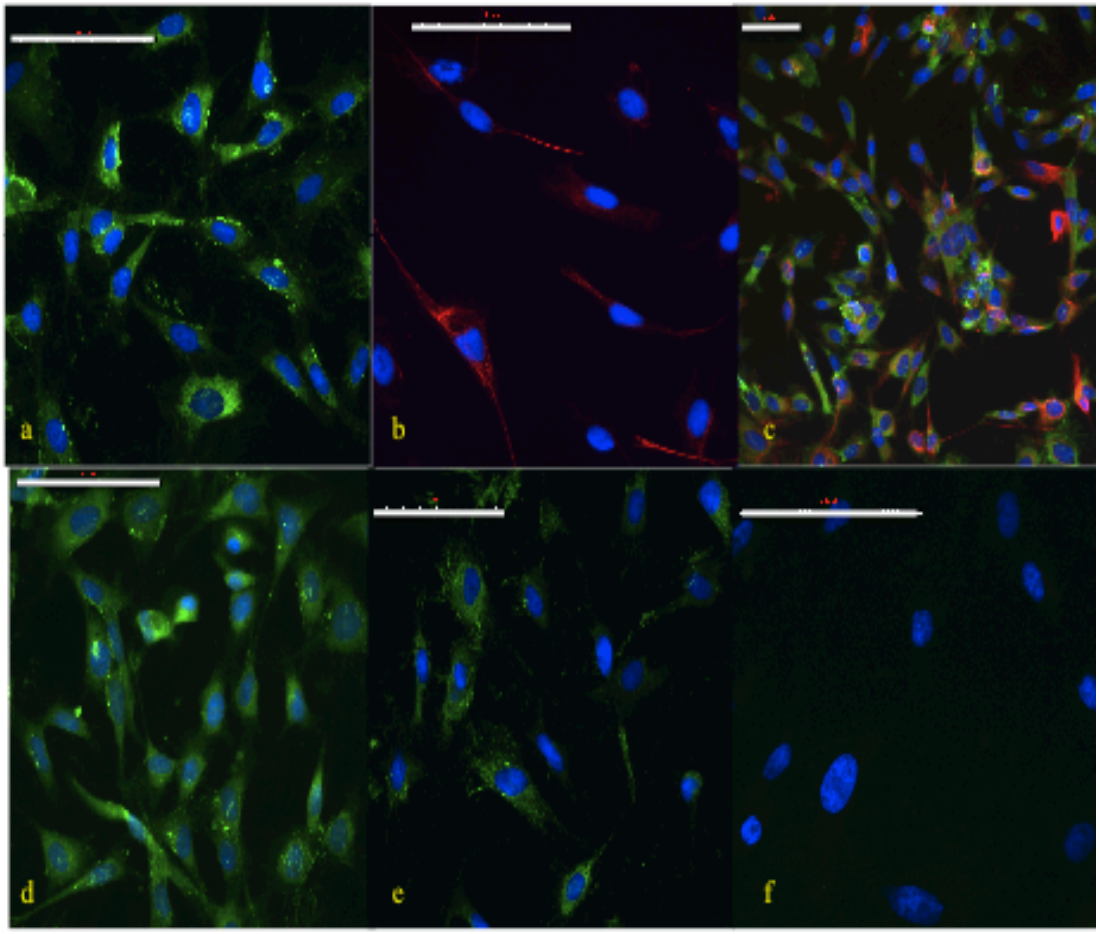

Figure 16 In culture, olfactory glia abundantly express p75NTR, GFAP, s100 and fibronectin.

Nucleii –blue. a-p75, b-s100, c-co-expression of p75 (green) and s100 (red), d-GFAP, e-fibronectin, f-control. The OEC cultures were on over 98% pure population expressing all relevant marker proteins namely p75NTR, s100, GFAP and fibronectin.

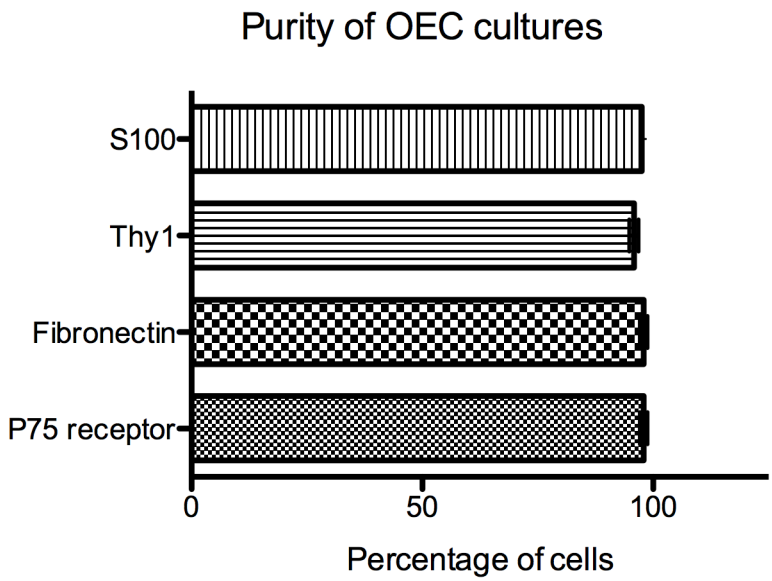

Figure 17 Over 97% of olfactory glial cells in culture express OEC specific proteins, confirming the purity of our cultures.

OEC were isolated and cultured for 6-7 days on matrigel coated glass slides; fixed and immunostained for p75 receptor, s100, fibronectin and Thy1. Over 97% of the cells in culture expressed the OEC specific markers p75 NTR and s100.

Electron microscopic study of the OEC in culture

We plated passage 0 (P0) OEC on poly-D lysine and laminin- coated glass cover slips for electron microscopy. The cells generally had a single large nucleus. The main cytoskeletal elements of OEC were intermediate filaments, placed at approximately 20nm apart. The cytoplasm had abundant rough endoplasmic reticulum and mitochondria. Membrane bound vesicles like lysosomes and peroxisomes were also common. Glycogen granules were dispersed throughout the cytoplasm Figure 18.

Neurotrophic factors expressed by OEC

We cultured P0 OEC from postnatal (day four to five) rats as well as adult rats (four weeks old) for about seven days and isolated RNA from the cells. We tested the samples for neurotrophins NGF, BDNF, GDNF and NT3. OEC from both adult rats and pups expressed BDNF, NT3, GDNF and NGF (Figure 20 and Figure 21).

Optimisation of OEC cultures

OEC cultured using serum pose various risks for human use. Culture of human cells with bovine/horse serum leads to the deposition of animal proteins on the cell surface resulting in immunological rejection as well elevation of the chances of prion and viral infections (Chachques et al., 2004). Therefore we developed a method of serum free culture of OEC using recombinant mitogens and growth factors.

OEC cultured with bovine serum form nests of cells, which divide to form a confluent layer of cells in the flask. Freshly isolated cells, when plated with growth factors in the absence of serum fail to form the initial nests of cells required for successful cultures. Any amount of growth factors does not help to form nests in the absence of serum.

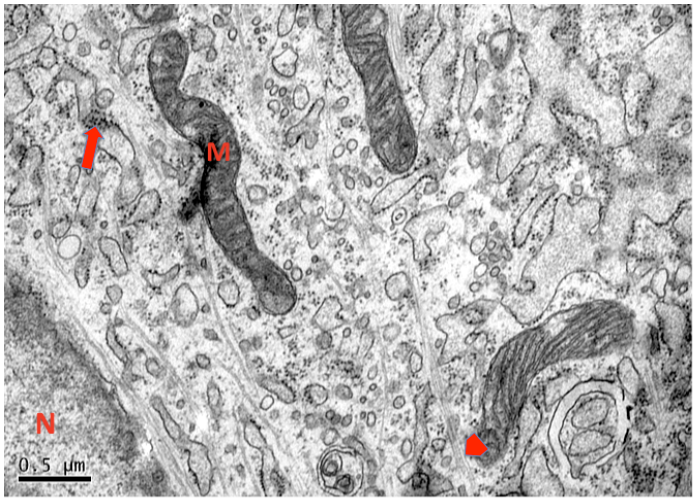

Figure 18 On EM, OEC display a large nucleus, abundant ER and mitochondria. The main cytoskeletal features are intermediate filaments.

P1 OEC were plated on glass cover slips coated with polylysine and laminin and fixed with Karnovsky's fixative, treated with osmium tetroxide and embedded in resin. Ultrathin sections were cut and stained using lead citrate and imaged with Transmission Electron Microscope. N-nucleus, M-Mitochondria, arrow- ribosomes, arrowhead- intermediate filaments.

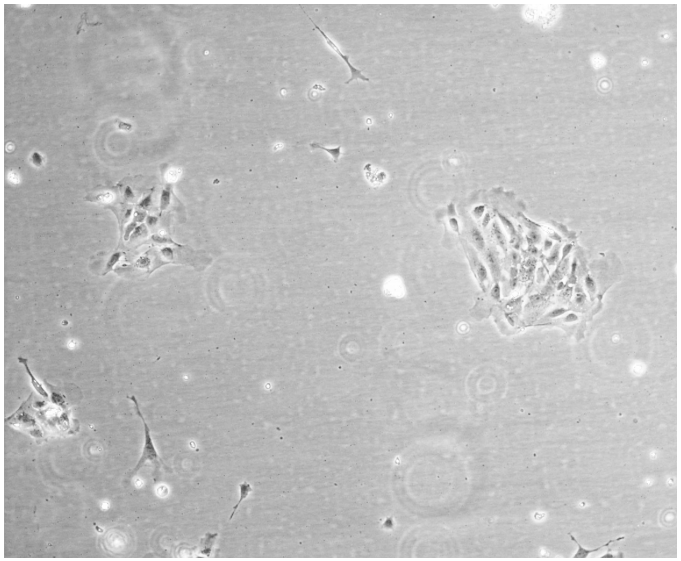

Figure 19 Nest of cells in OEC culture.

P0 OEC were isolated from postnatal rat pups and cultured in matrigel-coated flask. After 24hours in culture, nests or rosettes of cells were found in the flasks.

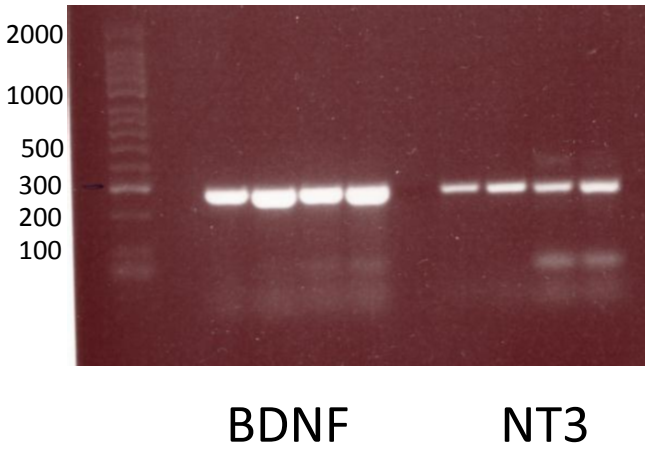

Figure 20 OEC in culture express mRNA of the neurotrophins BDNF and NT3.

OEC were isolated from adult rats and pups and cultured for about seven days with media containing serum. m-RNA was extracted from the cells. Neurotrophins NGF and GDNF were strongly expressed by OEC.

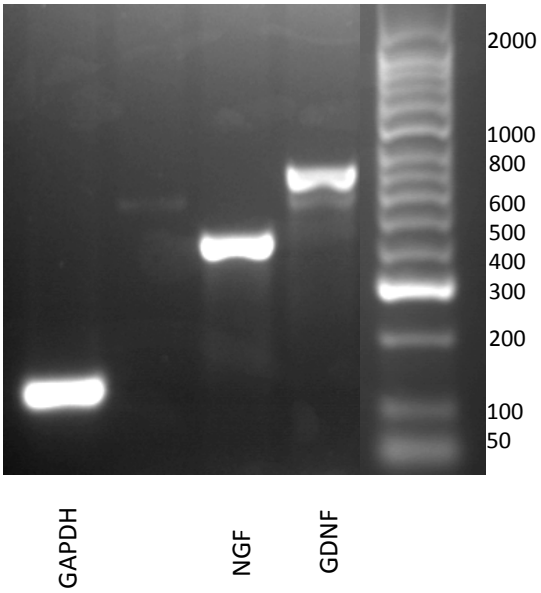

Figure 21 OEC in culture express mRNA of the neurotrophins NGF and GDNF.

OEC were isolated from adult rats and cultured for about seven days with media containing serum. m-RNA was extracted from the cells. Neurotrophins NGF and GDNF were strongly expressed by OEC.

Forskolin is a mitogen extracted from the root of *Coleus forskohli* that elevates the cyclic AMP levels in rat Schwann cell cultures. Proliferation occurs only by the synergistic activity of both EGF and forskolin to facilitate significant levels of cyclinD to promote cell proliferation (Rahmatullah et al., 1998).

OEC being similar to Schwann cells in their functional properties, we used forskolin for serum-free culture of OEC. OEC were isolated from the olfactory mucosa as described before, except that we used trypleExpress instead of trypsin. Trypsin is animal derived, but trypleExpress is not and also trypleExpress does not require deactivation with serum. The cells were plated on 48 well plates (Nunc) at a density of 5x 10^4 cells per well. The cells were grown in serum free DMEM/F12 medium containing forskolin (2µg/ml), EGF (40ng/ml), B27 and N2 supplements. We used DMEM/F12 medium with EGF, B27 and N2 supplements only as negative control. Positive control was DMEM/F12 medium with 10% FBS. To evaluate the effect of EGF, we used another group of cells grown in DMEM/F12 medium with forskolin and B27, N2 supplements in the absence of EGF.

Cell proliferation was quantified using the Alamar Blue assay. Absorbance was measured at day one (24 hours after plating), day five and day seven and the results compared using students t test. OEC cultured with forskolin and EGF proliferated significantly more than cells cultured in media with serum and other groups, $p< 0.0001$ (Figure 22). In the absence of EGF, forskolin could not support proliferation, the results being similar to that of Schwann cell cultures (Rahmatullah et al., 1998). EGF in the absence of forskolin did also not support proliferation. It can be concluded that successful proliferation of OEC in serum free conditions requires simultaneous supplements of both Forskolin and EGF.

OEC cultured with serum or forskolin/EGF were immunostained for P75 receptor, the marker for OEC. Both groups had remarkably similar expression of P75 receptor in the cytoplasm Figure 23.

Cell motility of OEC

In culture, OEC express p75 receptor and migrate actively. We tried to block the P75 receptors with P75 antibody and measured the movements of OEC.

OEC in culture exhibited vigorous protrusion and extraction of processes, but rarely sufficiently motile to translocate from one place to another. We used time-lapse light microscopy to capture the extension and retraction of the cell for 20 minutes and then added the antibody and recorded the same for another hour. We calculated the dynamic index (DI), which is the fraction of the cell that is remodelled at each time point (Dahlmann-Noor et al., 2007).

Addition of the P75 antibody reduces the dynamic index of OEC from about five minutes after the addition of the antibody. The DI was lowered for about 30minutes, after which it was fluctuating Figure 24. The experiment was repeated four times and a total of thirty motile cells were analyzed. Non-motile cells were not included in the study.

Scratch wound assay

We used a scratch wound assay to study the role of the p75NTR in OEC proliferation and migration *in vitro*. The wound closure in the groups treated with p75 antagonists was not significantly different from that of the controls. In our study, the p75 antibody, NGF inhibitor or TACE had no effect on the cell proliferation/migration of OEC at sixteen hours after the wound was induced Figure 25. The experiments were repeated four times.

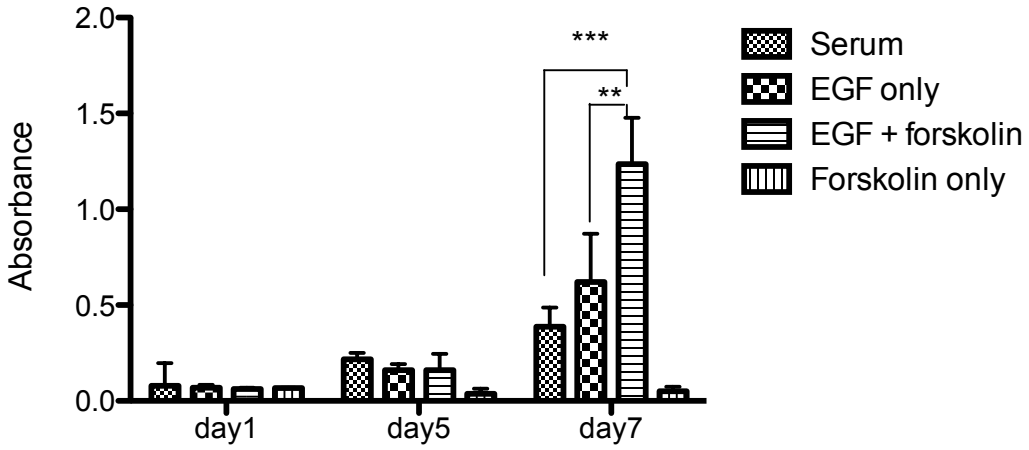

Figure 22 OEC proliferation is greatest in serum-free medium with forskolin and EGF supplements.

OEC isolated from rat mucosa and grown in serum free media in the presence of EGF and forskolin proliferated significantly more by day seven than OEC cultured in media with serum or media with forskolin or EGF alone. Alamar Blue assay was performed on the cultures on 48 well plates and absorbance was measured using a plate reader. The readings were compared using two-way ANOVA. Error bars =SEM.

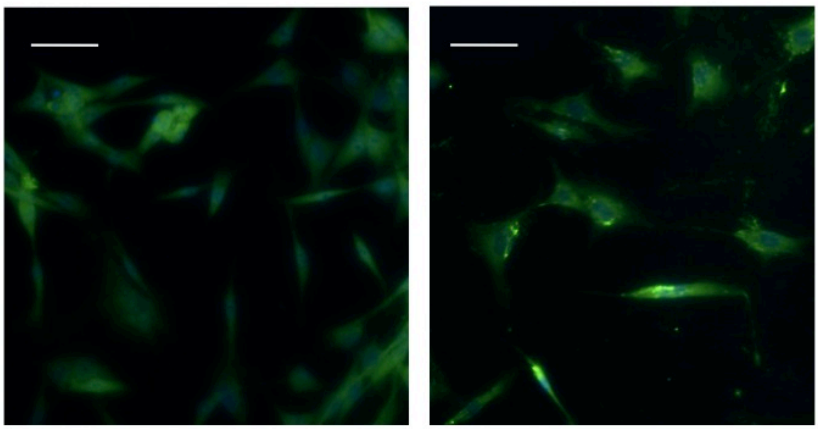

Figure 23 P75 NTR expression in forskolin/EGF treated OEC is similar to serum treated OEC.

OEC were grown in matrigel coated Labtek wells with DMEM/F12 with serum or forskolin/EGF. After seven days, the cells were fixed and immunostained for p75 NTR. The OEC in both groups showed strong staining for P75 NTR.

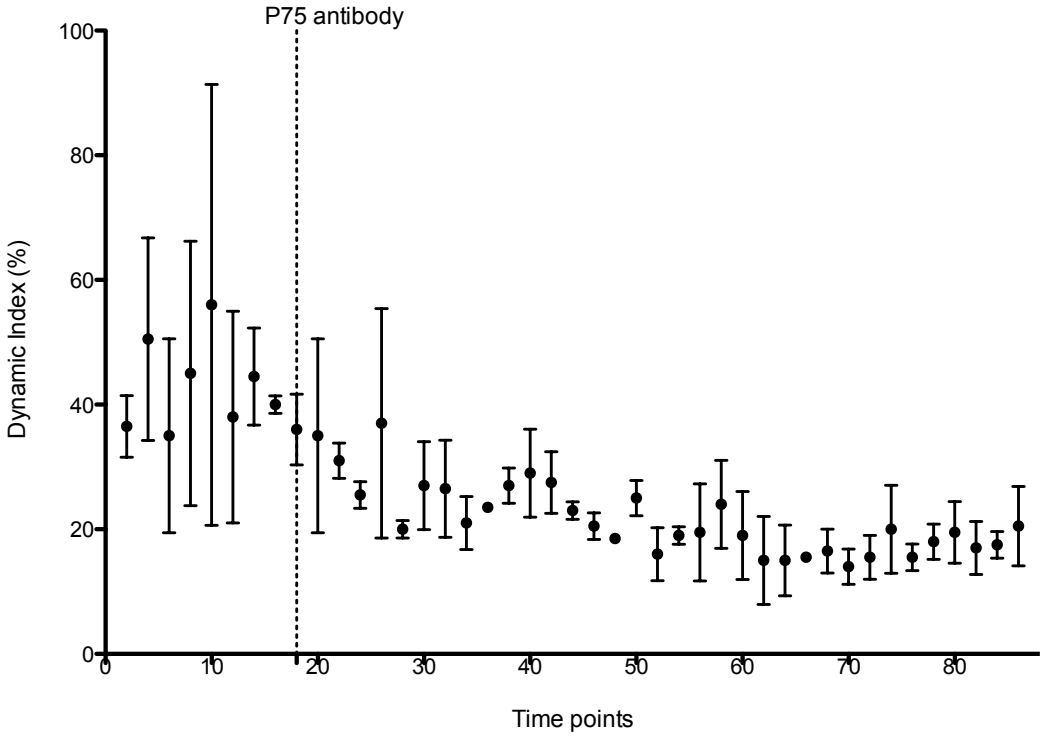

Figure 24 Blocking the P75 NTR by specific antibody reduces OEC motility.

We used time-lapse light microscopy to capture the extension and retraction of the OEC process for 20 minutes, then added P75 antibody and recorded cell motility for another hour. We calculated the dynamic index, which is the fraction of the cell that is remodeled at each time point. The addition of P75 antibody reduces cell motility. Error bars represent SEM. The experiment was repeated four times and a total of thirty motile cells were analyzed. Non-motile cells were not included in the study.

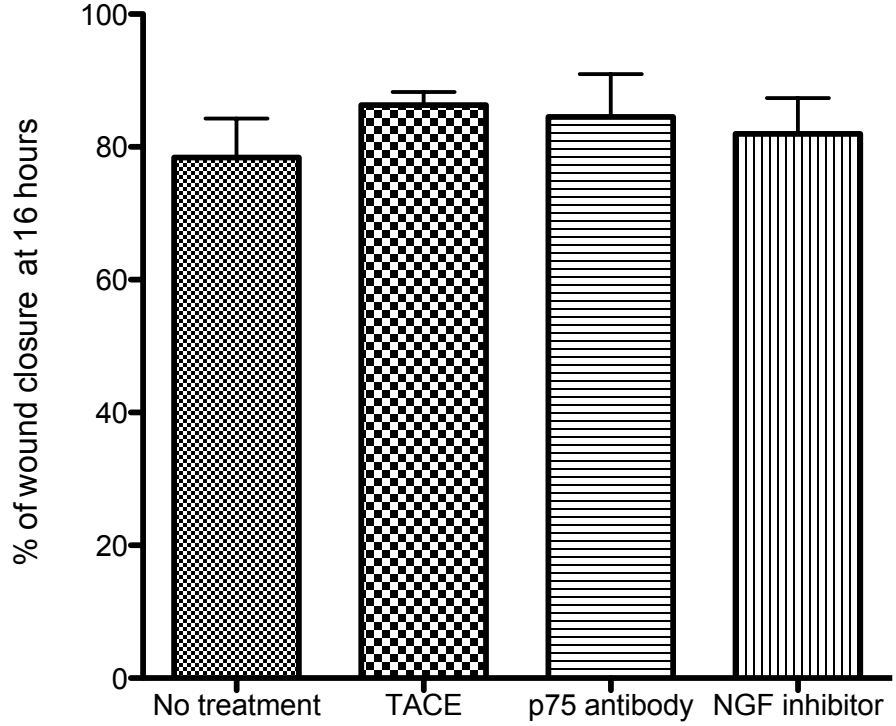

Figure 25 Substances inhibiting the binding of NGF to the p75 NTR have no significant effect on wound closure in an in vitro scratch wound assay.

P1 OEC were plated on 96 well flat bottom plates and incubated in DMEM/F12 media with 10% serum for 24 hours. The wound was made by scratching a straight line on the well using a sterile 10µl pipette tip held perpendicularly to the surface of the well. Fresh media with/without inhibitors replaced the previous media. The phase contrast images of the wound were captured at time points 0 hours and 16 hours using an inverted microscope. The percentage of area of wound was measured using Image J software and compared by one-way ANOVA. Inhibition of NGF binding to the p75 NTR has no significant effect on wound closure in this assay.

Phagocytosis by OEC

Experiments to study the interactions of RGC and OEC *in vitro* are discussed in detail in chapter two. Upon immunostaining the co-cultures for OEC and RGC markers and DAPI to stain for nucleus, we noticed that OEC cytoplasm (only in the co-cultures) had specs of nuclear material, but not in monocultures of OEC.

Therefore, we decided to study the potential phagocytic activity by the OEC. Since OEC are known to phagocytose neuronal debris (Chuah et al., 1995), we hypothesised that, in the co-culture of RGC and OEC, OEC endocytose apoptotic/necrotic RGC. Another possible source of the DNA material in the cytoplasm are other dead OEC in culture. However, we did not find DNA material when OEC were plated without RGC. Even though there are chances of OEC phagocytosing other unhealthy/dead OEC when plated with RGC, we wanted test the hypothesis of OEC phagocytosing dead RGC.

Primary RGC were cultured on cover slips for six days. On the sixth day, 3μM solution of propidium iodide (PI) were added to the culture media on the cells and incubated for 10 minutes at 37^0C. The media was removed and the cover slips were washed very carefully (not to detach any unhealthy RGC) with warm PBS and fresh, warm media was added. About 5000 OEC was added to each cover slip and cultured for 24 hours or 48 hours. Controls had OEC on PI treated cover slips.

The cultures were fixed and immunostained with Lysosomal-associated membrane protein 1 **(**LAMP1) antibody. The cover slips were mounted and imaged using confocal microscope.

We identified OEC by their glial morphology in the phase image. PI was imaged at 598nm.

PI staining was mostly confined to rounded RGC without any neurites. 48 hours after the co-culture, OEC cytoplasm showed specs of bright red

staining for PI. OEC nuclei were devoid of red staining. Monocultures of OEC did not have any PI staining in the cytoplasm.

It is therefore likely that in RGC/OEC co-cultures this nuclear material is derived from RGC. Alternatively, co-culture with RGC might induce OEC apoptosis. To confirm the source of the DNA material, we labelled the RGC nuclei before co-culture. This allowed us to track their fate after the OEC was added.

After 48 hours of co-culture, OEC displayed PI-positive cytoplasmic inclusions. In some OEC, the cytoplasm stained diffusely red. This could be due to digestion of the phagolysosomes and subsequent release of the PI dye in the whole cytoplasm. Importantly, PI staining was confined to the OEC cytoplasm; the OEC nuclei were devoid of PI.

The PI positive inclusions also colocalised with LAMP1 staining, which is a marker for lysosome. OEC cytoplasm generally expressed faint staining for LAMP1, but the LAMP1 staining was concentrated around the PI positive inclusions Figure 30. These findings confirm that RGC, not OEC, undergo apoptosis and that OEC display phagocytic /efferocytic activity when presented with apoptotic/ necrotic RGC.

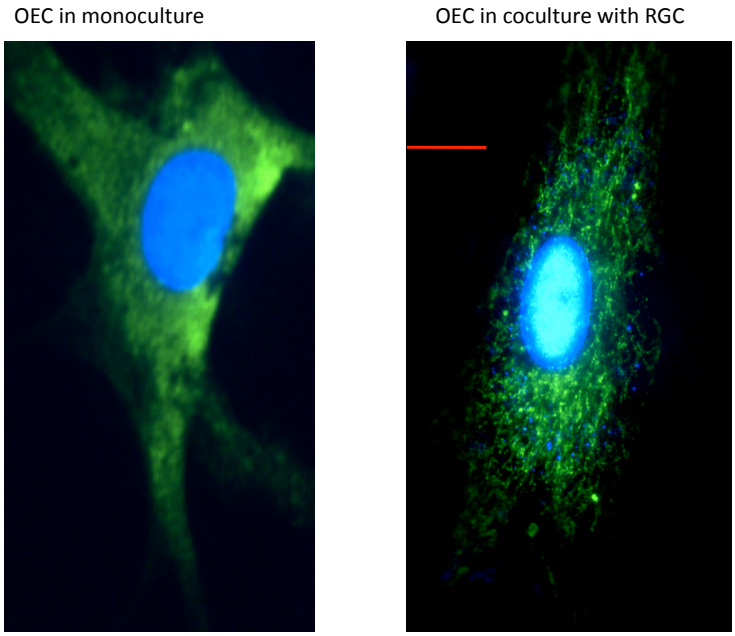

Figure 26 OEC cytoplasm contains fragmented nuclear material when co-cultured with RGC.

OEC and RGC were in co-culture for fifteen hours. The cells were fixed and immunostained for p75 receptor and DAPI. OEC in cocultures (right) has a strong P75 receptor expression in the cytoplasm and DNA material scattered throughout the cytoplasm. OEC in monoculture has diffuse p75 staining and do not display cytoplasmic nuclear material (left). Scale bars represent 25μm.

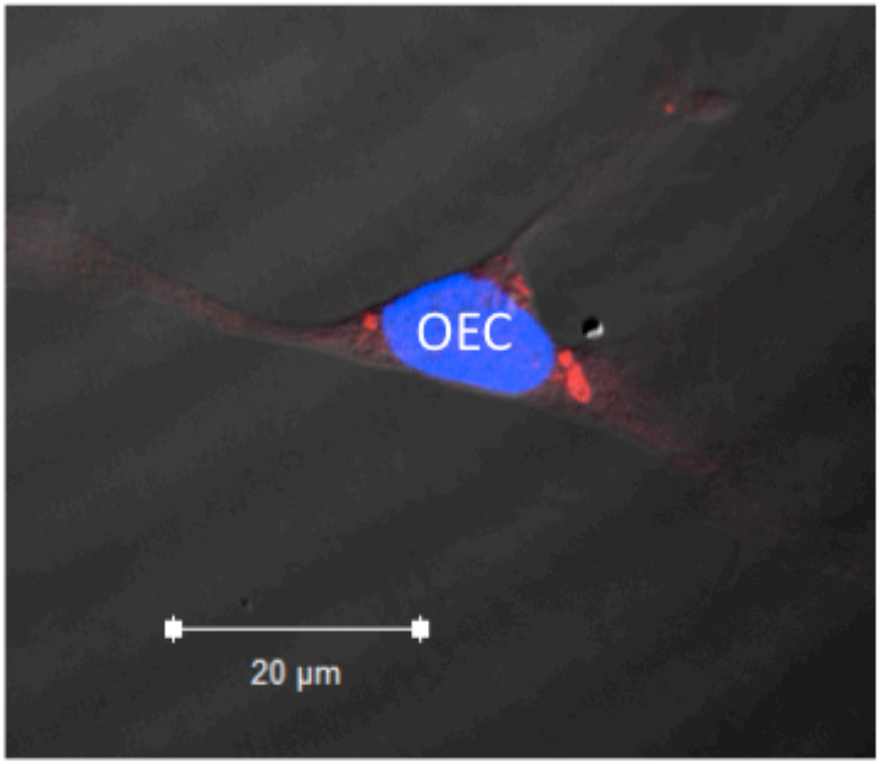

Figure 27 RGC debris in the OEC cytoplasm.

We labeled apoptotic/dead RGC with PI before adding OEC to the culture. After 48 hours of co-culture, cells were fixed and cover-slipped with Vectashield with DAPI. Phase and fluorescent images of OEC were captured with a confocal microscope. PI stained RGC nuclear material (red) is located in the cytoplasm of an OEC. The OEC nucleus stained blue with DAPI. The RGC nuclei in the OEC seem to be fragmented. The entire OEC cytoplasm appears slightly red. This could be due to residual PI in the cytoplasm after digestion of nuclear fragments.

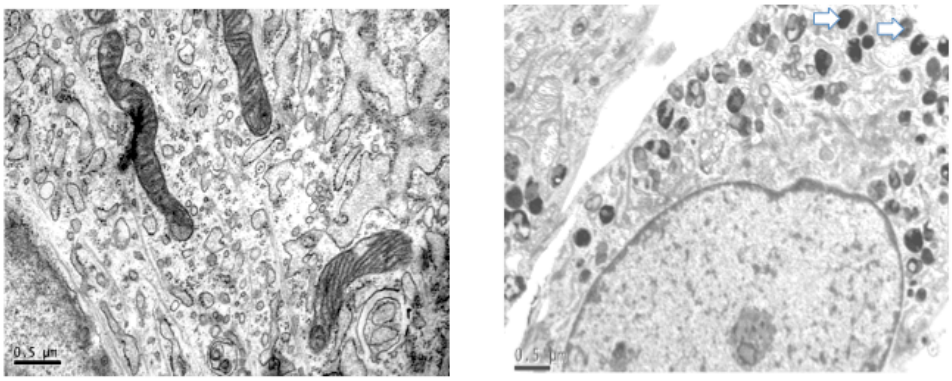

Figure 28 OEC in co-culture with RGC contain electron dense inclusions.

RGC and OEC were co-cultured for 48 hours, fixed and embedded in resin. Ultrathin sections were cut and imaged using TEM. The OEC cytoplasm displayed numerous electron dense inclusions, some of which were enclosed in a single membrane (arrows) and located at the periphery of the cytoplasm. OEC in monoculture (left) did not have similar inclusions. Scale bar represents 0.5µm.

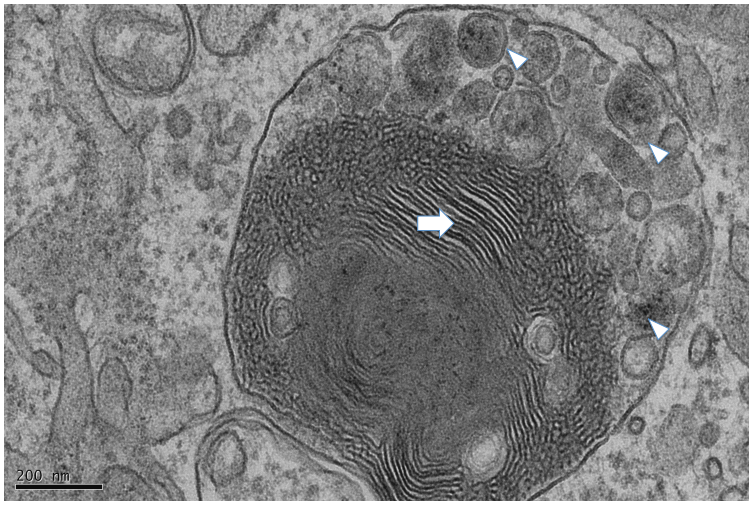

Figure 29 Vesicular organelles in OEC cytoplasm show phagolysosomal characteristics.

RGC and OEC were co-cultured for 48 hours, fixed and imaged using TEM. At higher magnification, vesicular organelles in the OEC cytoplasm displayed phagolysosomal characteristics such as enclosure within a single membrane (arrows) and electron-dense inclusions. Phagolysosome like single membrane bound structures were found with lysosomal membranes (arrows) and electron dense inclusions (arrowheads). Scale bar represents 200nm.

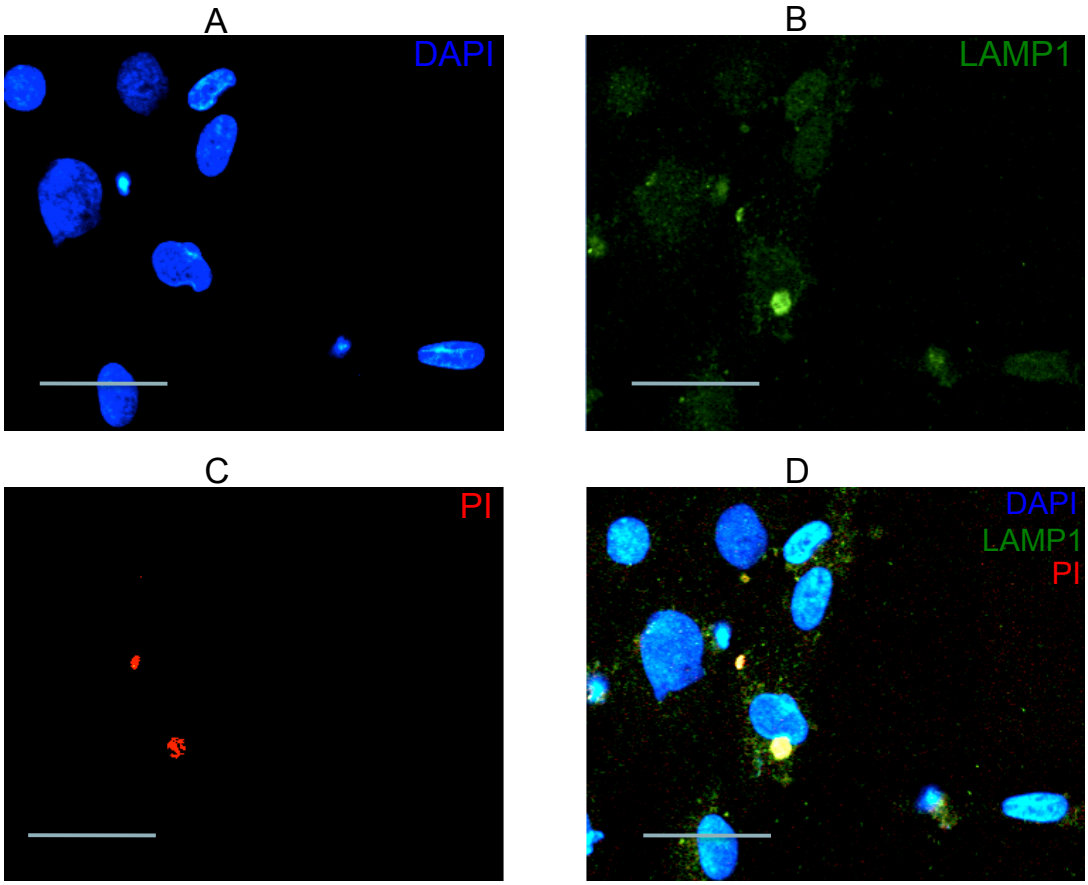

Figure 30 OEC lysosomes phagocytose RGC material.

We labeled apoptotic/necrotic RGC with PI (red) before adding OEC to the culture. After 48 hours of coculture, the cells were fixed and immunostained for lysosomal membrane protein (LAMP1) green. The cells were cover-slipped with Vectashield with DAPI to stain the nuclei blue. Two populations of OEC can be distinguished: those with and without cytoplasmic inclusions of nuclear debris. OEC without nuclear debris display uniform LAMP1 staining throughout the cytoplasm (green). In those with nuclear debris, LAMP1 staining is more intense around areas of debris stained with PI (red). A- Dapi staining only in blue. B- LAMP1 staining only in green. C- PI staining only in red. D- DAPI, LAMP1 and PI staining, areas of co-localisation of red and green appears as yellow. Scale bar represents 25µm.

Discussion

In rats, the p75 receptor in OEC is down regulated after birth and is strongly up regulated after lesion/injury (Gong et al., 1994). We did not find abundant p75 receptor expression in the adult rat mucosa, which could be due to the above-mentioned reason. Our antibodies were functional as we observed positive staining in cultured OEC. However, OEC *in situ* in the mucosa expressed other markers like GFAP and fibronectin.

We characterised our OEC cultures using immunostaining and RT-PCR techniques. Our cultures were over 97% pure population of OEC for at least two weeks in culture (based on GFAP, p75 and s100 expression). Olfactory mucosal cultures are generally reported to have p75+/gfap+/s100+ OEC and fibronectin+/thy1+ ONF, (Ramer et al., 2004), but in our assays, we did not find a major segregation until day 14. Keuh et al., has recently described highly proliferative stem cell-like p75+ cells derived from the olfactory mucosa that co-express fibroblast markers for over 14 days. These cells lose their proliferative ability after subsequent passages, but can provide sufficient cells for transplantation experiments (Kueh et al., 2011).

Our cultures are very similar to those mentioned by Keuh et al., (Kueh et al., 2011) in their proliferation and antigen expression.

The OEC also express mRNA of all the major neurotrophins including NGF, BDNF, NT3 and GDNF. Expression of BDNF, CNTF, and GDNF by OEC is well demonstrated (Woodhall et al., 2001, Wewetzer et al., 2001).

Electron micrograph of OEC showed abundant mitochondria, glycogen granules, rough endoplasmic reticulum and various membrane-bound organelles, which might sustain the highly active cells.

Serum free culture of OEC

We developed a serum free culture technique for OEC from the rat mucosa using forskolin and EGF. This could be applied to human

mucosal cultures which would be free of animal-borne pathogens and therefore safer. We have adapted the technique of Rahmatullah et al, for Schwann cell cultures. Similar to their observation, we found that forskolin or EGF alone did not promote the proliferation of OEC. These experiments also indicate that the functional mechanisms of both these cell populations might be quite similar. Proliferation of Schwann cells was attributed to the cyclic AMP (cAMP) release and *in situ* proliferation of glia in the phase of injury was proposed to be stimulated by cAMP release from the neurons (Rahmatullah et al., 1998).

Effects of P75 receptor antagonists in OEC migration and proliferation

Injury to the olfactory mucosa may induce OEC migration (Chehrehasa et al., 2011). As p75 receptor up-regulation coincides with the injury, the receptor could be a molecular switch, which activates migration in an otherwise dormant cell.

The scratch wound assay gives an idea of the rate of cell migration (Liang et al., 2007). The scratch wound assay showed that P75 receptor blocking does not affect the proliferation/migration of OEC. However, the calculation of dynamic indices of OEC following addition of P75 antibody showed that the cell movements are reduced to a certain extent by the blockage of the receptor. It is quite possible that the cell migration is controlled by multiple factors including the P75 receptor or, in the event of blockade of the P75 receptor; there might be alternative signalling pathways to facilitate migration and/or proliferation.

Serum starvation before the assay is supposed to keep cell proliferation to minimum. However, we could not serum starve the cells as OEC died during serum starvation. Therefore, cell proliferation may have contributed to wound closure in our experiment.

Phagolysosomes digest the endocytosed RGC debris

We have shown here for the first time that OEC can phagocytose dead RGC. Electron micrographs show dark, electron dense material enclosed in a single membrane in the periphery of the OEC cell body. OEC may internalise debris through phagocytosis- where the cell membrane of OEC engulf the debris, and pinch off into the cytoplasm forming an endosome. The endosome may fuse with lysosome(s). When the lysosomal enzymes are released, the debris could be digested completely. Electron micrographs show membrane bound structures with lysosomal membranes and electron dense material which support the formation of phagolysosomes.

Our experiments suggest that, OEC transplanted in the sites of neuronal injury might be able to clear the debris and thereby ease the problems associated with scar formation and inflammation, which might be a hindrance for regeneration.

Role of P75 receptor in phagocytosis

We have noticed that the OEC that phagocytose RGC debris had a strong P75 receptor expression than the surrounding OEC which did not phagocytose. This is a preliminary, but consistent observation in our studies. Wewetzer et al has reported that OEC that phagocytose axonal fragments and express them on their surface upregulate P75 receptor during the process (Wewetzer et al., 2005).

These data indicate the physiological relevance of upregulation of p75 receptor in OEC following olfactory nerve injury. The upregulation might be a key switch to initiate the sequence of signalling that regulates phagocytosis and regeneration.

Chapter two: Interaction of olfactory glia and neurites *in vitro*

Introduction

Olfactory ensheathing cell transplantation promotes regeneration of CNS neurites

In animal models of spinal cord injury, OEC transplantation contributes to the regeneration of axons with minimal branching and restoration of functional connections after spinal cord lesions (Li et al., 1997) (Verdu et al., 2001) (Lu et al., 2002) (Guntinas-Lichius et al., 2002). In successful axonal regeneration after transplantation, OECs exhibit a spindle shape, which may form a scaffold facilitating the regeneration of axons (Li et al., 1998). OEC also restore nerve function without noticeable axon regeneration, but the mechanism is unclear (Yamamoto et al., 2009).

OEC-filled conduits, transplanted into the transection site of facial motor neurons, encourage axonal sprouting but not functional improvement (Guntinas-Lichius et al., 2001). However, OEC transplantation along with microsurgical repair induces regeneration of sciatic nerve axons along with myelin formation by OEC. This results in functional recovery with formation of new nodes of Ranvier and enhanced conduction velocity due to the myelin formed by OEC around the regenerated axons (Radtke et al., 2009).

Regeneration of retinal ganglion cell neurites

Regeneration of RGC neurites has several challenges: overcoming glial scars (or activated astrocytes in the case of glaucoma), growth of axons and reconnection of axons at synapses. Experimental evidence shows that OEC can support the RGC axons in all these areas. But, in the case of RGC regeneration, the axons have to travel all the way from eye to the

lateral geniculate body and superior colliculus and therefore injection of OEC in the optic nerve alone might only be partially beneficial.

Effects of OEC in RGC regeneration

In vitro, OEC increase the number and length of RGC neurites that sprout from retinal explants (Leaver et al., 2006). This neurotrophic effect may be mediated by secreted, soluble factors and/or by direct contact with RGC. Direct contact of RGC with OEC stimulates neurite outgrowth significantly more than OEC conditioned medium from wild type OEC or OEC over-expressing CNTF (Plant et al., 2010).

RGC grown in the presence of OEC extend longer neurites than those cultured with Schwann cells or a mixture of Schwann cells and OEC (Moreno-Flores et al., 2003, Leaver et al., 2006). RGC neurites are longest in co-culture with OEC and astrocytes (Plant et al., 2010). Considering that astrocytes are inherently present in the optic nerve, OEC together with resident astrocytes might promote RGC regeneration.

Even though OEC are reported to successfully remyelinate CNS axons, OEC fail to myelinate RGC axons, whereas Schwann cells succeed *in vitro* and *in vivo* (Plant et al., 2002) (Li et al., 2007).

The co-culture of OEC with RGC *in vitro* is a useful tool to study the patterns of interaction of the two cell types as well as their effects on each other.

Markers for OEC and RGC in culture

We used immunocytochemistry to distinguish the antigenic differences between OEC and RGC. P75 neurotrophin receptor antibody was used to stain OEC selectively. RGC neurites were stained for neurofilament. Although early studies described the expression of p75 neurotrophin receptor by RGC, it was later well established that p75 receptor expression is located on Müller cell processes that cover the RGC cell body (Lebrun-Julien et al., 2009, Hu et al., 1999).

Electron microscopically, the two cell types can be differentiated according to their characteristic morphology and organelles. Glial cytoplasm has intermediate filaments and glycogen granules. Axons have parallel neurofilaments in the axoplasm. Synaptic terminals can be determined by the presence of synaptic vesicles in the presynaptic terminal and membrane thickening at the postsynaptic density.

We used three models of co-culture to study OEC/RGC interactions.

I. A cell line of ganglion cells (RGC5) isolated from rat pups
II. Primary RGC isolated from rat pups
III. Retinal organ culture from rat pups

RGC5 cell line

A cell line of RGC was developed and characterized by Krishnamoorthy et al. (Krishnamoorthy et al., 2001). The cells were isolated from P1 rat retina was transformed with the virus ψ2 EA1. Prof. Neeraj Agarwal (University of North Texas Health Science Center, Fort Worth, TX) kindly provided cells at passage 21. These cells express RGC markers including Brn3-c, Thy-1, intermediate filament proteins, NT like NGF, BDNF, NT-3, NT-4, CNTF and GDNF and neurotrophin receptors of the Trk family and p75 (Krishnamoorthy et al., 2001). RGC5 have been used to study pathways in apoptosis and regeneration of RGC (Tchedre and Yorio, 2008, Zheng et al., 2011). However, the cell line was re-characterised after controversial results, which led to the conclusion that RGC5 may be a progenitor of retinal photoreceptor rather than RGC (Van Bergen et al., 2009).

Aims

The aims of this chapter are

1. To culture RGC with long neurites to simulate the axons of the optic nerve.
2. To develop a stable culture technique to co-culture RGC and OEC *in vitro.*

3. To study the effects of OEC on RGC survival and neurite elongation.
4. To determine the effect of OEC-secreted factors and contact mediated response.
5. To study the effects of OEC on the formation of synapses between the RGC.
6. To study the effects of RGC on OEC.
7. To develop a model of optic nerve to study the functional effects of OEC on RGC neurites

Methods

Isolation of primary cells and culture techniques are explained in the general materials and methods section, page 61 and 62.

Under standard conditions, about 50% of RGC plated on the cover slips survive at six days in culture. The remaining 50% detach.

Six days after plating RGC on cover slips, we added OEC/OEC conditioned media/plain media (for controls). We studied the interaction of the cells by fixing the co-cultures at fifteen hours, six days and two weeks time points and analysed the results using ICC/transmission electron microscopy.

Effect of OEC on number of surviving RGC and neurites

To study the effects of OEC on the number of surviving RGC and to test the effects of OEC secreted factors on RGC survival, we compared

1. Monoculture of RGC
2. Co-cultures of RGC and OEC
3. Monocultures of RGC cultured with OEC conditioned media
4. Monocultures of OEC

We fixed the cultures and immunostained for neuronal nuclei (NeuN) antibody and DAPI. NeuN is a neuronal specific nuclear protein (Mullen et

al., 1992) and is expressed only by RGC in the co-cultures. Twelve images were taken from each cover slip using a Leica 700 confocal microscope. The number of nuclei stained with DAPI and NeuN was counted in each group and compared using ANOVA.

Prior to neuronal death, blockade of transport leads to accumulation of cytoskeletal structures referred to as beading (Takeuchi et al., 2005). To study if OEC offered any protection to neurites, we quantified the beads in monocultures of RGC and co-cultures of RGC and OEC Figure 43. We immunostained the cultures for neurofilament antibody and counted the number of beads along 1mm length of neurites starting from the nucleus. The two groups were compared using Student's t-test.

Effect of OEC on RGC synapse formation

Primary RGC cultured on glass cover slips can form synapses (Kucukdereli et al., 2011). We hypothesised that the increase in the number of surviving RGC and healthy neurites might increase synapse formation between RGC.

Synaptotagmins (Syn) are membrane proteins found in the presynaptic terminals of neurons. They are important calcium sensors and regulators of neurotransmitter release (Zimmerberg et al., 2006).

To study the effects of OEC on synapse formation, we co-cultured RGC and OEC for two weeks. We compared monocultures of RGC and monocultures of OEC with co-culture of RGC and OEC using Student's t test after immunostaining for synaptotagmin protein and neurofilaments.

Retinal explant culture

Approximately E15 rat retina was used for explants. The retinal quadrant was placed on polymerised Matrigel gels, and another 50µl of Matrigel was added on top of the explant so that the explant was sandwiched between two layers of Matrigel. The dishes were incubated at 37^0C for thirty minutes before adding neurobasal-A media with BDNF and CNTF.

To compare the length of neurites, retinal explants from embryonic and postnatal day three rats were cultured for three days and fixed with 4% PFA and imaged using a phase contrast microscope. The neurites were measured using Image J software and analyzed with Student's t-test.

In vitro model of optic nerve

To develop an in vitro model of the optic nerve, we filled a 100mm plastic petridish with resin and inserted a mould into the resin such that the resin had a groove of 1mm (width) x 2mm (depth) across the centre of the dish as it hardened. At one end of the groove, there was a slightly wider pocket of about 3mm width. The dish was washed with 100% ethanol followed by PBS before use.

A piece of retina was placed in the pocket at the end of the groove and the groove was filled with matrigel. The matrigel with the retina was allowed to set for about 15 minutes and Neurobasal-A media with supplements and growth factors was added and cultured at 37^0C.

Results

Co-culture of RGC5 and OEC

RGC5 have a fibroblast like morphology and do not form long axons or dendrites like primary RGC Figure 31 Figure 33.

When co-cultured with OEC on plastic dishes, RGC5 proliferate faster than OEC, resulting in the disappearance of OEC in about 48 hours. No interaction occurs between the two cell types.

When cultured on collagen or Matrigel gels, RGC5 do not produce long processes. On co-culture with OEC on gels, the two cell types do not show any interaction Figure 32.

To study the interactions of OEC and neurites and explore the possibility of RGC myelination by OEC, we needed neurons with longer extensions. Our attempts to induce long neurites in RGC5 by application of

hydroxyurea failed (data not shown). As an alternative, we studied primary RGC cultures from postnatal rats. Compared to RGC5, primary RGC form long neurites Figure 33.

Co-culture of primary RGC and OEC

Despite the well-established neuro-regenerative and neuroprotective roles of OEC, none of the studies demonstrated myelination of RGC axons *in vitro* or *in vivo* (Plant et al., 2002) (Li et al., 2007). We cultured primary RGC in an attempt to obtain long neurites to facilitate OEC myelination.

Primary RGC were isolated from rat pups, postnatal day one, and grown on cover slips as described in page 62. After six days in culture, the RGC formed neurites up to 4mm long.

At this stage, we plated around 10,000 p1 OEC on top of these RGC, and co-cultured them for up to six days.

Over the first 24 hours of co-culture, no ensheathment takes place. Cell-cell contacts remain temporary, with OEC protrusions transiently adhering to RGC bodies and neurites. The OEC form temporary contacts at various parts of the neurite to aid attachment and further alignment.

Fifteen hours of co-culture

On confocal images of immunolabelled cells, the initial point of contact of the two cell types appears to be at the bulbous growth cones of the neurons and the cell body of the glia. Processes of OEC make discontinuous contacts with the neurites, where they wrap around the neurites like tendrils Figure 34. The OEC exhibit a fibroblast-like morphology with short and stubby processes.

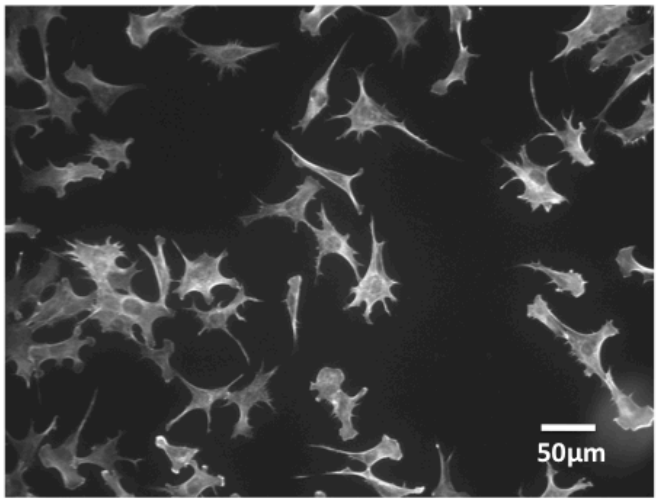

Figure 31 RGC5 have short processes and do not extend long neurites.

We grew RGC5 on matrigel coated glass cover slips; we stained for phalloidin to visualize the cytoskeleton. The cells have short processes and do not produce long neurites.

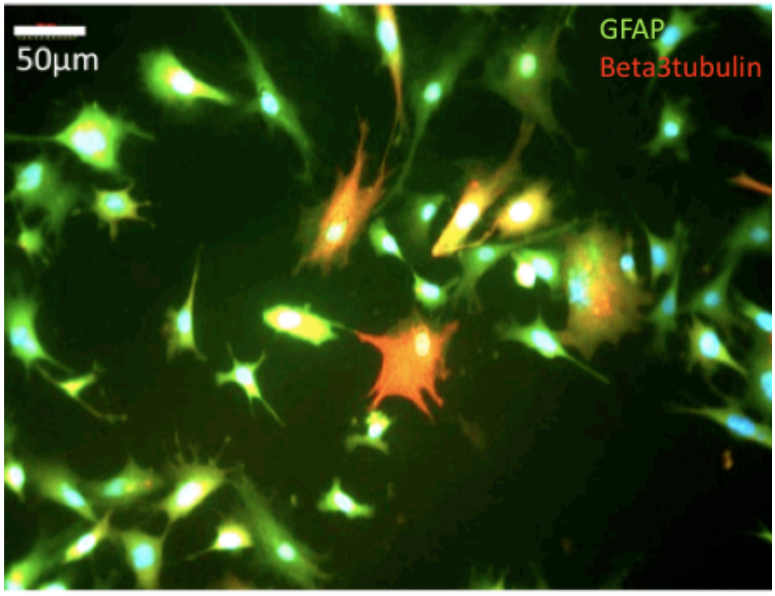

Figure 32 In co-cultures on matrigel, RGC5 and OEC intermingle, but do not form cell-cell contacts.

RGC5 cells and p1 OEC were mixed with matrigel and cast on circular wells of mattek dishes. After co-culturing for 48 hours, the cells were fixed. OEC were immunostained for GFAP in green and RGC5 in red for beta3tubulin. The cell types intermingle but do not form cell-cell contacts.

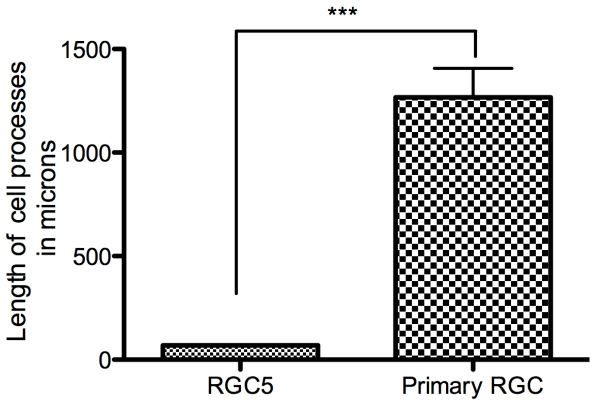

Figure 33 RGC5 cells have short processes when compared to primary RGC isolated from neonatal rat pups.

RGC5 cells and primary RGC isolated from neonatal rat pups were plated on separate glass cover slips. The cultures were maintained in their respective media for three to four days, fixed and immunostained for cytoskeletal markers (actin / neurofilaments). The images were viewed using an epifluorescence microcope and captured using a digital camera. The images were analyzed using Image J software and the length of the whole cell including the processes was measured. The length of the two cell types was compared using Students t test. Primary RGC were significantly longer than RGC5 cells; $p<0.0008$, $n=15$.

Six days in co-culture

At day six in co-culture, we observed two groups of OEC: those in close contact with the neurites; these extend thin, elongated processes around the neurites, partially enveloping them Figure 35. OEC without neuronal contact remain short and stubby. We also observed morphological differences between RGC that are in contact with OEC and those that are not. The neurites that were at least partially ensheathed by OEC were straight, whereas those that do not come in contact with OEC are tortuous Figure 38.

Electron micrographs show that neurites are indeed ensheathed by OEC processes Figure 36. Occasionally, the OEC processes engulf the bulbous tip of a neurite. The interface of the two cell types does not show morphological signs of signal transmission between RGC and OEC, i.e, no junctions.

Two weeks in co-culture

After two weeks in co-culture, three-dimensional images show that RGC neurites are completely surrounded by thick OEC processes Figure 37. Cells ensheathing neurites strongly express the p75 receptor, whilst OEC not in contact with neurites show only weak expression Figure 37 and Figure 42.

In areas of high neurite density, OEC bundle neurites together, resulting in parallel running neurites organised within a tube of OEC Figure 40 and Figure 41. In contrast, neurites of RGC in monoculture invariably follow a random course; bundling is never seen Figure 39. OEC tubes do not cover the neurites throughout their length. It is not clear whether the neurites in one bundle belong to different RGC.

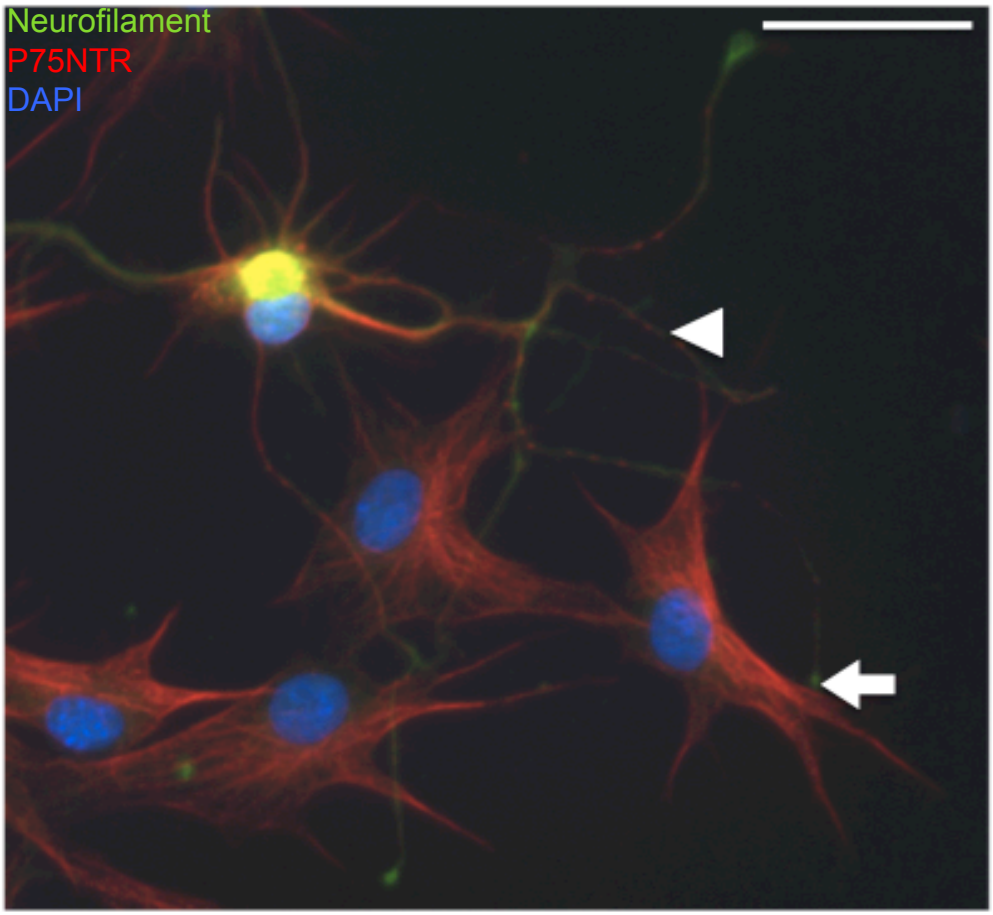

Figure 34 OEC (red) processes are apposed to RGC (green) neurites.

OEC and RGC were co-cultured on glass cover slips for fifteen hours, fixed with PFA and immunostained for P75 receptor and neurofilaments. The arrowhead indicates a point of contact. The neurite growth cone extends towards the OEC- indicated by the arrow. The experiments were repeated four times. Scale bar- 50µm.

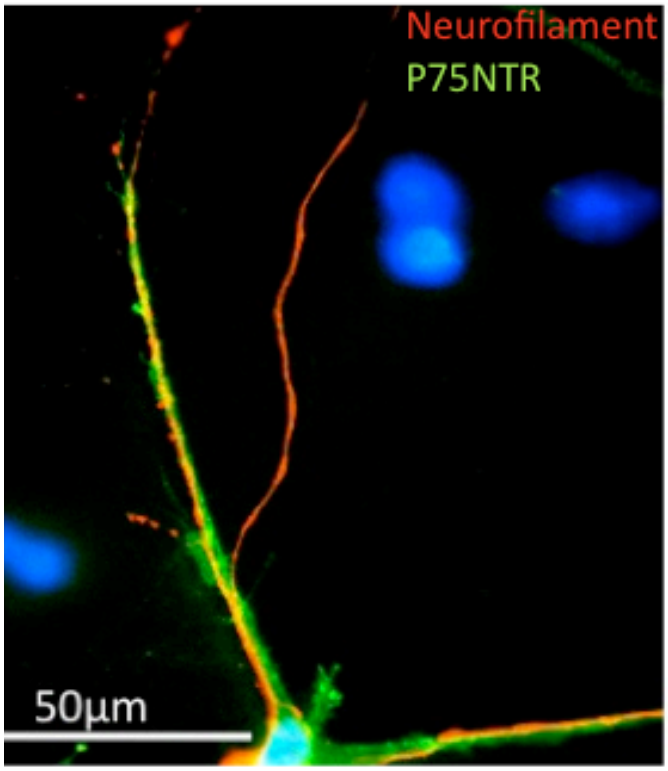

Figure 35 Partial ensheathment of a neurite in a co-culture of primary RGC and OEC after five days.

OEC and RGC were co-cultured on glass cover slips for five days, fixed with PFA and immunostained for P75 receptor in green for OEC processes and neurofilaments (red); ensheathment caused overlap of both colors (yellow). Branching off the ensheathed neurite is a non-ensheathed one which has a wavy course when compared to the ensheathed ones that are straight. The experiments were repeated four times.

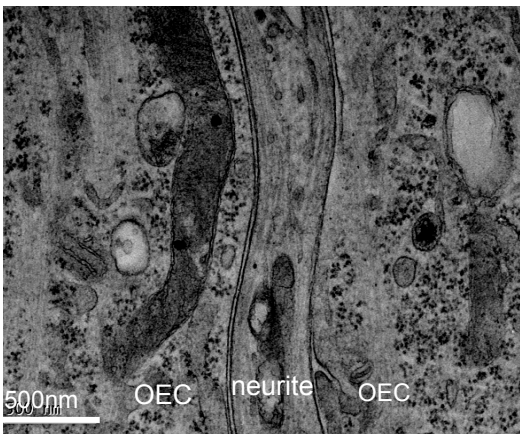

Figure 36 Olfactory glia ensheath RGC neurite at six days in co-culture.

Transmission electron micrograph of OEC and RGC co-cultured on glass cover slip for six days. In the figure, the neurite is identified by the parallel arrangement of neurofilaments and glia is identified by the presence of large amount of glycogen in the cytoplasm. The figure shows the intricate association of glia and neurite in culture. The experiments were repeated four times.

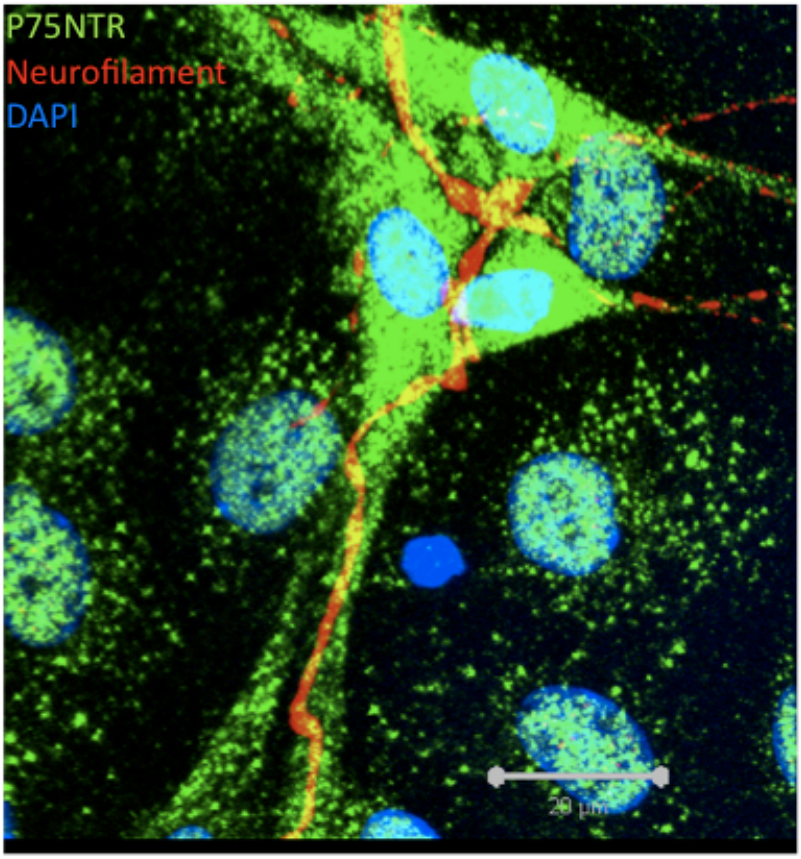

Figure 37 OEC that ensheath RGC neurites express p75 NTR more strongly than non-ensheathing OEC in the vicinity of RGC.

OEC are immunostained green for the marker p75 and neurites are stained red for neurofilament.Thick processes of OEC ensheath the neurites. Note the high p75 expression in the cytoplasm of OEC ensheathing the neurites. The OEC in the background that are not in contact with the neurites have scarce p75 expression. Scale bar represents 20µm. The experiments were repeated four times.

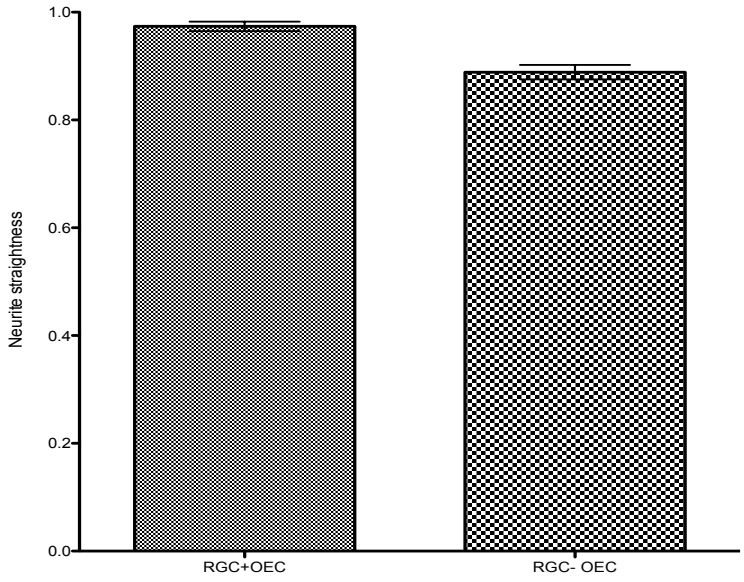

Figure 38 When co-cultured with OEC, RGC neurites are significantly straighter than in monoculture.

OEC and RGC were co-cultured on glass cover slips for six days, fixed with PFA and immunostained for neurofilaments; straightness of the neurites were calculated from ratio varying between 0 (not straight) and 1 (perfectly straight) defined as end-to-end distance between segment junctions divided by corresponding actual end-to-end lengths of neurites divided by the sum of curve lengths. The straightness was compared with unpaired t test. The straightness of RGC neurites is significantly greater in co-culture than in monocultures, $p<0.0001$. Error bars represent SEM, n=20.

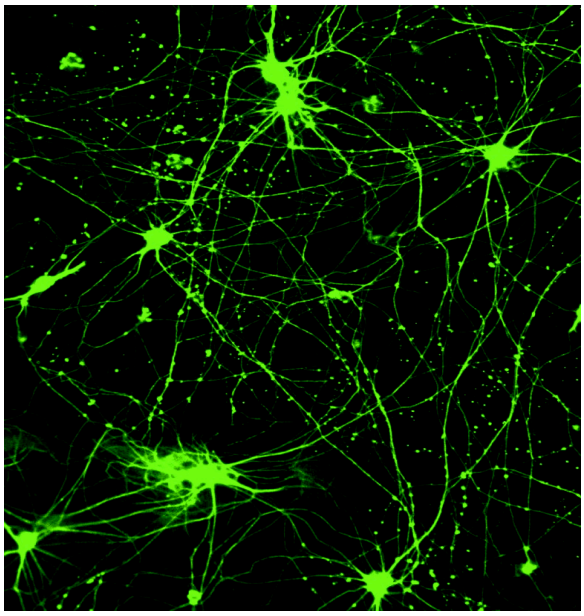

Figure 39 RGC neurites in monocultures have a random arrangement and do not form bundles.

Monoculture of RGC on cover slip; Neurofilaments are immunostained green. Note the RGC neurites spread at random on the cover slip.

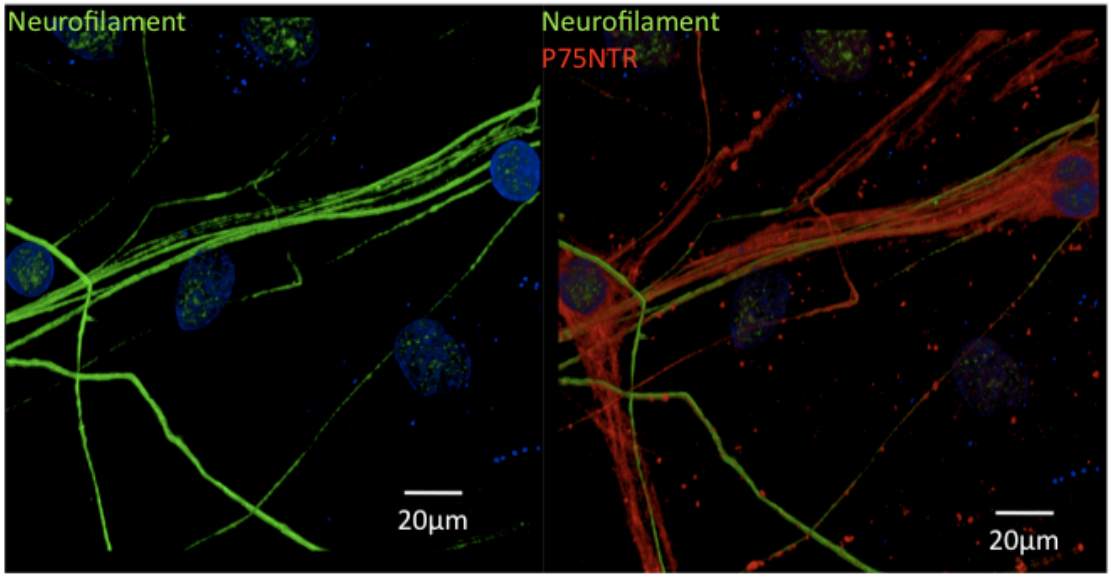

Figure 40 On co-culture, OEC arrange RGC neurites to form a bundle ensheathed by the OEC cytoplasm.

Co-culture of RGC and OEC; Neurofilaments are immunostained green, P75 is red and DAPI is blue. The figure in the left shows the number of neurites that are aligned in a straight line. The figure in the right shows the OEC processes engulfing the bundle. From the figure it is evident that an OEC need not be confined to one neurite, but can ensheath several neurites.

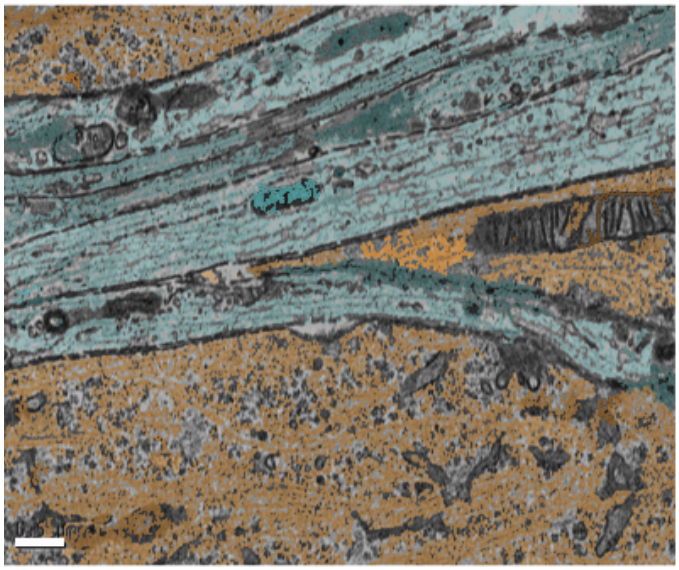

Figure 41 Transmission electron micrograph of OEC ensheathing a bundle of neurites.

Two weeks co-culture of RGC and OEC; image is false-colored, blue for neurites and orange for OEC processes. Neurites are identified by the parallel arrangement of neurofilaments and glia is identified by the presence of large amount of glycogen in the cytoplasm. Glial cytoplasm is seen surrounding the neurites. Scale bar represents 0.5µm.

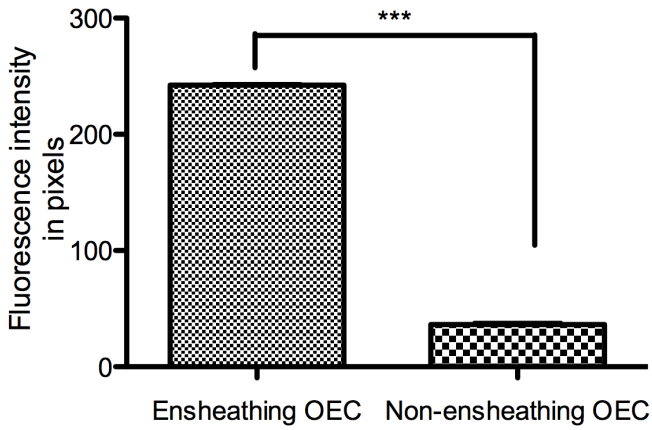

Figure 42 P75 receptor is heavily expressed by OEC that ensheath neurites when compared to OEC that are not in contact with neurites.

OEC and RGC were co-cultured on glass cover slips for two weeks, fixed with PFA and immunostained for P75 receptor and neurofilaments. The fluorescence intensity for P75 receptor along the cytoplasm of OEC was measured using image J software and the intensities of ensheathing and non-ensheathing OEC were compared using student t-tests. P75 expression was significantly stronger in OEC that ensheathed neurites than in OEC that did not contact any neurites, p=0.0002, n=6.

Long term co-culture

After three weeks of co-culture, OEC proliferation outgrows the culture dish. The cells lift off the cover slip as a sheet.

All the co-culture experiments involving primary RGC and OEC were repeated atleast four times. The cell interactions described above were consistent in all the experiments.

Effect of OEC on number of surviving RGC and neurites

In the presence of OEC, the number of surviving RGC is significantly higher than under the other conditions studied, namely the RGC treated with OEC conditioned media or RGC in monoculture $p<0.001$ Figure 46. OEC in monoculture do not express the marker for RGC nuclei, NeuN. There is no statistically significant difference between monocultures of RGC and RGC treated with OEC conditioned media.

In the presence of OEC, RGC neurites have significantly less beadings than in monoculture, $p<0.0001$ Figure 45.

Influence of OEC on synapse formation of RGC in culture

RGC neurites express significantly more pre-synaptic puncta in the presence of OEC than in monocultures, ($p<0.02$) Figure 47.

In the presence of RGC neurites, OEC also appear to express synatotagmin protein. This does not occur in OEC monocultures. Figure 49 demonstrates apparent synaptotagmin staining within the OEC cytoplasm surrounding a neurite on ICC. To investigate this further, we imaged RGC and OEC co-cultured for two weeks using TEM. TEM images reveal that OEC processes in fact closely surround synapses, indicating that synaptotagmin expression is restricted to RGC Figure 48.

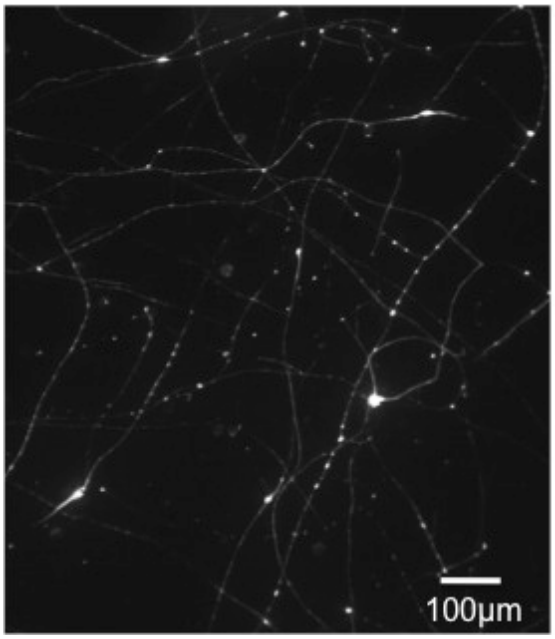

Figure 43 RGC neurites appear beaded after two weeks in culture.

RGC cultured on glass cover slip coated with laminin and poly-d-lysine for two weeks; fixed and immunostained for neurofilament antibody. Degenerating neurites appear beaded due to the accumulation of organelles.

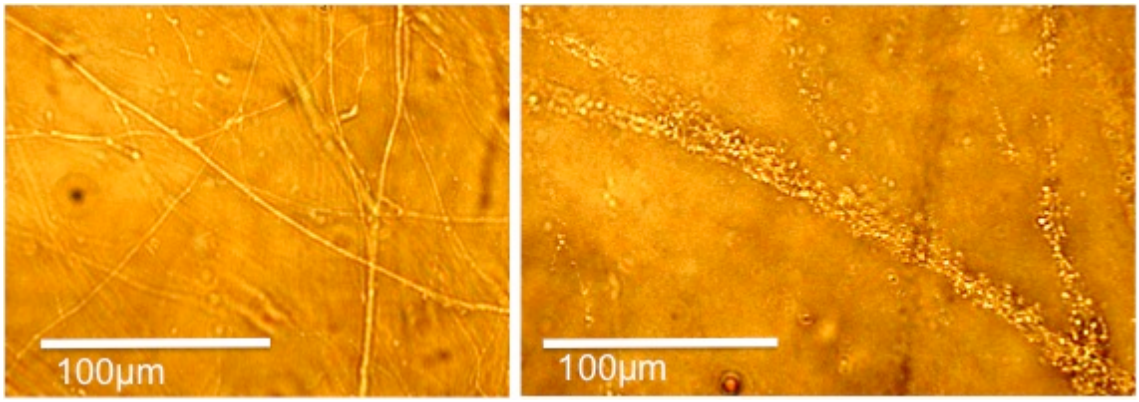

Figure 44 Phase contrast images of healthy and fragmented RGC neurites in culture.

The picture on the left is an intact neurite whereas the right one is fragmented. Upon addition of paraformaldehyde, the fragmented neurites lift off the cover-slip such that they can not be immunostained.

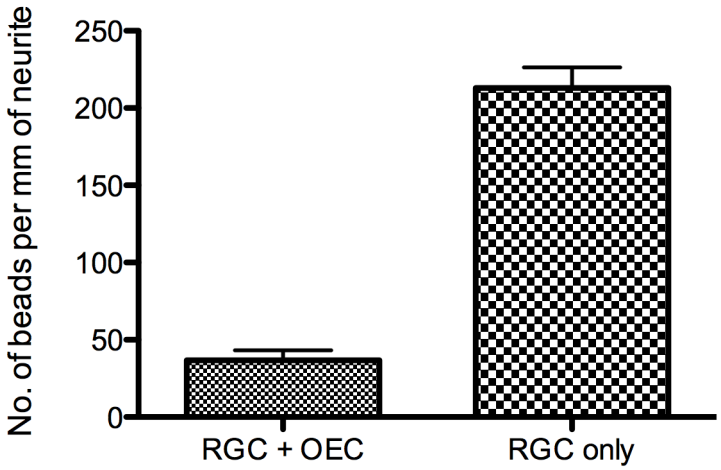

Figure 45 RGC neurites have significantly less beading in the presence of OEC than in monoculture.

Beads appear along the degenerating neurites as a result of accumulation of organelles and are therefore an indicator of neurite dysfunction. RGC neurites were found to have significantly higher number of beads in monocultures than in co-culture with OEC. The number of beads was counted and the two groups were compared with Students t test, $p<0.0001$. Error bars represent SEM.

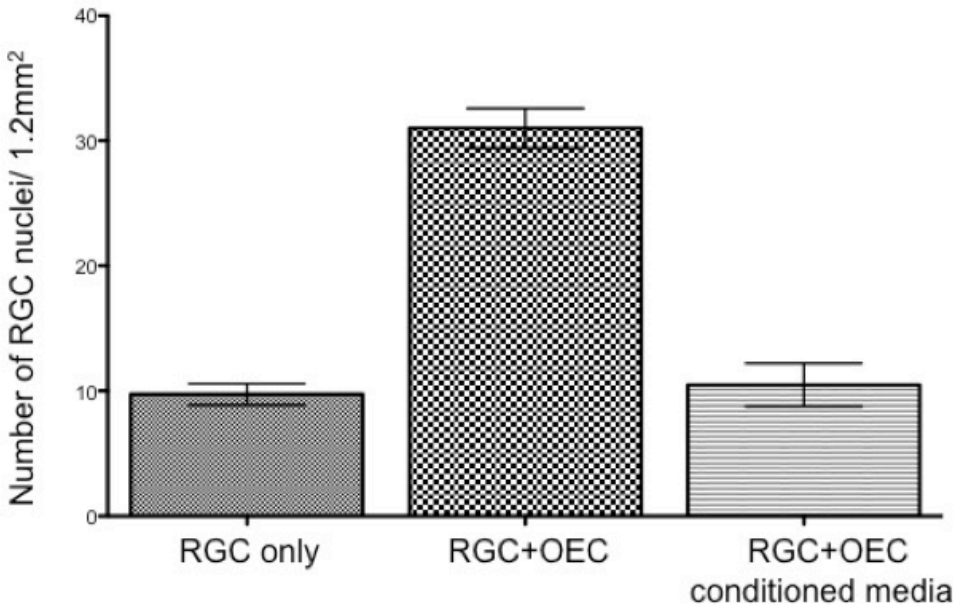

Figure 46 OEC enhance the number of surviving RGC after two weeks in co-culture.

The number of RGC in monoculture was compared to co-culture of RGC and OEC and RGC cultured with OEC conditioned media. The cultures were immunostained for NeuN, which selectively stains neuronal nuclei so that RGC could be distinguished from glia. The different groups were compared by ANOVA. In the presence of OEC, the number of surviving RGC is significantly higher than in the other groups, $p<0.001$. Error bars represent SEM.

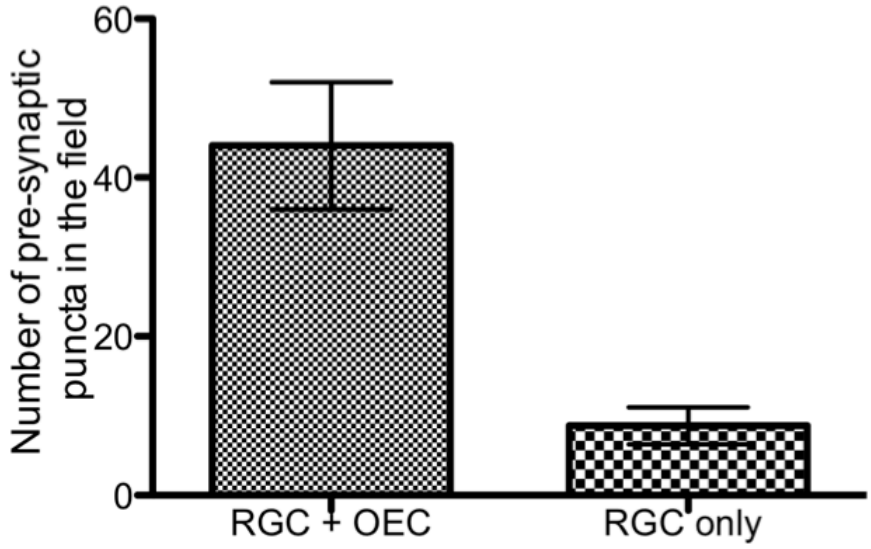

Figure 47 RGC neurites have a greater number of presynaptic puncta when co-cultured with OEC than in monoculture.

RGC and OEC co-cultured for 14 days and immunostained for synaptotagmin,which indicates the presence of pre-synaptic terminals. The number of pre-synaptic terminals in monocultures of RGC and co-culture of OEC and RGC were compared using students t test. The number of pre-synaptic terminals on RGC neurites is significantly higher in the RGC with OEC than RGC in monoculture, $p<0.02$. Error bars represent SEM.

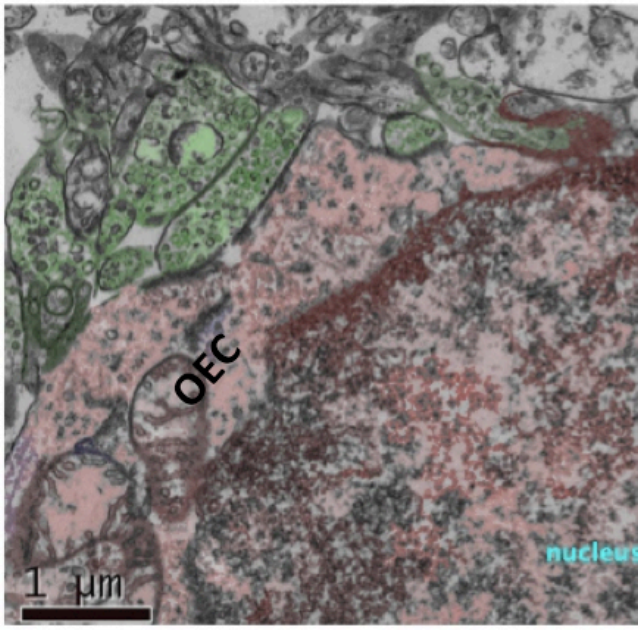

Figure 48 When co-cultured with OEC, RGC synaptic terminals were surrounded by an OEC.

RGC and OEC were co-cultured for 14 days and imaged using a transmission electron microscope. The image is false coloured, green for synapse and pink for OEC. The image shows the close association of OEC and the synapse. Scale bar represents 1µm.

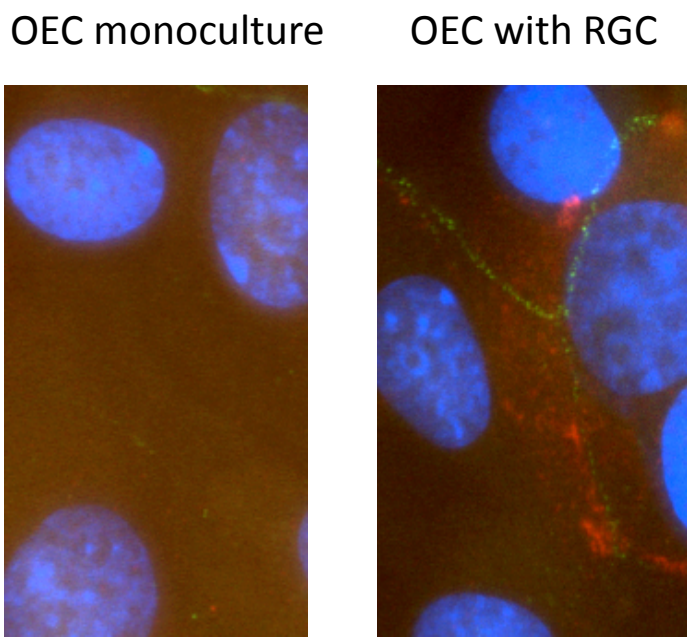

Figure 49 In the presence of RGC, OEC appear to express synaptotagmin protein.

RGC and OEC co-cultured (right) for 14 days and immunostained for neurofilament (green), synaptotagmin (red) and nuclei (stained blue with DAPI). OEC were identified by their large, oval shaped nuclei. Note that the synaptotagmin expression appears not to be on the neurite but in the OEC cytoplasm. The left figure is the OEC in monoculture which do not stain for synaptotagmin.

OEC and retinal culture on gels

Primary RGC isolated from the retina are sensitive to the matrix on which they grow. In our experiments, primary RGC survived only on laminin coated coverslips. Primary RGC plated on collagen/matrigel thick gels failed to produced neurites. Therefore, we tried to grow neurites from retinal explants cultured on thick gels. The methods of retinal explant culture is explained on page 63.

Samples with OEC and retinal explants display *in vitro* ensheathment of neurites by OEC. Initially, OEC attach to the outer border of the retina at right angle, parallel to the surface of the gel Figure 51. OEC, immunostained for p75 antibody, have long processes that wrapped around neurites Figure 52. Neurites ensheathed by OEC extend randomly through the gel, both horizontally and vertically.

Retinal explants from neonatal rats grew few neurites. In order to obtain longer neurites, explants were cultured from embryonic rats.

The retina from embryonic rats had significantly longer and denser neurites when compared to the explants from postnatal (day three) rats, $p<0.0001$.

Long neurites of the order of a few millimetres are necessary to perform electrophysiological studies. Measuring the nerve conduction velocity of the neurites in monoculture of RGC explants and co-culture of explants with OEC may contribute to our understanding of the effects of OEC on the function of neurites in future studies.

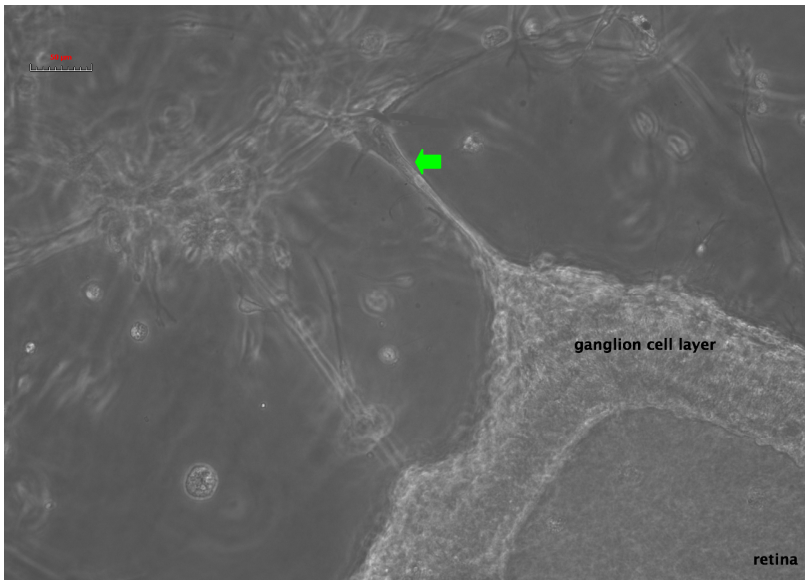

Figure 50 Retina and OEC (indicated by arrow) after 24 hours in culture on gel.

Pieces of retina were cultured on top of Matrigel gel, and OEC were added to the culture. After 24 hours, the culture was fixed with 4% PFA and the specimen was imaged using a phase contract microscope. OEC appear to extend cytoplasmic processes which adhere to the edges of the retinal explants and exert traction.

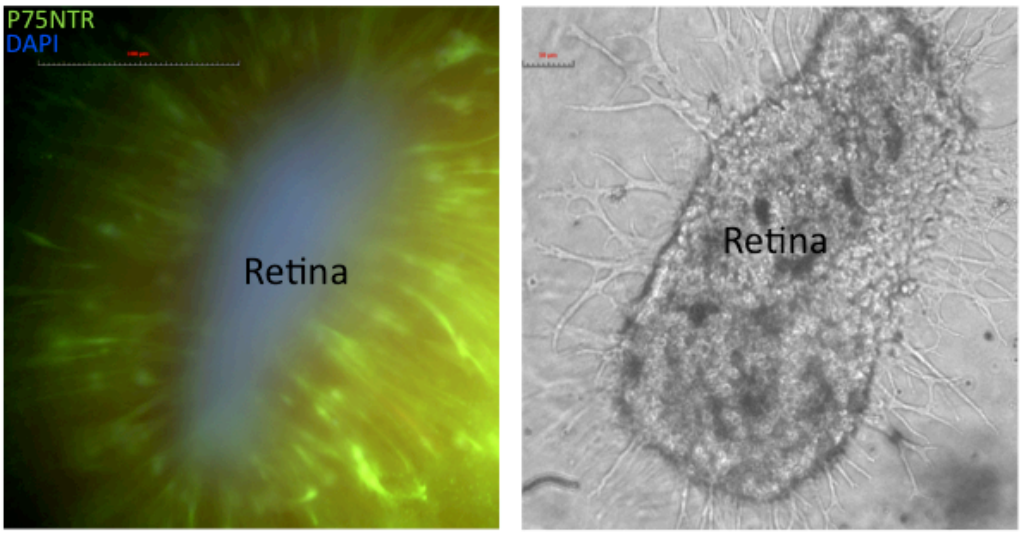

Figure 51 Fluorescent and light microscopic images of OEC anchored to a retinal explant on top of a gel.

Pieces of retina were cultured on top of Matrigel gel and OEC were added to the culture. After 24 hours, the culture was fixed and immunostained for p75 antibody (green) and DAPI (blue). The specimens were imaged using an epifluorescence microscope. The OEC in the culture appear to have attached to the retinal explants. The branching structures radiating from the sides of the retina stain positive for P75 receptor indicating that these cells are OEC. RGC neurites growing out from the explants are not clearly visible. Scale bar represents 100µm.

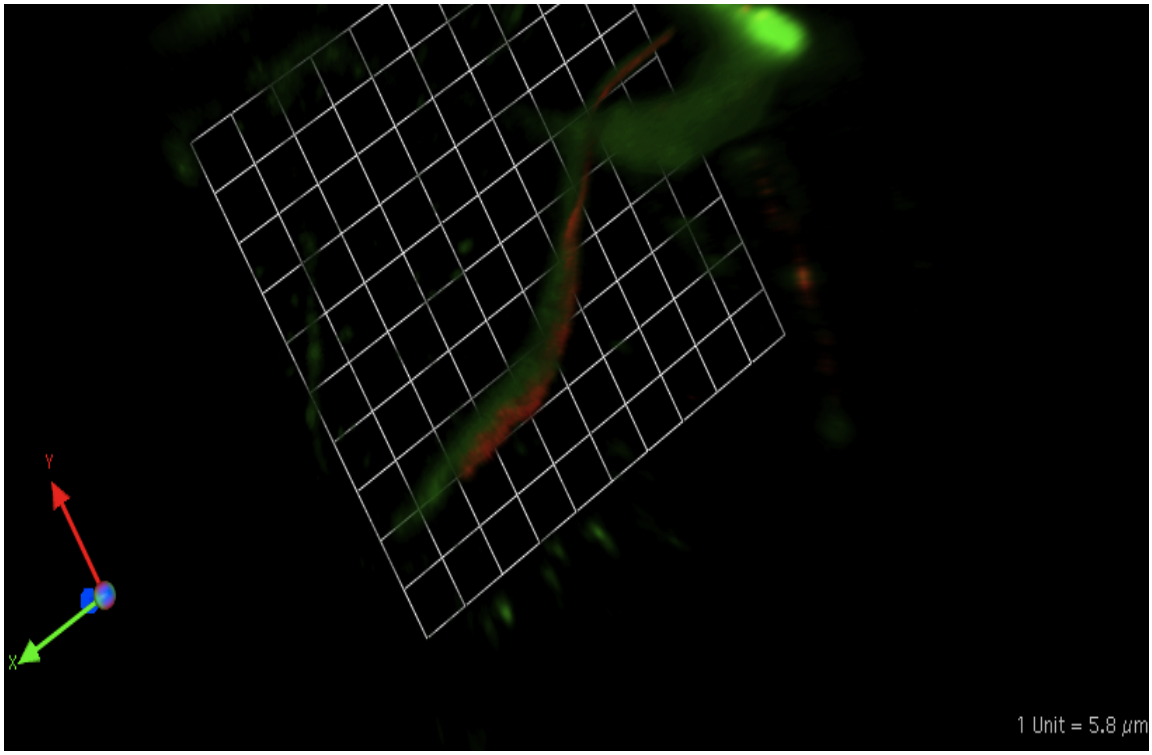

Figure 52 A three-dimensional reconstruction image of a neurite ensheathed by a process of an OEC in a gel.

Pieces of retina were cultured on top of Matrigel gel and OEC were added to the culture. After three days, the culture was fixed and immunostained for neurofilament (red) and for p75 receptor (green), the marker for OEC. The picture depicts the close apposition of the glial process to the back of the neurite and partial ensheathment at certain points.

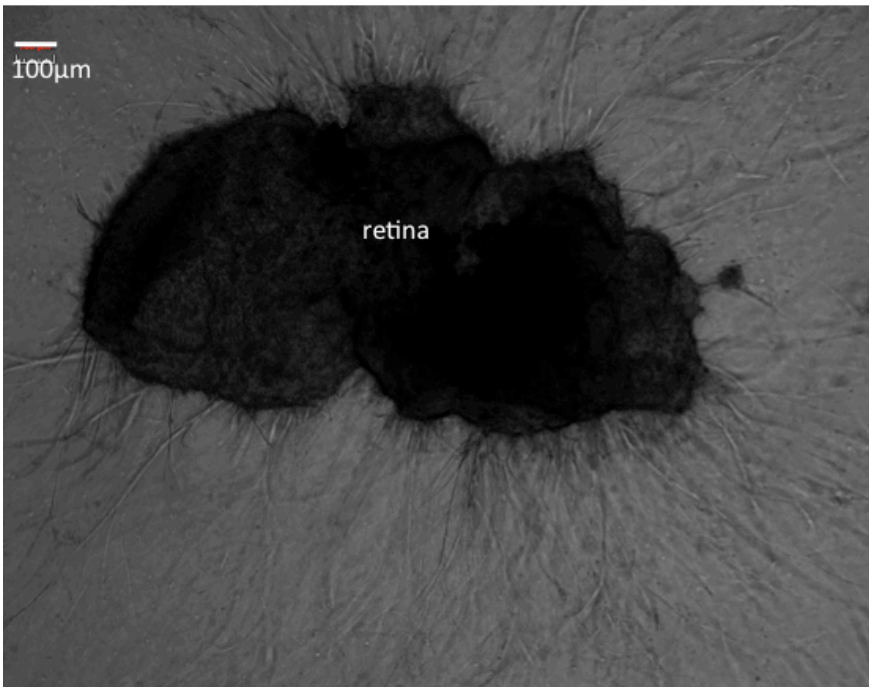

Figure 53 Retinal explants from (E15 rat pup) in a sandwich between two layers of matrigel.

Phase contrast image of tufts of neurites emerging out of the retina cultured on a dense Matrigel gel.

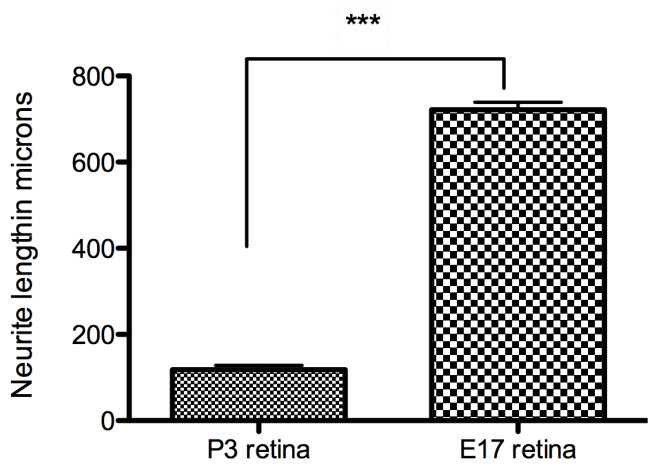

Figure 54 A comparison of neurite length from retinal explants of embryonic and postnatal rats.

Retinal explants from embryonic and postnatal day three rats were cultured for three days, fixed and imaged using a phase contrast microscope. The neurites were measured using Image J software and analyzed with Students t-test. The retina from embryonic rats had significantly longer and denser neurites when compared to the explants from postnatal day three rats, $p<0.0001$. Error bars represent SEM.

An *in vitro* model of optic nerve

Introduction

There is no established *in vitro* assay to study the optic nerve axonal structure and function. Primary RGC cultured on cover-slips and retinal explants on matrigel extend neurites in all directions. Neurite growth is not directional. This does not resemble the optic nerve where the axons travelling towards the brain are arranged closely within the nerve and are far from the cell bodies. In addition to morphology, functional assessment such as conduction studies would also be facilitated by the creation of structures with densely bundled axons. Therefore, we developed a new model where neurite outgrowth can be directed and concentrated in a grove such that it resembles the bundle of axons in the nerve.

Methods

35mm petridish was filled with resin. Before the resin polymerised, a mould was inserted into the centre to create a 2mm x 1mm groove with a pocket at one end Figure 55. After the resin has set, the dish was rinsed with ethanol, air dried and washed with PBS. A retinal explant was placed in the pocket which was then filled with matrigel. When the gel has set, media was added to the culture. After ten days the cultures were fixed using 4% PFA and images were captured using light microscope.

Results

After a week in culture, almost all the neurites that grow out from the explant are concentrated in the groove Figure 56. Even the neurites that sprout in the direction opposite to the groove turn around and grew through the matrigel in the groove. At ten days in co-culture, neurites grow to about five millimetres in the matrigel in the groove, away from the retinal explant.

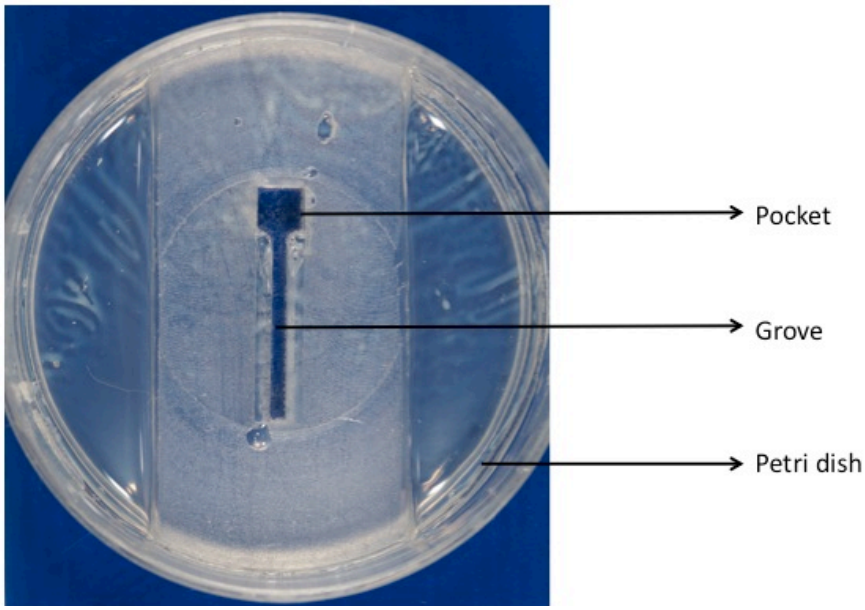

Figure 55 Custom made petridish for culture of an in vitro model of optic nerve.

The 35mm petridish was filled with resin. Before the resin polymerised, a mould was inserted into the centre to create a 2mm x 1mm groove with a pocket at one end. A retinal explant was placed in the pocket which was then filled with matrigel.

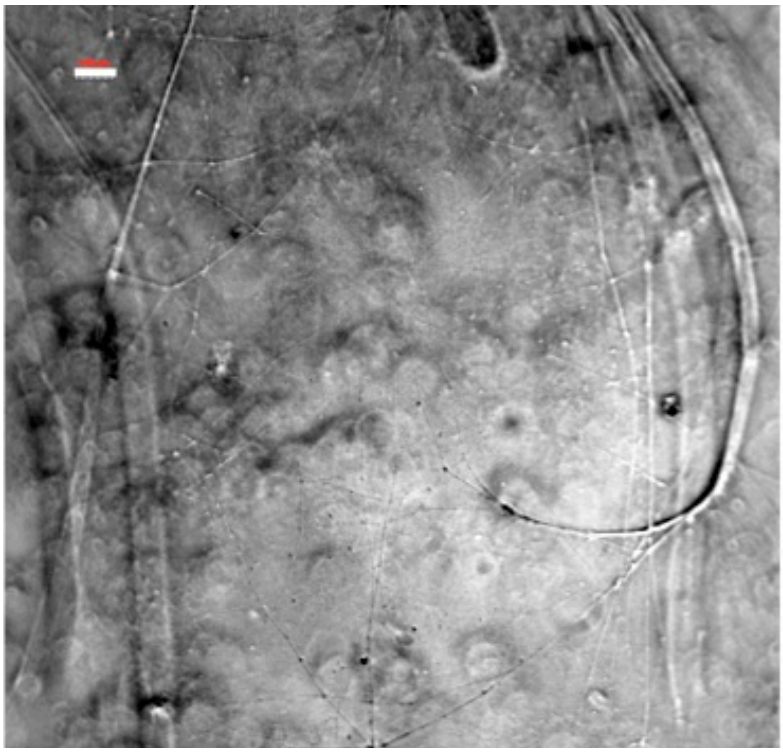

Figure 56 Retinal neurites were found in the groove of the Petri dish.

The neurites from the retinal explant in the pocket extend into the matrigel in the groove. After ten days in culture, the neurites extend about five millimeters in the groove. Scale bar represents 100μm.

Discussion

Our results indicate that, *in vitro*, OEC enhance the survival of RGC, support the maintenance of healthy neurites, ensheath RGC neurites and bundle them and influence their synaptic connectivity.

Ensheathment by OEC

In our assays, although OEC ensheathed the RGC neurites, they did not form “tubes” by aligning end-to-end neurite bundles. Longer observation periods may have resulted in tube formation rather than ensheathment.

Influence of OEC in RGC synaptic formation

We found that OEC participate in synapse formation like astrocytes and Schwann cells.

In the CNS, astrocytes surround synapses and modulate synaptic activity, a phenomenon known as “the tripartite synapse”. In tripartite synapses, in addition to the classic components of pre- and post-synaptic terminals, a third perisynaptic glial process also comes into action. In these synapses, astrocytes are responsible for information processing in response to synaptic activity and trigger neuronal firing in reaction to inputs (Araque et al., 1999), (Araque et al., 2002), (Parri et al., 2001, Pasti et al., 1997).

Schwann cells are another glial cell type known to control the release of neurotransmitters, such as at the neuromuscular junction in frog (Robitaille, 1998). Glial cells can possibly endocytose excess neurotransmitters released from the synapse and thereby prevent excitotoxicity (Bergles and Jahr, 1997).

One of the major hurdles in CNS regeneration experiments is the loss of synaptic plasticity past embryonic stages. The close association of OEC with synapses might indicate that OEC can play a role in the regeneration and rewiring of CNS axons. However, further studies are needed to

confirm the role of OEC in synaptogenesis in neuronal regeneration *in vivo*.

P75 receptor expression by OEC

We found that OEC that ensheath the neurites heavily express p75 receptors when compared to OEC that did not make contacts with neurites. Whether the P75 receptor expression is increased due to its contact with the neuron or whether only OEC with high P75 receptor expression were able to make contact with the neuron is not known.

OEC are often described as “olfactory Schwann cells” because of the similarity of the two cell types. Schwann cells facilitate axon regeneration associated with high expression of P75 receptor following nerve injury (You et al., 1997). Therefore, it is reasonable to suggest that a similar mechanism might be present in OEC.

Moreno-Flores et al., described enhancement of RGC regeneration by an OEC cell line. Their finding suggest that P75 receptor has no role in neurite regeneration (Moreno-Flores et al., 2003) . However, the cell line has a different expression profile from that of primary cells even though the reparative properties are not affected.

In the context of glaucoma, our studies provide an insight into the basic interactions of OEC with the axotomised and degenerating RGC axons. Importantly, we have shown that OEC can endocytose apoptotic RGC, which might have translational implications.

Disrupted axonal transport of RGC in glaucoma is well established (Hollander et al., 1995). Beading of neurites observed *in vitro* in our experiments could be due to compromised axonal transport. The fact that OEC can reduce RGC beading *in vitro* supports the possibility of neuroprotection of RGC by OEC.

Primary RGC and retinal explants undergo axotomy during isolation and regenerating neurites in these models are not exactly similar to the optic nerve axons *in vivo*. Also, our culture conditions lack extracellular matrix and cells that would modulate RGC behaviour, such as the astrocytes.

A three-dimensional culture of RGC, retinal astrocytes and OEC might even help us understand and predict the effects of OEC on glial scar and RGC regeneration in various retinal diseases.

In vitro model of optic nerve

This assay creates an *in vitro* model of the unmyelinated optic nerve which could be useful in testing the response of axons to experimental conditions without the interference of oligodendrocytes or astrocytes which are normally present in the nerve *in situ*. It could also be used for screening cell types for myelination/ensheathment studies *in vitro*.

Chapter three: Experimental glaucoma in rodent models

In the previous chapter we discussed the *in vitro* interactions of RGC and OEC and the protective effects of OEC on RGC neurites. We wanted to test if OEC can protect/ control the damage of RGC axons in glaucoma. In order to test this, we needed an experimental model of glaucoma where we could introduce OEC into the diseased eye.

Several animal models of glaucoma, especially cost effective rodent models are described in the literature Table 1. Since we wanted to eventually inject cells into the glaucomatous eyes, maintaining a clear visual axis along with minimal inflammation to the eyes were the main criteria to select an animal model.

The aim of this chapter is to develop a glaucoma model based on well established techniques and characterise the elevation of IOP and changes at the optic nerve head and axons.

We tried the following models of experimental glaucoma

- Steroid induced ocular hypertension in mouse eyes
- Hypertonic saline injection into the episcleral veins of rat eyes
- Polystyrene bead injection into the anterior chamber of rat eyes
- Magnetic micro-bead injection into the anterior chamber of rat eyes

Topical administration of corticosteroids to create a mouse model of experimental glaucoma

Corticosteroids and ocular hypertension

Corticosteroids (CS) are widely used in ophthalmologic treatments as anti-inflammatory agents. However, application of CS can induce a rise in intraocular pressure and subsequent glaucoma in some patients (Armaly, 1963a). About 30% of the general population might respond to corticosteroid treatment with a rise in IOP (Armaly, 1965). The percentage of steroid responders increase to 90% in primary open angle glaucoma patients and IOP falls at the cessation of steroid treatment (Armaly, 1963b). This increase in IOP is a significant side effect. CS that do not have an effect on IOP would have a significant clinical advantage.

CS treated eyes have extracellular matrix deposits (plaques) within the aqueous humour drainage pathway, in Schlemm's canal through the trabecular meshwork. These deposits increase resistance in the aqueous outflow pathway (Johnson et al., 1997). Since this condition is considered to be similar to primary open angle glaucoma, CS have been used to create experimental animal models of glaucoma (Sawaguchi et al., 2005) (Tektas et al., 2010). The use of CS to experimentally raise the IOP is well characterized in cattle, sheep, and rabbits and rats Table 4.

Table 4 summarizes animal models of steroid induced ocular hypertension. These animal models were mainly designed for the study of trabecular meshwork changes associated with ocular hypertension in glaucoma. Changes to retinal neurons or optic nerve axons were not assessed. In addition to pressure-induced changes, steroids entering the circulation might have secondary effects on the retinal neurons. This might complicate the understanding of primary glaucomatous damage in these animal models.

The effects of topically administered CS in mice however are not well characterized. Therefore we tested the effects of topically administered steroids in mouse eyes.

Methods

8 weeks old C57 BL/6J inbred mice were used in the study with 8 animals in each group. Each group received either prednisolone acetate 1% (Pred Forte) or loteprednol 0.5% (Lotemax), applied topically to the left eye using standard dropper bottles, average dropsize ~ 45µl. The right eye was the untreated control. The drops were stored at 4^0C and left at room temperature for about 30 minutes and shaken thoroughly just before application. The drops were applied twice daily during weekdays approximately at the same time (at 9.00 am and 4.30pm) and once daily during weekends for 35 days. Special care was taken not to allow the animal to accidentally ingest the drops from the dropper tips.

The IOP in both the eyes was measured using a rebound tonometer, the Tonolab (Tiolat), which is a well-established IOP measurement device (Johnson et al., 2008b) (Saeki et al., 2008). IOP measurements were taken before application of drops every day for the first week and thrice a week thereafter. IOP was measured by the same person throughout the experiment to reduce inter observer variability. An average of five readings were noted with all readings within three mm of Hg in each eye.

Results

There were no significant IOP changes in either group through out the 42-day observation period. However, the variability in the readings in each group was very high.

Table 4 Animal models of steroid induced hypertension.

Animal model	**Steroid tested**	**Frequency of administration of drops**	**Time required for IOP elevation**	**Reference**
Monkey	Dexamethasone and methyl prednisolone acetate	Thrice daily	**NO** IOP elevation after three months	(Armaly, 1964)
Cow	Prednisolone acetate (0.5%)	Thrice daily	IOP rise after 3 weeks; return to normal on cessation of drops.	(Gerometta et al., 2004), (Tektas et al., 2010)
Sheep	Prednisolone acetate (0.5%)	Thrice daily	IOP rise after a week and peaked after a week; return to normal on cessation of drops.	(Gerometta et al., 2009)
Cat	Prednisolone acetate (1%)/ dexamethasone (1%)	Twice/thrice daily	IOP rise in 2-3 weeks time; return to normal on cessation of drops.	(Zhan et al., 1992)
Rabbit	Dexamethasone, betamethasone, medrysone	Four times daily	IOP raise in four weeks data only	(Lorenzetti, 1970)

Rabbit	Betamethasone 4mg repository	Weekly/ thrice weekly subconjunctival injections	IOP rise within three weeks	(Bonomi et al., 1978)
Rabbit	dexamethasone	Four times daily	IOP rise in two weeks	(Knepper et al., 1978)
Rabbit	Dexamethasone (1%)	Thrice daily	IOP rise in 3-5 weeks	(Ticho et al., 1979)
Rabbit	dexamethasone and betamethasone	_	IOP rise in two weeks	(Knepper et al., 1985)
Rat	dexamethasone	Four times daily (both eyes)	IOP rise in two weeks	(Sawaguchi et al., 2005); (Miyara et al., 2008)
Mice	dexamethasone (0.09 mg/day)	Systemic administration with osmotic pumps	IOP rise (except in a subset)	(Whitlock et al., 2010)

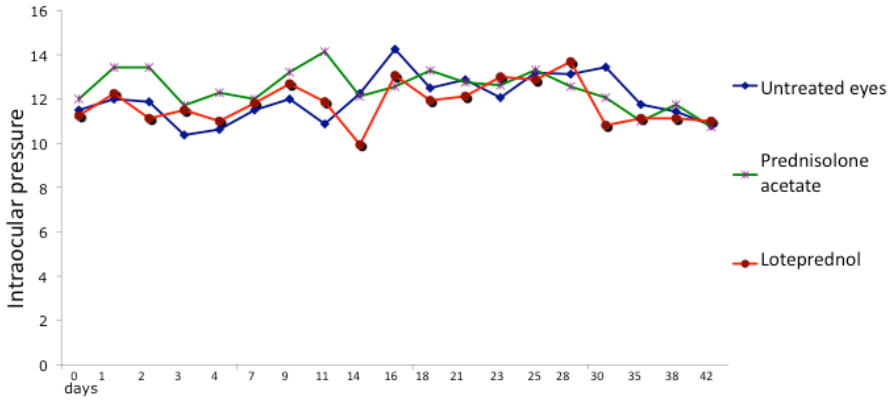

Figure 57 IOP fluctuations in treatment and control eyes over a period of 42 days.

Experimental glaucoma in rats

Several rat glaucoma models have been used to study the causes of and treatment options for glaucoma. Most models are based on the obstruction of the aqueous humour outflow pathways and secondary rise in IOP. However, the pressure increase is not gradual as in human chronic glaucoma. Also, inflammation occurs as a side effect of some of the surgical procedures used to raise IOP, which affects the validity of these models.

We raised IOP in rats using the following methods:

1. Injection of hypertonic saline into episcleral veins
2. Injection of polystyrene micro beads into the anterior chamber
3. Injection of magnetic micro beads into the anterior chamber

We used Brown Norway (BN) rats. Spontaneous axon damage is negligible in these animals (Cepurna et al., 2005). Also, BN rats are docile and tame enabling IOP measurements to be carried out in awake animals. The IOP was measured in non-anaesthetised animals using a Tonolab, a rebound tonometer calibrated for use in rats.

Injection of hypertonic saline into episcleral veins

Methods

Injection techniques are described in page 72. We sacrificed the animals 7, 14 or 30 days after the saline injection by transcardiac perfusion under terminal anesthesia. We dissected an optic nerve sample from 2mm behind the eye, where myelination begins. We stained semithin plastic sections with toluidine blue to study differences in axonal and glial structures. We imaged and photographed the sections using a light microscope at magnifications of 40x and 63x. We processed retinal whole mounts for TUNEL assay to assess RGC apoptosis. Confocal images of TUNEL staining were obtained using a digital camera fitted to a Biorad confocal microscope.

Results

There was no noticeable difference in the IOP of the saline injected eyes and unoperated eyes at any time point.

In about 40% of the rats, semithin sections of optic nerve showed that there were different degrees of axon damage in the saline injected eyes; varying from focal damage in one area of optic nerve to complete damage across the nerve. Axon damage characterized by collapsed myelin sheaths and/or damaged cytoskeleton appeared as inclusions in the axon or empty myelin sheath (without any cytoskeleton) Figure 58.

TUNEL staining of the retinal whole mounts showed varying extents of RGC apoptosis Figure 59.

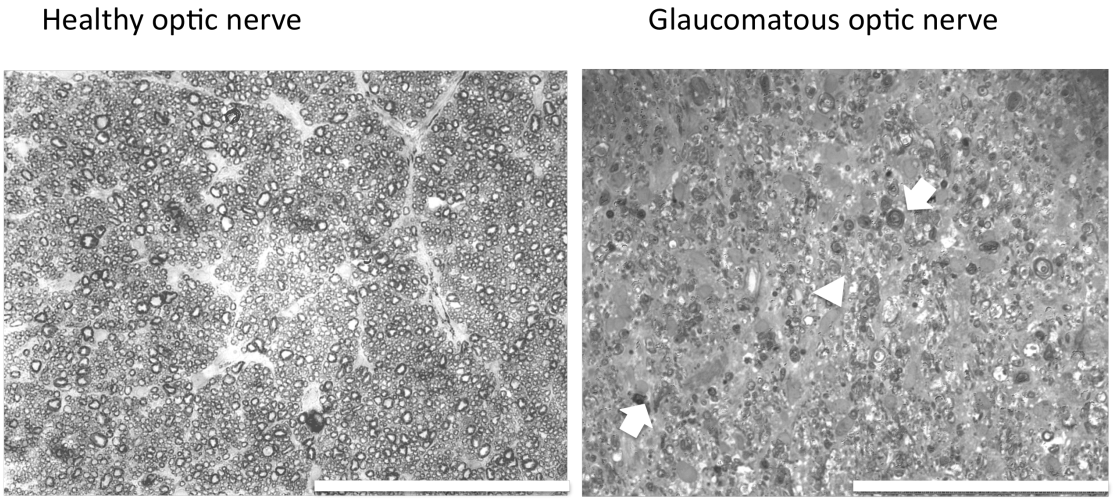

Figure 58 Episcleral hypertonic saline injection causes severe axon damage in the optic nerve.

Episcleral veins of rat eyes were injected with hypertonic saline solution. After four weeks, the rat was sacrificed and semi-thin cross-sections of optic nerve from 2mm behind the eye were stained with toluidine blue and imaged using a light microscope. Healthy optic nerves from unoperated eyes had clear circular axons and thin glial processes. Glaucomatous optic nerve from hypertonic saline injected eyes had axon damage as indicated by arrows and extensive gliosis as indicated by the arrowhead. Scale bar represents 100μm.

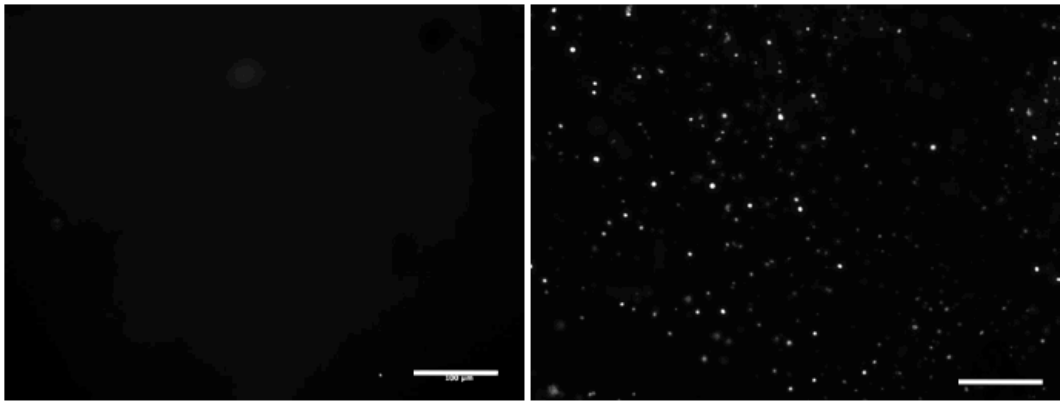

Figure 59 Retinal ganglion cell apoptosis in episcleral hypertonic saline injection model of glaucoma.

Episcleral veins of rat eyes were injected with hypertonic saline solution. After one week, the rat was sacrificed. Retinal whole mounts were stained for TUNEL, an apoptosis marker. The retina from saline injected (right) eyes stained positive for apoptosis while the control eye stained negative (left). Scale bar represents100μm.

Polystyrene microbead injection

Methods

Injection of polystyrene micro beads into the anterior chamber raises IOP in rats and mice (Sappington et al., 2009a).

We housed rats in a constant illumination chamber at 80lux light intensity from seven days prior to the injection in order to eliminate the circadian IOP fluctuations.

Fluorescently labelled polystyrene micro beads of 15μm diameter were purchased from Invitrogen. The beads were suspended in physiological saline. Circa 5000 beads were reconstituted in 5μl of saline and injected into the anterior chamber using a 33G needle attached to a Hamilton syringe. The needle was held in place for at least 15 seconds after the injection. There was a significant back flow of the beads in most animals. A drop of chloramphenicol was applied to the eye after the injection to prevent microbial infection. Only one eye of each animal was injected; the unoperated eye served as control. IOP was measured in non-anaesthetized animals three times a week for up to three weeks.

Results

Immediately after the injection, the beads appeared to be well distributed throughout the anterior chamber. But, after 24 hours, the majority of animals had clumps of beads towards the centre of anterior chamber Figure 60 and away from the iridocorneal angle. None of the animals showed a significant rise in the IOP at any time point.

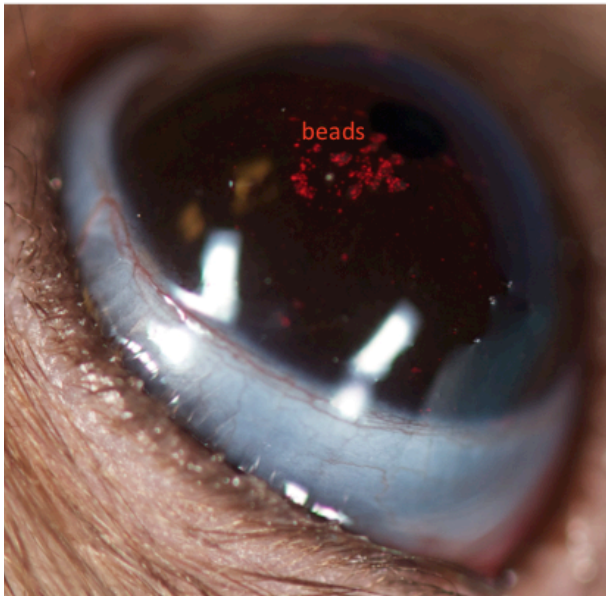

Figure 60 Red micro beads clumped together in the centre of the anterior chamber of a rat eye, seven days after injection.

Magnetic micro bead injection

Polystyrene bead injection does not allow control over the position of the injected beads. As a solution to this problem Samsel et al., injected magnetic micro beads, which can be directed using a strong, handheld magnet. The magnet can direct the beads to the iridocorneal angle and prevent the accumulation of beads in the centre of the anterior chamber (Samsel et al., 2010). Advantages of this method are the preservation of a clear visual axis, sustained increase in IOP and a subsequent reduction in the number of RGC.

Methods

We modified the micro bead injection model described by Samsel et al., for our experiments. We obtained magnetic micro beads of about 8µm diameter from Bangs laboratories, UK (UMC04N-0.5). We washed the beads thrice in PBS and incubated them overnight in Tris-buffered Saline. We washed the beads again and aliquoted them into 0.5ml eppendorf tubes. Tubes were sterilised by gamma irradiation (Isotron PLC) and stored at 4°C until use.

We resuspended around two million micro beads in physiological saline and injected these into the anterior chamber of the eye using a 32G needle attached to a Hamilton syringe. Once the beads were distributed uniformly in the anterior chamber, we guided the beads towards the limbus with a ring shaped neodymium magnet of 5mm internal diameter and 42 kilojoules per cubic meter strength (Supermagnete, Germany) placed around the globe such that the beads were closely apposed to the trabecular meshwork.

We measured the IOP twice a week, starting a week before the first intervention. Each measurement consisted of five sets of measurements, each set reflecting the average of six individual measurements. We

performed the measurements in both eyes of awake animals without topical anaesthetics.

We assessed the damage to the optic nerves using semi-thin sections of the nerve from two millimetres behind the globe. We also counted the number of RGC on retinal whole mounts.

Results

The time required for IOP rise in response to magnetic bead injection ranged from two to four days. To characterise the IOP rise in this glaucoma model, we conducted a pilot experiment with ten rats. We had to sacrifice two rats during the course of study due to severe hyphema and one rat due to infection in the eye. After eliminating the three rats, IOP from the remaining seven rats were plotted over 29 days. IOP rise in the bead-injected eyes were fluctuating but significantly higher than the uninjected eyes at 17, 21 and 29 days after the injection Figure 65. The IOP rise after bead injection varied from 20mmHg to 60mmHg. When the IOP was above 60mmHg, there was blood in the anterior chamber (hyphema) in about 50% of the animals, which were terminated from the study.

Eyes with elevated IOP always appeared enlarged and had a cloudy cornea. The anterior chamber appeared very deep which could be due to the excess amount of aqueous humour.

We also noticed that new blood vessels sprouted into the corneal stroma adjacent to the beads. The blood vessels were confined to the area of beads and never spread to the rest of the cornea.

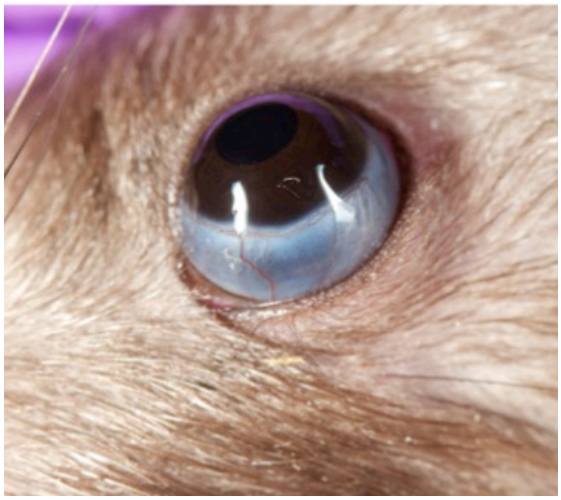

Figure 61 Rat eye before injection of magnetic beads.

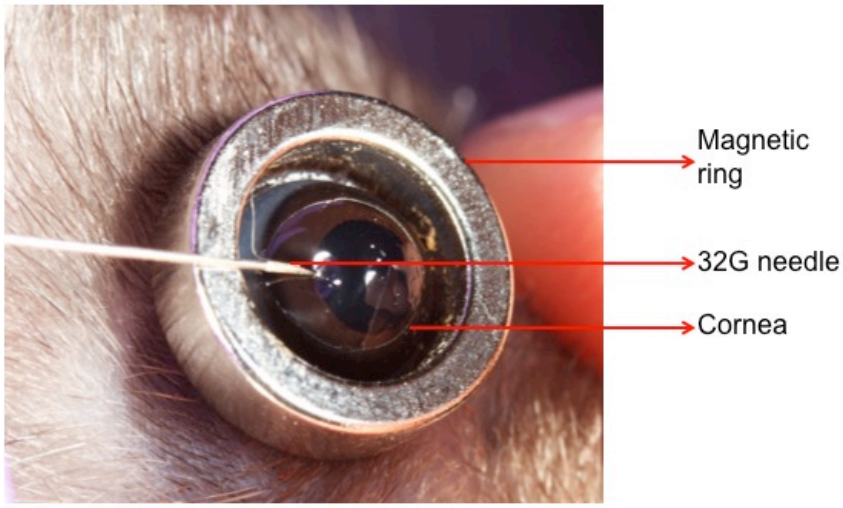

Figure 62 Magnetic beads injection set up.

A magnetic ring of 6mm inner diameter was placed around the globe prior to injection. A custom-made 1.5 cm long 32G needle was used to inject the beads. The tip of the needle was inserted into the anterior chamber without injuring the iris and the beads were injected slowly.

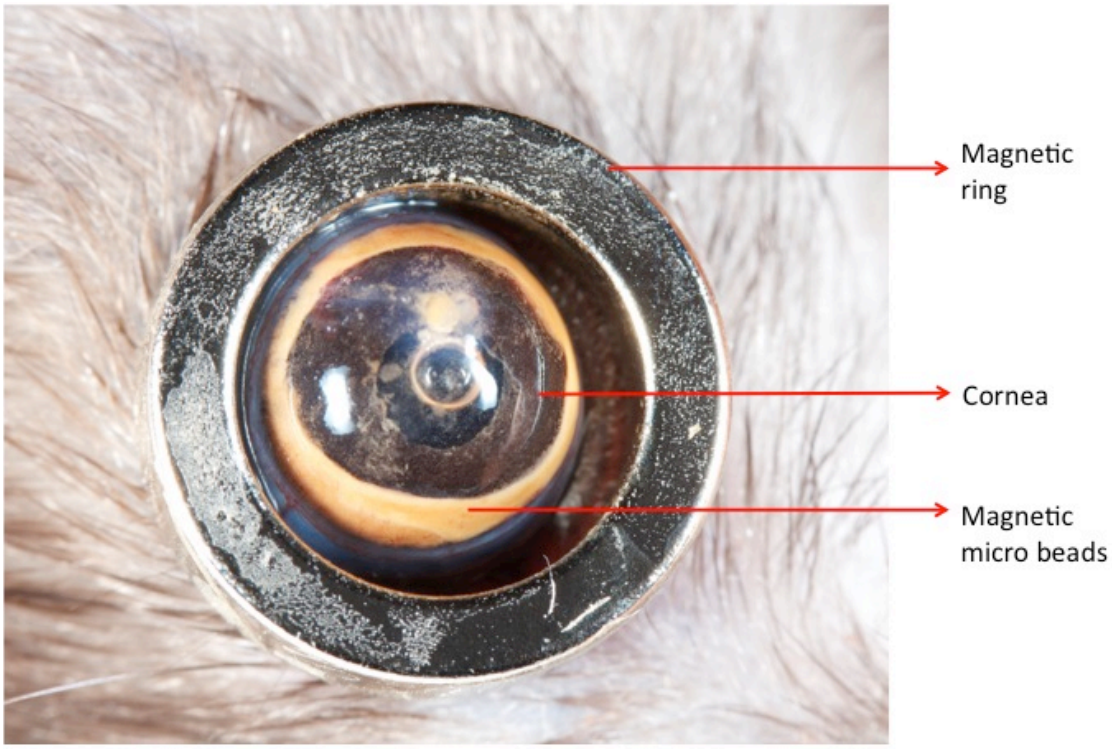

Figure 63 The magnetic ring placed around the globe of rat eye pulled the injected microbeads to the limbus.

The magnetic ring (inner diameter of 6mm; strength 42 kilojoules per cubic meter) was placed around the globe and the beads were injected just under the cornea without damaging the iris. The beads were immediately pulled to the iridocorneal angle by the magnetic ring and distributed in the form of a ring due to the magnetic field created by the magnet. After the injection, the magnet was left around the globe for 5-10 minutes so that the microbeads were firmly apposed to the trabecular meshwork pores. Later, when the magnet was removed, the beads did not fall back to the centre but stayed in the iridocorneal angle.

Figure 64 A comparison of magnetic microbeads injected eyes with and without the magnetic ring.

Left: The magnetic beads injected into the eye were pulled in the iridocorneal angle using a magnet placed around the globe so that the beads form a ring at the limbus. There are no beads in the centre of the anterior chamber. Right: the beads injected into the eye in the right stayed at the place of injection. The beads are in front of the pupil and also deposited on the iris. The use of the magnetic ring helps to concentrate the beads in the iridocorneal angle and does not block the path of light to the retina.

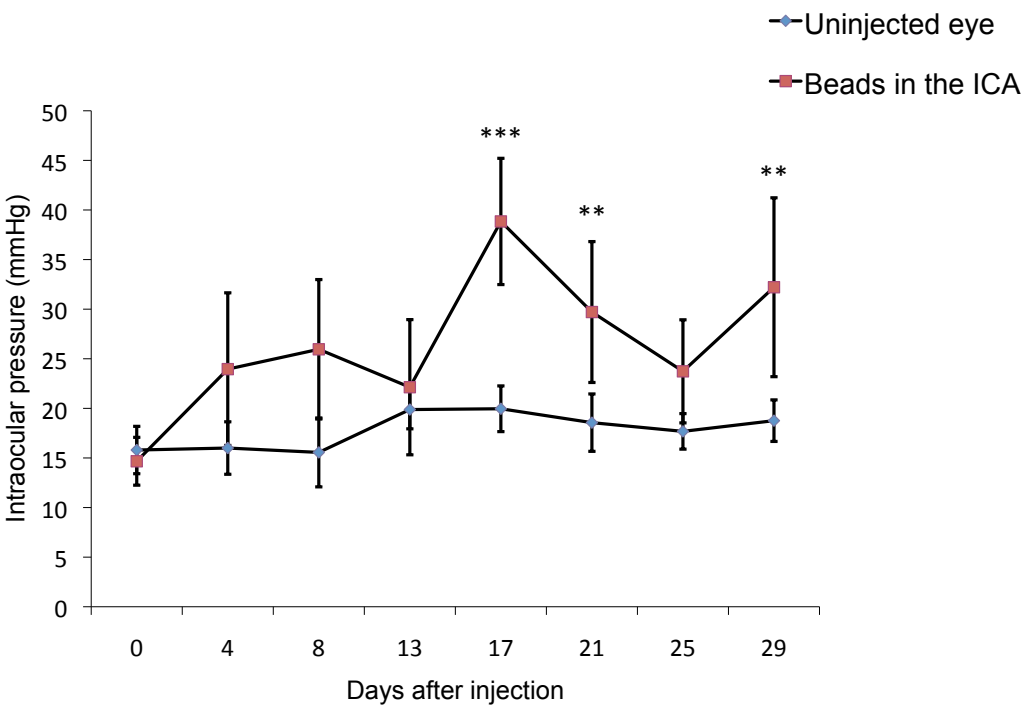

Figure 65 Intraocular pressure of bead-injected eyes and control eyes. *Left eyes were injected with paramagnetic beads which were pulled into the iridocorneal angle using a magnet placed around the globe. The right eyes served as uninjected controls. IOP was measured twice a week in both the eyes. IOP of the uninjected eyes fluctuated between 12-20 mmHg, while that of the bead-injected eyes fluctuated between 20-60 mmHg. The IOP of the bead-injected eyes were always higher than that of the uninjected eyes, but the difference was statistically significant only on days 17 (***, p<0.0001), 21 (**, p=0.003) and 29 (**, p=0.0026). Error bars represent SEM, n=7.*

Damage to the optic nerve

We noticed the earliest change in the axons of the optic nerve seven days after the bead injection. Some axons displayed dark and dense axoplasm and disorganised myelin. These were interspersed between normal axons with clear axoplasm and myelin sheaths Figure 69. In two animals, extensive gliosis was observed instead of axon damage at three days after bead injection.

In animals with minimal nerve damage, the axon damage was concentrated in the centre of the optic nerve. In the case of severe nerve damage, the damaged axons appeared to be evenly distributed throughout the nerve.

Blockage of axon transport

We observed accumulation of organelles in the axons of glaucomatous optic nerve both at the non-myelinated optic nerve head as well in the myelinated part. The accumulation of organelles was limited to glaucomatous nerves and never observed in the healthy optic nerves (Figure 68). Organelles accumulate because of the blockade of axonal transport.

Damage at the optic nerve head

At the optic nerve head, we found clumping of organelles in the axoplasm. The glial lamina in the optic nerve head of rat, which is composed of astrocytes, sends processes in a direction perpendicular to that of the optic nerve axons. In the glaucomatous nerve head, however, this organisation is compromised, and the glial cells seem to be dispersed and atrophied (Figure 66 and Figure 67).

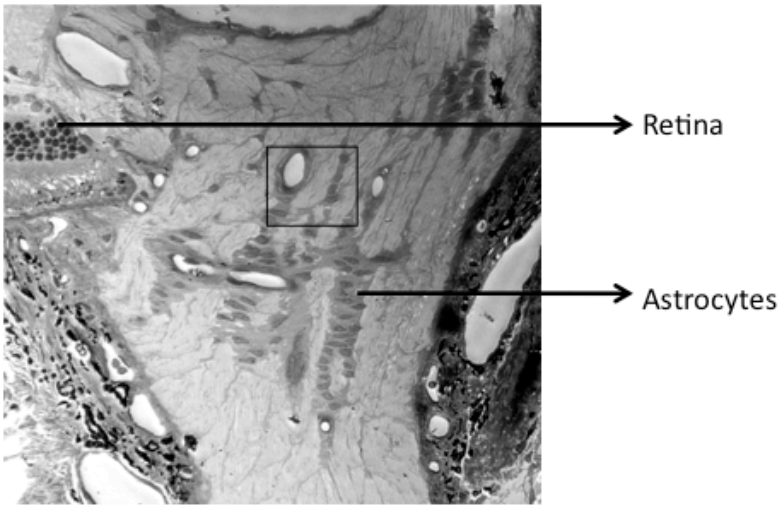

Figure 66 Anatomy of a healthy rat optic nerve head and glial lamina.

A healthy optic nerve head is supported by a glial lamina that spans the unmyelinated area of the nerve head. The cluster of astrocytes at the lamina lay perpendicular to the direction of axons. Higher magnification of the area in the box in healthy and glaucomatous nerve heads is presented in ***Figure 67****.*

Healthy lamina Glaucomatous lamina

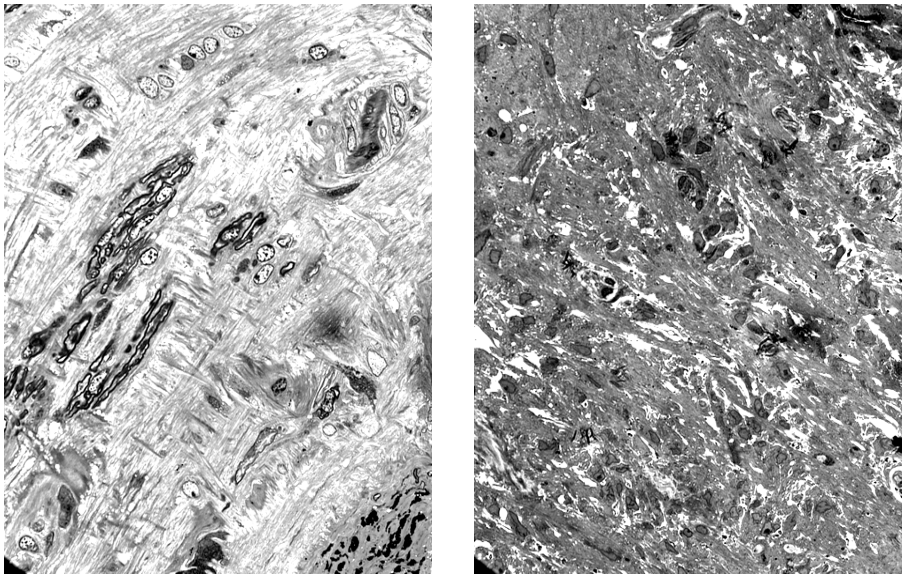

Figure 67 Glial lamina of glaucomatous optic nerve head is disorganized.

Left: Healthy glial lamina. The glial processes are arranged perpendicular to the direction of the optic nerve axons. Right: glaucomatous glial lamina. The glia is disorganized, the processes are not held perpendicular to the nerve.

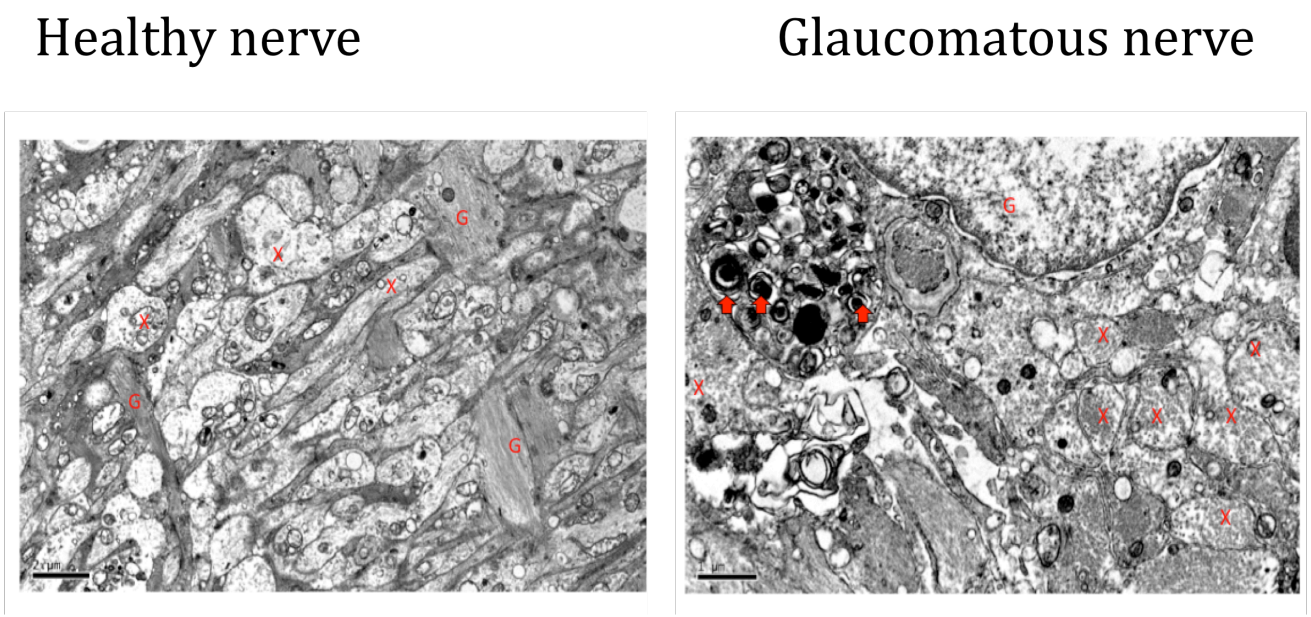

Figure 68 The optic nerve head of glaucomatous eye displays axons filled with accumulated organelles.

Electron micrograph of glaucomatous optic nerve head. Healthy axons (X in the figure) have clear cytoplasm. The axoplasm of unhealthy axon is occluded with organelles (arrows indicate dark, electron dense organelles trapped at the optic nerve head). The axon with the clump of organelles appears bigger than the other, healthy axons in the figure. The accumulation of organelles is attributed to the blockade of axonal transport. The image also has a glial nucleus (indicated by G). Scale bar represents 2µm

Healthy axon

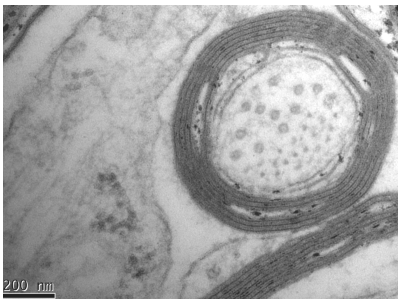

Damaged axons

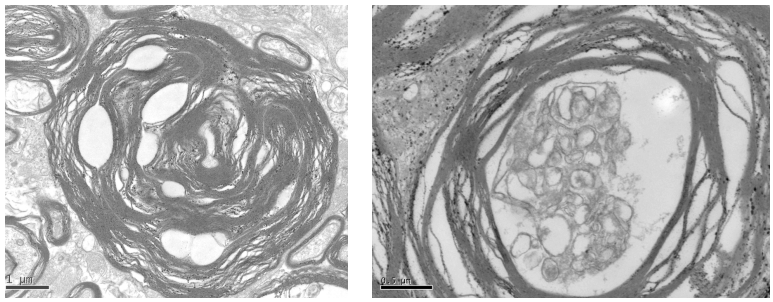

Figure 69 A comparison of healthy and damaged axons of the rat optic nerve.

Left eyes were injected with magnetic microbeads, right eyes were used as controls. IOP remained elevated for three weeks. The rats were transcardiacally perfused with a mixture of 3%PFA and 1% glutaraldehyde. The optic nerves of both eyes were collected from 2mm behind the globe and processed for electron microscopy and embedded in plastic. Ultrathin cross sections were stained and examined using the transmission electron microscope and images were captured. Top: healthy axon from uninjected eye with well-defined rings of evenly spaced myelin sheaths, clear cytoplasm with scattered rings of microtubules and spots of neurofilaments (scale bar represents 0.2µm). Bottom: Damaged axons from glaucomatous eye. The arrangements of the myelin sheaths are disrupted. Bottom right: Severely shrunken axoplasm (scale bar represents 1µm). Bottom right: vacuolated axoplasm detached from the myelin. The organelles cannot be recognized in the axoplasm (scale bar represents 0.5µm).

Healthy nerve Glaucomatous nerve

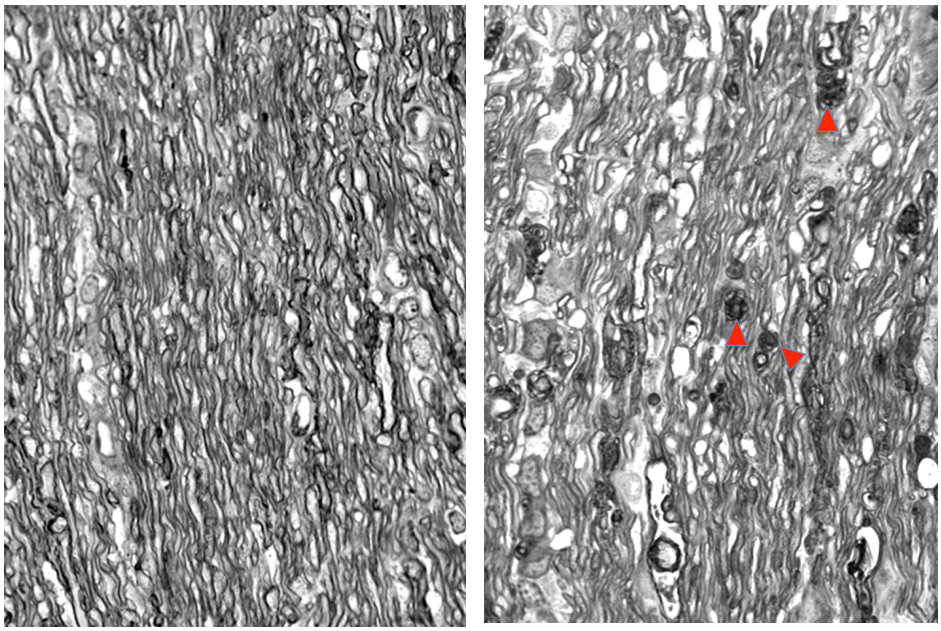

Figure 70 Longitudinal sections of glaucomatous and control rat optic nerves.

One eye was injected with magnetic microbeads and the other eye served as uninjected control. The injected eye had elevated IOP for eight days. Optic nerves were collected from 2mm behind the globe and embedded in plastic. Semi-thin, longitudinal sections of control (left) and glaucomatous (right) rat optic nerves were cut and stained with toluidine blue. The control nerve has evenly spaced, clear axonal cytoplasm while the glaucomatous nerve has dark and dense accumulations (arrowheads) in the axonal cytoplasm.

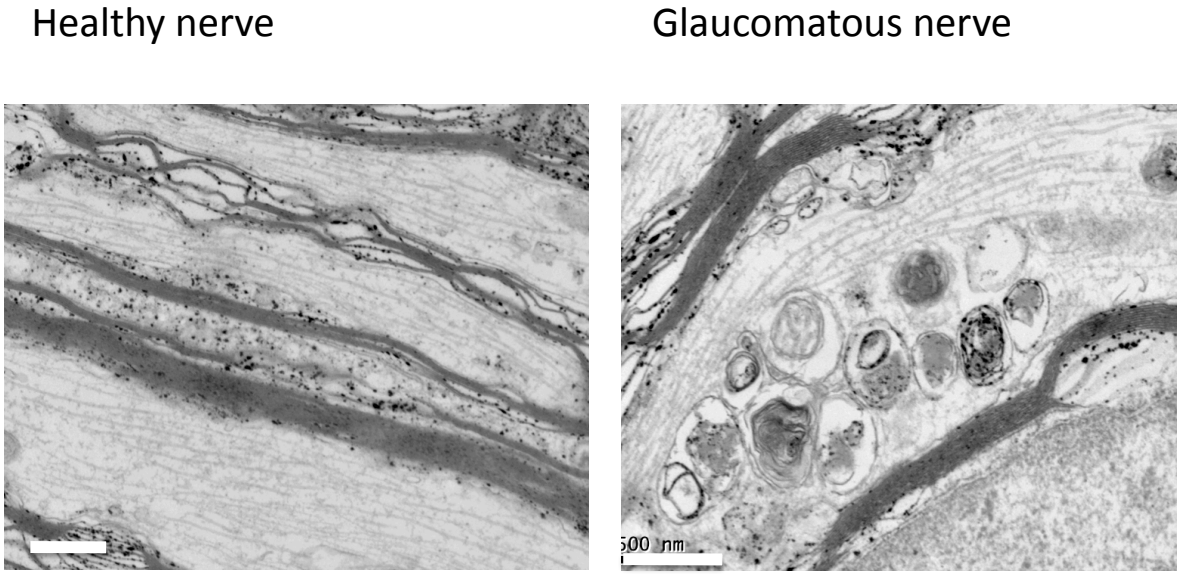

Figure 71 Transmission electron micrograph of a longitudinal section of rat optic nerve with healthy and glaucomatous axons.

One eye of the rat was injected with magnetic microbeads and the other eye served as uinjected control. The injected eye had elevated IOP for three weeks. Optic nerves were collected from 2mm behind the globe and embedded in plastic. Ultrathin sections were cut and examined under the transmission electron microscope. Left: healthy axons from the optic nerve of control eye have clear cytoplasm and evenly spaced, parallel microtubules and well dispersed organelles. Right: glaucomatous axon from the optic nerve of injected eye with accumulated organelles and disrupted microtubules indicating compromised axonal transport and microtubule disassembly (scale bar represents 500nm).

Discussion

Topical administration of corticosteroids to create a mouse model of experimental glaucoma

No significant rise in IOP was observed in either of the groups. However, there was a great fluctuation in IOP of a few animals on some days, which returned to normal on cessation of drops. Since we applied drops only to one eye, any systemic effect would have affected both the eyes, which could be the reason we observed similar IOP in both the eyes across the different groups. Whilst we ensured correct application of drops, we did not assess penetration into the eye.

Bonomi et al noted that different strains of rabbits respond differently to the same drug (Bonomi et al., 1978). It is currently not known as to whether the drug response in mice is also strain specific.

The frequency of application of drops in our experiments is lower than that in other animal models of steroid induced glaucoma. Increasing the frequency of drops was not feasible in our study because of the limited number of observers. Slow release preparations might have an effect.

Considering the fact that it is easier to measure IOP in rat eyes and that rats are more docile than mice, it might be worth repeating the experiment on rats. Studies on rat also applied steroid drops to both the eyes of animals and used untreated animals as controls, which might have led to accumulation of drug in the treated eyes.

Injection of hypertonic saline into episcleral veins

Episcleral vein injection is technically difficult. Conjunctival hemorrhage during the incision of conjunctiva and cannulation can impair visualization of episcleral veins. Moreover, holding the needle inside the vein throughout the injection is challenging.

The lack of IOP rise despite axon damage and RGC death might have been due to IOP fluctuation during the circadian cycle. The IOP rise might have gone undetected during our study because IOP elevation is more pronounced during the dark phase of circadian rhythm in rats (Jia et al., 2000).

While studying the rats with episcleral vein injection of saline, we carried out IOP measurements in standard housing conditions. For later models, i.e, bead injection models, we changed to constant illumination to abolish circadian fluctuations (Morrison et al., 2005). Lastly, the IOP measuring device (Tonolab), may not detect small changes in IOP (Morrison et al., 2009).

Polystyrene bead injection

The beads failed to localise in the iridocorneal angle and formed clumps in the centre of the cornea which interrupted the visual axis. Therefore we decided not to use the model for our experiments.

Magnetic bead injection

Magnetic bead injections were technically easy and IOP rise was observed within four days of initial injection. At day 29, IOP rise was significantly higher than that of the uninjected eyes without additional injections in between. However, the main drawback of the model is that the magnitude of IOP rise cannot be controlled and the IOP fluctuated throughout the experiment. These results were similar to that observed by Samsel et al., (Samsel et al.,2010). Although this model represents an acute rise of IOP, which can be used to study the effects of elevated IOP on retina and optic nerve, it does not exactly replicate the disease condition in humans where RGC and axon damage is due to chronic IOP rise.

Disruption of axonal transport and axonal death

Mechanical injury to cultured neurons can cause calcium influx through axolemmal pores, which lead to activation of calpains and disassembly of

cytoskeletal proteins, blockage of axonal transport and axonal beading (Kilinc et al., 2009). The same sequence of events might occur in glaucoma.

Increase in IOP is one of the main risk factors in glaucoma. Raised hydrostatic pressure induces apoptosis in cultured RGC, possibly due to the influx of calcium ions (Sappington et al., 2009b). RGC axons in humans and primates pass through the lamina cribrosa, an elastic connective tissue, as they leave the eye. In glaucoma, the lamina is deformed. This leads to optic nerve cupping and the lamina pores become smaller and elongated (Morrison et al., 1995a) (Miller and Quigley, 1988) (Tezel et al., 2004). Even though rats and mice have a glial lamina devoid of extracellular matrix, the pathology of glaucoma in experimental models is remarkably similar. The deformation of the lamina cribrosa may cause mechanical injury to the axons, given the fact that the fibres passing through weaker areas of lamina are more susceptible to early damage (Quigley et al., 1983). This stretch/mechanical insult might cause an influx of calcium ions into the axons. In rodent models of glaucoma, axonal swellings were found in the laminar region. Initial axon disruption in the optic nerve is followed by accumulation of phosphorylated neurofilament and loss of axonal transport in the intraocular part of the RGC axon and later by death of RGC soma (Soto et al., 2010) (Howell et al., 2007).

Calpains are calcium dependent proteolytic enzymes in the cytoplasm. Calpain activation in experimental glaucoma is well documented (Huang et al., 2010). Calpains in turn are capable of activating Calcineurin in neurons (Wu et al., 2004); calcineurin is activated in experimental glaucoma. Its deactivation prevents RGC death (Huang et al., 2005). Calcineurins mediate cytoskeletal damage in axonal injury (Staal et al., 2007), which could explain the loss of axonal transport in glaucoma. Once the axonal transport is disrupted, RGC are deprived of vital neurotrophins on which they depend to remain functional.

We evaluated different rodent models of glaucoma- steroid induced glaucoma, hypertonic saline injection model of glaucoma, polystyrene bead injection model of glaucoma and magnetic microbead injection model of glaucoma. Of these, the magnetic bead injection model is the most reliable and feasible model for our studies of neuroprotection in glaucoma.

Chapter four: Characterization of structural and functional retinal and optic nerve damage in the magnetic bead injection model of glaucoma.

Introduction

The recently described magnetic bead injection model of glaucoma combines the advantage of an uncomplicated technique and the possibility for re-treatment in case of an insufficient elevation of the IOP (Samsel et al., 2010). Whilst the original publication details the anatomical impact of raised IOP upon RGC, it does not present data on RGC function.

Traditional outcome measures in experimental models of glaucoma are the RGC axon count in optic nerve sections and the RGC count in retinal wholemounts or cross-sections. Whilst histological outcome measures give an accurate account of RGC survival or damage, they do not allow the longitudinal follow up of single animals. Importantly, they also lack information about visual function and the progression of visual loss.

A brief introduction about electroretinography is described in page 57. Recently, it was reported that glaucomatous damage in humans could be predicted by ERG recordings, years before clinical confirmation of the disease (Bode et al., 2011). This emphasises the fact that RGC function in glaucoma is potentially compromised long before clinically conclusive visual field and structural nerve changes are detected.

We therefore characterised the early and late functional and histological changes in the retina of glaucomatous rat eyes. From our pilot studies, it was evident that IOP rise was observed at four days after the bead injection. However, considering the fluctuations in IOP rise, we decided to

characterise the changes at day seven as representative of early glaucoma and day twenty-eight as late glaucoma.

Methods

We used adult female Brown Norway rats from Harlan, UK. Beginning one week before the induction of raised intraocular pressure, we housed rats under constant low illumination (40-90lux) chambers to reduce IOP fluctuations with circadian rhythm. The animals had food and water *ad libitum*. We measured the IOP twice a week, starting a week before the first intervention. Each measurement consisted of five sets of measurements, each set reflecting the average of six individual measurements. We performed the measurements in both the eyes of awake animals without topical anaesthetics using a rebound tonometer calibrated for use in rats (TonoLab, Tiolat). We induced raised IOP by injecting paramagnetic beads into the anterior chamber of the rat eyes (refer page 162). This blocks aqueous outflow.

Experimental groups

We had three experimental groups.

1. We injected the magnetic microbeads suspended in balanced salt solution into the anterior chamber of rats and distributed the beads at the iridocorneal angle using the magnetic ring.
2. We injected the magnetic microbeads into the anterior chamber, but without the use of the ring magnet so that the beads were distributed randomly. This group was used to study if the beads had any effect on the electric potentials such that it could interfere with the ERG results.
3. We injected balanced salt solution only into the anterior chamber of the rats (negative control).

Seven days after the injection of beads, the IOP was measured and the rats were subjected to ERG. Half of the animals from each group were

kept for another three weeks with regular IOP measurements. The other half of the animals were sacrificed and eyes were fixed in 4% PFA. We prepared retinal whole mounts and quantified the number of surviving RGC. A flowchart details the experiment layout (Figure 72).

Electroretinography

Prior to ERG recordings rats were dark adapted overnight for a minimum of 12 hours and handled in red light. We anaesthetized animals by intraperitoneal injection of ketamine hydrochloride and medetomidine hydrochloride. We dilated both pupils with a drop each of phenylephrine hydrochloride 2.5% and tropicamide 1% (Bausch and Lomb, UK). We also applied a drop of topical proxymetacaine hydrochloride 0.5%. Throughout the examination we kept rats on a 37^0C heating pad. We recorded full field flash ERG in both eyes simultaneously using a gold ring electrode, 3mm in diameter (Roland Consult, Germany) placed on the cornea, held in position using a drop of hypromellose solution. We placed a reference electrode subcutaneously on the forehead and a neutral electrode sub-dermally above the tail.

LED stimulators from Color Dome (Color Dome, Espion system, Diagnosys) Figure 73 generated the white flashes of intensities of -6.5 to 1 log cd s m^{-2} for a duration of about 4ms. We averaged 35 recordings of each intensity to pick up maximum signal and avoid background noise. Very significant outliers such as heartbeats were rejected manually.

pSTR were measured at 120ms crest and nSTR at 220ms trough of the responses to flashes below -3.5 log cd s m^{-2} . A waves were measured at 8ms trough and b wave at 50ms crest of the responses to the bright flashes of 1 log cd s m-2.

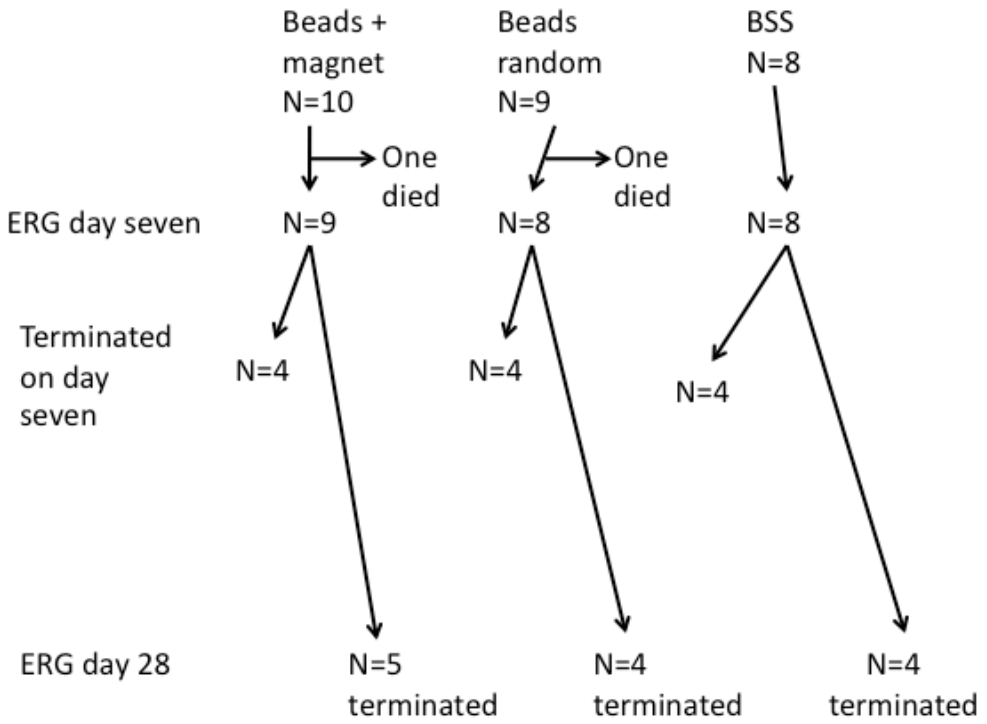

Figure 72 Flow chart explaining the experimental set up for the study of RGC function in early and late glaucoma.

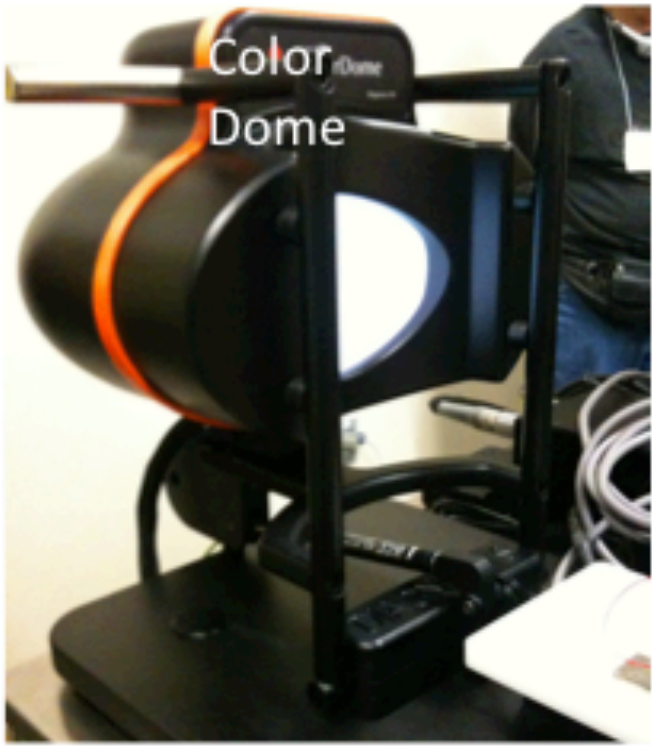

Figure 73 The Color Dome.

LED stimulators from Color Dome generated white flashes of of intensities of -6.5 to 1 log cd s m-2 for a duration of about 4ms.

Results

Intraocular pressure for seven days

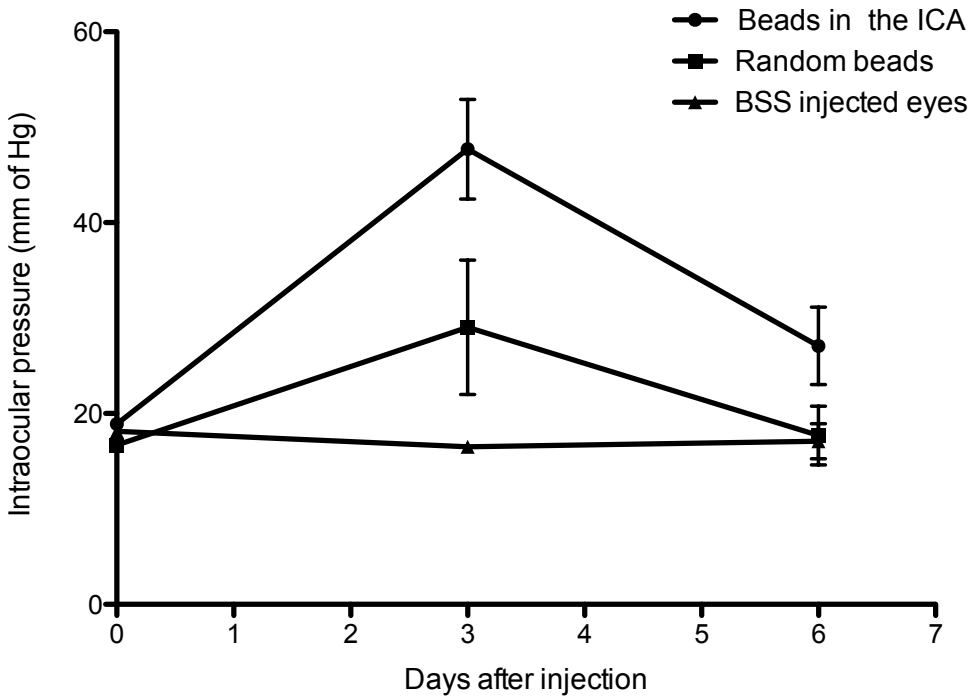

Figure 74 IOP recordings across the different groups over six days.

IOP of different groups were analyzed using two-way ANOVA and the groups were compared using Bonferroni's correction. On day three- IOP of the eyes with beads at the iridocorneal angle were significantly higher than that of the BSS injected eyes ($p<0.001$) and random beads injected eyes ($p<0.01$). IOP of random bead-injected eyes were significantly higher than that of the BSS injected eyes ($p<0.05$). At day six, there was no significant difference in the IOP across the different groups.

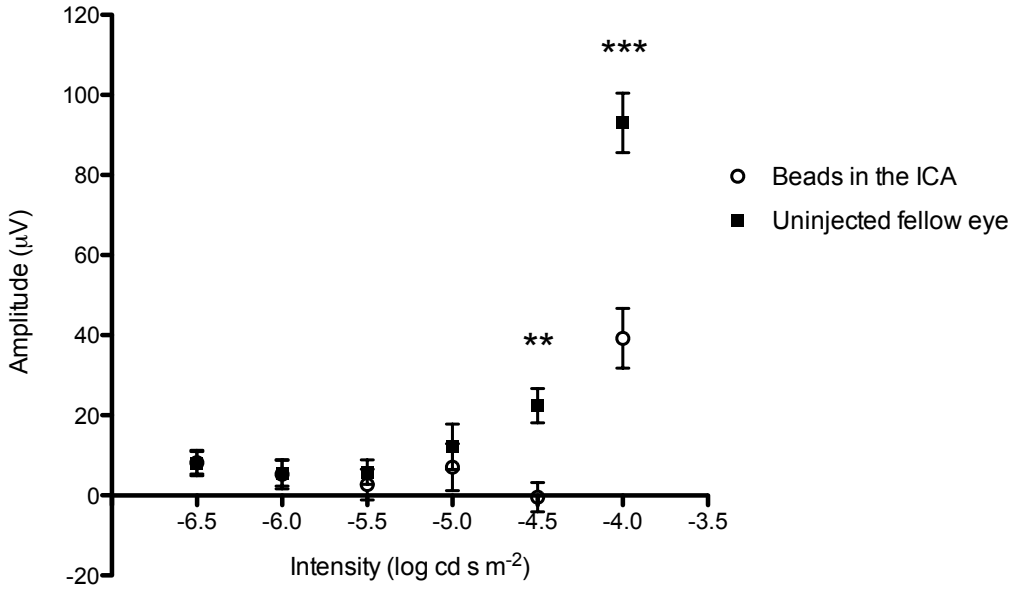

Figure 75 Seven days after the obstruction of trabecular meshwork by paramagnetic beads, the pSTR to a light stimulus of -4 log cd sm^{-2} is significantly reduced.

*The figure shows pSTR at low intensities at seven days after the injection. At an intensity of -4 log cd s m^{-2}, a strong pSTR was recorded in the uninjected fellow eyes, but the amplitude of pSTR of the beads injected eyes was significantly smaller (**p<0.01, ***p<0.001, p>0.05 at lower intensities). Error bars represent SEM.*

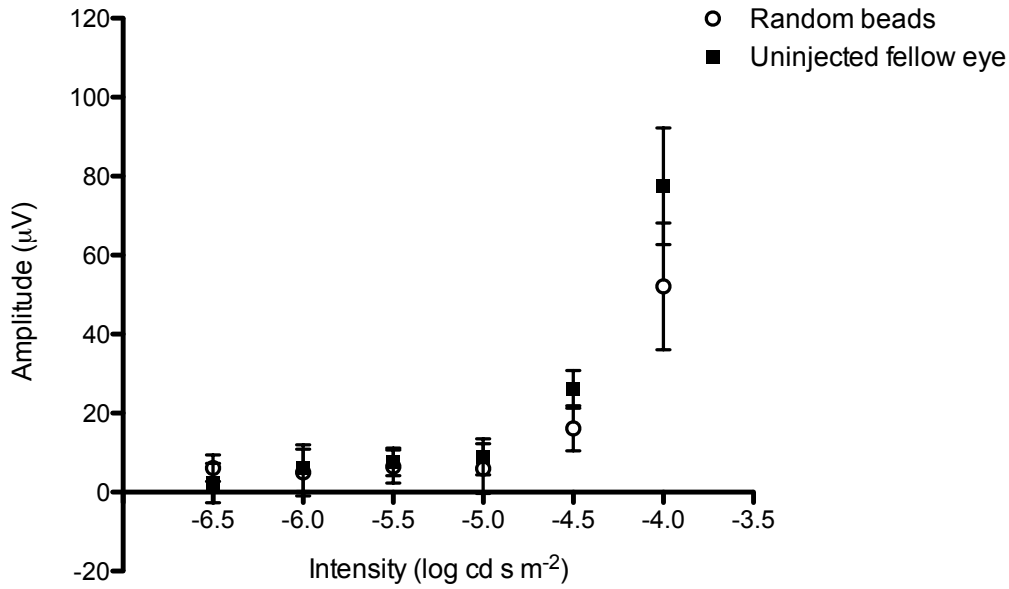

Figure 76 Paramagnetic beads distributed randomly in the anterior chamber do not significantly affect the pSTR.

At an intensity of -4 log cd s m^{-2}, a strong pSTR was recorded in the uninjected fellow eyes. The amplitude of the pSTR of the beads injected eyes was not significantly different from that of the fellow eyes ($p>0.05$) at all intensities. Error bars represent SEM.

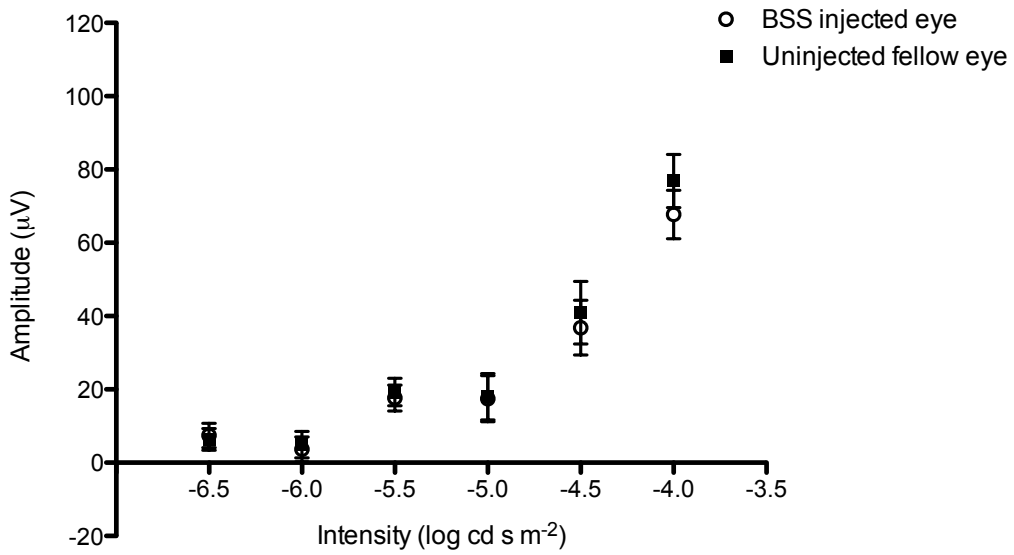

Figure 77 Injection of BSS (carrier solution) into the anterior chamber does not affect the pSTR.

At an intensity of -4 log cd s m-2, a strong pSTR was recorded in the uninjected fellow eyes. The amplitude of pSTR of the salt solution injected eyes was not significantly different from that of the fellow eyes ($p>0.05$ at all intensities). Error bars represent SEM.

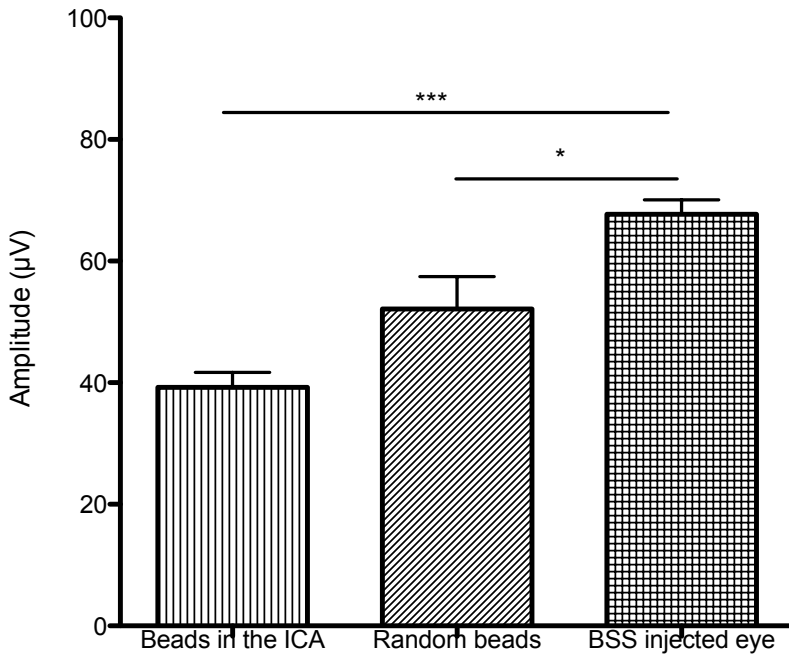

Figure 78 A comparison of pSTR of bead injected and saline injected eyes at seven days after the injection.

The amplitude of pSTR of the bead-injected eyes (at the iridocorneal angle and the random beads) was compared with that of the balanced saline solution injected eyes using one-way ANOVA with Bonferroni correction. The pSTR of the eyes with beads directed to the iridocorneal angle with a magnet was significantly smaller than that of the BSS injected eyes, $p<0.001$, while the pSTR of the eyes with random beads in the eye (without use of magnet) was significantly smaller than the BSS injected eyes, but $p<0.01$. Only the pSTR at an intensity of -4 log cd s m-2 was considered because the STR was most pronounced at that intensity. Error bars represent SEM.

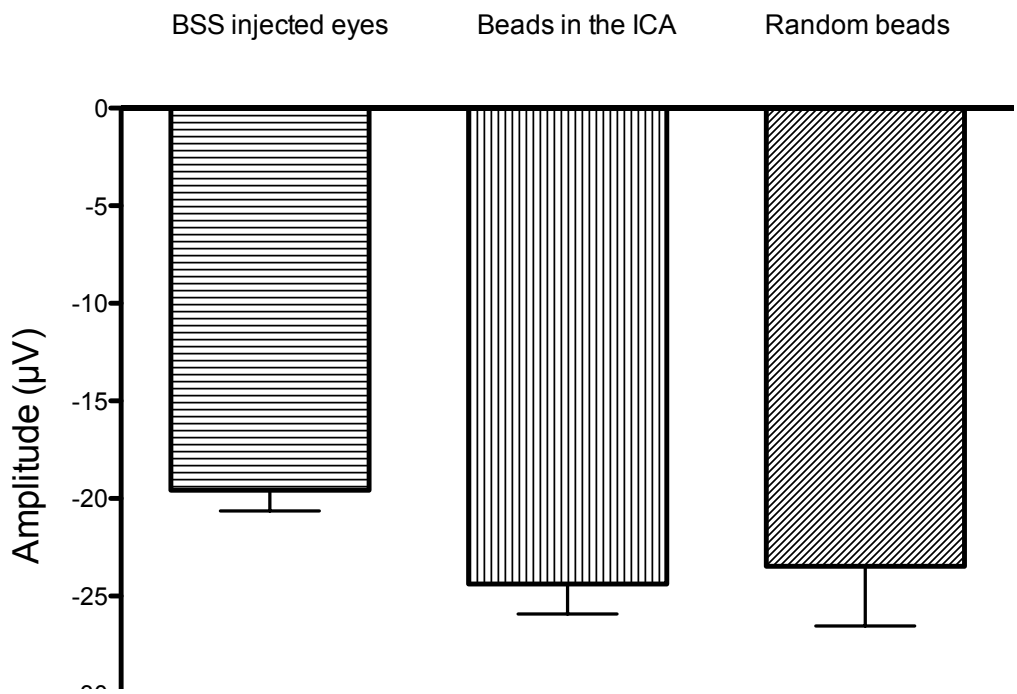

Figure 79 A comparison of the nSTR of bead injected and BSS injected eyes at seven days after the injection.

The amplitude of the nSTR of the bead-injected eyes (at the iridocorneal angle and the random beads) was compared to that of the balanced saline solution (BSS) injected eyes using one-way ANOVA with Bonferroni correction. The nSTR of the eyes with beads at the iridocorneal angle was not significantly different from that of the BSS injected eyes ($p>0.05$). The nSTR of the eyes with random beads in the eye (without use of magnet) was also no different to that of the BSS injected eyes ($p>0.05$). Only the nSTR at an intensity of -4 log cd s m-2 was considered because the STR was most pronounced at that intensity. Error bars represent SEM.

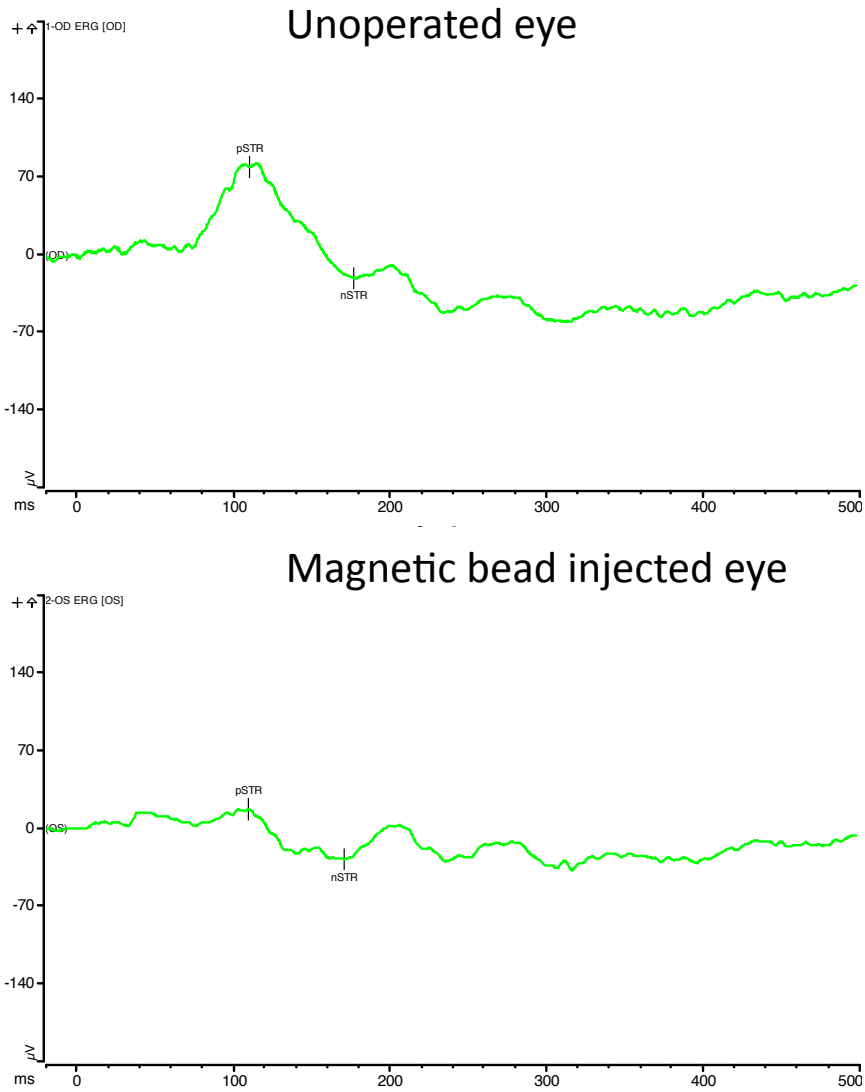

Figure 80 A comparison of the STR waves of the uninjected fellow eyes and bead-injected eyes.

The figure is a comparison of the pSTR and nSTR waves of eyes with beads at the iridocorneal angle and the uninjected right eye at seven days after injection. The IOP of the bead-injected eye was 40mm of Hg higher than that of the un-injected eye at three days after the injection and 6mm of Hg at six days. The pSTR of the right eye had amplitude of 79.61μV (top) while that of the beads injected eye had amplitude of 18.22μV (bottom). The amplitude of nSTR of the control eye was -21μV, while that of the beads injected eye was -27μV.

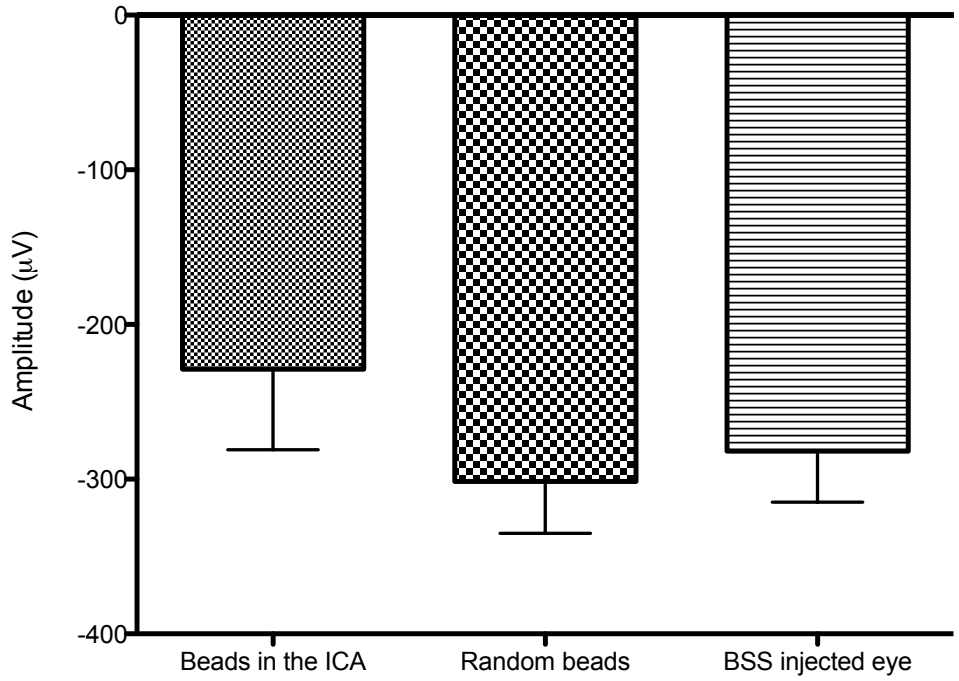

Figure 81 A comparison of A waves of beads injected eyes and BSS injected eyes at seven days after the injection.

The amplitude of the A wave of the bead-injected eyes (at the iridocorneal angle and the random beads) was compared with that of the balanced saline solution (BSS) injected eyes using one way ANOVA with Bonferroni correction. The A wave of the eyes with beads at the iridocorneal angle was smaller than that of the BSS injected eyes, but the difference was not statistically significant ($p>0.05$). The A wave of the eyes with random beads (without use of magnet) was not different from the BSS injected eyes ($p>0.05$). Only the A wave at an intensity of 1 log cd s m-2 was considered, because the A wave was most pronounced at that intensity. Error bars represent SEM.

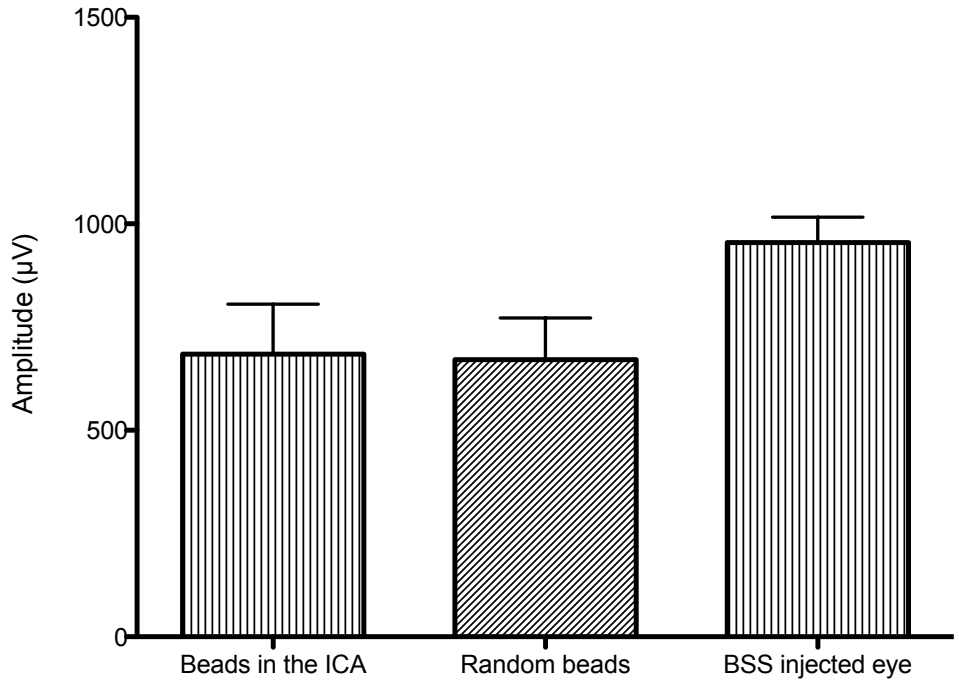

Figure 82 A comparison of B waves of beads injected and BSS injected eyes at seven days after the injection.

The amplitude of the B wave in bead-injected eyes (at the iridocorneal angle and random) was compared with that of the balanced saline solution (BSS) injected eyes using one-way ANOVA with Bonferroni correction. The B wave of the glaucomatous eyes with beads directed at the iridocorneal angle as well as that of the eyes with random beads (without use of magnet) was smaller than that of the BSS injected eyes, but the difference was not statistically significant ($p>0.05$). Only the B wave at an intensity of 1 log cd s m-2 was considered because the B wave was most pronounced at that intensity. Error bars represent SEM.

At seven days after the injection, the ERG data of injected and uninjected eyes were recorded. We recorded STR from a very low intensity of -6.5log cd s m-2 onwards, where the amplitude was minimal. The STR started to increase in amplitude at an intensity of -5 log cd s m-2. At an intensity of -4 log cd s m-2, we recorded the highest amplitudes for both pSTR and nSTR.

At higher intensities of illumination, pSTR in the eyes with beads in the iridocorneal angle was significantly reduced in the experimental eye compared to the uninjected control eye. In the random bead group, the amplitude of the pSTR did not show a difference between the uninjected control eyes and bead injected eyes.

To study the effect of bead injection on the ERG, the bead-injected eyes were compared to the BSS injected eyes using one-way ANOVA, and Bonferroni's correction was applied.

Comparison of pSTR and nSTR amplitude of beads injected eyes versus BSS injected eyes

Since the STR was most pronounced at an intensity of -4 log cd s m-2, we compared the STR amplitudes of the different groups at that intensity. The eyes where the beads were directed to the iridocorneal angle had a significant reduction of the pSTR when compared to the BSS injected eyes, $p<0.0001$ (***). The eyes with random injection of beads without the help of a magnet also had a significant reduction in the pSTR when compared to the BSS injected eyes, but the significance was $p=0.04$(*). There was no significant difference in the amplitude of pSTR between the random beads injected eyes and eyes with beads in the iridocorneal angle Figure 78.

However, there was no significant difference in the amplitudes of nSTR between the eyes with beads at the iridocorneal angle, eyes with random beads or the BSS injected eyes (Figure 79).

Reduction of pSTR amplitudes was only found in eyes with increased IOP

After seven days from the injections, we divided the bead-injected animals into two groups-

a) Bead injected eyes with elevated IOP (IOP recorded above 23mm of Hg during the seven days before ERG)
b) Bead injected eyes without elevated IOP (never recorded IOP above 23mm of HG during the seven days before ERG)

The amplitudes of pSTR and nSTR of the two groups were compared using Student's t test. The pSTR of the bead-injected eyes with IOP elevation was significantly smaller than that of the bead injected eyes without IOP elevation (Figure 83), but the nSTR was not significantly different (Figure 84).

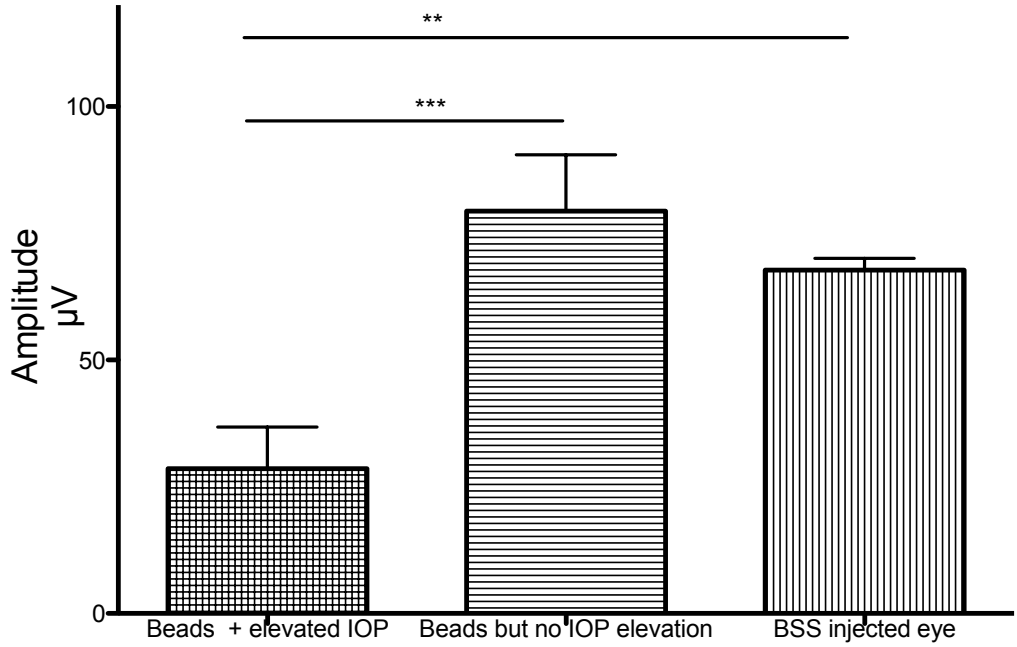

Figure 83 Reduction in pSTR correlates with IOP elevation.

To investigate the effect of IOP on the pSTR, we compared the amplitudes of pSTR waves in the bead-injected eyes with elevated IOP with the bead-injected eyes without any recorded IOP elevation using t test. The amplitudes of pSTR of the eyes with elevated IOP was significantly smaller than that of the eyes without IOP elevation, $p<0.001$. Only the pSTR at an intensity of -4 log cd s m-2 was considered because the STR was most pronounced at that intensity. Error bars represent SEM.

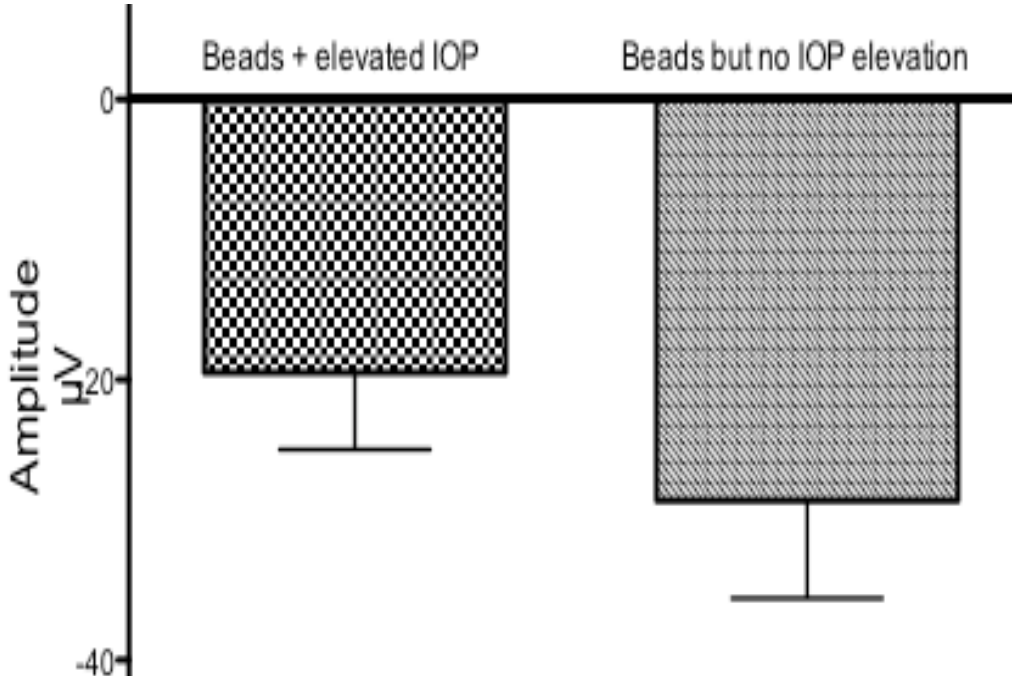

Figure 84 nSTR amplitudes do not differ significantly between bead-injected eyes with and without IOP elevation.

To investigate the effect of IOP on the nSTR, we compared the amplitudes of nSTR waves in the bead-injected eyes with elevated IOP with the bead-injected eyes without any recorded IOP elevation using t test. The amplitudes of nSTR of the eyes with elevated IOP was smaller than that of the eyes without IOP elevation, but the difference was not statistically significant, p=0.069. Only the pSTR at an intensity of -4 log cd s m-2 was considered because the STR was most pronounced at that intensity. Error bars represent SEM.

Comparison of A- and B-wave amplitudes of bead injected eyes versus BSS injected eyes

The A waves and B waves were most pronounced at an intensity of 1 log cd s m-2. Therefore, we compared the A and B waves of bead-injected eyes to that of BSS injected eyes using one-way ANOVA, and Bonferroni's correction was applied.

The amplitude of A wave of eyes with beads at the iridocorneal angle was smaller than that of the BSS injected eyes, but the difference was not statistically significant ($p>0.05$). The A wave of the eyes with random beads did not differ significantly from that in BSS injected eyes ($p>0.05$) Figure 81.

The amplitude of the B wave of eyes with beads at the iridocorneal angle as well as the eyes with random beads was smaller than that of BSS injected eyes, but the difference was statistically not significant ($p>0.05$) Figure 82.

Quantification of RGC at 7 days after the beads injections

At seven days after the bead injections, we sacrificed half of the animals and prepared retinal whole-mounts from the eyes. RGC from these eyes were quantified and the number of RGC in the eyes with beads at the iridocorneal angle and random beads were compared statistically with that of the BSS injected eyes. We analyzed the three groups using ANOVA and applying Bonferroni's correction, compared individual groups. There was no significant difference in the number of RGC in the BSS injected eyes and bead-injected eyes Figure 85.

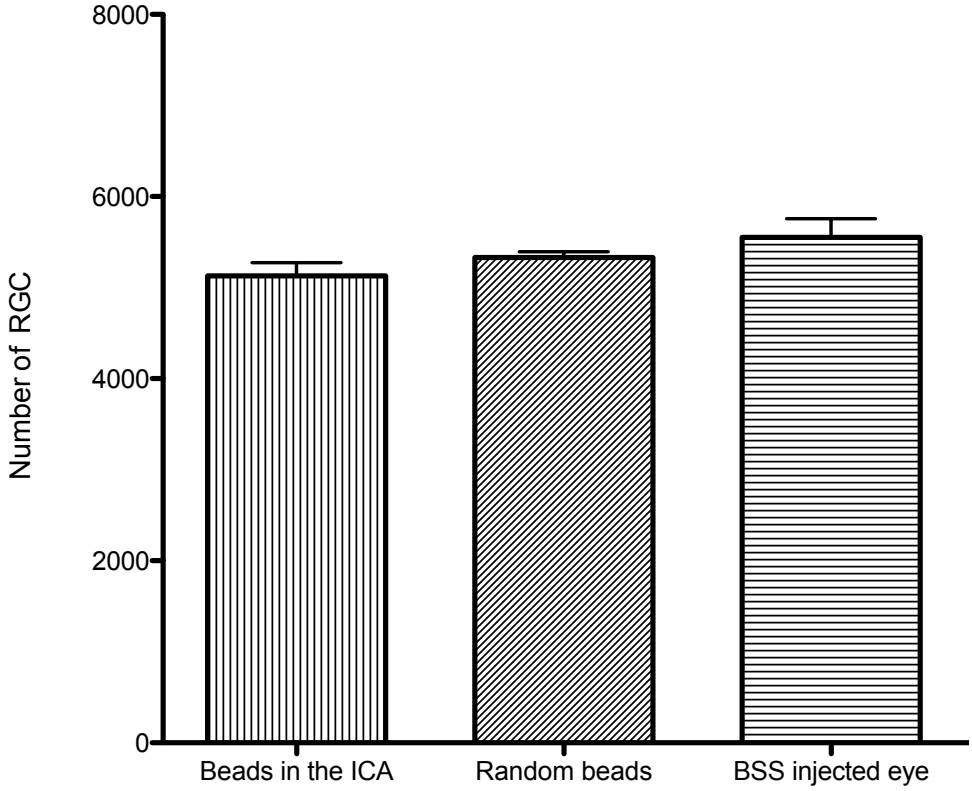

Figure 85 Number of RGC in the bead-injected eyes did not differ significantly from the BSS injected eyes at seven days after the injections.

At seven days after the injections, the rats were sacrificed and RGC were counted. The RGC counts across different groups were compared using one-way ANOVA with Bonferroni correction. There was no significant difference in the number of RGC of bead-injected eyes or BSS injected eyes ($p>0.05$). There was no significant difference in the number of RGC between eyes with beads at iridocorneal angle and random beads ($p>0.05$). Error bars represent SEM.

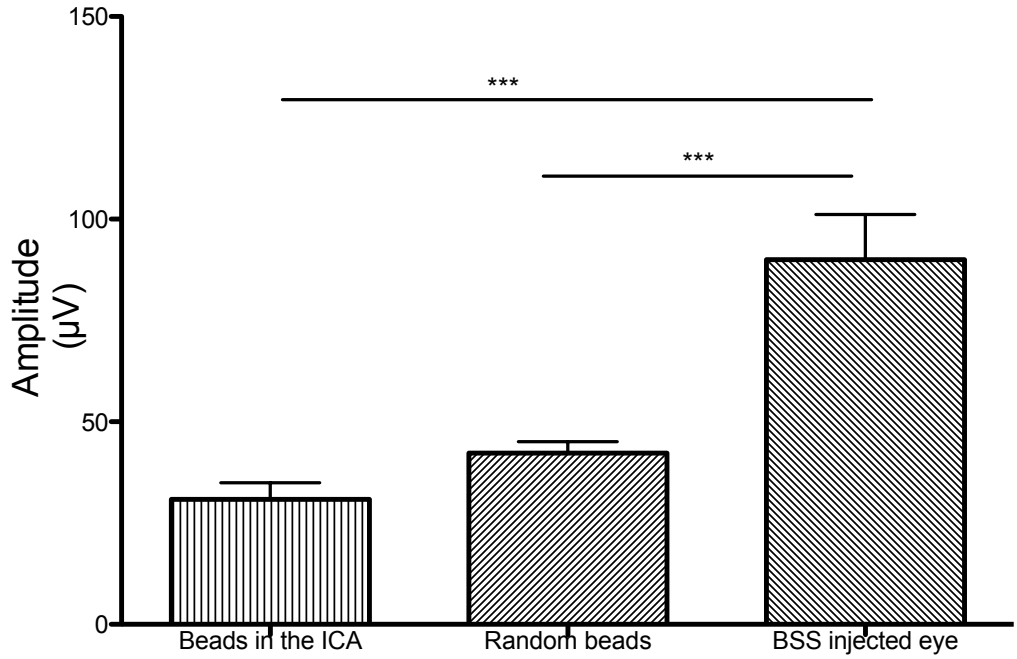

Figure 86 Comparison of pSTR amplitude between bead-injected eyes and BSS-injected eyes at four weeks after the injection.

The pSTR amplitudes of the bead-injected eyes (in the iridocorneal angle and the random beads) was compared with that of the balanced salt solution (BSS) injected eyes using one-way ANOVA with Bonferroni's correction. The pSTR of the eyes with beads was significantly smaller than that of the BSS injected eyes, $p<0.0001$, regardless of the use of a magnet to position the beads in the trabecular meshwork. Only the pSTR at an intensity of -4 log cd s m-2 was considered, because the STR was most pronounced at that intensity. Error bars represent SEM.

Four weeks after the injection of beads, the animals were again subjected to ERG. The pSTR of the bead-injected eyes and the BSS injected eyes was compared using one-way ANOVA, and Bonferroni's correction was applied to compare individual groups.

The amplitude of the pSTR of the eyes with beads at the iridocorneal angle was significantly smaller than that of the BSS injected eyes, $p<0.0001$. There was no significant difference in the amplitude of pSTR of beads in the iridocorneal angle and random bead injected eyes Figure 86.

Quantification of RGC 4 weeks after bead injection

At 28 days after the injection, the number of surviving RGC in the eyes with beads at the iridocorneal angle as well that of the random beads was significantly lower than that of the BSS injected eyes, $p<0.0001$, beads in the iridocorneal angle n=5, random beads and BSS injected n=4 each Figure 87.

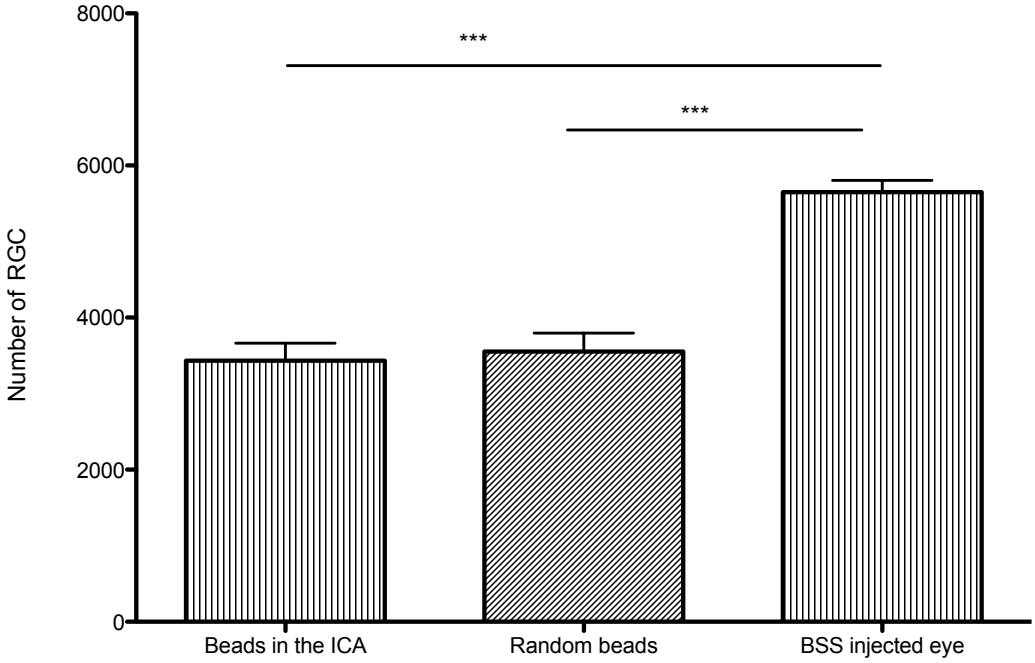

Figure 87 At 28 days after the injections, the number of RGC in the bead-injected eyes was significantly less than that in the BSS injected eyes.

At 28 days after the injections, the rats were sacrificed and RGC were counted. The RGC counts across different groups were compared using one-way ANOVA and Bonferroni correction was applied. The number of RGC in the eyes with beads in the iridocorneal angle were significantly less than that of the BSS injected eyes $p<0.0001$. The eyes with random bead injections also had significantly lower RGC counts than the BSS injected eyes, $p<0.0001$. However, there was no significant difference in the number of RGC of eyes with beads in the iridocorneal angle or random beads. Error bars represent SEM.

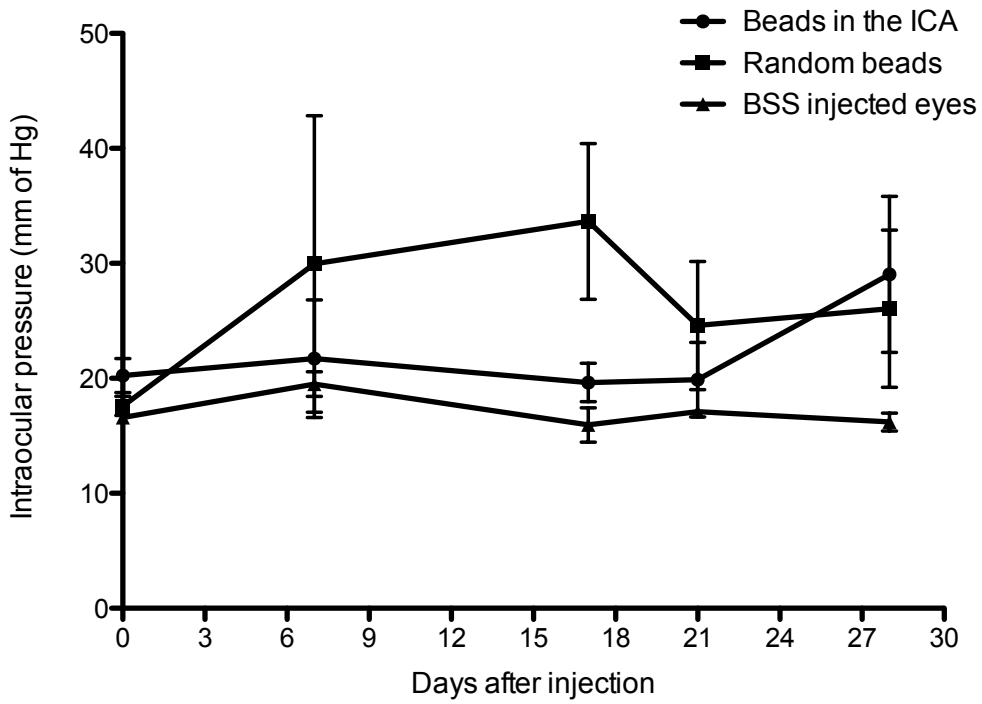

Figure 88 IOP recordings across the different groups over 28 days.

The IOP of different groups was analyzed using two-way ANOVA and the groups were compared using Bonferroni's correction. While the BSS injected eyes had an IOP around 20 mm of Hg throughout the study, the bead-injected eyes had fluctuating IOP, but the difference between the bead injected and BSS injected eyes was not statistically significant, except for day 17 ($p<0.0001$). Error bars represent SEM.

Discussion

ERG at seven days after the injection of paramagnetic beads.

Our data show that RGC function is affected at seven days after the injection of beads, even though there is no significant RGC loss or axon damage at that time point. However, the eyes where the beads were positioned at the iridocorneal angle using a magnetic ring had a more significant reduction in pSTR amplitude.

IOP rise in the bead-injected groups were fluctuating throughout the study. A similar fluctuation in IOP in the magnetic bead injection model was described by Samsel et al., (Samsel et al., 2010). Considering the fact that the rats were housed in constant illumination chamber to eliminate circadian cycle, the reasons for IOP fluctuations in our study remains unclear. However, large fluctuations in IOP cause progressive visual field loss and is considered a significant risk factor in patients with glaucoma irrespective of baseline pressure (Asrani et al., 2000, Caprioli, 2007, Hong et al., 2007).

We also correlated the elevation of IOP with the reduction of pSTR amplitudes by comparing the eyes with elevation of IOP and the eyes without elevation of IOP after the bead injection. We found that the eyes with elevated IOP had a significant reduction of amplitude of pSTR compared with bead-injected eyes without elevated IOP. Therefore, it is clear that the reduction in pSTR amplitude is due to the effect of elevation in IOP, and that the mere presence of beads in the anterior chamber does not affect the ERG response.

We did not detect a negative STR in all rats. Although some animals showed a negative deflection in the STR, the positive component, pSTR was the most consistent and larger component at lower intensities of

stimulation in Brown Norway rats. The near absence of negative STR in rats has been reported previously (Bui and Fortune, 2004).

Although we found that the amplitudes of a and b waves in the bead injected groups were slightly reduced, these reductions were not overall statistically significant. Since there was no significant reduction, we can assume that the photoreceptor and bipolar cell functions were minimally affected in most eyes.

However, when we consider individual cases, we did find eyes where b waves were reduced. This could be due to the fact that very high IOP (above 50mm of Hg) could cause non specific changes in the ERG response (Bui et al., 2005). Extreme rise of IOP causes ischemia and associated defects in the ERG. We noticed that IOP rise above 60 mm of Hg is associated with anterior chamber haemorrhage. In this study, however, we excluded animals with hyphema from the analysis.

ERG at four weeks after the bead injection

At four weeks after the bead injection, the pSTR amplitudes of both bead-injected groups were significantly reduced compared with the saline injected eyes. These animals had a significant loss of RGC as well. The number of animals for ERG at four weeks after the bead injection was very small. The IOP in those animals fell back to normal after the ERG recordings at one week after the injections. This could be due to the fact that we dilated the pupils in these animals for ERG recordings, which may have displaced the beads from the trabecular meshwork.

The drop in IOP after seven days did not stop the progression of RGC damage in these animals. Repeating the study with a higher number of animals may give a clearer understanding of the time-courses of functional damage in this model of experimental glaucoma, so that we can compare it with that of the human disease. This study underlines the fact that the initial insult of raised IOP could continue to damage RGC function and survival even after reduction of IOP to normal levels.

Our findings agree with previous ERG studies in the hypertonic saline injection model of rat glaucoma in the fact that only the pSTR is affected in rat glaucoma while the nSTR remains unaffected (Fortune et al., 2004).

For the glaucoma model we used, the time course and location of RGC damage had not been established previously. The finding that the ERG changes began earlier than significant loss of RGC raises the question of the possible sequence of events in this rat model of glaucoma. This thesis takes the view that the primary injury in glaucoma is in the region where the RGC axons pass through the ONH. To determine at what point the axons fragment and degenerate in the ONH and the optic nerve would require an extensive detailed study of the time courses in these two structures. However, there is poor agreement about the most appropriate structural outcome in animal models of glaucoma. It is documented that the retrograde changes in the cell bodies of the RGC in the retina occur over a prolonged and asynchronous time course after complete optic nerve transection (Madison et al., 1984) (Alarcon-Martinez et al., 2010), a situation in which the presence of surviving RGC can convey no visual function.

Chapter five: Olfactory ensheathing cells for neuro-protection in the glaucomatous rat eye

We characterised the RGC damage in magnetic bead injection model of glaucoma (chapter 4). Upon *in vitro* co-culture with OEC, we found that primary RGC survival was greatly enhanced by OEC (page 131). Also, we found that the RGC had significantly higher number of healthier neurites in the presence of OEC (page 131). Considering the above-mentioned neuroprotective effects of OEC on RGC as well as their neurites, we hypothesised that OEC could protect the optic nerve axons from glaucomatous degeneration.

To evaluate the effects of OEC on glaucomatous retina and optic nerve, we decided to inject OEC into the glaucomatous eyes.

Li et al., has injected OEC into the vitreous of healthy rat eyes and found that the OEC preferentially associated with the RGC layer of the retina (Li et al., 2008). The authors also described that the OEC survived in the rat eye for one month without immunosuppression.

In our *in vitro* co-culture experiments of OEC and primary RGC, we found that one OEC can ensheath three to five neurites (page 128). Since the Brown Norway rat optic nerve has circa 115,000 axons (Cepurna et al., 2005), we decided to inject ~50,000 into the rat vitreous.

Intravitreal injection of cells targeting the optic nerve head in the rat is technically challenging because of the small size of the eye and the large lens. The adult rat eye measures about 6 mm in diameter. In contrast to the human eye, the rat lens is occupies the majority of the posterior chamber and is about 3.8 mm in diameter (Baldo and Mathias, 1992).

Inadvertent injury to the lens causes activation of macrophages which secrete factors into the vitreous humour which in turn can affect the retinal

ganglion cells (Yin et al., 2003). Lens injury also causes cataract and inflammation in the eye. Therefore, the needle has to be inserted very carefully into the narrow space between the lens and the retina to avoid injuring the lens, which could compromise the survival of cells transplanted into the vitreous. To determine a safe route to deliver OEC, we tried transplanting OEC into the vitreous and subretinal space.

The volume of the vitreous humour in the rat is about 56µl (Berkowitz et al., 1998). Vitreous has limited oxygen and nutrients required for the survival of the transplanted cells; cells might be trapped in the vitreous and might not be able to migrate to retinal surface (Bull and Martin, 2009). Physical vitrectomy in rat eye is difficult because of the big lens and the miniscule amount of vitreous. Chemical vitreolysis can be achieved by enzymes which digest collagen (collagenase) and hyaluronic acid (hyaluronidase). However, injection of collagenase into the vitreous is known to cause retinal haemorrhage, an unacceptable complication for transplantation experiments (Johnson et al., 2009b). Therefore we decided to try chemical vitreoctomy using a combination of enzymes.

Labelling the cells for tracking after transplantation

In the *in vitro* co-culture experiments involving OEC and RGC, we could differentiate the two cell types by immunostaining for their markers, p75 neurotrophin receptor and neurofilaments respectively, because the markers were expressed exclusively by the individual cell types. In the retina, however, Müller cells express p75 receptor (Lebrun-Julien et al., 2009) and therefore we cannot detect the OEC injected into the eye by ICC, hence the need for labelling OEC prior to transplantation.

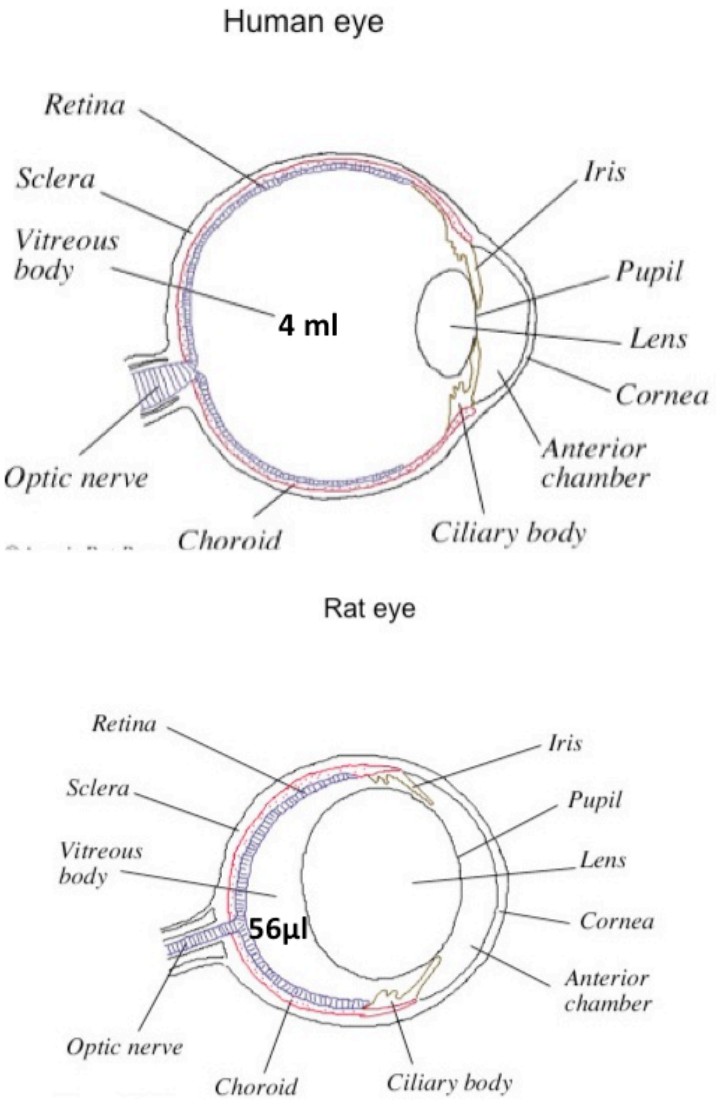

Figure 89 Comparison of human and rat eye.

Top: diagrammatic representation of a cross section through a human eye. Bottom: representation of the rat eye. The lens occupies the majority of the posterior chamber while the human lens occupies a much smaller part of the vitreous chamber. Figure adapted from http://www.ratbehavior.org.

Aims

The aims of this chapter are to

1. Determine a safe technique to deliver OEC to the proximity of RGC.
2. Evaluate the effects of OEC on glaucomatous optic nerve damage.

Methods

OEC culture and labelling of cells- See Materials and methods (Page 61).

Transplantation of cells

After anaesthetizing the rats (page 72), pupils were dilated with a drop of 1% tropicamide and 2.5% phenylephrine. The fundus was visualized under a surgical microscope with a cover slip held in place with a drop of the eye lubricant, visco-tears.

Injection techniques

About 50,000 cells were suspended in 2µl of carbon dioxide independent serum free media and drawn into a 5µl Nanofil syringe.

A 32 gauge bevelled needle was used to pierce the conjunctiva and sclera. A 32gauge blunt needle was attached to the Nanofil syringe to inject the OEC. The blunt needle was guided into the vitreous chamber through the hole created by the bevelled needle.

Intravitreal injections

The cells were injected in front of the ONH, just behind the lens without damaging the retina.

Subretinal injections

A sharp needle tip was inserted carefully through the retina, near the optic nerve head avoiding blood vessels. Cells were slowly injected. Injected cells and fluid spread under the retina. Accidental damage of blood

vessels caused severe haemorrhage in some animals which were terminated immediately.

The needle was held in place for ten seconds to prevent the escape of cells along the needle track. The cover slip was removed and a drop of Maxitrol (antibiotic and steroid) was applied on the eye.

Enzymatic vitreolysis

We injected a mixture of collagenase (Sigma) (0.05U), hyaluronidase (Sigma) and plasmin (1U) (Sigma) into the vitreous to digest collagen, hyaluronic acid and laminin, the components of vitreous. We injected the cells after 24 hours after the injection of enzymes.

Effect of OEC in glaucomatous rat eyes

To study the effect of OEC on the progression of glaucoma, we designed the following experiment- we used four months old female Brown Norway rats.

The rats were housed in constant illumination at 80-lux to eliminate IOP fluctuation due to Circadian rhythm throughout the experiment. The rats were in the illumination chamber from at least ten days prior to surgery. Intraocular pressure was measured twice weekly; the first measurements were taken prior to surgery to identify the baseline pressures.

There were two groups of rats in the study. One group received intravitreal injections of OEC suspended in 2µl of serum free carbondioxide independent media. The other group (placebo) received intravitreal injections of the same amount of serum free carbondioxide independent media without OEC. Four days after the injections, magnetic microbeads were injected to the anterior chamber of the eyes that received either OEC or placebo. The microbeads were distributed in the iridocornneal angle using a ring magnet in order to induce ocular hypertension and glaucoma. IOP was measured at six days after the bead injections.

One further injection of microbeads was required in seven rats at one week after the first injection the IOP failed to raise. We eliminated four rats from the study because of intravitreal haemorrhage. The experimental set up is detailed in Figure 99. We further eliminated seven rats which had blood in the anterior chamber and/or severe inflammation, such that OEC injected group had n=7 and placebo had n=5.

We sacrificed the rats at 28 days after successful induction of glaucoma. The rats were trancardially perfused with 4% PFA and the eyes and optic nerves were collected. The optic nerves from 2mm behind the globe were embedded in plastic. Semi-thin sections were stained with toluidine blue and micrographed for axonal quantification.

Axon quantification

We quantified the number of healthy axons in the optic nerves of OEC/carrier injected eyes and the two groups as mentioned in the materials and methods (page 79), were compared using t test. About 50% of the area of the nerve was included in the quantification.

Optic nerve grading

A healthy optic nerve with no axon damage was assigned a grade one, the nerve with a focal damage was grade two, the nerve with damage spread to more than one area was grade three (medium sized axons still survived), the nerve with only the smallest axons surviving was grade 4 and the nerve with no healthy axons was grade 5. Representative images of the different grades of optic nerve damage are illustrated in Figure 90.

The eyes were fixed, dehydrated and embedded in OCT. Longitudinal sections were cut and stained for DAPI to locate the relative position of OEC in the retina.

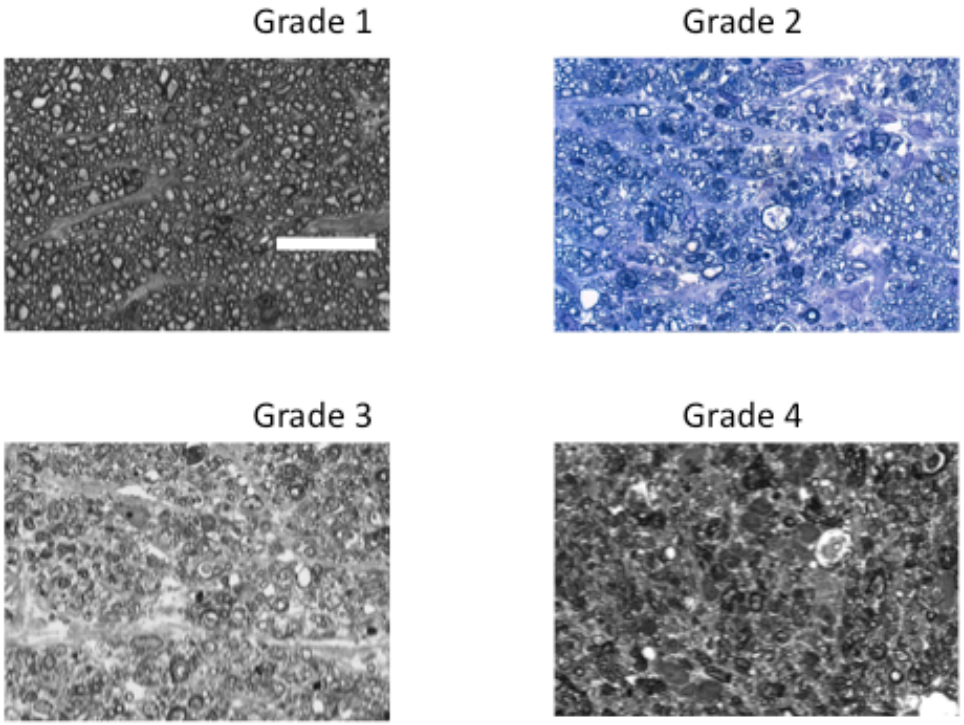

Figure 90 Grades of optic nerve damage

Grade 1- A healthy optic nerve with no axon damage. Grade 2- Nerve with a focal damage. Grade 3- Nerve with damage spread to more than one area (medium sized axons still survived). Grade 4- Nerve with only the smallest axons surviving. Scale bar represents 25μm.

Results

Intravitreal injections

The cells stay suspended as a clump in the vitreous. Analysis of retinal sections failed to show integration of transplanted cells into the retinal layers except for one occasion. Sometimes, OEC clumped behind the lens Figure 91.

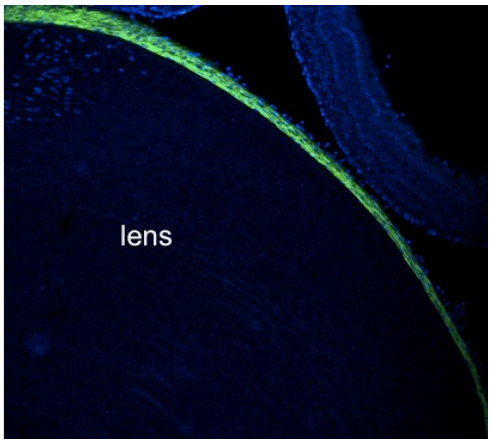

Figure 91 Intravitreally injected OEC deposited on the posterior lens surface.

GFP-OEC was injected intravitreally in normal adult rat eyes. Two weeks after the transplantation, the rats were sacrificed. Eyes were fixed, embedded in OCT and sectioned. The sections were stained with DAPI and imaged. Green OEC were detected behind the lens in the vitreal cavity. No OEC were detected in the retina.

Four days after OEC injection

Four days after the OEC injection, we found OEC on the retina in one eye. The OEC exhibit long spindle shaped migratory morphology and lay on top of the ganglion cell layer (GCL) Figure 92. They seem to migrate from the injection point towards the ONH Figure 93. The injection site was evident by the needle mark on the retina and a localised high concentration of OEC. In the retina, the OEC lay flat, parallel to the nerve fibres, while in the ONH, the OEC align themselves perpendicular to the axis of the nerve head Figure 94. Interestingly, there was no OEC migration in the direction away from the ONH.

However, in subsequent experiments, OEC injected intravitreally did not integrate into the retinal layers at one week or four weeks after the injection.

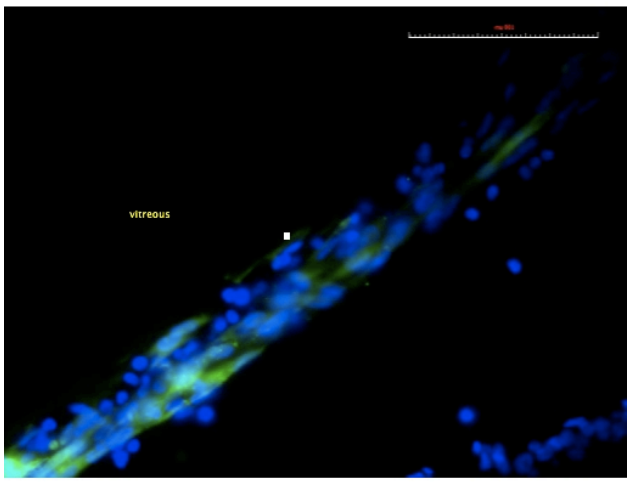

Figure 92 Spindle shaped OEC aligned on the ganglion cell layer of the rat retina.

We injected green OEC (stained with cell tracker dye, CMFDA) intravitreally in the adult rat eye. After four days, we sacrificed the animal; the eye was fixed, embedded in OCT and sectioned. The sections were stained blue with DAPI. Spindle shaped green OEC align parallel to the ganglion cell layer, but do not integrate into other layers of retina. Scale bar represents 100µm.

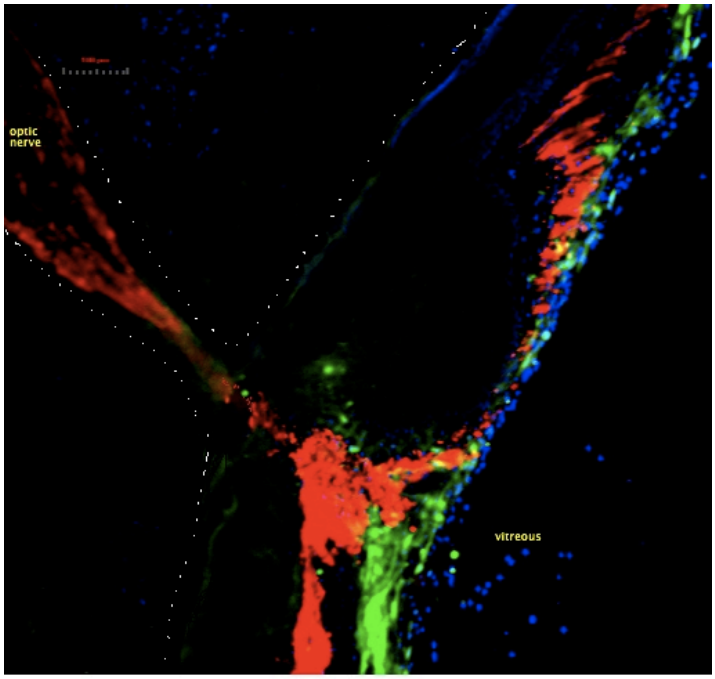

Figure 93 Spindle shaped green OEC lay on the inner nuclear layer and did not integrate into other layers of retina.

We injected green OEC (stained with cell tracker dye, CMFDA) intravitreally in the adult rat eye. After four days, we sacrificed the animal; the eye was fixed, embedded in OCT and sectioned. The sections were immunostained for neurofilament (red) and DAPI (blue). Spindle shaped green OEC lay on the inner nuclear layer and do not integrate into other layers of retina. OEC seem to migrate towards the ONH through the nerve fibre layer.

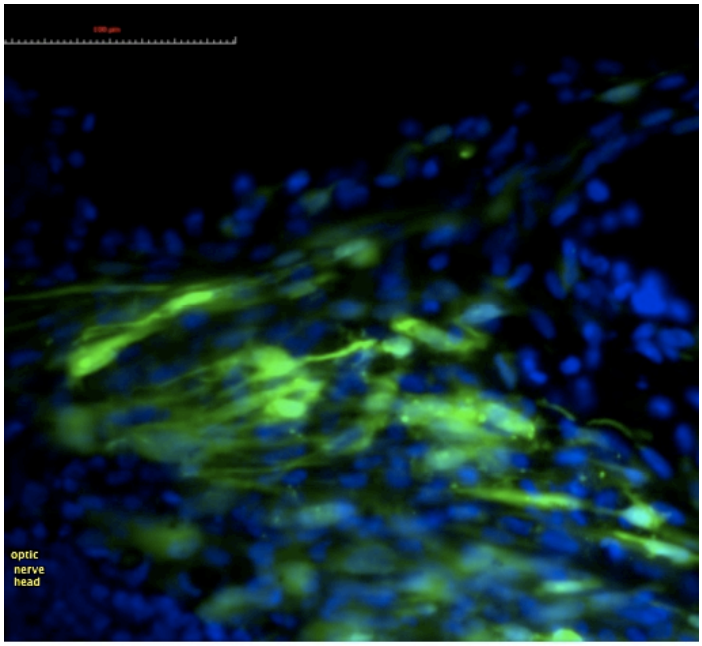

Figure 94 OEC at optic nerve head in a normal rat eye.

At four days after intravitreal injection of OEC, we sacrificed the rat, fixed and sectioned the eyes. The nuclei in the sections were stained blue with DAPI. Spindle shaped green OEC lay perpendicular to the retina at the ONH. Scale bar represents 100μm.

Subretinal injection

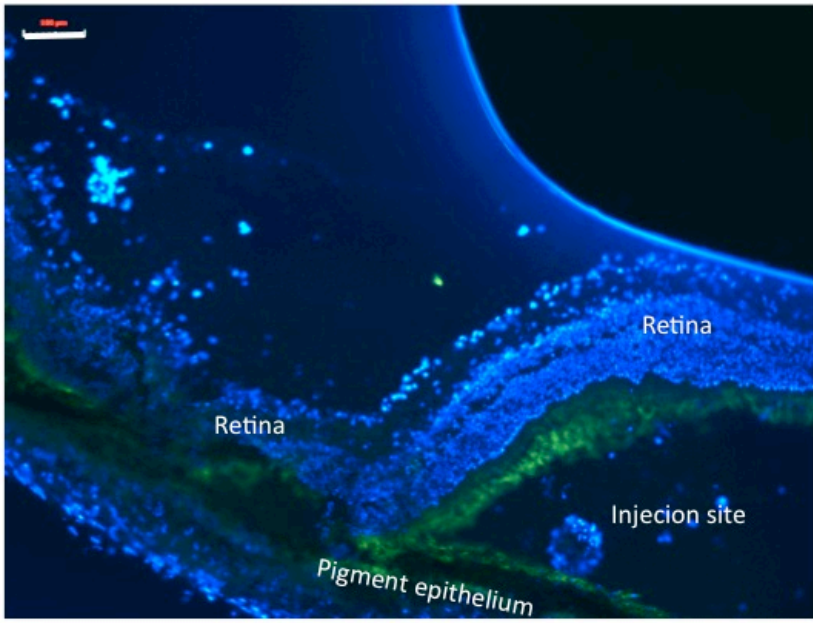

Figure 95 Subretinal injection of OEC in the rat eye causes retinal detachment.

GFP-OEC were injected subretinally in the normal rat eye. One week later, the animal was sacrificed, the eyes were fixed and embedded in OCT. Sections were collected and nuclei were stained with DAPI. The injection site showed retinal detachment from the underlying pigment epithelium. Scale bar represents 100µm.

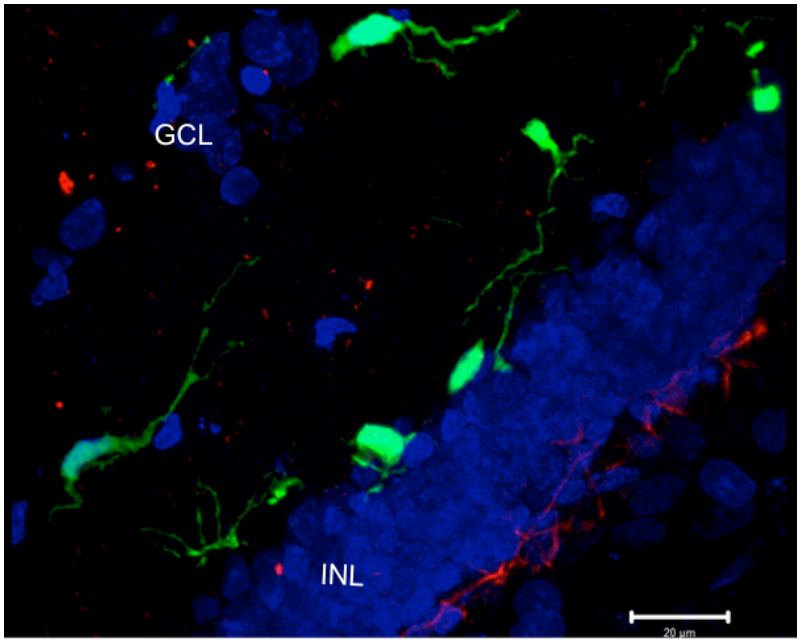

Figure 96 Subretinal injection of OEC in a normal rat eye.

eGFP-OEC were injected sub-retinally in the normal rat eyes. The rats were sacrificed after fifteen days and eyes were fixed, dehydrated and embedded in OCT and sectioned. The sections were immunostained for neurofilament antibody and DAPI to detect the postion of OEC relative to nerve fibre layer. The sections were imaged using a fluorescent confocal microscope. OEC (green) with spindle shaped elongated processes extend across the inner plexiform layer between the inner nuclear layer and ganglion cell layer. However, the retina is not intact throughout the section; there areas of localized retinal detachment. The staining pattern of neurofilaments indicates nerve fibre layer fragmentation, probably due to complications of sub-retinal injection.

Enzymatic vitreolysis

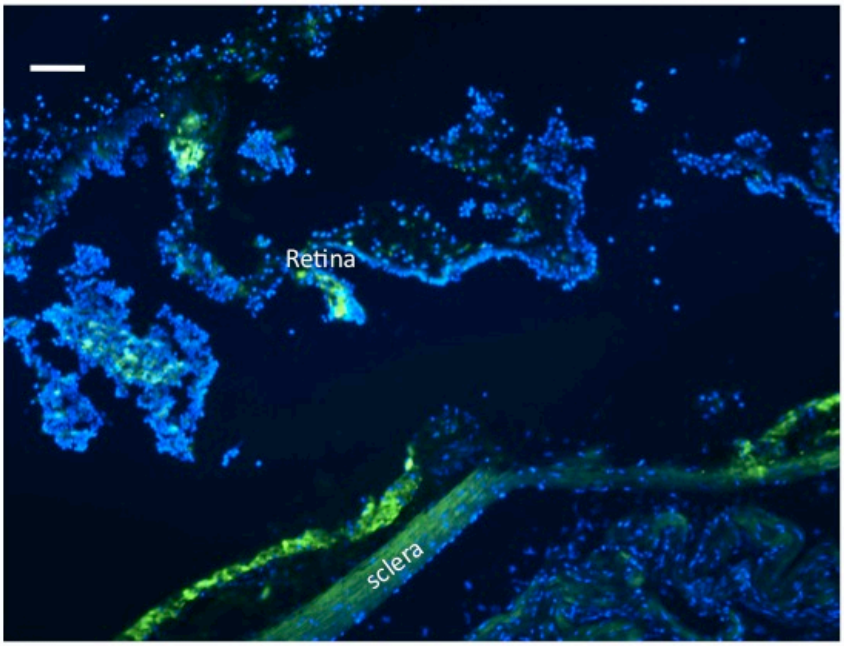

Figure 97 Retinal damage due to chemical vitreolysis.

We injected a mixture of collagenase, hyaluronidase and plasmin intravitreally to induce chemical vitreolysis, which could facilitate better adherence of OEC to the retinal surface. One week after the vitreolysis, we injected GFP OEC intravitreally. They spread well and did not remain in a cluster in the vitreous. Two weeks after injection, the rats were sacrificed by transcardiac perfusion and the eyes were fixed, embedded in OCT. Sections were collected on glass slides and stained with DAPI to recognize the nuclear layers of retina and imaged using fluorescent confocal microscope. The retina was disintegrated and the various layers were not recognizable. Scale bar represents 100µm.

The main caveat of sub-retinal injection is that the cell injections cause massive retinal detachment, compromising the structure and anatomy of retina.

OEC from rat pups

Initially, we obtained eGFP expressing OEC for transplantation from postnatal rat pups. About 50,000 OEC were transplanted intravitreally into healthy rat eyes. Animals were sacrificed two weeks after transplantation. The eyes were fixed in PFA and retinal explants were prepared. The retina was stained with DAPI and the RGC layer was imaged using fluorescent confocal microscope. Green OEC formed a sheet of cells on the RGC layer and the RGC nuclei were not visible from the top Figure 98. The OEC did not show spindle shaped morphology; they were rather rounded, which suggests proliferative rather than migratory activity.

As the aim of the transplantation experiment was to establish a cellular transplant in contact with RGC or ILM so as to protect the RGC/axons, we switched from pups to adult rats as donors of OEC for transplantation in glaucomatous rat eyes. Proliferation of OEC cultures from adult rats was slower, but over 97% of cells expressed the marker proteins p75NTR and s100 as well as mRNA for the neurotrophins BDNF, NT3, NGF and GDNF (Figure 20 and Figure 21). We hypothesised that OEC from adult animals might display a less proliferative morphology on the retina and migrate and adhere to the ILM.

Effect of OEC in glaucomatous rat eyes

We did not succeed in chemical vitreoctomy with preservation on retinal structure. We also did not manage to inject subretinally with preservation of retinal structure. Therefore, to evaluate the effect of OEC on glaucomatous eyes, we relied on intravitreal injection of OEC without vitreoctomy.

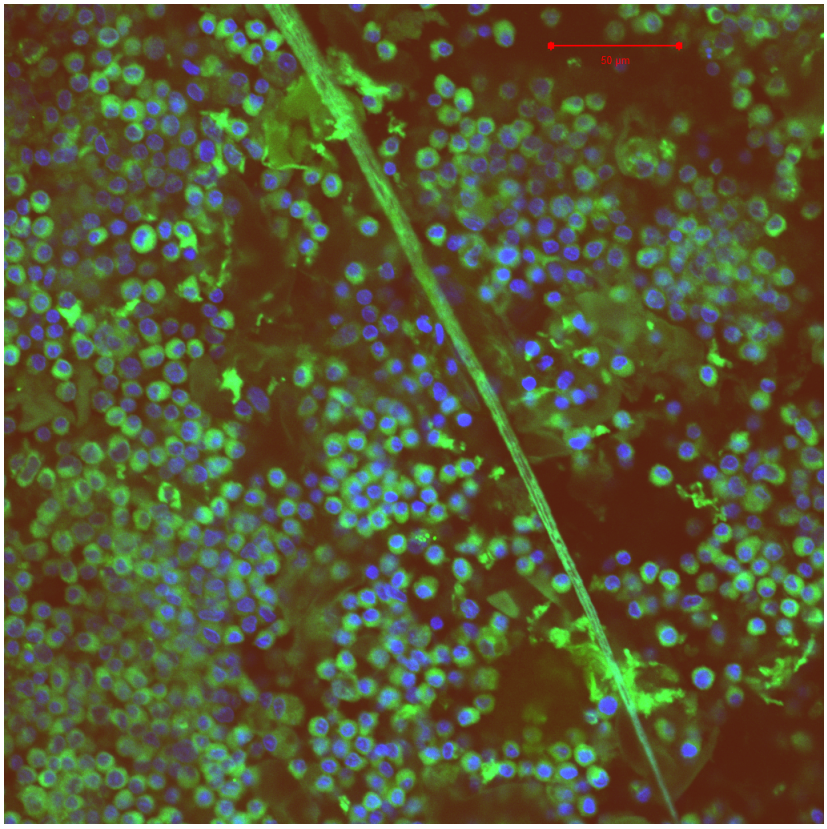

Figure 98 OEC from rat pups on retinal whole mount exhibited proliferative morphology.

eGFP-OEC were isolated from rat pups and cultured for seven days. The cells were trypsinised and injected intravitreally into rat eyes. After two weeks, the rats were sacrificed. Eyes were fixed in PFA and retinal whole mounts were prepared. The retina was stained with DAPI and the RGC layer was imaged using fluorescent confocal microscope. The OEC formed a sheet on the retinal surface, but did not exhibit a spindle shaped migratory morphology. RGC nuclei were not visible due to the overcrowding of OEC above the RGC layer. Scale bar represents 50µm.

Cryosections of the OEC injected eyes showed that the OEC adhered to the posterior surface of the lens. OEC behind the lens in the vitreous in front of the retina were identified by their green fluorescence. Retinal layers were demonstrated by the nuclei stained with DAPI Figure 100.

Intraocular pressure during the course of the study

The course of IOP in the OEC/carrier injected eyes is shown on Figure 101. Among the eyes with only one bead injection, the rate of IOP rise was different in the OEC injected and carrier injected groups. The OEC injected eyes had IOP of the order of 30 mmHg (with fluctuations) throughout the study (figure C), whereas the carrier injected eyes had IOP of 50mmHg for 20 days after the bead injections (figure A). Where the initial bead injection failed to raise the IOP, a second injection was performed after seven days. Then, the carrier eyes had IOP in the range of 30-40mmHg for 20 days, after which IOP fell to the twenties (figure B). In the OEC injected eyes, IOP rose to 50 mmHg by day 15 but fell to the twenties by day 20 (figure D). The presence of OEC seems to affect the IOP in eyes with one bead injection.

Optic nerve axon damage evaluation- grading and quantification

The optic nerves of carrier injected eyes were of grades 2, 3 and 4 (n=2 in each group) where as the nerves of half of OEC injected eyes were healthy, grade one (n=4). Two of the OEC injected eyes had grade two damage and one had grade three damage. Overall, the OEC injected eyes had higher number of healthier axons than the carrier injected eyes Figure 104.

OEC injected eyes (n=8) had a significantly higher number of healthy axons than the carrier injected eyes (n=6) P=0.001 Figure 105.

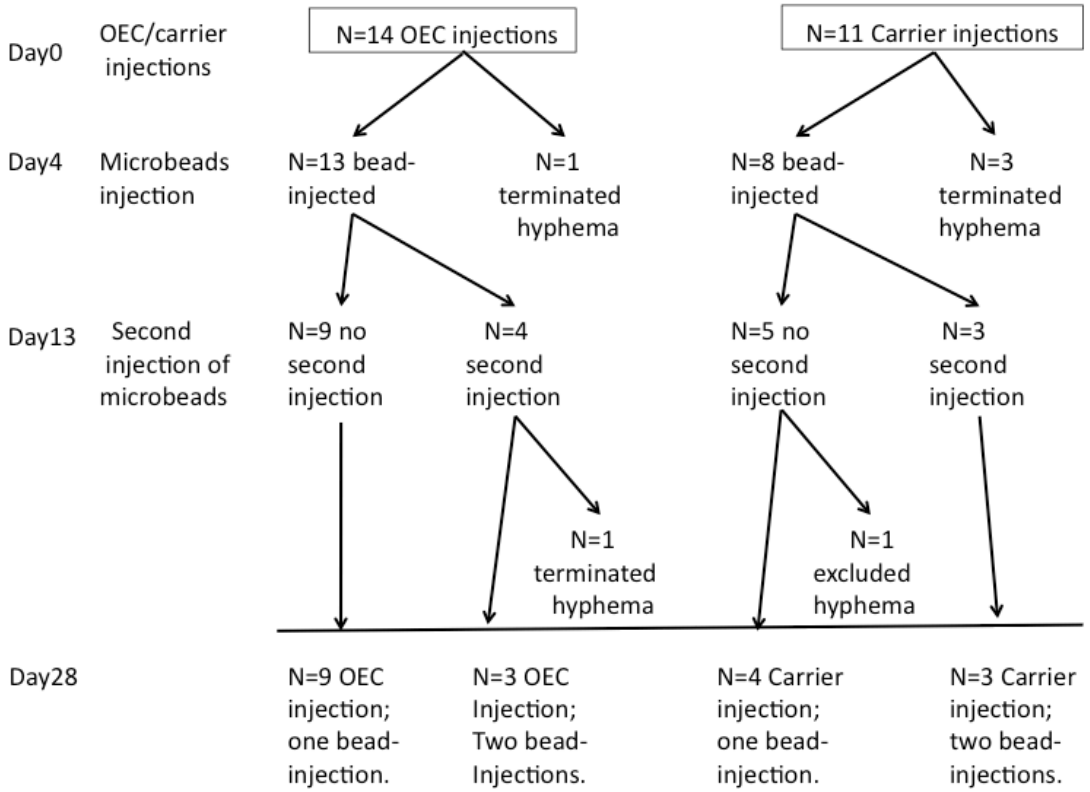

Figure 99 A flow chart describing the experiment set up to study the effects of intravitreal injection of OEC on glaucomatous optic nerve damage.

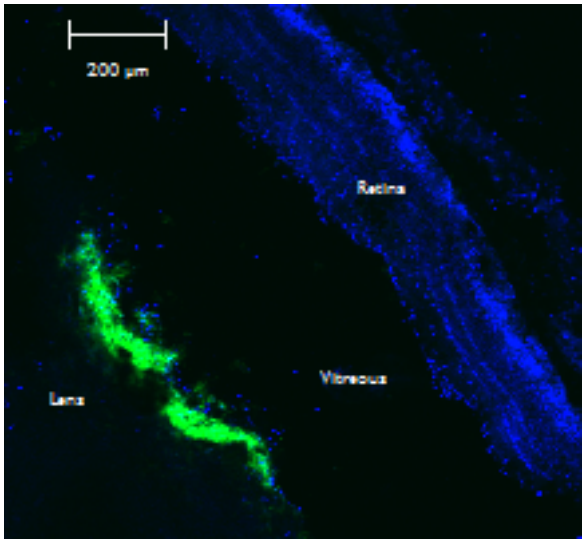

Figure 100 OEC cluster on the posterior surface of the lens after intravitreal injection of GFP-OEC and subsequent induction of glaucoma.

GFP-OEC was injected into the vitreous of rat eye prior to induction of glaucoma. 28 days after the induction of glaucoma, the rats were perfused transcardially and eyes were fixed and dehydrated. The eyes were embedded in OCT and sectioned longitudinally. The sections were stained with DAPI. GFP-OEC were found to adhere to the posterior lens surface. Scale bar represents 200µm.

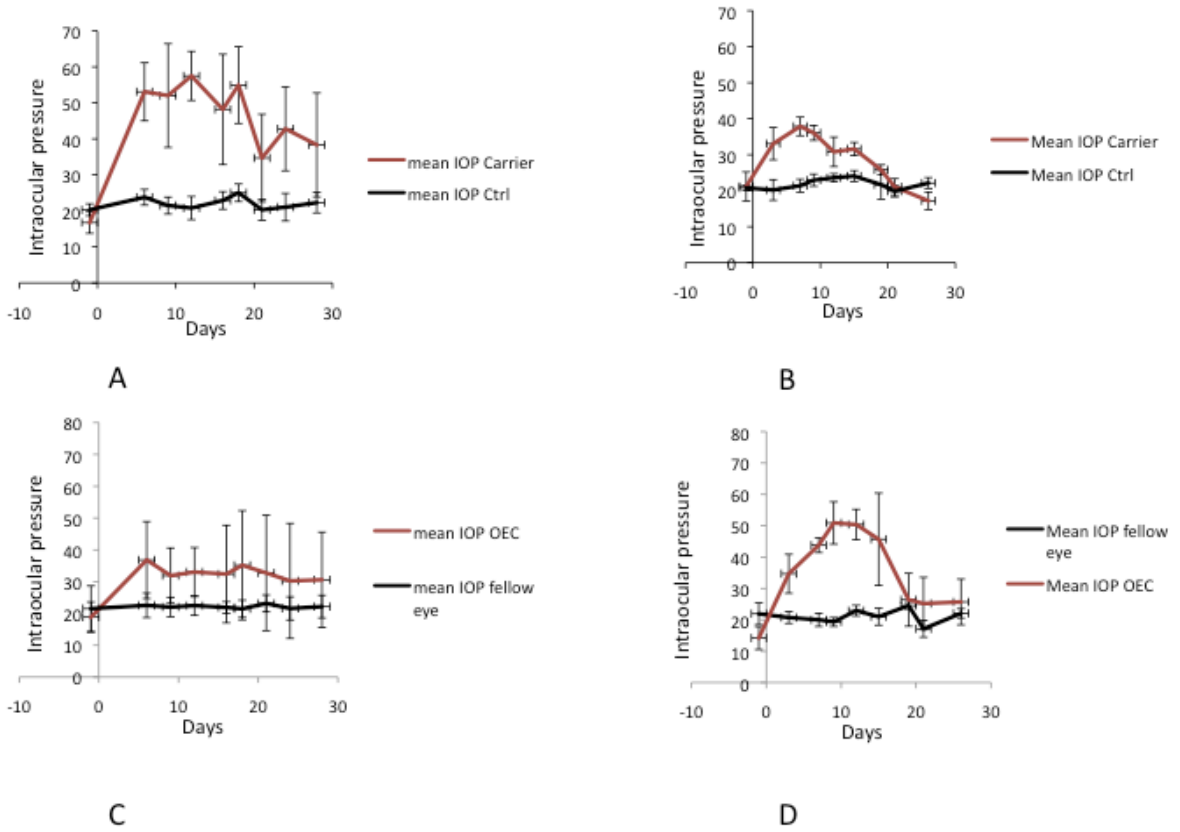

Figure 101 Course of intraocular pressure (IOP) in the OEC/carrier injected eyes for 28 days after induction of glaucoma.

A- IOP of carrier injected eyes (with one bead injection on day zero) was above 50mmHg after induction of glaucoma for about 15 days while the fellow control eyes had IOP of around 20mm of Hg throughout the study. At about day 20, the IOP of carrier-injected eyes fell between 30 and 40mmHg, n=5. B- Where the IOP did not raise after initial bead injection, a second injection was required

in the carrier injected eye (which is counted as day zero), n=1. IOP stayed between 30 and 40mm Hg for 15 days and then fell to the twenties. The control eyes were in the range of 20mmHg. C- IOP of OEC injected eyes (with one bead injection on day zero) mostly stayed above 30mmHg throughout the study n=6, however the IOP was heavily fluctuating. The control eyes were in the range of 20mmHg throughout the study. D- Where the IOP did not raise after initial bead injection, a second injection was required in the OEC injected eye (which is counted as day zero), n=2. Here the IOP rose to 50mmHg over ten days and then fell to twenties by day 20. The control eyes were in the range of 20mmHg throughout the study.

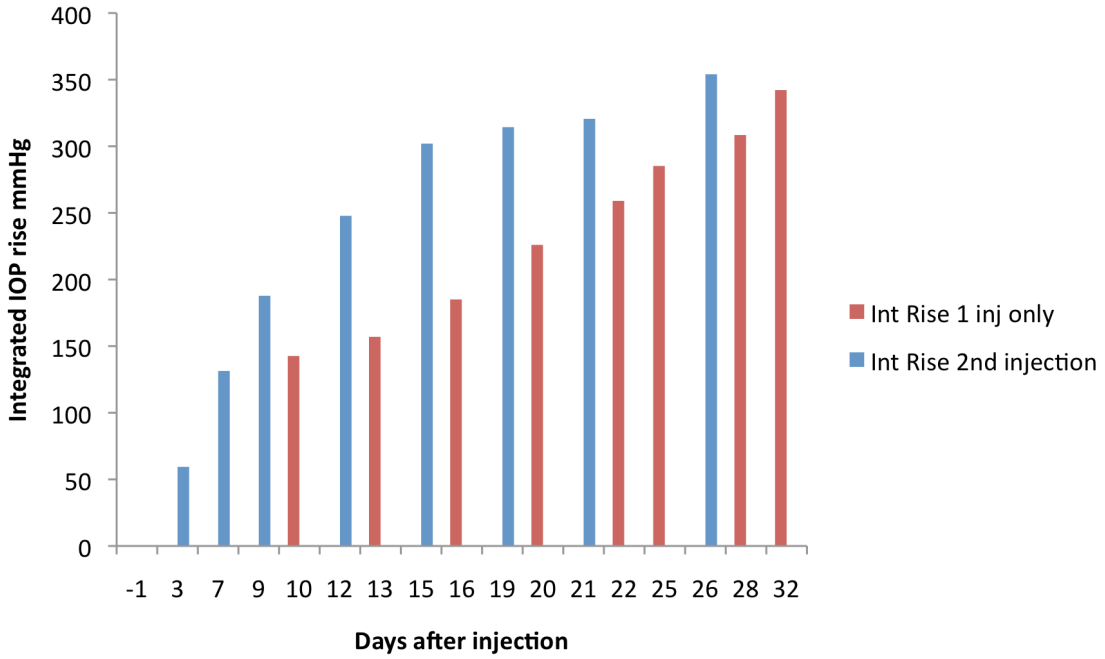

Figure 102 Course of integral IOP rise (Int rise) in the OEC injected eyes.

For 28 days after induction of glaucoma, Int rise was gradual in the group that received one dose of magnetic beads. Where the IOP did not rise with the first injection of beads, a subsequent injection was required. The integral IOP rise was very rapid after the second injection when compared to the gradual rise after the first injection. Integral IOP is the difference in IOP between the bead-injected and control eyes, calculated as the function of number of days after the injection.

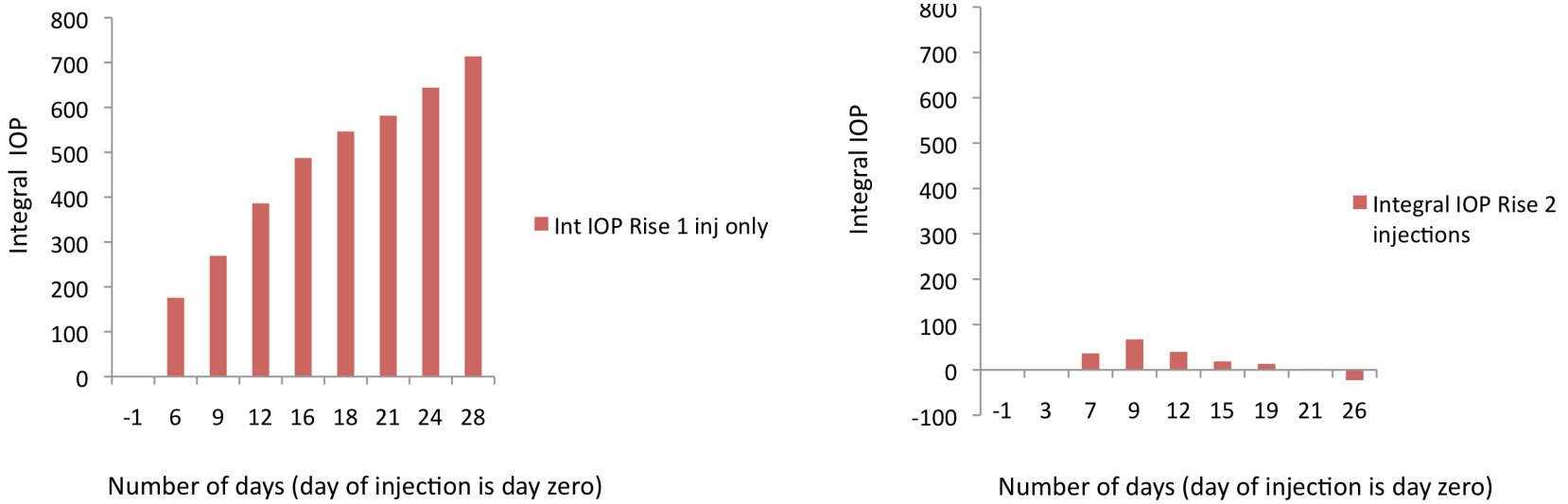

Figure 103 Course of integral IOP rise in the carrier-injected eyes

For 28 days after induction of glaucoma, IOP rose rapidly in the eyes with successful bead injections; where the IOP did not rise, a subsequent injection of beads was required. But the second injection also failed to rise the IOP considerably when compared to the successful initial injections.

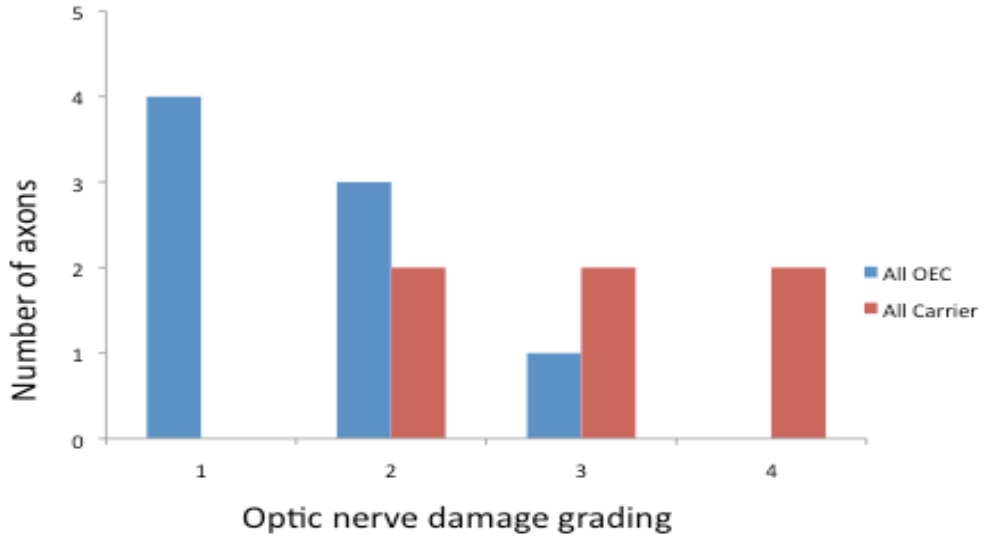

Figure 104 OEC injected eyes have lower grades of optic nerve damage due to glaucoma than the carrier solution injected eyes.

Intravitreal injections of OEC/carrier solution were made prior to induction of glaucoma. 28 days after the induction of glaucoma, the rats were perfused transcardially and optic nerves from 2mm behind the globe were collected. The nerves were processed and semi-thin sections were stained with toluidine blue. The extent of damage of nerves was graded by two observers from grade 1(healthy) to grade 5 (no healthy axons left). Half of the OEC injected eyes had healthy optic nerves while there were no healthy nerves in the carrier injected eyes. Overall, OEC injected eyes (n=8) had lower grades of optic nerve axon damage when compared to that of the carrier injected eyes (n=6).

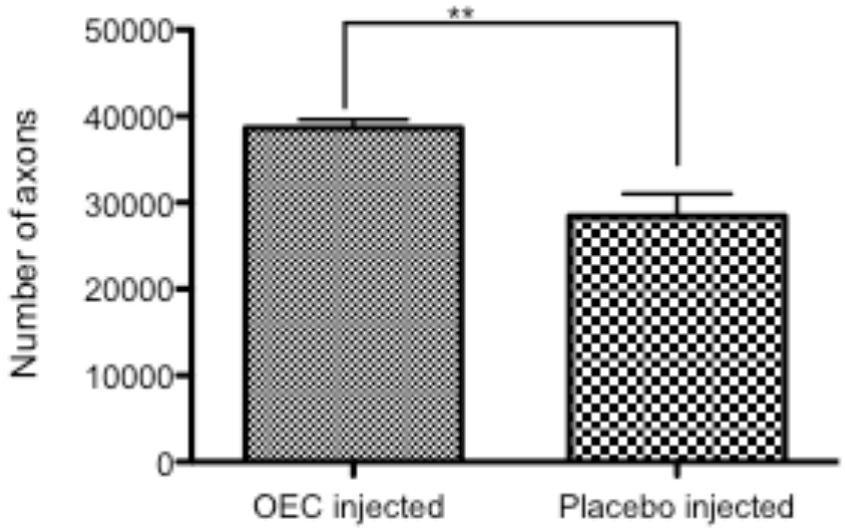

Figure 105 Glaucomatous eyes had more surviving axons with intravitreal injections of OEC than placebo.

Intravitreal injections of OEC/carrier solution were made prior to induction of glaucoma. 28 days after the induction of glaucoma, the rats were perfused transcardially and optic nerves from 2mm behind the globe were collected. The nerves were processed and semi-thin sections were stained with toluidine blue. The number of axons were counted manually using ImageJ software and the two groups were compared statistically using t test. OEC injected eyes (n=8) had a significantly higher number of axons than the placebo injected eyes (n=6), p=0.001.

Discussion

Labelling of OEC with cell tracker dye

One week after intravitreal injection, we could not detect CMFDA labelled green fluorescent cells in the eye. This could be due to the loss of green dye from the cells or the cells might have divided after transplantation and the green fluorescence would have been reduced beyond detection limits. In culture, OEC would divide continuously and any cell tracker dye is lost after a few divisions.

Finally, we isolated green fluorescent OEC from transgenic rats expressing eGFP in its genome.

Injection of OEC in glaucomatous rat eyes

In the *in vitro* experiments to characterise the interactions of OEC and RGC, we used OEC from rat pups. However, we found that OEC from pups proliferated on the retinal surface and had to switch to adult rats for OEC transplantation. In the *in vitro* co-culture experiments, we used serum free media with supplements necessary for facilitate ensheathment. But in the retina, we could not control the availability of growth factors to the cells, which would have contributed to their excessive proliferation.

Despite their excessive proliferation, OEC isolated from pups and adults were comparable in terms of neurotrophin expression as well as expression of marker proteins. Therefore, the neuroprotective effects of OEC on RGC might not be dependent on the age of the donor rats from which the OEC are derived.

Other studies have shown that intact retina posses several barriers for transplanted cells to integrate to the different layers. Glaucomatous retina might effectively facilitate the integration of intravitreally transplanted OEC because the integrity of inner limiting membrane and Müller glia is lost in glaucoma.

To simulate the human disease, it would be better to induce glaucoma first followed by OEC transplantation. But, targeted intravitreal delivery of OEC requires direct visualisation of the retina to minimise lens and retina damage. Visualising the retina requires dilation of the pupils. However, dilating the pupils in glaucomatous eyes could in effect, force the magnetic beads out of the iridocorneal angle. The reduction in IOP due to the efflux of beads from the iridocorneal angle may compromise the glaucoma model. Therefore, we decided to inject the OEC into the eyes before induction of glaucoma.

For the treatment of human glaucoma, where the patient already has structural and functional changes of retina and optic nerve, our experiment is not an exact simulation. However, injection of OEC prior to glaucoma onset can be used to investigate their effects in the presence of raised IOP.

Effect of OEC on IOP of glaucomatous eyes

We found that the IOP rise in the OEC injected eyes were less than in carrier-injected eyes, where IOP was very high.

The OEC could have reduced the aqeous humour production by the secretion of vasoconstrictors. One such vasoconstrictor, endothelin, which is also a neuroprotective agent is synthesised in the olfactory mucosa and prevents apoptosis of neurons (Gouadon et al., 2010). OEC could also have lowered the IOP by increasing the aqueous outflow through secretion of prostaglandins or their promoters. OEC transplantation resulted in the upregulation of cyclohexogenases that promote the synthesis of prostaglandins in models of spinal cord injury (Lopez-Vales et al., 2004). Prostaglandins are also known to be neuroprotective (Akaike et al., 1994).

Neuroprotection by OEC

We found that OEC injection can reduce axon damage in glaucomatous eyes. However, a part of the protection could be attributed to lower IOP in these eyes compared to the carrier-injected eyes.

OEC are known to secrete neurotrophins like BDNF, NGF and GDNF (Woodhall et al., 2001). These neurotrophins are neuroprotective to RGC in glaucoma (reviewed in the introduction chapter). Therefore the protective effects of OEC in glaucomatous eyes in our study might be partly due to the secretion of neurotrophins.

Even though we studied the axon regenerative abilities of OEC *in vitro*, this was not relevant in the context of glaucomatous axon damage, as we were aiming at neuroprotection of existing axons only.

Possibilities of OEC transplantation in bigger eyes

To overcome the limitations of the size of rat eye, OEC transplantation experiments could be done in bigger eyes of pigs or primates. The merits of pig/primate eyes would be

1. The possibility of physical vitrectomy prior to OEC transplantation.
2. Insertion of extracellular matrix laden with OEC in the retina/optic nerve
3. The possibility of injecting OEC into the optic nerve head.
4. Presence of lamina cribrosa.

Physical vitrectomy

Vitrectomy would be possible because of the relatively bigger size of the eye and vitreous. The positioning of OEC in the vitreous hampers the chances of OEC to attach to a firm surface and migrate into the retinal layers. After the removal of the vitreous close to the retina, the OEC could be injected onto the retinal surface.

OEC injection in the optic nerve head

In glaucoma, the initial insult seems to occur at the nerve head (Quigley et al., 1981, Soto et al., 2010) (Soto et al., 2010). Therefore, introducing OEC that could ensheath the RGC axons could possibly protect them from IOP induced insult. Injection of OEC directly into the nerve head would limit the possibilities of OEC migrating into peripheral retina or attaching to the lens surface. Since the nerve head in pigs and primates are big enough, OEC

injection would be a plausible surgical option. However, in rats the presence of large blood vessel in the centre of the optic nerve head poses a high risk of haemorrhage.

Presence of lamina cribrosa

Lamina cribrosa is one of the important tissues affected in human glaucoma (Quigley et al., 1981). Although the rats posses a glial lamina, critics claim that the absence of a robust lamina cribrosa makes the pathology of glaucoma in these animals very different and therefore not comparable. Pigs and monkeys posses a lamina cribrosa that is very similar to that of humans and therefore the injection of OEC in a glaucoma model of pig/monkey eyes would truly reflect the possibilities in human eye.

Possible effects of OEC on the RGC function

OEC partially preserve optic nerve axons in the presence of glaucoma. This might in turn improve the RGC function. The functional rescue of RGC should be evaluated to confirm the benefits of OEC transplantation. On the other hand, cells injected into the vitreous/retina possess risks of blocking the entry of light and thereby blocking vision.

From the OEC transplants to date, we have understood that intact retina does not allow the integration and further migration of OECs into the retinal layers.

Other studies have shown that the retinal barrier is indeed an obstacle to intravitreally-transplanted cells even in diseased retina (Young et al., 2000) (Bull et al., 2008).

The retinal barrier makes it extremely difficult for the OECs to enter the retina; therefore a physical rupture/lesions at the vitreal interphase of retina could help in the integration of OECs into the retina. However, the fact that the integrity of retinal barriers is compromised in glaucoma might facilitate the migration of OEC into the RGC layer or the optic nerve head.

Given our premise that the primary targets of the raised IOP are the RGC axons in the ONH, the protective effect of the OEC transplants on the ganglion cells themselves in the retina, whether due to lower IOP, or neuroprotective/neurotrophic effects from the transplanted cells, could not overcome the visual loss caused by axotomy in the ONH.

However, the rats also showed a protective effect on the numbers of axons in the optic nerve. One possibility is that stimulatory effects of the OECs on the RGCs may enable their axons better to resist insult at the ONH level.

Conclusions

Our main aims were to characterise a rat glaucoma model and to study the structural and functional changes associated with glaucoma. We modified the magnetic beads injection model of rat glaucoma to achieve a consistent rise of intraocular pressure using strong neodymium ring magnets. We conducted the first study of early functional changes in the retina in this rat glaucoma model. We found that there is a marked reduction in ganglion cell function without reduction in the number of RGC at one week after the induction of ocular hypertension, which progresses over four weeks, resulting in further attenuation of RGC function along with a decline in RGC number. We also demonstrated that in the magnetic bead model of ocular hypertension, RGC function was selectively attenuated, while the bipolar and photoreceptor neurons were not significantly affected.

We then tested whether transplantation of OEC can prevent pressure-induced axonal damage. Prior to in vivo experiments, we co-cultured the RGC and OEC in vitro to gain a better understanding of the interactions of the two cell types. Using the co-culture model, we were able to demonstrate the protective role of OEC on RGC survival, maintenance of healthy neurites, ensheathment and bundling of RGC axons. The protective role of OEC was mainly contact-mediated rather than via secreted factors. We also showed that the OEC phagocytosed dead RGC in the culture; this implies that OEC transplantation in the CNS could help clear dead neurons and reduce inflammation to facilitate a better milieu for regeneration.

We also developed cell culture techniques for serum-free culture of rat OEC with the intention of ensuring sufficient and safe human OEC cultures in the future.

OEC protect optic nerve axons in glaucoma.

Intravitreal injection of OEC prior to induction of ocular hypertension protected optic nerve axons at four weeks after the induction of glaucoma.

OEC deposited in the vitreous behind the lens. OEC seem to lower the IOP; this could be one of the reasons for reduced axonal damage in the OEC-injected glaucomatous eyes. The neuroprotection offered by OEC could also be due to neurotrophins secreted into the vitreous.

Future work

Introduction of OEC into the vitreous after induction of ocular hypertension

Intraocular transplantation studies indicate that the main barrier to cell integration into the retina is the inner limiting membrane (Young et al., 2000) (Bull et al., 2008). In animal models of glaucoma, grafted cells only appear to integrate into damaged retina (Li et al., 2008) (Huo et al., 2011). Future OEC transplantation studies will therefore investigate whether cell injection after introduction of ocular hypertension facilitates integration into the retina/optic nerve. Further functional investigations such as rat electroretinography or ex-vivo nerve conduction studies will explore the effect of ensheathment of RGC axons. It will be important to confirm that the ensheathment of axons does not cause a disruption of nerve conduction.

OEC in extracellular matrix

Injection of OEC in suspension as a bolus may not be the optimal way to transplant these cells. Trypsinisation and lack of adhesion to a surface following intravitreal injection may result in a number of cells not surviving transplantation. Growing OEC on extracellular matrix or biodegradable membranes suitable for intraocular delivery may enhance survival and gradual migration of cells. This method would also suit to introduce OEC into a localised region of retina.

However, the relatively small size of the rat eye may be a practical limitation to delivery of OEC grown on a scaffold, as available instruments suitable for surgery on the rat eye may not have lumen sufficiently wide to allow delivery of membranes.

Importance of OEC in treatment of glaucoma

Glial activation in glaucoma was initially considered to be either a protective response to glaucomatous axon damage or a factor adding to the glaucomatous axonal injury (Johnson and Morrison, 2009). However, recent evidence indicates that glaucomatous axonal damage may be secondary to glial damage (Dai et al., 2012). The authors suggest that axonal damage could be a result of lack of metabolic support due to glial atrophy.

Since Muller glial end feet contribute to maintenance of healthy nerve fibre layer, their damage would lead to dystrophy of retinal ganglion cells. Ensheathment of the nerve fibre layer/ optic nerve axons by OEC processes could possibly be an alternative source of metabolic support to the ailing axons in glaucoma.

Optic nerve model

In human glaucoma, the ONH assumes a characteristic appearance described as “cupping”. Pores of the lamina cribrosa through which axons pass as they leave the eye undergo deformation, exposing axons to shear stress. This mechanical stretching of axons could be simulated *in vitro* using the culture of RGC neurites on deformable gels. The effect of the stretch on neurites could be quantified histologically as well as by monitoring axonal transport. Upon addition of OEC to the neurites and subsequent ensheathment, we could evaluate the effect of OEC on stretch-induced neurite injury.

The effect of OEC ensheathment of neurites on nerve conduction could be tested using electrophysiological techniques. However, this could be technically very challenging using neurites in culture, as the longest RGC neurites we cultured are about 4-5 mm in length. The cell body of the neurites lie in the retinal explant and therefore, visual tracking of the neurite along with a single cell body could be very difficult.

In order to grow long neurites from retinal explants, we etched grooves in plastic petridishes. However, the plastic dishes were not sterile and we regularly had bacterial infection in the cultures (data not shown). The dishes

would melt upon autoclaving or chip upon treatment with alcohol. Therefore, a glass petridish would be ideal for growing neurites from the explant. We are currently exploring options of sourcing custom-made grooved glass dishes. Glass would be the ideal material for the dish, because it would allow live cell microscopy on the explants inside the groove. It would also enable us to conduct electrophysiological tests on the neurites in the groove.

Role of p75NTR in ensheathment

To study the role of p75NTR in ensheathment by OEC, we tried to knock down receptor expression using si-RNA (small interfering RNA) targeted at p75NTR. However, OEC did not survive the treatment with si-RNA reagents (data not shown).

Successful transfection of OEC with si-RNA against p75NTR would enable us to study the role of this receptor not only in ensheathment, but also in migration, proliferation and phagocytosis.

A p75NTR knockout mouse has been developed and used to study the effect of the receptor on olfactory neurons and olfactory memory (Barrett et al., 2010). Only natural turn over of olfactory neurons was considered; experiments to damage olfactory mucosa or bulb to induce synchronous regeneration of the olfactory system were not conducted. In this model, there was no evidence to support a role of the p75NTR in olfactory memory formation. Functional redundancies often make it difficult to understand the role of a neurotrophin receptor in knockout animal models (Snider, 1994) (Geddes et al., 2006).

OEC cell line

Different from other investigators, we were unsuccessful in transfecting primary OEC using viral transduction via adeno- or lentivirus. Development of a cell line of OEC might make transfection experiments easier. Moreno-Flores et al., successfully generated a cell line of OEC. The authors demonstrated that the OEC cell line supported axonal regeneration to a similar degree as primary cells do (Moreno-Flores et al., 2003).

However, the cell line would need to be well characterized before the effects of neurotrophin receptors could be compared to that of primary cells. For *in-vivo* experiments, any OEC cell line may pose a risk of tumour formation due to uncontrolled proliferation.

References

Abelson, M. B., Gilbert, C. M. & Smith, L. M. (1988) Sustained reduction of intraocular pressure in humans with the calcium channel blocker verapamil. *Am J Ophthalmol,* 105**,** 155-9.

Agapova, O. A., Ricard, C. S., Salvador-Silva, M. & Hernandez, M. R. (2001) Expression of matrix metalloproteinases and tissue inhibitors of metalloproteinases in human optic nerve head astrocytes. *Glia,* 33**,** 205-16.

Agarwal, N., Agarwal, R., Kumar, D. M., Ondricek, A., Clark, A. F., Wordinger, R. J. & Pang, I. H. (2007) Comparison of expression profile of neurotrophins and their receptors in primary and transformed rat retinal ganglion cells. *Mol Vis,* 13**,** 1311-8.

Ahmed, Z., Mazibrada, G., Seabright, R. J., Dent, R. G., Berry, M. & Logan, A. (2006) TACE-induced cleavage of NgR and p75NTR in dorsal root ganglion cultures disinhibits outgrowth and promotes branching of neurites in the presence of inhibitory CNS myelin. *FASEB J,* 20**,** 1939-41.

Akaike, A., Kaneko, S., Tamura, Y., Nakata, N., Shiomi, H., Ushikubi, F. & Narumiya, S. (1994) Prostaglandin E2 protects cultured cortical neurons against N-methyl-D-aspartate receptor-mediated glutamate cytotoxicity. *Brain Res,* 663**,** 237-43.

Alarcon-Martinez, L., Aviles-Trigueros, M., Galindo-Romero, C., Valiente-Soriano, J., Agudo-Barriuso, M., Villa Pde, L., Villegas-Perez, M. P. & Vidal-Sanz, M. (2010) ERG changes in albino and pigmented mice after optic nerve transection. *Vision Res,* 50**,** 2176-87.

Alm, A. & Nilsson, S. F. (2009) Uveoscleral outflow--a review. *Exp Eye Res,* 88**,** 760-8.

Alvarado, J., Murphy, C. & Juster, R. (1984) Trabecular meshwork cellularity in primary open-angle glaucoma and nonglaucomatous normals. *Ophthalmology,* 91**,** 564-79.

Anton, E. S., Weskamp, G., Reichardt, L. F. & Matthew, W. D. (1994) Nerve growth factor and its low-affinity receptor promote Schwann cell migration. *Proc Natl Acad Sci U S A,* 91**,** 2795-9.

Araque, A., Martin, E. D., Perea, G., Arellano, J. I. & Buno, W. (2002) Synaptically released acetylcholine evokes Ca2+ elevations in astrocytes in hippocampal slices. *J Neurosci,* 22**,** 2443-50.

Araque, A., Parpura, V., Sanzgiri, R. P. & Haydon, P. G. (1999) Tripartite synapses: glia, the unacknowledged partner. *Trends Neurosci,* 22**,** 208-15.

Armaly, M. F. (1963a) Effect of Corticosteroids on Intraocular Pressure and Fluid Dynamics. I. The Effect of Dexamethasone in the Normal Eye. *Arch Ophthalmol,* 70**,** 482-91.

Armaly, M. F. (1963b) Effect of Corticosteroids on Intraocular Pressure and Fluid Dynamics. Ii. The Effect of Dexamethasone in the Glaucomatous Eye. *Arch Ophthalmol,* 70**,** 492-9.

Armaly, M. F. (1964) Aqueous Outflow Facility in Monkeys and the Effect of Topical Corticoids. *Invest Ophthalmol,* 3**,** 534-8.

Armaly, M. F. (1965) Statistical Attributes of the Steroid Hypertensive Response in the Clinically Normal Eye. I. The Demonstration of Three Levels of Response. *Invest Ophthalmol,* 4**,** 187-97.

Asrani, S., Zeimer, R., Wilensky, J., Gieser, D., Vitale, S. & Lindenmuth, K. (2000) Large diurnal fluctuations in intraocular pressure are an independent risk factor in patients with glaucoma. *J Glaucoma,* 9**,** 134-42.

Au, E. & Roskams, A. J. (2003) Olfactory ensheathing cells of the lamina propria in vivo and in vitro. *Glia,* 41**,** 224-36.
Baldo, G. J. & Mathias, R. T. (1992) Spatial variations in membrane properties in the intact rat lens. *Biophys J,* 63**,** 518-29.
Barnett, S. C., Hutchins, A. M. & Noble, M. (1993) Purification of olfactory nerve ensheathing cells from the olfactory bulb. *Dev Biol,* 155**,** 337-50.
Barnett, S. C., Thompson, R. J., Lakatos, A. & Pitts, J. (2001) Gap junctional communication and connexin expression in cultured olfactory ensheathing cells. *J Neurosci Res,* 65**,** 520-8.
Barrett, G. L., Reid, C. A., Tsafoulis, C., Zhu, W., Williams, D. A., Paolini, A. G., Trieu, J. & Murphy, M. (2010) Enhanced spatial memory and hippocampal long-term potentiation in p75 neurotrophin receptor knockout mice. *Hippocampus,* 20**,** 145-52.
Becker, B. (1959) Carbonic anhydrase and the formation of aqueous humor. *Am J Ophthalmol,* 47**,** 342-61.
Bentley, C. A. & Lee, K. F. (2000) p75 is important for axon growth and schwann cell migration during development. *J Neurosci,* 20**,** 7706-15.
Bergles, D. E. & Jahr, C. E. (1997) Synaptic activation of glutamate transporters in hippocampal astrocytes. *Neuron,* 19**,** 1297-308.
Berkowitz, B. A., Lukaszew, R. A., Mullins, C. M. & Penn, J. S. (1998) Impaired hyaloidal circulation function and uncoordinated ocular growth patterns in experimental retinopathy of prematurity. *Invest Ophthalmol Vis Sci,* 39**,** 391-6.
Bernardos, R. L., Barthel, L. K., Meyers, J. R. & Raymond, P. A. (2007) Late-stage neuronal progenitors in the retina are radial Muller glia that function as retinal stem cells. *J Neurosci,* 27**,** 7028-40.
Bianco, J. I., Perry, C., Harkin, D. G., Mackay-Sim, A. & Feron, F. (2004) Neurotrophin 3 promotes purification and proliferation of olfactory ensheathing cells from human nose. *Glia,* 45**,** 111-23.
Bishop, P. N. (2000) Structural macromolecules and supramolecular organisation of the vitreous gel. *Prog Retin Eye Res,* 19**,** 323-44.
Black, J. A., Waxman, S. G. & Hildebrand, C. (1984) Membrane specialization and axo-glial association in the rat retinal nerve fibre layer: freeze-fracture observations. *J Neurocytol,* 13**,** 417-30.
Bode, S. F., Jehle, T. & Bach, M. (2011) Pattern electroretinogram in glaucoma suspects: new findings from a longitudinal study. *Invest Ophthalmol Vis Sci,* 52**,** 4300-6.
Bonomi, L., Perfetti, S., Noya, E., Bellucci, R. & Tomazzoli, L. (1978) Experimental corticosteroid ocular hypertension in the rabbit. *Albrecht Von Graefes Arch Klin Exp Ophthalmol,* 209**,** 73-82.
Bornstein, P. & Sage, E. H. (2002) Matricellular proteins: extracellular modulators of cell function. *Curr Opin Cell Biol,* 14**,** 608-16.
Bos, K. J., Holmes, D. F., Meadows, R. S., Kadler, K. E., McLeod, D. & Bishop, P. N. (2001) Collagen fibril organisation in mammalian vitreous by freeze etch/rotary shadowing electron microscopy. *Micron,* 32**,** 301-6.
Bristow, E. A., Griffiths, P. G., Andrews, R. M., Johnson, M. A. & Turnbull, D. M. (2002) The distribution of mitochondrial activity in relation to optic nerve structure. *Arch Ophthalmol,* 120**,** 791-6.
Bui, B. V., Edmunds, B., Cioffi, G. A. & Fortune, B. (2005) The gradient of retinal functional changes during acute intraocular pressure elevation. *Invest Ophthalmol Vis Sci,* 46**,** 202-13.
Bui, B. V. & Fortune, B. (2004) Ganglion cell contributions to the rat full-field electroretinogram. *J Physiol,* 555**,** 153-73.
Bull, N. D., Limb, G. A. & Martin, K. R. (2008) Human Muller stem cell (MIO-M1) transplantation in a rat model of glaucoma: survival, differentiation, and integration. *Invest Ophthalmol Vis Sci,* 49**,** 3449-56.

Bull, N. D. & Martin, K. R. (2009) Using stem cells to mend the retina in ocular disease. *Regen Med,* 4**,** 855-64.
Burgoyne, C. F., Downs, J. C., Bellezza, A. J., Suh, J. K. & Hart, R. T. (2005) The optic nerve head as a biomechanical structure: a new paradigm for understanding the role of IOP-related stress and strain in the pathophysiology of glaucomatous optic nerve head damage. *Prog Retin Eye Res,* 24**,** 39-73.
Caggiano, M., Kauer, J. S. & Hunter, D. D. (1994) Globose basal cells are neuronal progenitors in the olfactory epithelium: a lineage analysis using a replication-incompetent retrovirus. *Neuron,* 13**,** 339-52.
Caleo, M., Menna, E., Chierzi, S., Cenni, M. C. & Maffei, L. (2000) Brain-derived neurotrophic factor is an anterograde survival factor in the rat visual system. *Curr Biol,* 10**,** 1155-61.
Campana, G., Bucolo, C., Murari, G. & Spampinato, S. (2002) Ocular hypotensive action of topical flunarizine in the rabbit: role of sigma 1 recognition sites. *J Pharmacol Exp Ther,* 303**,** 1086-94.
Caprioli, J. (2007) Intraocular pressure fluctuation: an independent risk factor for glaucoma? *Arch Ophthalmol,* 125**,** 1124-5.
Carr, A. J., Vugler, A. A., Hikita, S. T., Lawrence, J. M., Gias, C., Chen, L. L., Buchholz, D. E., Ahmado, A., Semo, M., Smart, M. J., Hasan, S., da Cruz, L., Johnson, L. V., Clegg, D. O. & Coffey, P. J. (2009) Protective effects of human iPS-derived retinal pigment epithelium cell transplantation in the retinal dystrophic rat. *PLoS One,* 4**,** e8152.
Carter, D. A., Bray, G. M. & Aguayo, A. J. (1989) Regenerated retinal ganglion cell axons can form well-differentiated synapses in the superior colliculus of adult hamsters. *J Neurosci,* 9**,** 4042-50.
Carter, L. A., MacDonald, J. L. & Roskams, A. J. (2004) Olfactory horizontal basal cells demonstrate a conserved multipotent progenitor phenotype. *J Neurosci,* 24**,** 5670-83.
Carter-Dawson, L., Crawford, M. L., Harwerth, R. S., Smith, E. L., 3rd, Feldman, R., Shen, F. F., Mitchell, C. K. & Whitetree, A. (2002) Vitreal glutamate concentration in monkeys with experimental glaucoma. *Invest Ophthalmol Vis Sci,* 43**,** 2633-7.
Cepurna, W. O., Kayton, R. J., Johnson, E. C. & Morrison, J. C. (2005) Age related optic nerve axonal loss in adult Brown Norway rats. *Exp Eye Res,* 80**,** 877-84.
Chachques, J. C., Herreros, J., Trainini, J., Juffe, A., Rendal, E., Prosper, F. & Genovese, J. (2004) Autologous human serum for cell culture avoids the implantation of cardioverter-defibrillators in cellular cardiomyoplasty. *Int J Cardiol,* 95 Suppl 1**,** S29-33.
Chan, K. C., Fu, Q. L., Hui, E. S., So, K. F. & Wu, E. X. (2008) Evaluation of the retina and optic nerve in a rat model of chronic glaucoma using in vivo manganese-enhanced magnetic resonance imaging. *Neuroimage,* 40**,** 1166-74.
Chang, B., Smith, R. S., Hawes, N. L., Anderson, M. G., Zabaleta, A., Savinova, O., Roderick, T. H., Heckenlively, J. R., Davisson, M. T. & John, S. W. (1999) Interacting loci cause severe iris atrophy and glaucoma in DBA/2J mice. *Nat Genet,* 21**,** 405-9.
Chauhan, B. C. (2008) Endothelin and its potential role in glaucoma. *Can J Ophthalmol,* 43**,** 356-60.
Chehrehasa, F., Ekberg, J. A., Lineburg, K., Amaya, D., Mackay-Sim, A. & St John, J. A. (2011) Two phases of replacement replenish the olfactory ensheathing cell population after injury in postnatal mice. *Glia*.
Chen, Q., Long, Y., Yuan, X., Zou, L., Sun, J., Chen, S., Perez-Polo, J. R. & Yang, K. (2005) Protective effects of bone marrow stromal cell transplantation in injured rodent brain: synthesis of neurotrophic factors. *J Neurosci Res,* 80**,** 611-9.
Chen, X., Fang, H. & Schwob, J. E. (2004) Multipotency of purified, transplanted globose basal cells in olfactory epithelium. *J Comp Neurol,* 469**,** 457-74.

Cheng, L., Sapieha, P., Kittlerova, P., Hauswirth, W. W. & Di Polo, A. (2002) TrkB gene transfer protects retinal ganglion cells from axotomy-induced death in vivo. *J Neurosci,* 22**,** 3977-86.
Chintala, S. K., Zhang, X., Austin, J. S. & Fini, M. E. (2002) Deficiency in matrix metalloproteinase gelatinase B (MMP-9) protects against retinal ganglion cell death after optic nerve ligation. *J Biol Chem,* 277**,** 47461-8.
Cho, K. S. & Chen, D. F. (2008) Promoting optic nerve regeneration in adult mice with pharmaceutical approach. *Neurochem Res,* 33**,** 2126-33.
Cho, K. S., Yang, L., Lu, B., Feng Ma, H., Huang, X., Pekny, M. & Chen, D. F. (2005) Re-establishing the regenerative potential of central nervous system axons in postnatal mice. *J Cell Sci,* 118**,** 863-72.
Chuah, M. I., Tennent, R. & Jacobs, I. (1995) Response of olfactory Schwann cells to intranasal zinc sulfate irrigation. *J Neurosci Res,* 42**,** 470-8.
Chung, R. S., Woodhouse, A., Fung, S., Dickson, T. C., West, A. K., Vickers, J. C. & Chuah, M. I. (2004) Olfactory ensheathing cells promote neurite sprouting of injured axons in vitro by direct cellular contact and secretion of soluble factors. *Cell Mol Life Sci,* 61**,** 1238-45.
Cioffi, G. A. & Sullivan, P. (1999) The effect of chronic ischemia on the primate optic nerve. *Eur J Ophthalmol,* 9 Suppl 1**,** S34-6.
Civan, M. M. & Macknight, A. D. (2004) The ins and outs of aqueous humour secretion. *Exp Eye Res,* 78**,** 625-31.
Coassin, M., Lambiase, A., Sposato, V., Micera, A., Bonini, S. & Aloe, L. (2008) Retinal p75 and bax overexpression is associated with retinal ganglion cells apoptosis in a rat model of glaucoma. *Graefes Arch Clin Exp Ophthalmol,* 246**,** 1743-9.
Cole, D. F. (1977) Secretion of the aqueous humour. *Exp Eye Res,* 25 Suppl**,** 161-76.
Court, F. A., Hendriks, W. T., MacGillavry, H. D., Alvarez, J. & van Minnen, J. (2008) Schwann cell to axon transfer of ribosomes: toward a novel understanding of the role of glia in the nervous system. *J Neurosci,* 28**,** 11024-9.
Cragnolini, A. B. & Friedman, W. J. (2008) The function of p75NTR in glia. *Trends Neurosci,* 31**,** 99-104.
Crigler, L., Robey, R. C., Asawachaicharn, A., Gaupp, D. & Phinney, D. G. (2006) Human mesenchymal stem cell subpopulations express a variety of neuro-regulatory molecules and promote neuronal cell survival and neuritogenesis. *Exp Neurol,* 198**,** 54-64.
Dahlmann-Noor, A. H., Martin-Martin, B., Eastwood, M., Khaw, P. T. & Bailly, M. (2007) Dynamic protrusive cell behaviour generates force and drives early matrix contraction by fibroblasts. *Exp Cell Res,* 313**,** 4158-69.
Dai, C., Khaw, P. T., Yin, Z. Q., Li, D., Raisman, G. & Li, Y. (2012) Structural basis of glaucoma: the fortified astrocytes of the optic nerve head are the target of raised intraocular pressure. *Glia,* 60**,** 13-28.
Das, A. V., Mallya, K. B., Zhao, X., Ahmad, F., Bhattacharya, S., Thoreson, W. B., Hegde, G. V. & Ahmad, I. (2006) Neural stem cell properties of Muller glia in the mammalian retina: regulation by Notch and Wnt signaling. *Dev Biol,* 299**,** 283-302.
Davies, R., Hayat, S., Wigley, C. B. & Robbins, J. (2004) The calcium influx pathway in rat olfactory ensheathing cells shows TRPC channel pharmacology. *Brain Res,* 1023**,** 154-6.
Dezawa, M., Kanno, H., Hoshino, M., Cho, H., Matsumoto, N., Itokazu, Y., Tajima, N., Yamada, H., Sawada, H., Ishikawa, H., Mimura, T., Kitada, M., Suzuki, Y. & Ide, C. (2004) Specific induction of neuronal cells from bone marrow stromal cells and application for autologous transplantation. *J Clin Invest,* 113**,** 1701-10.
Diestelhorst, M. & Krieglstein, G. K. (1989) The intraocular pressure response of human atrial natriuretic factor in glaucoma. *Int Ophthalmol,* 13**,** 99-101.

Doherty, J., Logan, M. A., Tasdemir, O. E. & Freeman, M. R. (2009) Ensheathing glia function as phagocytes in the adult Drosophila brain. *J Neurosci,* 29**,** 4768-81.
Doucette, J. R. (1984) The glial cells in the nerve fiber layer of the rat olfactory bulb. *Anat Rec,* 210**,** 385-91.
Doucette, J. R., Kiernan, J. A. & Flumerfelt, B. A. (1983) The re-innervation of olfactory glomeruli following transection of primary olfactory axons in the central or peripheral nervous system. *J Anat,* 137 (Pt 1)**,** 1-19.
Doucette, R. (1990) Glial influences on axonal growth in the primary olfactory system. *Glia,* 3**,** 433-49.
Doucette, R. (1991) PNS-CNS transitional zone of the first cranial nerve. *J Comp Neurol,* 312**,** 451-66.
Doucette, R. (1995) Olfactory ensheathing cells: potential for glial cell transplantation into areas of CNS injury. *Histol Histopathol,* 10**,** 503-7.
Dreyer, E. B., Zurakowski, D., Schumer, R. A., Podos, S. M. & Lipton, S. A. (1996) Elevated glutamate levels in the vitreous body of humans and monkeys with glaucoma. *Arch Ophthalmol,* 114**,** 299-305.
Duijm, H. F., van den Berg, T. J. & Greve, E. L. (1997) Choroidal haemodynamics in glaucoma. *Br J Ophthalmol,* 81**,** 735-42.
Endres, M., Fan, G., Hirt, L., Fujii, M., Matsushita, K., Liu, X., Jaenisch, R. & Moskowitz, M. A. (2000) Ischemic brain damage in mice after selectively modifying BDNF or NT4 gene expression. *J Cereb Blood Flow Metab,* 20**,** 139-44.
Fan, B. J., Pasquale, L., Grosskreutz, C. L., Rhee, D., Chen, T., DeAngelis, M. M., Kim, I., del Bono, E., Miller, J. W., Li, T., Haines, J. L. & Wiggs, J. L. (2008) DNA sequence variants in the LOXL1 gene are associated with pseudoexfoliation glaucoma in a U.S. clinic-based population with broad ethnic diversity. *BMC Med Genet,* 9**,** 5.
Farbman, A. I. & Margolis, F. L. (1980) Olfactory marker protein during ontogeny: immunohistochemical localization. *Dev Biol,* 74**,** 205-15.
Fernandez-Durango, R., Ramirez, J. M., Trivino, A., Sanchez, D., Paraiso, P., Garcia De Lacoba, M., Ramirez, A., Salazar, J. J., Fernandez-Cruz, A. & Gutkowska, J. (1991) Experimental glaucoma significantly decreases atrial natriuretic factor (ANF) receptors in the ciliary processes of the rabbit eye. *Exp Eye Res,* 53**,** 591-6.
Fernandez-Durango, R., Trivino, A., Ramirez, J. M., Garcia de Lacoba, M., Ramirez, A., Salazar, J. J., Fernandez-Cruz, A. & Gutkowska, J. (1990) Immunoreactive atrial natriuretic factor in aqueous humor: its concentration is increased with high intraocular pressure in rabbit eyes. *Vision Res,* 30**,** 1305-10.
Field, P., Li, Y. & Raisman, G. (2003) Ensheathment of the olfactory nerves in the adult rat. *J Neurocytol,* 32**,** 317-24.
Flugel-Koch, C., Ohlmann, A., Fuchshofer, R., Welge-Lussen, U. & Tamm, E. R. (2004) Thrombospondin-1 in the trabecular meshwork: localization in normal and glaucomatous eyes, and induction by TGF-beta1 and dexamethasone in vitro. *Exp Eye Res,* 79**,** 649-63.
Fortune, B., Bui, B. V., Morrison, J. C., Johnson, E. C., Dong, J., Cepurna, W. O., Jia, L., Barber, S. & Cioffi, G. A. (2004) Selective ganglion cell functional loss in rats with experimental glaucoma. *Invest Ophthalmol Vis Sci,* 45**,** 1854-62.
Frade, J. M. (2005) Nuclear translocation of the p75 neurotrophin receptor cytoplasmic domain in response to neurotrophin binding. *J Neurosci,* 25**,** 1407-11.
Franceschini, I. A. & Barnett, S. C. (1996) Low-affinity NGF-receptor and E-N-CAM expression define two types of olfactory nerve ensheathing cells that share a common lineage. *Dev Biol,* 173**,** 327-43.
Franklin, R. J., Gilson, J. M., Franceschini, I. A. & Barnett, S. C. (1996) Schwann cell-like myelination following transplantation of an olfactory bulb-ensheathing cell line into areas of demyelination in the adult CNS. *Glia,* 17**,** 217-24.

Frishman, L. J., Shen, F. F., Du, L., Robson, J. G., Harwerth, R. S., Smith, E. L., 3rd, Carter-Dawson, L. & Crawford, M. L. (1996) The scotopic electroretinogram of macaque after retinal ganglion cell loss from experimental glaucoma. *Invest Ophthalmol Vis Sci,* 37**,** 125-41.
Frishman, L. J. & Steinberg, R. H. (1989) Light-evoked increases in [K+]o in proximal portion of the dark-adapted cat retina. *J Neurophysiol,* 61**,** 1233-43.
Fu, Q. L., Li, X., Shi, J., Xu, G., Wen, W., Lee, D. H. & So, K. F. (2009) Synaptic Degeneration of Retinal Ganglion Cells in a Rat Ocular Hypertension Glaucoma Model. *Cell Mol Neurobiol*.
Gaasterland, D. & Kupfer, C. (1974) Experimental glaucoma in the rhesus monkey. *Invest Ophthalmol,* 13**,** 455-7.
Gasser, P. (1989) Ocular vasospasm: a risk factor in the pathogenesis of low-tension glaucoma. *Int Ophthalmol,* 13**,** 281-90.
Gasser, P. & Flammer, J. (1987) Influence of vasospasm on visual function. *Doc Ophthalmol,* 66**,** 3-18.
Gasser, P., Flammer, J. & Mahler, F. (1988) [The use of calcium antagonists in the treatment of ocular circulation symptoms in the framework of a vasospastic syndrome]. *Schweiz Med Wochenschr,* 118**,** 201-2.
Geddes, A. J., Angka, H. E., Davies, K. A. & Kablar, B. (2006) Subpopulations of motor and sensory neurons respond differently to brain-derived neurotrophic factor depending on the presence of the skeletal muscle. *Dev Dyn,* 235**,** 2175-84.
Geijer, C. & Bill, A. (1979) Effects of raised intraocular pressure on retinal, prelaminar, laminar, and retrolaminar optic nerve blood flow in monkeys. *Invest Ophthalmol Vis Sci,* 18**,** 1030-42.
Georgoulas, S., Dahlmann-Noor, A., Brocchini, S. & Khaw, P. T. (2008) Modulation of wound healing during and after glaucoma surgery. *Prog Brain Res,* 173**,** 237-54.
Gerometta, R., Podos, S. M., Candia, O. A., Wu, B., Malgor, L. A., Mittag, T. & Danias, J. (2004) Steroid-induced ocular hypertension in normal cattle. *Arch Ophthalmol,* 122**,** 1492-7.
Gerometta, R., Podos, S. M., Danias, J. & Candia, O. A. (2009) Steroid-induced ocular hypertension in normal sheep. *Invest Ophthalmol Vis Sci,* 50**,** 669-73.
Getchell, M. L. & Getchell, T. V. (1991) Immunohistochemical localization of components of the immune barrier in the olfactory mucosae of salamanders and rats. *Anat Rec,* 231**,** 358-74.
Ginty, D. D. & Segal, R. A. (2002) Retrograde neurotrophin signaling: Trk-ing along the axon. *Curr Opin Neurobiol,* 12**,** 268-74.
Goel, M., Picciani, R. G., Lee, R. K. & Bhattacharya, S. K. (2010) Aqueous humor dynamics: a review. *Open Ophthalmol J,* 4**,** 52-9.
Gomez, T. M. & Spitzer, N. C. (1999) In vivo regulation of axon extension and pathfinding by growth-cone calcium transients. *Nature,* 397**,** 350-5.
Gong, G., Kosoko-Lasaki, O., Haynatzki, G. R. & Wilson, M. R. (2004) Genetic dissection of myocilin glaucoma. *Hum Mol Genet,* 13 Spec No 1**,** R91-102.
Gong, Q., Bailey, M. S., Pixley, S. K., Ennis, M., Liu, W. & Shipley, M. T. (1994) Localization and regulation of low affinity nerve growth factor receptor expression in the rat olfactory system during development and regeneration. *J Comp Neurol,* 344**,** 336-48.
Gorrie, C. A., Hayward, I., Cameron, N., Kailainathan, G., Nandapalan, N., Sutharsan, R., Wang, J., Mackay-Sim, A. & Waite, P. M. (2010) Effects of human OEC-derived cell transplants in rodent spinal cord contusion injury. *Brain Res,* 1337**,** 8-20.
Gottanka, J., Johnson, D. H., Martus, P. & Lutjen-Drecoll, E. (1997) Severity of optic nerve damage in eyes with POAG is correlated with changes in the trabecular meshwork. *J Glaucoma,* 6**,** 123-32.

Gouadon, E., Meunier, N., Grebert, D., Durieux, D., Baly, C., Salesse, R., Caillol, M. & Congar, P. (2010) Endothelin evokes distinct calcium transients in neuronal and non-neuronal cells of rat olfactory mucosa primary cultures. *Neuroscience,* 165**,** 584-600.
Goyal, J. K., Khilnani, G., Sharma, D. P. & Singh, J. (1989) The hypotensive effect of verapamil eye drops on ocular hypertension. *Indian J Ophthalmol,* 37**,** 176-8.
Granit, R. (1933) The components of the retinal action potential in mammals and their relation to the discharge in the optic nerve. *J Physiol,* 77**,** 207-39.
Graziadei, P. P. & Graziadei, G. A. (1979) Neurogenesis and neuron regeneration in the olfactory system of mammals. I. Morphological aspects of differentiation and structural organization of the olfactory sensory neurons. *J Neurocytol,* 8**,** 1-18.
Graziadei, P. P. & Monti Graziadei, G. A. (1980) Neurogenesis and neuron regeneration in the olfactory system of mammals. III. Deafferentation and reinnervation of the olfactory bulb following section of the fila olfactoria in rat. *J Neurocytol,* 9**,** 145-62.
Gudino-Cabrera, G., Pastor, A. M., de la Cruz, R. R., Delgado-Garcia, J. M. & Nieto-Sampedro, M. (2000) Limits to the capacity of transplants of olfactory glia to promote axonal regrowth in the CNS. *Neuroreport,* 11**,** 467-71.
Guerout, N., Duclos, C., Drouot, L., Abramovici, O., Bon-Mardion, N., Lacoume, Y., Jean, L., Boyer, O. & Marie, J. P. (2011a) Transplantation of olfactory ensheathing cells promotes axonal regeneration and functional recovery of peripheral nerve lesion in rats. *Muscle Nerve,* 43**,** 543-51.
Guerout, N., Paviot, A., Bon-Mardion, N., Duclos, C., Genty, D., Jean, L., Boyer, O. & Marie, J. P. (2011b) Co-transplantation of olfactory ensheathing cells from mucosa and bulb origin enhances functional recovery after peripheral nerve lesion. *PLoS One,* 6**,** e22816.
Guntinas-Lichius, O., Angelov, D. N., Tomov, T. L., Dramiga, J., Neiss, W. F. & Wewetzer, K. (2001) Transplantation of olfactory ensheathing cells stimulates the collateral sprouting from axotomized adult rat facial motoneurons. *Exp Neurol,* 172**,** 70-80.
Guntinas-Lichius, O., Wewetzer, K., Tomov, T. L., Azzolin, N., Kazemi, S., Streppel, M., Neiss, W. F. & Angelov, D. N. (2002) Transplantation of olfactory mucosa minimizes axonal branching and promotes the recovery of vibrissae motor performance after facial nerve repair in rats. *J Neurosci,* 22**,** 7121-31.
Guo, L., Moss, S. E., Alexander, R. A., Ali, R. R., Fitzke, F. W. & Cordeiro, M. F. (2005) Retinal ganglion cell apoptosis in glaucoma is related to intraocular pressure and IOP-induced effects on extracellular matrix. *Invest Ophthalmol Vis Sci,* 46**,** 175-82.
Guo, Y., Johnson, E., Cepurna, W., Jia, L., Dyck, J. & Morrison, J. C. (2009) Does elevated intraocular pressure reduce retinal TRKB-mediated survival signaling in experimental glaucoma? *Exp Eye Res*.
Guo, Y., Saloupis, P., Shaw, S. J. & Rickman, D. W. (2003) Engraftment of adult neural progenitor cells transplanted to rat retina injured by transient ischemia. *Invest Ophthalmol Vis Sci,* 44**,** 3194-201.
Gupta, N., Ly, T., Zhang, Q., Kaufman, P. L., Weinreb, R. N. & Yucel, Y. H. (2007) Chronic ocular hypertension induces dendrite pathology in the lateral geniculate nucleus of the brain. *Exp Eye Res,* 84**,** 176-84.
Hains, B. C. & Waxman, S. G. (2005) Neuroprotection by sodium channel blockade with phenytoin in an experimental model of glaucoma. *Invest Ophthalmol Vis Sci,* 46**,** 4164-9.
Harada, C., Harada, T., Quah, H. M., Namekata, K., Yoshida, K., Ohno, S., Tanaka, K. & Parada, L. F. (2005) Role of neurotrophin-4/5 in neural cell death during retinal development and ischemic retinal injury in vivo. *Invest Ophthalmol Vis Sci,* 46**,** 669-73.

Harberts, E., Yao, K., Wohler, J. E., Maric, D., Ohayon, J., Henkin, R. & Jacobson, S. (2011) Human herpesvirus-6 entry into the central nervous system through the olfactory pathway. *Proc Natl Acad Sci U S A,* 108**,** 13734-9.
Hayat, S., Thomas, A., Afshar, F., Sonigra, R. & Wigley, C. B. (2003a) Manipulation of olfactory ensheathing cell signaling mechanisms: effects on their support for neurite regrowth from adult CNS neurons in coculture. *Glia,* 44**,** 232-41.
Hayat, S., Wigley, C. B. & Robbins, J. (2003b) Intracellular calcium handling in rat olfactory ensheathing cells and its role in axonal regeneration. *Mol Cell Neurosci,* 22**,** 259-70.
He, S., Prasanna, G. & Yorio, T. (2007) Endothelin-1-mediated signaling in the expression of matrix metalloproteinases and tissue inhibitors of metalloproteinases in astrocytes. *Invest Ophthalmol Vis Sci,* 48**,** 3737-45.
He, Y., Leung, K. W., Zhang, Y. H., Duan, S., Zhong, X. F., Jiang, R. Z., Peng, Z., Tombran-Tink, J. & Ge, J. (2008) Mitochondrial complex I defect induces ROS release and degeneration in trabecular meshwork cells of POAG patients: protection by antioxidants. *Invest Ophthalmol Vis Sci,* 49**,** 1447-58.
Hernandez, M. R. (2000) The optic nerve head in glaucoma: role of astrocytes in tissue remodeling. *Prog Retin Eye Res,* 19**,** 297-321.
Hollander, H., Makarov, F., Stefani, F. H. & Stone, J. (1995) Evidence of constriction of optic nerve axons at the lamina cribrosa in the normotensive eye in humans and other mammals. *Ophthalmic Res,* 27**,** 296-309.
Hong, S., Seong, G. J. & Hong, Y. J. (2007) Long-term intraocular pressure fluctuation and progressive visual field deterioration in patients with glaucoma and low intraocular pressures after a triple procedure. *Arch Ophthalmol,* 125**,** 1010-3.
Howell, G. R., Libby, R. T., Jakobs, T. C., Smith, R. S., Phalan, F. C., Barter, J. W., Barbay, J. M., Marchant, J. K., Mahesh, N., Porciatti, V., Whitmore, A. V., Masland, R. H. & John, S. W. (2007) Axons of retinal ganglion cells are insulted in the optic nerve early in DBA/2J glaucoma. *J Cell Biol,* 179**,** 1523-37.
Hu, B., Yip, H. K. & So, K. F. (1999) Expression of p75 neurotrophin receptor in the injured and regenerating rat retina. *Neuroreport,* 10**,** 1293-7.
Huang, W., Fileta, J., Rawe, I., Qu, J. & Grosskreutz, C. L. (2010) Calpain activation in experimental glaucoma. *Invest Ophthalmol Vis Sci,* 51**,** 3049-54.
Huang, W., Fileta, J. B., Dobberfuhl, A., Filippopolous, T., Guo, Y., Kwon, G. & Grosskreutz, C. L. (2005) Calcineurin cleavage is triggered by elevated intraocular pressure, and calcineurin inhibition blocks retinal ganglion cell death in experimental glaucoma. *Proc Natl Acad Sci U S A,* 102**,** 12242-7.
Huang, Z. H., Wang, Y., Cao, L., Su, Z. D., Zhu, Y. L., Chen, Y. Z., Yuan, X. B. & He, C. (2008) Migratory properties of cultured olfactory ensheathing cells by single-cell migration assay. *Cell Res,* 18**,** 479-90.
Huo, S. J., Li, Y., Raisman, G. & Yin, Z. Q. (2011) Transplanted olfactory ensheathing cells reduce the gliotic injury response of Muller cells in a rat model of retinitis pigmentosa. *Brain Res,* 1382**,** 238-44.
Ide, C. (1996) Peripheral nerve regeneration. *Neurosci Res,* 25**,** 101-21.
Imper, V. & Van Wart, H. E. (1998) Recognition of the matrix metalloproteinases. In: Matrix metalloproteinases. *New York: Academic Press.***,** pp 219-242.
Inoue, Y., Iriyama, A., Ueno, S., Takahashi, H., Kondo, M., Tamaki, Y., Araie, M. & Yanagi, Y. (2007) Subretinal transplantation of bone marrow mesenchymal stem cells delays retinal degeneration in the RCS rat model of retinal degeneration. *Exp Eye Res,* 85**,** 234-41.
Isenmann, S., Kretz, A. & Cellerino, A. (2003) Molecular determinants of retinal ganglion cell development, survival, and regeneration. *Prog Retin Eye Res,* 22**,** 483-543.

Ishii, Y., Kwong, J. M. & Caprioli, J. (2003) Retinal ganglion cell protection with geranylgeranylacetone, a heat shock protein inducer, in a rat glaucoma model. *Invest Ophthalmol Vis Sci,* 44**,** 1982-92.
Izzotti, A., Longobardi, M., Cartiglia, C. & Sacca, S. C. (2011) Mitochondrial damage in the trabecular meshwork occurs only in primary open-angle glaucoma and in pseudoexfoliative glaucoma. *PLoS One,* 6**,** e14567.
Jacobson, N., Andrews, M., Shepard, A. R., Nishimura, D., Searby, C., Fingert, J. H., Hageman, G., Mullins, R., Davidson, B. L., Kwon, Y. H., Alward, W. L., Stone, E. M., Clark, A. F. & Sheffield, V. C. (2001) Non-secretion of mutant proteins of the glaucoma gene myocilin in cultured trabecular meshwork cells and in aqueous humor. *Hum Mol Genet,* 10**,** 117-25.
Jeng, S. M., Karger, R. A., Hodge, D. O., Burke, J. P., Johnson, D. H. & Good, M. S. (2007) The risk of glaucoma in pseudoexfoliation syndrome. *J Glaucoma,* 16**,** 117-21.
Ji, J. Z., Elyaman, W., Yip, H. K., Lee, V. W., Yick, L. W., Hugon, J. & So, K. F. (2004) CNTF promotes survival of retinal ganglion cells after induction of ocular hypertension in rats: the possible involvement of STAT3 pathway. *Eur J Neurosci,* 19**,** 265-72.
Jia, L., Cepurna, W. O., Barber, S. L., Morrison, J. C. & Johnson, E. C. (2004) Retinal neurotrophin and Trk receptor mRNA expression following elevated intraocular pressure or optic nerve transection. *Investig. Ophthalmol. Vis. Sci. ,* 45**,** p.U787.
Jia, L., Cepurna, W. O., Johnson, E. C. & Morrison, J. C. (2000) Patterns of intraocular pressure elevation after aqueous humor outflow obstruction in rats. *Invest Ophthalmol Vis Sci,* 41**,** 1380-5.
Joachim, S. C., Bruns, K., Lackner, K. J., Pfeiffer, N. & Grus, F. H. (2007) Antibodies to alpha B-crystallin, vimentin, and heat shock protein 70 in aqueous humor of patients with normal tension glaucoma and IgG antibody patterns against retinal antigen in aqueous humor. *Curr Eye Res,* 32**,** 501-9.
Johnson, D., Gottanka, J., Flugel, C., Hoffmann, F., Futa, R. & Lutjen-Drecoll, E. (1997) Ultrastructural changes in the trabecular meshwork of human eyes treated with corticosteroids. *Arch Ophthalmol,* 115**,** 375-83.
Johnson, E. C., Guo, Y., Cepurna, W. O. & Morrison, J. C. (2009a) Neurotrophin roles in retinal ganglion cell survival: lessons from rat glaucoma models. *Exp Eye Res,* 88**,** 808-15.
Johnson, E. C. & Morrison, J. C. (2009) Friend or foe? Resolving the impact of glial responses in glaucoma. *J Glaucoma,* 18**,** 341-53.
Johnson, E. C., Morrison, J. C., Farrell, S., Deppmeier, L., Moore, C. G. & McGinty, M. R. (1996) The effect of chronically elevated intraocular pressure on the rat optic nerve head extracellular matrix. *Exp Eye Res,* 62**,** 663-74.
Johnson, T. V., Bull, N. D., Hunt, D. P., Marina, N., Tomarev, S. I. & Martin, K. R. (2010) Neuroprotective effects of intravitreal mesenchymal stem cell transplantation in experimental glaucoma. *Invest Ophthalmol Vis Sci,* 51**,** 2051-9.
Johnson, T. V., Bull, N. D. & Martin, K. R. (2008a) Transplantation prospects for the inner retina. *Eye*.
Johnson, T. V., Bull, N. D. & Martin, K. R. (2009b) Identification of barriers to retinal engraftment of transplanted stem cells. *Invest Ophthalmol Vis Sci,* 51**,** 960-70.
Johnson, T. V., Fan, S. & Toris, C. B. (2008b) Rebound tonometry in conscious, conditioned mice avoids the acute and profound effects of anesthesia on intraocular pressure. *J Ocul Pharmacol Ther,* 24**,** 175-85.
Kafitz, K. W. & Greer, C. A. (1997) Role of laminin in axonal extension from olfactory receptor cells. *J Neurobiol,* 32**,** 298-310.
Kanning, K. C., Hudson, M., Amieux, P. S., Wiley, J. C., Bothwell, M. & Schecterson, L. C. (2003) Proteolytic processing of the p75 neurotrophin receptor

and two homologs generates C-terminal fragments with signaling capability. *J Neurosci,* 23**,** 5425-36.
Karwoski, C. J., Lu, H. K. & Newman, E. A. (1989) Spatial buffering of light-evoked potassium increases by retinal Muller (glial) cells. *Science,* 244**,** 578-80.
Katai, N. & Yoshimura, N. (1999) Apoptotic retinal neuronal death by ischemia-reperfusion is executed by two distinct caspase family proteases. *Invest Ophthalmol Vis Sci,* 40**,** 2697-705.
Keirstead, S. A., Rasminsky, M., Fukuda, Y., Carter, D. A., Aguayo, A. J. & Vidal-Sanz, M. (1989) Electrophysiologic responses in hamster superior colliculus evoked by regenerating retinal axons. *Science,* 246**,** 255-7.
Keller, K. E., Kelley, M. J. & Acott, T. S. (2007) Extracellular matrix gene alternative splicing by trabecular meshwork cells in response to mechanical stretching. *Invest Ophthalmol Vis Sci,* 48**,** 1164-72.
Kerrigan, L. A., Zack, D. J., Quigley, H. A., Smith, S. D. & Pease, M. E. (1997) TUNEL-positive ganglion cells in human primary open-angle glaucoma. *Arch Ophthalmol,* 115**,** 1031-5.
Kilinc, D., Gallo, G. & Barbee, K. A. (2009) Mechanical membrane injury induces axonal beading through localized activation of calpain. *Exp Neurol,* 219**,** 553-61.
Kinsey, V. E. (1951) The chemical composition and the osmotic pressure of the aqueous humor and plasma of the rabbit. *J Gen Physiol,* 34**,** 389-402.
Knepper, P. A., Breen, M., Weinstein, H. G. & Blacik, J. L. (1978) Intraocular pressure and glycosaminoglycan distribution in the rabbit eye: effect of age and dexamethasone. *Exp Eye Res,* 27**,** 567-75.
Knepper, P. A., Collins, J. A. & Frederick, R. (1985) Effects of dexamethasone, progesterone, and testosterone on IOP and GAGs in the rabbit eye. *Invest Ophthalmol Vis Sci,* 26**,** 1093-100.
Ko, M. L., Hu, D. N., Ritch, R., Sharma, S. C. & Chen, C. F. (2001) Patterns of retinal ganglion cell survival after brain-derived neurotrophic factor administration in hypertensive eyes of rats. *Neurosci Lett,* 305**,** 139-42.
Kohno, H., Sakai, T. & Kitahara, K. (2006) Induction of nestin, Ki-67, and cyclin D1 expression in Muller cells after laser injury in adult rat retina. *Graefes Arch Clin Exp Ophthalmol,* 244**,** 90-5.
Kondo, T. & Raff, M. (2000) Oligodendrocyte precursor cells reprogrammed to become multipotential CNS stem cells. *Science,* 289**,** 1754-7.
Koriyama, Y., Tanii, H., Ohno, M., Kimura, T. & Kato, S. (2008) A novel neuroprotective role of a small peptide from flesh fly, 5-S-GAD in the rat retina in vivo. *Brain Res*.
Krishnamoorthy, R. R., Agarwal, P., Prasanna, G., Vopat, K., Lambert, W., Sheedlo, H. J., Pang, I. H., Shade, D., Wordinger, R. J., Yorio, T., Clark, A. F. & Agarwal, N. (2001) Characterization of a transformed rat retinal ganglion cell line. *Brain Res Mol Brain Res,* 86**,** 1-12.
Kucukdereli, H., Allen, N. J., Lee, A. T., Feng, A., Ozlu, M. I., Conatser, L. M., Chakraborty, C., Workman, G., Weaver, M., Sage, E. H., Barres, B. A. & Eroglu, C. (2011) Control of excitatory CNS synaptogenesis by astrocyte-secreted proteins Hevin and SPARC. *Proc Natl Acad Sci U S A,* 108**,** E440-9.
Kueh, J. L., Raisman, G., Li, Y., Stevens, R. & Li, D. (2011) Comparison of bulbar and mucosal olfactory ensheathing cells using FACS and simultaneous antigenic bivariate cell cycle analysis. *Glia*.
Kumar, R., Hayat, S., Felts, P., Bunting, S. & Wigley, C. (2005) Functional differences and interactions between phenotypic subpopulations of olfactory ensheathing cells in promoting CNS axonal regeneration. *Glia,* 50**,** 12-20.
Lakatos, A., Barnett, S. C. & Franklin, R. J. (2003) Olfactory ensheathing cells induce less host astrocyte response and chondroitin sulphate proteoglycan

expression than Schwann cells following transplantation into adult CNS white matter. *Exp Neurol,* 184**,** 237-46.
Lakatos, A., Franklin, R. J. & Barnett, S. C. (2000) Olfactory ensheathing cells and Schwann cells differ in their in vitro interactions with astrocytes. *Glia,* 32**,** 214-25.
Lam, T. T., Abler, A. S., Kwong, J. M. & Tso, M. O. (1999) N-methyl-D-aspartate (NMDA)--induced apoptosis in rat retina. *Invest Ophthalmol Vis Sci,* 40**,** 2391-7.
Lambert, W., Agarwal, R., Howe, W., Clark, A. F. & Wordinger, R. J. (2001) Neurotrophin and neurotrophin receptor expression by cells of the human lamina cribrosa. *Invest Ophthalmol Vis Sci,* 42**,** 2315-23.
Lawrence, J. M., Singhal, S., Bhatia, B., Keegan, D. J., Reh, T. A., Luthert, P. J., Khaw, P. T. & Limb, G. A. (2007) MIO-M1 cells and similar muller glial cell lines derived from adult human retina exhibit neural stem cell characteristics. *Stem Cells,* 25**,** 2033-43.
Leaver, S. G., Harvey, A. R. & Plant, G. W. (2006) Adult olfactory ensheathing glia promote the long-distance growth of adult retinal ganglion cell neurites in vitro. *Glia,* 53**,** 467-76.
Lebrun-Julien, F., Bertrand, M. J., De Backer, O., Stellwagen, D., Morales, C. R., Di Polo, A. & Barker, P. A. (2010) ProNGF induces TNFalpha-dependent death of retinal ganglion cells through a p75NTR non-cell-autonomous signaling pathway. *Proc Natl Acad Sci U S A,* 107**,** 3817-22.
Lebrun-Julien, F., Morquette, B., Douillette, A., Saragovi, H. U. & Di Polo, A. (2009) Inhibition of p75(NTR) in glia potentiates TrkA-mediated survival of injured retinal ganglion cells. *Mol Cell Neurosci,* 40**,** 410-20.
Lee, A. J., Rochtchina, E., Wang, J. J., Healey, P. R. & Mitchell, P. (2003) Does smoking affect intraocular pressure? Findings from the Blue Mountains Eye Study. *J Glaucoma,* 12**,** 209-12.
Leung, C. T., Coulombe, P. A. & Reed, R. R. (2007) Contribution of olfactory neural stem cells to tissue maintenance and regeneration. *Nat Neurosci,* 10**,** 720-6.
Leung, J. Y., Chapman, J. A., Harris, J. A., Hale, D., Chung, R. S., West, A. K. & Chuah, M. I. (2008) Olfactory ensheathing cells are attracted to, and can endocytose, bacteria. *Cell Mol Life Sci,* 65**,** 2732-9.
Levkovitch-Verbin, H., Martin, K. R., Quigley, H. A., Baumrind, L. A., Pease, M. E. & Valenta, D. (2002a) Measurement of amino acid levels in the vitreous humor of rats after chronic intraocular pressure elevation or optic nerve transection. *J Glaucoma,* 11**,** 396-405.
Levkovitch-Verbin, H., Quigley, H. A., Martin, K. R., Valenta, D., Baumrind, L. A. & Pease, M. E. (2002b) Translimbal laser photocoagulation to the trabecular meshwork as a model of glaucoma in rats. *Invest Ophthalmol Vis Sci,* 43**,** 402-10.
Li, Y., Decherchi, P. & Raisman, G. (2003) Transplantation of olfactory ensheathing cells into spinal cord lesions restores breathing and climbing. *J Neurosci,* 23**,** 727-31.
Li, Y., Field, P. M. & Raisman, G. (1997) Repair of adult rat corticospinal tract by transplants of olfactory ensheathing cells. *Science,* 277**,** 2000-2.
Li, Y., Field, P. M. & Raisman, G. (1998) Regeneration of adult rat corticospinal axons induced by transplanted olfactory ensheathing cells. *J Neurosci,* 18**,** 10514-24.
Li, Y., Field, P. M. & Raisman, G. (2005) Olfactory ensheathing cells and olfactory nerve fibroblasts maintain continuous open channels for regrowth of olfactory nerve fibres. *Glia,* 52**,** 245-51.
Li, Y., Li, D., Khaw, P. T. & Raisman, G. (2008) Transplanted olfactory ensheathing cells incorporated into the optic nerve head ensheathe retinal ganglion cell axons: possible relevance to glaucoma. *Neurosci Lett,* 440**,** 251-4.
Li, Y., Li, D. & Raisman, G. (2007) Transplanted Schwann cells, not olfactory ensheathing cells, myelinate optic nerve fibres. *Glia,* 55**,** 312-6.

Liang, C. C., Park, A. Y. & Guan, J. L. (2007) In vitro scratch assay: a convenient and inexpensive method for analysis of cell migration in vitro. *Nat Protoc,* 2**,** 329-33.
Liao, S. Y., Ivanov, S., Ivanova, A., Ghosh, S., Cote, M. A., Keefe, K., Coca-Prados, M., Stanbridge, E. J. & Lerman, M. I. (2003) Expression of cell surface transmembrane carbonic anhydrase genes CA9 and CA12 in the human eye: overexpression of CA12 (CAXII) in glaucoma. *J Med Genet,* 40**,** 257-61.
Limb, G. A., Salt, T. E., Munro, P. M., Moss, S. E. & Khaw, P. T. (2002) In vitro characterization of a spontaneously immortalized human Muller cell line (MIO-M1). *Invest Ophthalmol Vis Sci,* 43**,** 864-9.
Lipson, A. C., Widenfalk, J., Lindqvist, E., Ebendal, T. & Olson, L. (2003) Neurotrophic properties of olfactory ensheathing glia. *Exp Neurol,* 180**,** 167-71.
Liu, H., Fan, S., Gulati, V., Camras, L. J., Zhan, G., Ghate, D., Camras, C. B. & Toris, C. B. (2011) Aqueous humor dynamics during the day and night in healthy mature volunteers. *Arch Ophthalmol,* 129**,** 269-75.
Liu, X., Zhao, Y., Gao, J., Pawlyk, B., Starcher, B., Spencer, J. A., Yanagisawa, H., Zuo, J. & Li, T. (2004) Elastic fiber homeostasis requires lysyl oxidase-like 1 protein. *Nat Genet,* 36**,** 178-82.
Lom, B. & Cohen-Cory, S. (1999) Brain-derived neurotrophic factor differentially regulates retinal ganglion cell dendritic and axonal arborization in vivo. *J Neurosci,* 19**,** 9928-38.
Lopez-Vales, R., Garcia-Alias, G., Fores, J., Navarro, X. & Verdu, E. (2004) Increased expression of cyclo-oxygenase 2 and vascular endothelial growth factor in lesioned spinal cord by transplanted olfactory ensheathing cells. *J Neurotrauma,* 21**,** 1031-43.
Lorenzetti, O. J. (1970) Effects of corticosteroids on ocular dynamics in rabbits. *J Pharmacol Exp Ther,* 175**,** 763-72.
Lowe, D. G., Klisak, I., Sparkes, R. S., Mohandas, T. & Goeddel, D. V. (1990) Chromosomal distribution of three members of the human natriuretic peptide receptor/guanylyl cyclase gene family. *Genomics,* 8**,** 304-12.
Lowe, R. F. (1977) Primary angle-closure glaucoma: a reveiw of ocular biometry. *Australian Journal of Ophthalmology,* 5**,** 9-17.
Lu, J., Feron, F., Mackay-Sim, A. & Waite, P. M. (2002) Olfactory ensheathing cells promote locomotor recovery after delayed transplantation into transected spinal cord. *Brain,* 125**,** 14-21.
Luo, X., Wei, H., Liu, S., Lu, Y. & Zhang, Y. (1998) [The influence of pressure on human lamina cribrosa cell and its collagen synthesis]. *Zhonghua Yan Ke Za Zhi,* 34**,** 65-7.
Lutjen-Drecoll, E., Futa, R. & Rohen, J. W. (1981) Ultrahistochemical studies on tangential sections of the trabecular meshwork in normal and glaucomatous eyes. *Invest Ophthalmol Vis Sci,* 21**,** 563-73.
Mackay-Sim, A., Feron, F., Cochrane, J., Bassingthwaighte, L., Bayliss, C., Davies, W., Fronek, P., Gray, C., Kerr, G., Licina, P., Nowitzke, A., Perry, C., Silburn, P. A., Urquhart, S. & Geraghty, T. (2008) Autologous olfactory ensheathing cell transplantation in human paraplegia: a 3-year clinical trial. *Brain,* 131**,** 2376-86.
Madison, R., Moore, M. R. & Sidman, R. L. (1984) Retinal ganglion cells and axons survive optic nerve transection. *Int J Neurosci,* 23**,** 15-32.
Malone, P., Miao, H., Parker, A., Juarez, S. & Hernandez, M. R. (2007) Pressure induces loss of gap junction communication and redistribution of connexin 43 in astrocytes. *Glia,* 55**,** 1085-98.
Manabe, S., Gu, Z. & Lipton, S. A. (2005) Activation of matrix metalloproteinase-9 via neuronal nitric oxide synthase contributes to NMDA-induced retinal ganglion cell death. *Invest Ophthalmol Vis Sci,* 46**,** 4747-53.
Mandel, S. A., Avramovich-Tirosh, Y., Reznichenko, L., Zheng, H., Weinreb, O., Amit, T. & Youdim, M. B. (2005) Multifunctional activities of green tea catechins in

neuroprotection. Modulation of cell survival genes, iron-dependent oxidative stress and PKC signaling pathway. *Neurosignals,* 14**,** 46-60.
Mann, I. C. (1928) The Relations of the Hyaloid Canal in the Foetus and in the Adult. *J Anat,* 62**,** 290-6.
Marano, J. E., Sun, D., Zama, A. M., Young, W. & Uzumcu, M. (2008) Orthotopic transplantation of neonatal GFP rat ovary as experimental model to study ovarian development and toxicology. *Reprod Toxicol,* 26**,** 191-6.
Martin, K. R., Quigley, H. A., Zack, D. J., Levkovitch-Verbin, H., Kielczewski, J., Valenta, D., Baumrind, L., Pease, M. E., Klein, R. L. & Hauswirth, W. W. (2003) Gene therapy with brain-derived neurotrophic factor as a protection: retinal ganglion cells in a rat glaucoma model. *Invest Ophthalmol Vis Sci,* 44**,** 4357-65.
Martinou, J. C., Dubois-Dauphin, M., Staple, J. K., Rodriguez, I., Frankowski, H., Missotten, M., Albertini, P., Talabot, D., Catsicas, S., Pietra, C. & et al. (1994) Overexpression of BCL-2 in transgenic mice protects neurons from naturally occurring cell death and experimental ischemia. *Neuron,* 13**,** 1017-30.
Maruyama, I., Ohguro, H. & Ikeda, Y. (2000) Retinal ganglion cells recognized by serum autoantibody against gamma-enolase found in glaucoma patients. *Invest Ophthalmol Vis Sci,* 41**,** 1657-65.
Matrisian, L. M. (1992) The matrix-degrading metalloproteinases. *Bioessays,* 14**,** 455-63.
Maus, T. L., Young, W. F., Jr. & Brubaker, R. F. (1994) Aqueous flow in humans after adrenalectomy. *Invest Ophthalmol Vis Sci,* 35**,** 3325-31.
McElnea, E. M., Quill, B., Docherty, N. G., Irnaten, M., Siah, W. F., Clark, A. F., O'Brien, C. J. & Wallace, D. M. (2011) Oxidative stress, mitochondrial dysfunction and calcium overload in human lamina cribrosa cells from glaucoma donors. *Mol Vis,* 17**,** 1182-91.
Miller, K. M. & Quigley, H. A. (1988) The clinical appearance of the lamina cribrosa as a function of the extent of glaucomatous optic nerve damage. *Ophthalmology,* 95**,** 135-8.
Miyara, N., Shinzato, M., Yamashiro, Y., Iwamatsu, A., Kariya, K. & Sawaguchi, S. (2008) Proteomic analysis of rat retina in a steroid-induced ocular hypertension model: potential vulnerability to oxidative stress. *Jpn J Ophthalmol,* 52**,** 84-90.
Mizumoto, H., Mizumoto, K., Shatos, M. A., Klassen, H. & Young, M. J. (2003) Retinal transplantation of neural progenitor cells derived from the brain of GFP transgenic mice. *Vision Res,* 43**,** 1699-708.
Moreno-Flores, M. T., Lim, F., Martin-Bermejo, M. J., Diaz-Nido, J., Avila, J. & Wandosell, F. (2003) Immortalized olfactory ensheathing glia promote axonal regeneration of rat retinal ganglion neurons. *J Neurochem,* 85**,** 861-71.
Mori, I., Nishiyama, Y., Yokochi, T. & Kimura, Y. (2005) Olfactory transmission of neurotropic viruses. *J Neurovirol,* 11**,** 129-37.
Mori, K., Ando, F., Nomura, H., Sato, Y. & Shimokata, H. (2000) Relationship between intraocular pressure and obesity in Japan. *Int J Epidemiol,* 29**,** 661-6.
Morrison, J., Farrell, S., Johnson, E., Deppmeier, L., Moore, C. G. & Grossmann, E. (1995a) Structure and composition of the rodent lamina cribrosa. *Exp Eye Res,* 60**,** 127-35.
Morrison, J. C., Dorman-Pease, M. E., Dunkelberger, G. R. & Quigley, H. A. (1990) Optic nerve head extracellular matrix in primary optic atrophy and experimental glaucoma. *Arch Ophthalmol,* 108**,** 1020-4.
Morrison, J. C., Fraunfelder, F. W., Milne, S. T. & Moore, C. G. (1995b) Limbal microvasculature of the rat eye. *Invest Ophthalmol Vis Sci,* 36**,** 751-6.
Morrison, J. C., Jia, L., Cepurna, W., Guo, Y. & Johnson, E. (2009) Reliability and sensitivity of the TonoLab rebound tonometer in awake Brown Norway rats. *Invest Ophthalmol Vis Sci,* 50**,** 2802-8.

Morrison, J. C., Johnson, E. C., Cepurna, W. & Jia, L. (2005) Understanding mechanisms of pressure-induced optic nerve damage. *Prog Retin Eye Res,* 24**,** 217-40.
Morrison, J. C., Moore, C. G., Deppmeier, L. M., Gold, B. G., Meshul, C. K. & Johnson, E. C. (1997) A rat model of chronic pressure-induced optic nerve damage. *Exp Eye Res,* 64**,** 85-96.
Mullen, R. J., Buck, C. R. & Smith, A. M. (1992) NeuN, a neuronal specific nuclear protein in vertebrates. *Development,* 116**,** 201-11.
Muller, A., Hauk, T. G., Leibinger, M., Marienfeld, R. & Fischer, D. (2009) Exogenous CNTF stimulates axon regeneration of retinal ganglion cells partially via endogenous CNTF. *Mol Cell Neurosci*.
Murdoch, B. & Roskams, A. J. (2007) Olfactory epithelium progenitors: insights from transgenic mice and in vitro biology. *J Mol Histol,* 38**,** 581-99.
Nan, B., Getchell, M. L., Partin, J. V. & Getchell, T. V. (2001) Leukemia inhibitory factor, interleukin-6, and their receptors are expressed transiently in the olfactory mucosa after target ablation. *J Comp Neurol,* 435**,** 60-77.
Naska, S., Lin, D. C., Miller, F. D. & Kaplan, D. R. (2010) p75NTR is an obligate signaling receptor required for cues that cause sympathetic neuron growth cone collapse. *Mol Cell Neurosci,* 45**,** 108-20.
Neufeld, A. H., Das, S., Vora, S., Gachie, E., Kawai, S., Manning, P. T. & Connor, J. R. (2002) A prodrug of a selective inhibitor of inducible nitric oxide synthase is neuroprotective in the rat model of glaucoma. *J Glaucoma,* 11**,** 221-5.
Neufeld, A. H., Hernandez, M. R. & Gonzalez, M. (1997) Nitric oxide synthase in the human glaucomatous optic nerve head. *Arch Ophthalmol,* 115**,** 497-503.
Neufeld, A. H., Sawada, A. & Becker, B. (1999) Inhibition of nitric-oxide synthase 2 by aminoguanidine provides neuroprotection of retinal ganglion cells in a rat model of chronic glaucoma. *Proc Natl Acad Sci U S A,* 96**,** 9944-8.
Newman, E. A. (2001) Propagation of intercellular calcium waves in retinal astrocytes and Muller cells. *J Neurosci,* 21**,** 2215-23.
Newman, E. A., Frambach, D. A. & Odette, L. L. (1984) Control of extracellular potassium levels by retinal glial cell K+ siphoning. *Science,* 225**,** 1174-5.
Nicolela, M. T., Walman, B. E., Buckley, A. R. & Drance, S. M. (1996) Ocular hypertension and primary open-angle glaucoma: a comparative study of their retrobulbar blood flow velocity. *J Glaucoma,* 5**,** 308-10.
Niederhauser, O., Mangold, M., Schubenel, R., Kusznir, E. A., Schmidt, D. & Hertel, C. (2000) NGF ligand alters NGF signaling via p75(NTR) and trkA. *J Neurosci Res,* 61**,** 263-72.
Nivet, E., Vignes, M., Girard, S. D., Pierrisnard, C., Baril, N., Deveze, A., Magnan, J., Lante, F., Khrestchatisky, M., Feron, F. & Roman, F. S. (2011) Engraftment of human nasal olfactory stem cells restores neuroplasticity in mice with hippocampal lesions. *J Clin Invest,* 121**,** 2808-20.
O'Toole, D. A., West, A. K. & Chuah, M. I. (2007) Effect of olfactory ensheathing cells on reactive astrocytes in vitro. *Cell Mol Life Sci,* 64**,** 1303-9.
Ohuchi, E., Imai, K., Fujii, Y., Sato, H., Seiki, M. & Okada, Y. (1997) Membrane type 1 matrix metalloproteinase digests interstitial collagens and other extracellular matrix macromolecules. *J Biol Chem,* 272**,** 2446-51.
Ooto, S., Akagi, T., Kageyama, R., Akita, J., Mandai, M., Honda, Y. & Takahashi, M. (2004) Potential for neural regeneration after neurotoxic injury in the adult mammalian retina. *Proc Natl Acad Sci U S A,* 101**,** 13654-9.
Osborne, N. N. (2008) Pathogenesis of ganglion "cell death" in glaucoma and neuroprotection: focus on ganglion cell axonal mitochondria. *Prog Brain Res,* 173**,** 339-52.

Osborne, N. N., Block, F. & Sontag, K. H. (1991) Reduction of ocular blood flow results in glial fibrillary acidic protein (GFAP) expression in rat retinal Muller cells. *Vis Neurosci,* 7**,** 637-9.
Osborne, N. N., Lascaratos, G., Bron, A. J., Chidlow, G. & Wood, J. P. (2006) A hypothesis to suggest that light is a risk factor in glaucoma and the mitochondrial optic neuropathies. *Br J Ophthalmol,* 90**,** 237-41.
Osborne, N. N., Li, G. Y., Ji, D., Mortiboys, H. J. & Jackson, S. (2008) Light affects mitochondria to cause apoptosis to cultured cells: possible relevance to ganglion cell death in certain optic neuropathies. *J Neurochem,* 105**,** 2013-28.
Parri, H. R., Gould, T. M. & Crunelli, V. (2001) Spontaneous astrocytic Ca2+ oscillations in situ drive NMDAR-mediated neuronal excitation. *Nat Neurosci,* 4**,** 803-12.
Pasti, L., Volterra, A., Pozzan, T. & Carmignoto, G. (1997) Intracellular calcium oscillations in astrocytes: a highly plastic, bidirectional form of communication between neurons and astrocytes in situ. *J Neurosci,* 17**,** 7817-30.
Pastrana, E., Moreno-Flores, M. T., Gurzov, E. N., Avila, J., Wandosell, F. & Diaz-Nido, J. (2006) Genes associated with adult axon regeneration promoted by olfactory ensheathing cells: a new role for matrix metalloproteinase 2. *J Neurosci,* 26**,** 5347-59.
Paviot, A., Guerout, N., Bon-Mardion, N., Duclos, C., Jean, L., Boyer, O. & Marie, J. P. (2011) Efficiency of laryngeal motor nerve repair is greater with bulbar than with mucosal olfactory ensheathing cells. *Neurobiol Dis,* 41**,** 688-94.
Pease, M. E., McKinnon, S. J., Quigley, H. A., Kerrigan-Baumrind, L. A. & Zack, D. J. (2000) Obstructed axonal transport of BDNF and its receptor TrkB in experimental glaucoma. *Invest Ophthalmol Vis Sci,* 41**,** 764-74.
Pixley, S. K. (1992) The olfactory nerve contains two populations of glia, identified both in vivo and in vitro. *Glia,* 5**,** 269-84.
Plant, G. W., Currier, P. F., Cuervo, E. P., Bates, M. L., Pressman, Y., Bunge, M. B. & Wood, P. M. (2002) Purified adult ensheathing glia fail to myelinate axons under culture conditions that enable Schwann cells to form myelin. *J Neurosci,* 22**,** 6083-91.
Plant, G. W., Harvey, A. R., Leaver, S. G. & Lee, S. V. (2010) Olfactory ensheathing glia: repairing injury to the mammalian visual system. *Exp Neurol,* 229**,** 99-108.
Prasanna, G., Krishnamoorthy, R., Clark, A. F., Wordinger, R. J. & Yorio, T. (2002) Human optic nerve head astrocytes as a target for endothelin-1. *Invest Ophthalmol Vis Sci,* 43**,** 2704-13.
Puro, D. G., Yuan, J. P. & Sucher, N. J. (1996) Activation of NMDA receptor-channels in human retinal Muller glial cells inhibits inward-rectifying potassium currents. *Vis Neurosci,* 13**,** 319-26.
Quigley, H. & Anderson, D. R. (1976) The dynamics and location of axonal transport blockade by acute intraocular pressure elevation in primate optic nerve. *Invest Ophthalmol,* 15**,** 606-16.
Quigley, H. A. & Addicks, E. M. (1980) Chronic experimental glaucoma in primates. I. Production of elevated intraocular pressure by anterior chamber injection of autologous ghost red blood cells. *Invest Ophthalmol Vis Sci,* 19**,** 126-36.
Quigley, H. A., Addicks, E. M., Green, W. R. & Maumenee, A. E. (1981) Optic nerve damage in human glaucoma. II. The site of injury and susceptibility to damage. *Arch Ophthalmol,* 99**,** 635-49.
Quigley, H. A. & Broman, A. T. (2006) The number of people with glaucoma worldwide in 2010 and 2020. *Br J Ophthalmol,* 90**,** 262-7.
Quigley, H. A. & Green, W. R. (1979) The histology of human glaucoma cupping and optic nerve damage: clinicopathologic correlation in 21 eyes. *Ophthalmology,* 86**,** 1803-30.

Quigley, H. A., Hohman, R. M., Addicks, E. M., Massof, R. W. & Green, W. R. (1983) Morphologic changes in the lamina cribrosa correlated with neural loss in open-angle glaucoma. *Am J Ophthalmol,* 95**,** 673-91.
Quigley, H. A., McKinnon, S. J., Zack, D. J., Pease, M. E., Kerrigan-Baumrind, L. A., Kerrigan, D. F. & Mitchell, R. S. (2000) Retrograde axonal transport of BDNF in retinal ganglion cells is blocked by acute IOP elevation in rats. *Invest Ophthalmol Vis Sci,* 41**,** 3460-6.
Quigley, H. A., Nickells, R. W., Kerrigan, L. A., Pease, M. E., Thibault, D. J. & Zack, D. J. (1995) Retinal ganglion cell death in experimental glaucoma and after axotomy occurs by apoptosis. *Invest Ophthalmol Vis Sci,* 36**,** 774-86.
Radius, R. L. & Gonzales, M. (1981) Anatomy of the lamina cribrosa in human eyes. *Arch Ophthalmol,* 99**,** 2159-62.
Radtke, C., Aizer, A. A., Agulian, S. K., Lankford, K. L., Vogt, P. M. & Kocsis, J. D. (2009) Transplantation of olfactory ensheathing cells enhances peripheral nerve regeneration after microsurgical nerve repair. *Brain Res,* 1254**,** 10-7.
Rahmatullah, M., Schroering, A., Rothblum, K., Stahl, R. C., Urban, B. & Carey, D. J. (1998) Synergistic regulation of Schwann cell proliferation by heregulin and forskolin. *Mol Cell Biol,* 18**,** 6245-52.
Raisman, G. (1985) Specialized neuroglial arrangement may explain the capacity of vomeronasal axons to reinnervate central neurons. *Neuroscience,* 14**,** 237-54.
Ramer, L. M., Au, E., Richter, M. W., Liu, J., Tetzlaff, W. & Roskams, A. J. (2004) Peripheral olfactory ensheathing cells reduce scar and cavity formation and promote regeneration after spinal cord injury. *J Comp Neurol,* 473**,** 1-15.
Rao, V. R., Krishnamoorthy, R. R. & Yorio, T. (2007) Endothelin-1, endothelin A and B receptor expression and their pharmacological properties in GFAP negative human lamina cribrosa cells. *Exp Eye Res,* 84**,** 1115-24.
Rhee, D. J., Fariss, R. N., Brekken, R., Sage, E. H. & Russell, P. (2003) The matricellular protein SPARC is expressed in human trabecular meshwork. *Exp Eye Res,* 77**,** 601-7.
Rhee, D. J., Haddadin, R. I., Kang, M. H. & Oh, D. J. (2009) Matricellular proteins in the trabecular meshwork. *Exp Eye Res,* 88**,** 694-703.
Richter, M. W., Fletcher, P. A., Liu, J., Tetzlaff, W. & Roskams, A. J. (2005) Lamina propria and olfactory bulb ensheathing cells exhibit differential integration and migration and promote differential axon sprouting in the lesioned spinal cord. *J Neurosci,* 25**,** 10700-11.
Riddell, J. S., Enriquez-Denton, M., Toft, A., Fairless, R. & Barnett, S. C. (2004) Olfactory ensheathing cell grafts have minimal influence on regeneration at the dorsal root entry zone following rhizotomy. *Glia,* 47**,** 150-67.
Robitaille, R. (1998) Modulation of synaptic efficacy and synaptic depression by glial cells at the frog neuromuscular junction. *Neuron,* 21**,** 847-55.
Rohen, J. W. & van der Zypen, E. (1968) The phagocytic activity of the trabecularmeshwork endothelium. An electron-microscopic study of the vervet (Cercopithecus aethiops). *Albrecht Von Graefes Arch Klin Exp Ophthalmol,* 175**,** 143-60.
Roux, P. P. & Barker, P. A. (2002) Neurotrophin signaling through the p75 neurotrophin receptor. *Prog Neurobiol,* 67**,** 203-33.
Saeki, T., Aihara, M., Ohashi, M. & Araie, M. (2008) The efficacy of TonoLab in detecting physiological and pharmacological changes of mouse intraocular pressure--comparison with TonoPen and microneedle manometery. *Curr Eye Res,* 33**,** 247-52.
Sakamoto, T. & Ishibashi, T. (2011) Hyalocytes: essential cells of the vitreous cavity in vitreoretinal pathophysiology? *Retina,* 31**,** 222-8.

Samsel, P. A., Kisiswa, L., Erichsen, J. T., Cross, S. D. & Morgan, J. E. (2010) A novel method for the induction of experimental glaucoma using magnetic microspheres. *Invest Ophthalmol Vis Sci*.
Sappington, R. M., Carlson, B. J., Crish, S. D. & Calkins, D. (2009a) The Microbead Occlusion Model: A Paradigm for Induced Ocular Hypertension in Rats and Mice. *Invest Ophthalmol Vis Sci*.
Sappington, R. M., Sidorova, T., Long, D. J. & Calkins, D. J. (2009b) TRPV1: contribution to retinal ganglion cell apoptosis and increased intracellular Ca2+ with exposure to hydrostatic pressure. *Invest Ophthalmol Vis Sci,* 50**,** 717-28.
Sasaki, M., Black, J. A., Lankford, K. L., Tokuno, H. A., Waxman, S. G. & Kocsis, J. D. (2006) Molecular reconstruction of nodes of Ranvier after remyelination by transplanted olfactory ensheathing cells in the demyelinated spinal cord. *J Neurosci,* 26**,** 1803-12.
Sawaguchi, K., Nakamura, Y., Sakai, H. & Sawaguchi, S. (2005) Myocilin gene expression in the trabecular meshwork of rats in a steroid-induced ocular hypertension model. *Ophthalmic Res,* 37**,** 235-42.
Schwartzman, M. L., Balazy, M., Masferrer, J., Abraham, N. G., McGiff, J. C. & Murphy, R. C. (1987) 12(R)-hydroxyicosatetraenoic acid: a cytochrome-P450-dependent arachidonate metabolite that inhibits Na+,K+-ATPase in the cornea. *Proc Natl Acad Sci U S A,* 84**,** 8125-9.
Seki, M., Tanaka, T., Sakai, Y., Fukuchi, T., Abe, H., Nawa, H. & Takei, N. (2005) Muller Cells as a source of brain-derived neurotrophic factor in the retina: noradrenaline upregulates brain-derived neurotrophic factor levels in cultured rat Muller cells. *Neurochem Res,* 30**,** 1163-70.
Sekirnjak, C., Hottowy, P., Sher, A., Dabrowski, W., Litke, A. M. & Chichilnisky, E. J. (2008) High-resolution electrical stimulation of primate retina for epiretinal implant design. *J Neurosci,* 28**,** 4446-56.
Shareef, S. R., Garcia-Valenzuela, E., Salierno, A., Walsh, J. & Sharma, S. C. (1995) Chronic ocular hypertension following episcleral venous occlusion in rats. *Exp Eye Res,* 61**,** 379-82.
Sheffield, V. C., Stone, E. M., Alward, W. L., Drack, A. V., Johnson, A. T., Streb, L. M. & Nichols, B. E. (1993) Genetic linkage of familial open angle glaucoma to chromosome 1q21-q31. *Nat Genet,* 4**,** 47-50.
Siegner, S. W., Netland, P. A., Schroeder, A. & Erickson, K. A. (2000) Effect of calcium channel blockers alone and in combination with antiglaucoma medications on intraocular pressure in the primate eye. *J Glaucoma,* 9**,** 334-9.
Sieving, P. A. (1991) Retinal ganglion cell loss does not abolish the scotopic threshold response (STR) of the cat and human ERG. *Clin Vision Sci,* 6**,** 149-158.
Sieving, P. A., Frishman, L. J. & Steinberg, R. H. (1986) Scotopic threshold response of proximal retina in cat. *J Neurophysiol,* 56**,** 1049-61.
Singh, K. K., Park, K. J., Hong, E. J., Kramer, B. M., Greenberg, M. E., Kaplan, D. R. & Miller, F. D. (2008) Developmental axon pruning mediated by BDNF-p75NTR-dependent axon degeneration. *Nat Neurosci,* 11**,** 649-58.
Siu, A. W., Leung, M. C., To, C. H., Siu, F. K., Ji, J. Z. & So, K. F. (2002) Total retinal nitric oxide production is increased in intraocular pressure-elevated rats. *Exp Eye Res,* 75**,** 401-6.
Snider, W. D. (1994) Functions of the neurotrophins during nervous system development: what the knockouts are teaching us. *Cell,* 77**,** 627-38.
Sommer, A., Tielsch, J. M., Katz, J., Quigley, H. A., Gottsch, J. D., Javitt, J. & Singh, K. (1991) Relationship between intraocular pressure and primary open angle glaucoma among white and black Americans. The Baltimore Eye Survey. *Arch Ophthalmol,* 109**,** 1090-5.

Soto, I., Pease, M. E., Son, J. L., Shi, X., Quigley, H. A. & Marsh-Armstrong, N. (2010) Retinal Ganglion Cell Loss in a Rat Ocular Hypertension Model is Sectorial and Involves Early Optic Nerve Axon Loss. *Invest Ophthalmol Vis Sci*.
Sperber, G. O. & Bill, A. (1985) Blood flow and glucose consumption in the optic nerve, retina and brain: effects of high intraocular pressure. *Exp Eye Res,* 41**,** 639-53.
Staal, J. A., Dickson, T. C., Chung, R. S. & Vickers, J. C. (2007) Cyclosporin-A treatment attenuates delayed cytoskeletal alterations and secondary axotomy following mild axonal stretch injury. *Dev Neurobiol,* 67**,** 1831-42.
Stewart, W. C., Sine, C., Sutherland, S. & Stewart, J. A. (1996) Total cholesterol and high-density lipoprotein levels as risk factors for increased intraocular pressure. *Am J Ophthalmol,* 122**,** 575-7.
Stockton, R. A. & Slaughter, M. M. (1989) B-wave of the electroretinogram. A reflection of ON bipolar cell activity. *J Gen Physiol,* 93**,** 101-22.
Stoilov, I., Akarsu, A. N. & Sarfarazi, M. (1997) Identification of three different truncating mutations in cytochrome P4501B1 (CYP1B1) as the principal cause of primary congenital glaucoma (Buphthalmos) in families linked to the GLC3A locus on chromosome 2p21. *Hum Mol Genet,* 6**,** 641-7.
Stone, E. M., Fingert, J. H., Alward, W. L., Nguyen, T. D., Polansky, J. R., Sunden, S. L., Nishimura, D., Clark, A. F., Nystuen, A., Nichols, B. E., Mackey, D. A., Ritch, R., Kalenak, J. W., Craven, E. R. & Sheffield, V. C. (1997) Identification of a gene that causes primary open angle glaucoma. *Science,* 275**,** 668-70.
Suzuki, Y., Takeda, M. & Farbman, A. I. (1996) Supporting cells as phagocytes in the olfactory epithelium after bulbectomy. *J Comp Neurol,* 376**,** 509-17.
Takami, T., Oudega, M., Bates, M. L., Wood, P. M., Kleitman, N. & Bunge, M. B. (2002) Schwann cell but not olfactory ensheathing glia transplants improve hindlimb locomotor performance in the moderately contused adult rat thoracic spinal cord. *J Neurosci,* 22**,** 6670-81.
Takeuchi, H., Mizuno, T., Zhang, G., Wang, J., Kawanokuchi, J., Kuno, R. & Suzumura, A. (2005) Neuritic beading induced by activated microglia is an early feature of neuronal dysfunction toward neuronal death by inhibition of mitochondrial respiration and axonal transport. *J Biol Chem,* 280**,** 10444-54.
Tamm, E. R. (2009) The trabecular meshwork outflow pathways: structural and functional aspects. *Exp Eye Res,* 88**,** 648-55.
Taniuchi, M., Clark, H. B., Schweitzer, J. B. & Johnson, E. M., Jr. (1988) Expression of nerve growth factor receptors by Schwann cells of axotomized peripheral nerves: ultrastructural location, suppression by axonal contact, and binding properties. *J Neurosci,* 8**,** 664-81.
Tawara, A., Tou, N., Kubota, T., Harada, Y. & Yokota, K. (2008) Immunohistochemical evaluation of the extracellular matrix in trabecular meshwork in steroid-induced glaucoma. *Graefes Arch Clin Exp Ophthalmol,* 246**,** 1021-8.
Tchedre, K. T. & Yorio, T. (2008) sigma-1 receptors protect RGC-5 cells from apoptosis by regulating intracellular calcium, Bax levels, and caspase-3 activation. *Invest Ophthalmol Vis Sci,* 49**,** 2577-88.
Tektas, O. Y., Hammer, C. M., Danias, J., Candia, O., Gerometta, R., Podos, S. M. & Lutjen-Drecoll, E. (2010) Morphologic changes in the outflow pathways of bovine eyes treated with corticosteroids. *Invest Ophthalmol Vis Sci,* 51**,** 4060-6.
Tezel, G., Edward, D. P. & Wax, M. B. (1999) Serum autoantibodies to optic nerve head glycosaminoglycans in patients with glaucoma. *Arch Ophthalmol,* 117**,** 917-24.
Tezel, G., Hernandez, R. & Wax, M. B. (2000) Immunostaining of heat shock proteins in the retina and optic nerve head of normal and glaucomatous eyes. *Arch Ophthalmol,* 118**,** 511-8.

Tezel, G., Li, L. Y., Patil, R. V. & Wax, M. B. (2001) TNF-alpha and TNF-alpha receptor-1 in the retina of normal and glaucomatous eyes. *Invest Ophthalmol Vis Sci,* 42**,** 1787-94.
Tezel, G., Seigel, G. M. & Wax, M. B. (1998) Autoantibodies to small heat shock proteins in glaucoma. *Invest Ophthalmol Vis Sci,* 39**,** 2277-87.
Tezel, G., Trinkaus, K. & Wax, M. B. (2004) Alterations in the morphology of lamina cribrosa pores in glaucomatous eyes. *Br J Ophthalmol,* 88**,** 251-6.
Thummel, R., Kassen, S. C., Montgomery, J. E., Enright, J. M. & Hyde, D. R. (2008) Inhibition of Muller glial cell division blocks regeneration of the light-damaged zebrafish retina. *Dev Neurobiol,* 68**,** 392-408.
Thuret, S., Moon, L. D. & Gage, F. H. (2006) Therapeutic interventions after spinal cord injury. *Nat Rev Neurosci,* 7**,** 628-43.
Ticho, U., Lahav, M., Berkowitz, S. & Yoffe, P. (1979) Ocular changes in rabbits with corticosteroid-induced ocular hypertension. *Br J Ophthalmol,* 63**,** 646-50.
Tielsch, J. M., Katz, J., Singh, K., Quigley, H. A., Gottsch, J. D., Javitt, J. & Sommer, A. (1991) A population-based evaluation of glaucoma screening: the Baltimore Eye Survey. *Am J Epidemiol,* 134**,** 1102-10.
Todd, P. A. & Benfield, P. (1989) Flunarizine. A reappraisal of its pharmacological properties and therapeutic use in neurological disorders. *Drugs,* 38**,** 481-99.
Tomita, K., Kubo, T., Matsuda, K., Fujiwara, T., Yano, K., Winograd, J. M., Tohyama, M. & Hosokawa, K. (2007) The neurotrophin receptor p75NTR in Schwann cells is implicated in remyelination and motor recovery after peripheral nerve injury. *Glia,* 55**,** 1199-208.
Toris, C. B., Yablonski, M. E., Wang, Y. L. & Camras, C. B. (1999) Aqueous humor dynamics in the aging human eye. *Am J Ophthalmol,* 127**,** 407-12.
Trick, G. L. (1993) Visual dysfunction in normotensive glaucoma. *Doc Ophthalmol,* 85**,** 125-33.
Tumminia, S. J., Mitton, K. P., Arora, J., Zelenka, P., Epstein, D. L. & Russell, P. (1998) Mechanical stretch alters the actin cytoskeletal network and signal transduction in human trabecular meshwork cells. *Invest Ophthalmol Vis Sci,* 39**,** 1361-71.
Turner, D. L. & Cepko, C. L. (1987) A common progenitor for neurons and glia persists in rat retina late in development. *Nature,* 328**,** 131-6.
Ueda, J., Sawaguchi, S., Hanyu, T., Yaoeda, K., Fukuchi, T., Abe, H. & Ozawa, H. (1998) Experimental glaucoma model in the rat induced by laser trabecular photocoagulation after an intracameral injection of India ink. *Jpn J Ophthalmol,* 42**,** 337-44.
Van Bergen, N. J., Wood, J. P., Chidlow, G., Trounce, I. A., Casson, R. J., Ju, W. K., Weinreb, R. N. & Crowston, J. G. (2009) Recharacterization of the RGC-5 retinal ganglion cell line. *Invest Ophthalmol Vis Sci,* 50**,** 4267-72.
van den Pol, A. N. & Santarelli, J. G. (2003) Olfactory ensheathing cells: time lapse imaging of cellular interactions, axonal support, rapid morphologic shifts, and mitosis. *J Comp Neurol,* 458**,** 175-94.
Verdu, E., Garcia-Alias, G., Fores, J., Gudino-Cabrera, G., Muneton, V. C., Nieto-Sampedro, M. & Navarro, X. (2001) Effects of ensheathing cells transplanted into photochemically damaged spinal cord. *Neuroreport,* 12**,** 2303-9.
Vincent, A. J., Taylor, J. M., Choi-Lundberg, D. L., West, A. K. & Chuah, M. I. (2005) Genetic expression profile of olfactory ensheathing cells is distinct from that of Schwann cells and astrocytes. *Glia,* 51**,** 132-47.
Vincent, A. J., West, A. K. & Chuah, M. I. (2003) Morphological plasticity of olfactory ensheathing cells is regulated by cAMP and endothelin-1. *Glia,* 41**,** 393-403.
Vittal, V., Rose, A., Gregory, K. E., Kelley, M. J. & Acott, T. S. (2005) Changes in gene expression by trabecular meshwork cells in response to mechanical stretching. *Invest Ophthalmol Vis Sci,* 46**,** 2857-68.

von Bartheld, C. S. & Butowt, R. (2000) Expression of neurotrophin-3 (NT-3) and anterograde axonal transport of endogenous NT-3 by retinal ganglion cells in chick embryos. *J Neurosci,* 20**,** 736-48.
Wang, R. F., Gagliuso, D. J. & Podos, S. M. (2008) Effect of flunarizine, a calcium channel blocker, on intraocular pressure and aqueous humor dynamics in monkeys. *J Glaucoma,* 17**,** 73-8.
Wax, M. B. (2000) Is there a role for the immune system in glaucomatous optic neuropathy? *Curr Opin Ophthalmol,* 11**,** 145-50.
Waxman, S. G. & Black, J. A. (1984) Freeze-fracture ultrastructure of the perinodal astrocyte and associated glial junctions. *Brain Res,* 308**,** 77-87.
Weber, A. J., Kalil, R. E. & Stanford, L. R. (1998) Dendritic field development of retinal ganglion cells in the cat following neonatal damage to visual cortex: evidence for cell class specific interactions. *J Comp Neurol,* 390**,** 470-80.
Weber, A. J. & Zelenak, D. (2001) Experimental glaucoma in the primate induced by latex microspheres. *J Neurosci Methods,* 111**,** 39-48.
Wen, R. & Oakley, B., 2nd (1990) K(+)-evoked Muller cell depolarization generates b-wave of electroretinogram in toad retina. *Proc Natl Acad Sci U S A,* 87**,** 2117-21.
Wewetzer, K., Grothe, C. & Claus, P. (2001) In vitro expression and regulation of ciliary neurotrophic factor and its alpha receptor subunit in neonatal rat olfactory ensheathing cells. *Neurosci Lett,* 306**,** 165-8.
Wewetzer, K., Kern, N., Ebel, C., Radtke, C. & Brandes, G. (2005) Phagocytosis of O4+ axonal fragments in vitro by p75- neonatal rat olfactory ensheathing cells. *Glia,* 49**,** 577-87.
Whitlock, N. A., McKnight, B., Corcoran, K. N., Rodriguez, L. A. & Rice, D. S. (2010) Increased intraocular pressure in mice treated with dexamethasone. *Invest Ophthalmol Vis Sci,* 51**,** 6496-503.
Woodhall, E., West, A. K. & Chuah, M. I. (2001) Cultured olfactory ensheathing cells express nerve growth factor, brain-derived neurotrophic factor, glia cell line-derived neurotrophic factor and their receptors. *Brain Res Mol Brain Res,* 88**,** 203-13.
Wu, H. Y., Tomizawa, K., Oda, Y., Wei, F. Y., Lu, Y. F., Matsushita, M., Li, S. T., Moriwaki, A. & Matsui, H. (2004) Critical role of calpain-mediated cleavage of calcineurin in excitotoxic neurodegeneration. *J Biol Chem,* 279**,** 4929-40.
Yam, G., Gaplovska-Kysela, K., Roth, J. (2006) Aggregatedmyocilin induces Russell bodies and causes apoptosis. *Am J Pathol***,** 100-109.
Yamaguchi, Y., Watanabe, T., Hirakata, A. & Hida, T. (2006) Localization and ontogeny of aquaporin-1 and -4 expression in iris and ciliary epithelial cells in rats. *Cell Tissue Res,* 325**,** 101-9.
Yamamoto, M., Raisman, G., Li, D. & Li, Y. (2009) Transplanted olfactory mucosal cells restore paw reaching function without regeneration of severed corticospinal tract fibres across the lesion. *Brain Res,* 1303**,** 26-31.
Yan, X., Tezel, G., Wax, M. B. & Edward, D. P. (2000) Matrix metalloproteinases and tumor necrosis factor alpha in glaucomatous optic nerve head. *Arch Ophthalmol,* 118**,** 666-73.
Yang, J., Tezel, G., Patil, R. V., Romano, C. & Wax, M. B. (2001) Serum autoantibody against glutathione S-transferase in patients with glaucoma. *Invest Ophthalmol Vis Sci,* 42**,** 1273-6.
Yang, P., Agapova, O., Parker, A., Shannon, W., Pecen, P., Duncan, J., Salvador-Silva, M. & Hernandez, M. R. (2004) DNA microarray analysis of gene expression in human optic nerve head astrocytes in response to hydrostatic pressure. *Physiol Genomics,* 17**,** 157-69.
Yin, Y., Cui, Q., Li, Y., Irwin, N., Fischer, D., Harvey, A. R. & Benowitz, L. I. (2003) Macrophage-derived factors stimulate optic nerve regeneration. *J Neurosci,* 23**,** 2284-93.

You, S., Petrov, T., Chung, P. H. & Gordon, T. (1997) The expression of the low affinity nerve growth factor receptor in long-term denervated Schwann cells. *Glia,* 20**,** 87-100.
Young, M. J., Ray, J., Whiteley, S. J., Klassen, H. & Gage, F. H. (2000) Neuronal differentiation and morphological integration of hippocampal progenitor cells transplanted to the retina of immature and mature dystrophic rats. *Mol Cell Neurosci,* 16**,** 197-205.
Yu, S., Tanabe, T., Dezawa, M., Ishikawa, H. & Yoshimura, N. (2006a) Effects of bone marrow stromal cell injection in an experimental glaucoma model. *Biochem Biophys Res Commun,* 344**,** 1071-9.
Yu, S., Tanabe, T. & Yoshimura, N. (2006b) A rat model of glaucoma induced by episcleral vein ligation. *Exp Eye Res,* 83**,** 758-70.
Yue, P. Y., Leung, E. P., Mak, N. K. & Wong, R. N. (2010) A simplified method for quantifying cell migration/wound healing in 96-well plates. *J Biomol Screen,* 15**,** 427-33.
Zahs, K. R., Kofuji, P., Meier, C. & Dermietzel, R. (2003) Connexin immunoreactivity in glial cells of the rat retina. *J Comp Neurol,* 455**,** 531-46.
Zhan, G. L., Miranda, O. C. & Bito, L. Z. (1992) Steroid glaucoma: corticosteroid-induced ocular hypertension in cats. *Exp Eye Res,* 54**,** 211-8.
Zheng, J., Feng, X., Hou, L., Cui, Y., Zhu, L., Ma, J., Xia, Z., Zhou, W. & Chen, H. (2011) Latanoprost Promotes Neurite Outgrowth in Differentiated RGC-5 Cells via the PI3K-Akt-mTOR Signaling Pathway. *Cell Mol Neurobiol*.
Zimmerberg, J., Akimov, S. A. & Frolov, V. (2006) Synaptotagmin: fusogenic role for calcium sensor? *Nat Struct Mol Biol,* 13**,** 301-3.